Functional and safe encapsulation of *Escherichia coli* in Pluronic hydrogels for engineered living materials

Dissertation

zur Erlangung des Grades

des **Doktors der Naturwissenschaften**

der Naturwissenschaftlich-Technischen Fakultät

der Universität des Saarlandes

von

Shardul Bhusari

Saarbrücken, March 2023

Tag des Kolloquiums:	22. Juni 2023
Dekan:	Prof. Dr. Ludger Santen
Berichterstatter:	Prof. Dr. Aránzazu del Campo Bécares
	Prof. Dr. Karen Lienkamp
Akad. Mitglied:	Dr. Angelika Ullrich
Vorsitz:	Prof. Dr.-Ing. Markus Gallei

Abstract

Bacterial growth and metabolic activity are sensitive to the mechanical properties of their environment. Understanding how the 3D spatial confinement regulates the cell behavior is crucial not only for understanding biofilm development but also for the design and safe application of engineered materials containing living cells. This Thesis explores the use of Pluronic-based hydrogels to encapsulate genetically modified *Escherichia coli* bacteria. Hydrogels with different viscoelastic properties were prepared by mixing Pluronic and Pluronic diacrylate components in different ratios, giving physical hydrogels with variable degree of covalent crosslinking and different mechanical responses. Rheological properties of the hydrogels as well as the growth rate and morphology of the embedded bacterial colonies were characterized. The results provided correlations between material parameters and bacterial cell responses. Further, a bilayer thin film model was developed for long term encapsulation of the organisms, preventing leakage of cells for up to two weeks while maintaining their activity as drug/protein eluting devices or biosensing units. The bacterial bilayer thin films did not elicit significant immune responses in primary immune cells from healthy donors. The results of this Thesis demonstrate the potential of Pluronic-based biohybrid as a suitable and safe prototype for further *in vitro* and *in vivo* testing of engineered living material designs.

Kurzzusammenfassung

Wachstum und Stoffwechselaktivität von Bakterien sind sensitiv gegenüber den mechanischen Eigenschaften ihrer Umgebung. Das Verständnis, wie der räumliche 3D-Einschluss das Zellverhalten reguliert, ist sowohl für die Entwicklung von Biofilmen als auch für das Design und die sichere Anwendung von technischen Materialien, die lebende Zellen enthalten, essenziell. Diese Thesis untersucht die Verwendung von Hydrogelen auf Pluronic-Basis zur Verkapselung von genetisch veränderten *Escherichia coli* Bakterien. Durch die Mischung von Pluronic und Pluronic-Diacrylat in verschiedenen Verhältnissen wurden physische Hydrogele mit unterschiedlichem kovalenten Vernetzungsgrad und viskoelastischen Eigenschaften hergestellt. Die Charakterisierung der rheologischen Eigenschaften der Hydrogele sowie der Wachstumsrate und Morphologie der eingebetteten Bakterien zeigte eine Korrelation zwischen den Materialparametern und dem Zellverhalten. Darüber hinaus wurde ein Doppelschicht-Dünnfilmmodell entwickelt, in dem die Organismen bis zu zwei Wochen ohne Austreten eingeschlossen wurden, während gleichzeitig Medikamenten-, Proteinfreisetzung oder die Aktivität der Zellen als Biosensoren beibehalten wird. Das Modell löste bei primären Immunzellen von gesunden Spendern keine signifikanten Immunreaktionen aus. Diese Thesis zeigt das Potenzial von Biohybriden auf Pluronic-Basis als geeigneten und sicheren Prototyp für weitere *in vitro* und *in vivo* Tests von technischen lebenden Materialien.

Acknowledgments

The research that led to this thesis was conducted at the INM – Leibniz Institute for New Materials in the Dynamic Biomaterials group under the scientific guidance of Prof. Dr. Aránzazu del Campo. I am truly grateful to all the mentors and colleagues who participated in this amazing journey towards the completion of this work.

First and foremost, I would extend my deepest and sincerest gratitude to my supervisor, Prof. Dr. Aránzazu del Campo, for giving me the opportunity to work on such an exciting topic. I am grateful to her for providing a nurturing environment, ample resources, and the freedom to learn and improve as a researcher. Her continuous encouragement and support, whether it was for attending international conferences or competing in business competitions, have been invaluable to me. She has helped me build my confidence and push beyond my limits.

I am extremely thankful to Dr. Shrikrishnan Sankaran for being a wonderful mentor. I feel fortunate to have started my work under his immediate supervision. His passion for the field and cheerful attitude towards life were inspiring and taught me a great deal. I would also like to thank other amazing colleagues in the lab for lending me their knowledge and skills whenever I needed them, especially Dr. Mitchell Han, Dr. Jun Feng, Dr. Malgorzata Katarzyna Wlodarczyk-Biegun, Dr. María Puertas Bartolomé, Dr. Samuel Pearson, and Dr. Julieta Paez.

I am very grateful to all the collaborators without whom it would have been impossible to complete this work: Prof. Dr. Manfred Wilhelm and Maxi Hoffmann from Karlsruher Institut für Technologie (KIT), Dr. Bin Qu and Archana Yanamandra from School of Medicine at Saarland University (Homburg), and Prof. Karen Polizzi from Imperial College, London. I am extremely thankful to Dr. Hans Smola (Hartmann) for teaching me a great deal about the field of technology transfers.

I feel extremely lucky to have worked alongside many bright minds. Many thanks to all my amazing friends in the Dynamic Biomaterials group: Rocío, Priyanka, Adrían, Ana Díaz, Minye, Frano, Sara, Hanuman, Stefan, Gülistan, Zahra, Qiyang, Maria Villiou, Desna, Essak, Yijun, Emmanuel, Jingnan, Mokhamad, Javier, Syuzanna, Jennifer, Nguyen, Sandipan, Rinku, Usama, Lara, Joelle, Namine, Britta, Krupansh, Ketaki, Kathrin, Simon and also members from the Bioprogrammable Materials' group: Varun, Marc, Sourik, Florian, Lorena, and Waranya, for always being kind and generous in helping me. I am thankful to Therese Steudter for her help

in the German translation of the abstract. I also want to thank Christina Muth for her ever so friendly demeanor and immense help in the microbiology labs. I want to thank Dr. Claudia Fink-Straube and Ha Rimbach-Nguyen for their support in GPC measurements. I thank Petra Herbeck-Engel for her help with the Raman measurements. I am grateful for getting the SFB 1027 scholarship for funding the initial months of my research. Special thanks to Martina Bonnard for her kind support during my stay in Germany.

Finally, I would like to thank my parents, my brother, my relatives, and my friends for their unconditional love through all my ups and downs. I could never be as strong and reached this far without so much of your love and rock-solid support. I feel blessed to have all of you in my life.

“Arise, awake and stop not till the goal is reached.”

Swami Vivekananda

Table of Contents

1 MOTIVATION. BACTERIA-CONTAINING HYDROGELS: MAKING MATERIALS ALIVE?

Engineered Living Materials (ELMs) integrate living microbes into non-living materials and acquire properties and functionalities which are impossible to attain with non-living matter. ELMs strive to replicate and integrate the properties of living materials like self-growth, self-organization, adaptability, or evolvability.[1] Genetic programming allows the living components to react to external stimuli to perform functions such as releasing specific molecules or reactants. The matrix provides a stable structure and a supportive environment for the embedded organisms to survive and carry out their biological functions (**Figure 1**).

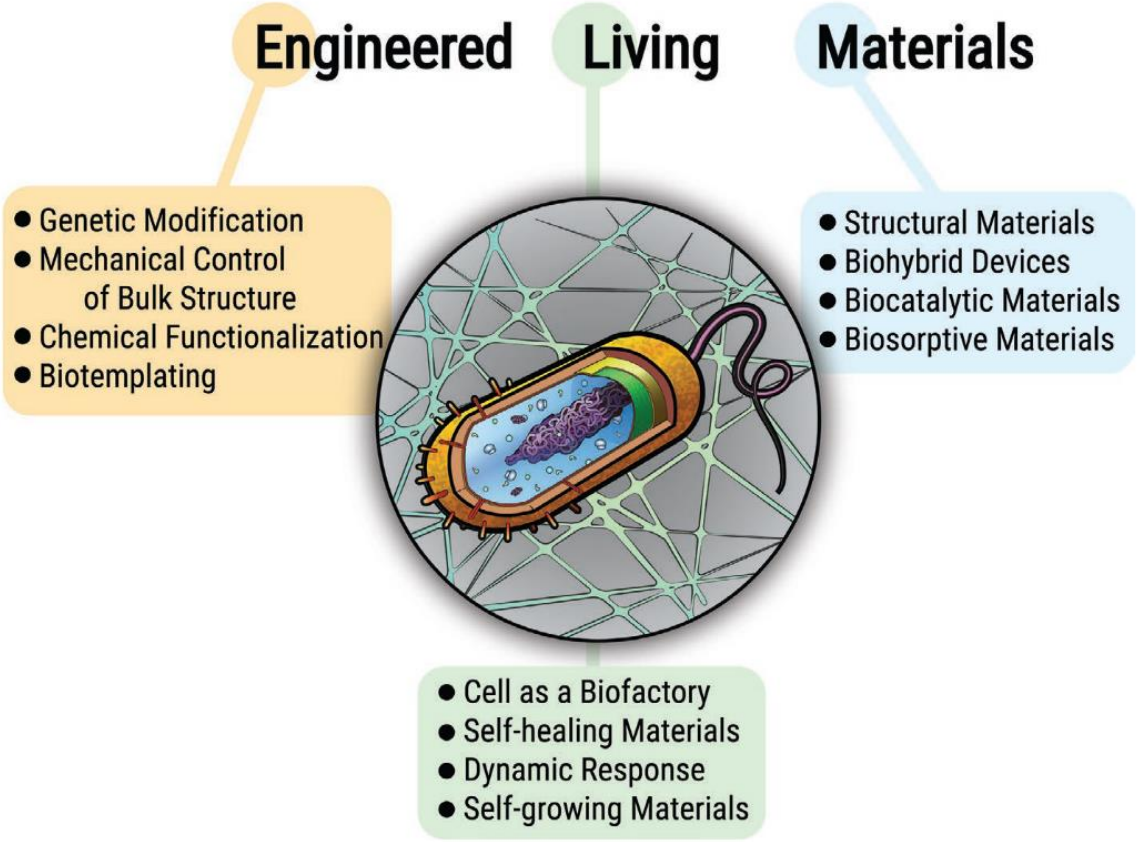

Figure 1: Engineered Living Materials (ELMs) harness the abilities of living systems, such as adaptability, self-replication, and resilience, to become programmable and responsive.[2] Reprinted (adapted) with permission from ref.[2] © 2018 WILEY-VCH Verlag GmbH & Co. KGaA, Weinheim.

Pioneering works in the ELM field have demonstrated the potential of ELMs across various applications.[1][3] Although the excitement in the field is big, there is little understanding of the interactions between the embedded microorganisms and the encapsulating matrices, and how they influence the activity and functionality of the organisms. Genetic manipulation has

been used to achieve tunable and on-demand functionality, but there is still much to be explored in terms of how the properties of the materials can be used to control the behavior of the embedded microorganisms. Inspiration from biofilm-related studies could be utilized for the same. Another open question is the lifespan of ELMs which is related to the diffusive and stability properties of the matrix. Model systems that allow tunability of the matrix properties and the study of cellular responses are needed to progress in the design and improvement of functional and useful ELMs.

An interesting model matrix to encapsulate organisms and study their functionality is the polymer Pluronic F127. Pluronic is easy to process and biocompatible. It is clinically approved and used for drug delivery, tissue engineering, and biotechnology applications. Pluronic forms thermosensitive physical hydrogels and has been used to encapsulate bacteria and yeast in ELMs.[4][5] In this Thesis, Pluronic hydrogels are used to encapsulate *E. coli* to study the growth and metabolic activity of the embedded bacteria as well as the stability of the living hydrogel as a function of the mechanical properties of the matrix. The resulting bacterial hydrogels are tested for their ability to deliver drugs/proteins (therapeutic devices) or to detect analytes (biosensors). The results of this work contribute to the understanding of bacteria-material interactions and pave the road to a functional and safe design of ELMs for the future.

2 INTRODUCTION

2.1 Engineered Living Materials (ELMs)

The ELMs field has grown as consequence of the increasing understanding of how living cells interact with materials, and the progress in genetic programming of microorganisms with specific functions beyond the natural ones.[6] By engineering cells, the production of metabolites can be enhanced or suppressed. By incorporating sensors and switches into their genetic code, the synthesis of these molecules can be controlled by external cues like light, pH, small molecules, temperature etc. alone or in combination.[1][7] By encapsulating programmed microbes within synthetic matrices, ELMs with features like externally guided or self-organization, growth, healing, or environmental responsiveness have been realized (**Figure 2**).[8] Photosynthetic garments[9], autonomously ventilating fabrics[10], self-healing concrete[11], shape morphing materials[12], biofilters for metal sequestration[13], biosensors for hazardous molecules in the environment[14], biofilters to remediate water[15], self-replenishable drug depots[16], wearable skin-sensors which can measure physiological parameters from sweat [17] etc. are some of the advanced applications of the ELMs, also depicted in **Figure 2**.

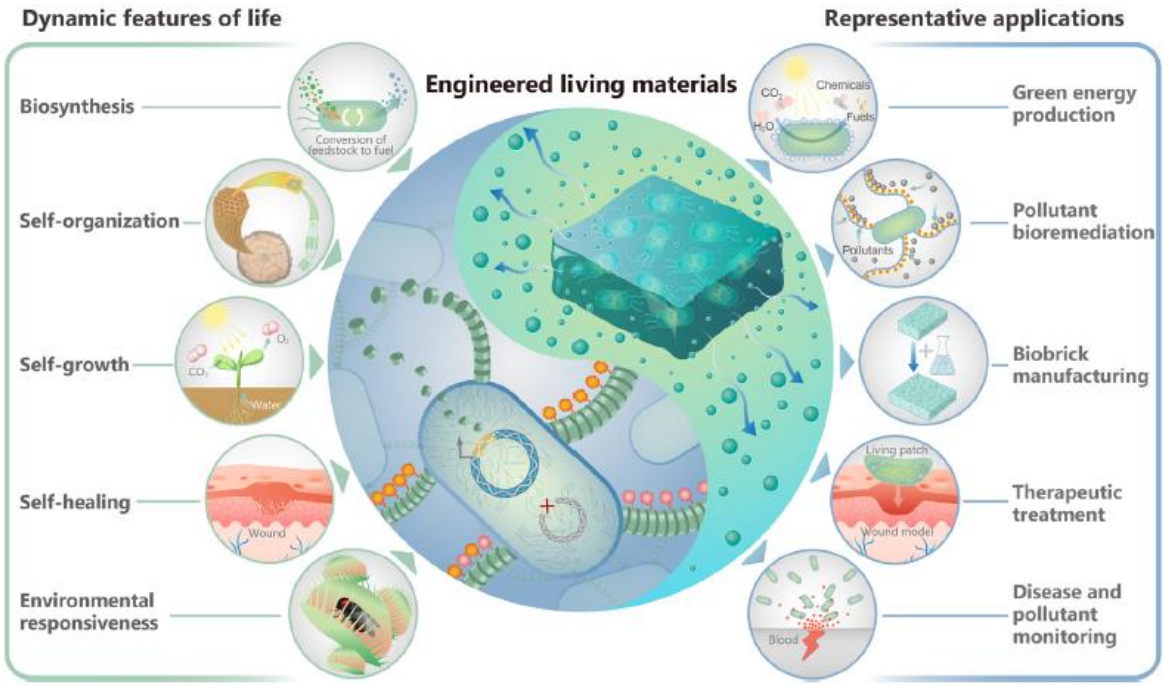

Figure 2: Schematic illustration highlighting envisioned properties of ELMs and their possible applications. ELMs are composed of cells embedded in natural or artificial scaffolds which can showcase different features of living systems like biosynthesis, self-organization, self-growth, self-healing, and respond to their surroundings. These properties lead to a range of applications for ELMs including production of green energy, bioremediation of pollutants, manufacturing of building blocks, diagnosis or therapeutics. Reprinted with permission from reference[8]. Copyright 2022 American Chemical Society.

ELMs can be classified in two types: bottom-up and top-down ELMs. When the living components self-generate their own matrix like polysaccharides, proteins, biomineralization etc., ELMs are called bottom-up ELMs or biological ELMs.[18][19] On the other hand, when living components are combined with abiotic scaffolds, they are termed as top-down or hybrid engineered living materials.[19][3] Tang et al. described various design parameters that can be considered when designing an ELM such as the extent of artificial scaffolding materials used, size scale of the ELM and approach taken for their morphogenesis, bottom-up vs top-down (**Figure 3**).[7] ELMs augment the properties of the materials, which can evolve, be customized with the help of artificial gene regulation, autonomously self-repair in case of biological ELMs and provide sustainable solutions to tackle the shortcomings of existing bio-hybrid systems.[8]

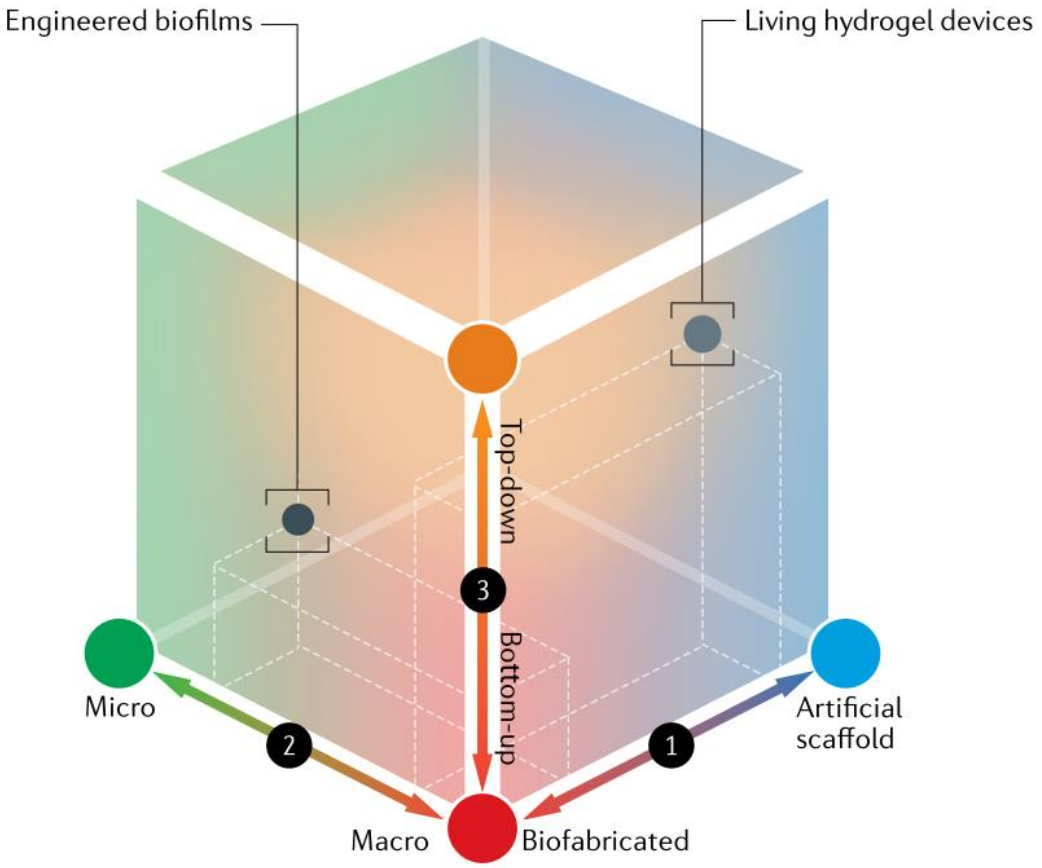

Figure 3: The cube represents the design parameter space for ELMs. On axis 1, the possibility to fabricate ELMs by seeding synthetic scaffolds or by using biofabrication technologies is represented. The other two axes represent the difference length scales (axis 2) and the bottom-up and top-down approaches (axis 3). Reprinted after permission from ref[7] Copyright © 2020, Springer Nature Limited.

2.2 Composition of ELMs

2.2.1 Encapsulating matrix and essential properties

The integration of living, functional microorganisms into non-living matrices presents special challenges in the engineering of ELMs. Two fundamental considerations are hydration and permeability of the matrix to nutrients, metabolic products and gases.[20][21] Hydration is the ability of the matrix to retain water and depends on its polarity or hydrophilicity and its morphology, i.e. the presence of pores or the ability to swell. The availability of oxygen to the embedded organism determines the choice of microorganism to be used for encapsulation and influence its metabolic pathways (aerobic, anaerobic). The permeability to nutrients is mandatory for the growth and metabolic function of the organisms inside the matrix. Non-toxicity of the material itself or its precursors, the mechanical properties of the matrix, the temperature, humidity, pH required for processing the material etc. are some of the considerations for ELM fabrication. Another relevant design parameter for the encapsulating matrix is its ability to contain and retain the living organisms during the application to ensure biosafety.[14]

Most reported ELMs use hydrogels as encapsulating matrices.[8][20] ELMs using porous silica matrices have also been reported.[22] Hydrogel ELMs are water-swollen polymeric networks[23] and also include cell-generated matrices of curli proteins[1][24][25] and polysachharides like bacterial cellulose.[26] Hydrogels have numerous advantages for cell encapsulation. They are soft, hydrated materials with properties similar to those of the extracellular matrix of natural tissues or the extracellular polymeric substances (EPS) of bacteria biofilms. Hydrogels are convenient matrices since their swelling, permeability and mechanical properties can be easily tailored by changes in the formulation of the precursor mixtures.[27] In addition, responsive elements can be incorporated in the polymeric network to enable external control of hydrogel properties and the embedded organisms. Stimuli-responsive hydrogels which respond to solvent composition, pH, temperature, electric fields, or light have been developed.[28][29] **Figure 4** highlights the use of combination of engineered living microbial cells with hydrogels for fabrication of ELMs of diverse and bio-programmable capabilities.

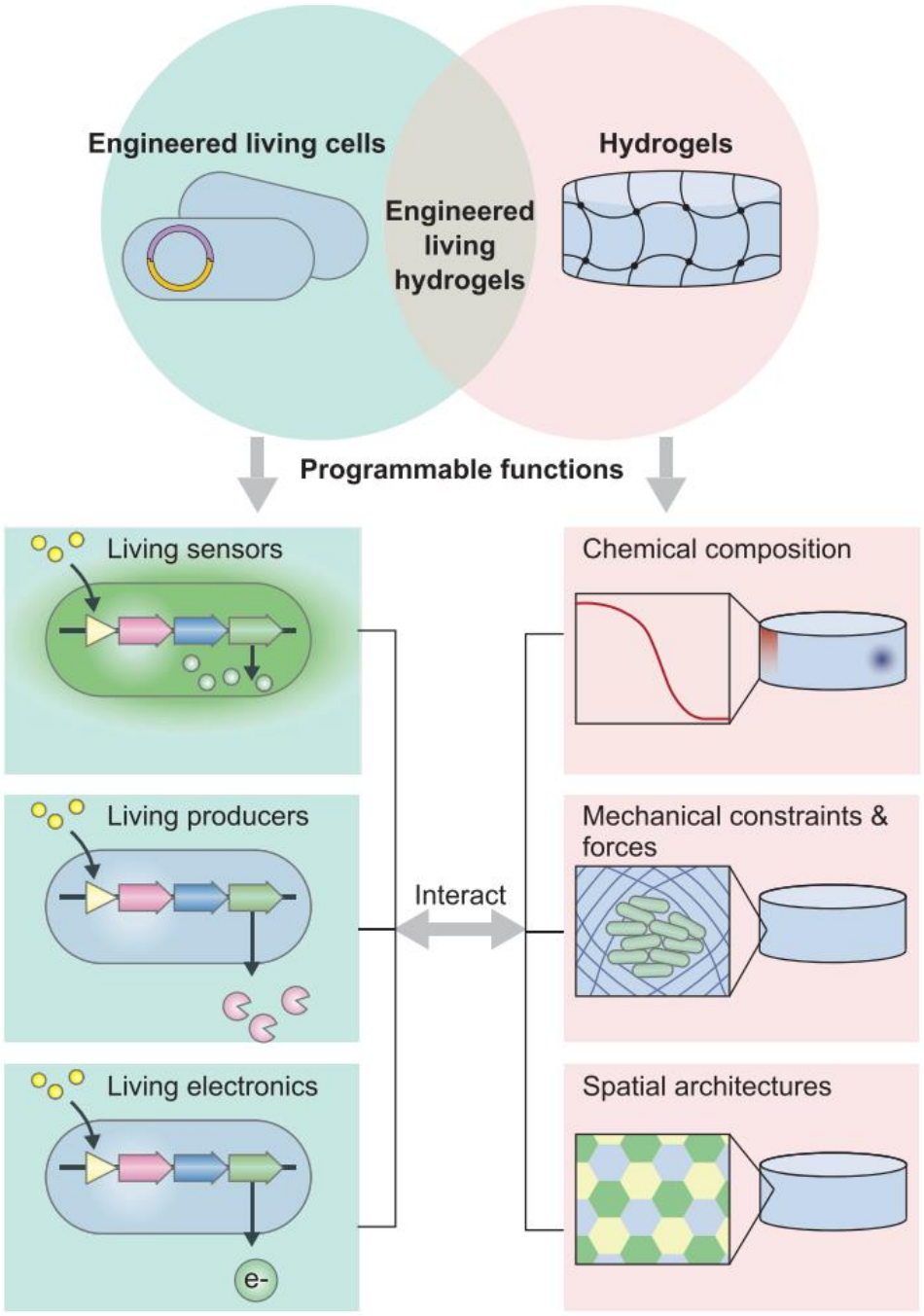

Figure 4: The tunability of hydrogels and programmed organisms allows for augmenting the functionality of ELMs due to the manipulation of chemical gradients, mechanical constraints and forces and the spatial distribution of the living components within. Reprinted (adapted) with permission from ref[20]. Copyright © 2022 Wiley-VCH GmbH.

Different hydrogels have been used for encapsulation of microorganisms. Reported examples include natural polymers such as agarose[30][31], alginate[29][32][33], chitosan[33], gellan gum[29], gelatin[29], xanthan gum[29] or dextran[34], or hydrogels from synthetic polymers such as

polyvinyl alcohol[32] or polyoxamers[17][4][35] which have been used to entrap bacteria.[29][36] For example, alginate beads containing genetically engineered bioluminescent bacteria were developed as sensors to detect water toxicity.[37] Extruding the sodium alginate solution through a needle and generating electrostatic potential between the needle and collector, 900-1000 µm beads were synthesized upon dropping in calcium chloride ($CaCl_2$) solution. These beads encapsulating bioluminescent bacteria and fluorescent microspheres were optically relevant for bioluminescent and fluorescent readouts and could be synthesized in submillimeter range to be used as portable sensors.[37] Agar[1][38][39], agarose[16][40], pluronic F127[4][35] etc. are thermosensitive hydrogels and have distinct working temperatures, making it one of the important aspects for their use as ELM matrices.[1] The thermosensitivity dictates the microbial encapsulation methodologies to enable a viable living population and the working temperature of the final ELM device. Combination of different polymers to synergize the qualities of the individual components has also been used as a strategy to fabricate matrices for ELMs. For example, Schaffner et al. encapsulated bacteria in biocompatible hyaluronic acid, k-carrageenan, and fumed silica for bioremediation and biomedical applications.[41] Variations in elastic and viscous behaviors of these individual components led to an optimal shear thinning ink ideal for fabrication of complex designs using 3D printing allowing a spatial control over the bacterial population growing within. Moreover, hyaluronic acid and k-carrageenan enabled good water retention favorable for a viable population. Heveran et al. incorporated a photosynthetic cyanobacterium *Synechococcus sp.* within a sand-hydrogel (gelatin) hybrid to induce biomineralization for living building materials.[42] Gelatin was the material of choice due to its ability to melt at 37 °C and increase of strength upon dehydration through physical crosslinks.[42] It also bridged sand particles providing a substrate for microbially induced mineralization of calcium carbonate ($CaCO_3$), which further toughened the hydrogel matrix.[42]

The selection of an appropriate encapsulating matrix for an ELM device is crucial. The composition and design can significantly impact the properties of the matrix and the behavior of encapsulated microorganisms. Next, we discuss the most important properties to consider when selecting a matrix for an ELM.

2.2.1.1 Porosity, swelling and diffusion

The porosity of the matrix and the spatial architecture impacts the ability of solutes to diffuse through it. Permeability to nutrients, gases like oxygen and waste products is essential to ensure survival of the embedded microorganisms.[1][21] The monomer and crosslinker concentration and the type of interactions (hydrogen bonding, electrostatic, hydrophobic interactions)[29] between the polymeric chains influence the mesh size of the network and thereby the swelling and the size-dependent permeability properties of solutes through the hydrogel.[20] Swelling is a process by which hydrogel increases in volume upon absorption of water without dissolving.[43] The extent of swelling depends on the pore size of the hydrogel.[44] Molecules like oxygen (~0.1 nm), glucose, lactose, acetate, and ammonium, which are essential for the microbes are in the range of 0.1-1 nm (**Figure 5a**).[20] The hydrodynamic diameters of biopolymers like proteins are comparable to the hydrogel mesh size[20][45], thus making it an important aspect to account for when designing ELMs for delivering protein cargo outside of the hydrogels. Diffusion of small molecules can be hindered if they interact with the polymeric chains of the network (**Figure 5b**).[20] Hence the structure and chemical backbone of the matrix material can affect the transport and molecular diffusion of different molecules. The size and shape of the molecules and the matrix morphology determine the diffusion rate of those molecules.[46] A slow or gradient distribution of the small molecules or nutrients within the hydrogel matrix can lead to heterogeneity of cell growth, viability and metabolic activity of the ELM (**Figure 5c, 5d**).[20]

Microbial cells (bacteria: ~ 0.5-5 µm in length, fungi filaments: ~ 5-10 µm in width, virus diameter: ~ 20-500 nm)[47] can move within the matrix if the pore size is bigger than the cell dimensions. Therefore, in order to hinder migration or outgrowth of the cells from the hydrogel matrix, the pore size should be smaller than the size of the embedded microorganisms. Networks with gradients in the pore size are used for biocontainment in PVA/PEG based Lentikats® (**Figure 5e**). These are lens-shaped structures with a pore gradient in the radial direction. They have microscale pores where bacteria are entrapped and nanoscale pores at the surface which prevent bacterial escape.[48][49] The tuning of the hydrogel porosity can also be used to avoid diffusion of larger molecules, like DNA and proteins.[14] For example, Tang et al. encapsulated *E. coli* within 2.5 wt. % of alginate coated with nanoporous (5-50 nm) alginate/polyacrylamide hydrogel shell. The coating prevented bacterial escape for 72 h and also the diffusion of large biopolymers.[14] Macroporous

networks have also been used to entrap bacteria in polyvinyl alcohol (PVA) using cryogenic process (**Figure 5f**). In the presence of glucose as a cryoprotectant, bacteria entrapped in 2 wt. % calcium-alginate beads were dispersed in an 8 wt. % PVA matrix formed using unidirectional freezing and freeze-drying process.[32] Subsequent calcium chelation using culture medium containing sodium citrate allowed for dissolution of the alginate beads and formation of cavities supporting bacterial proliferation for 24 h.[32]

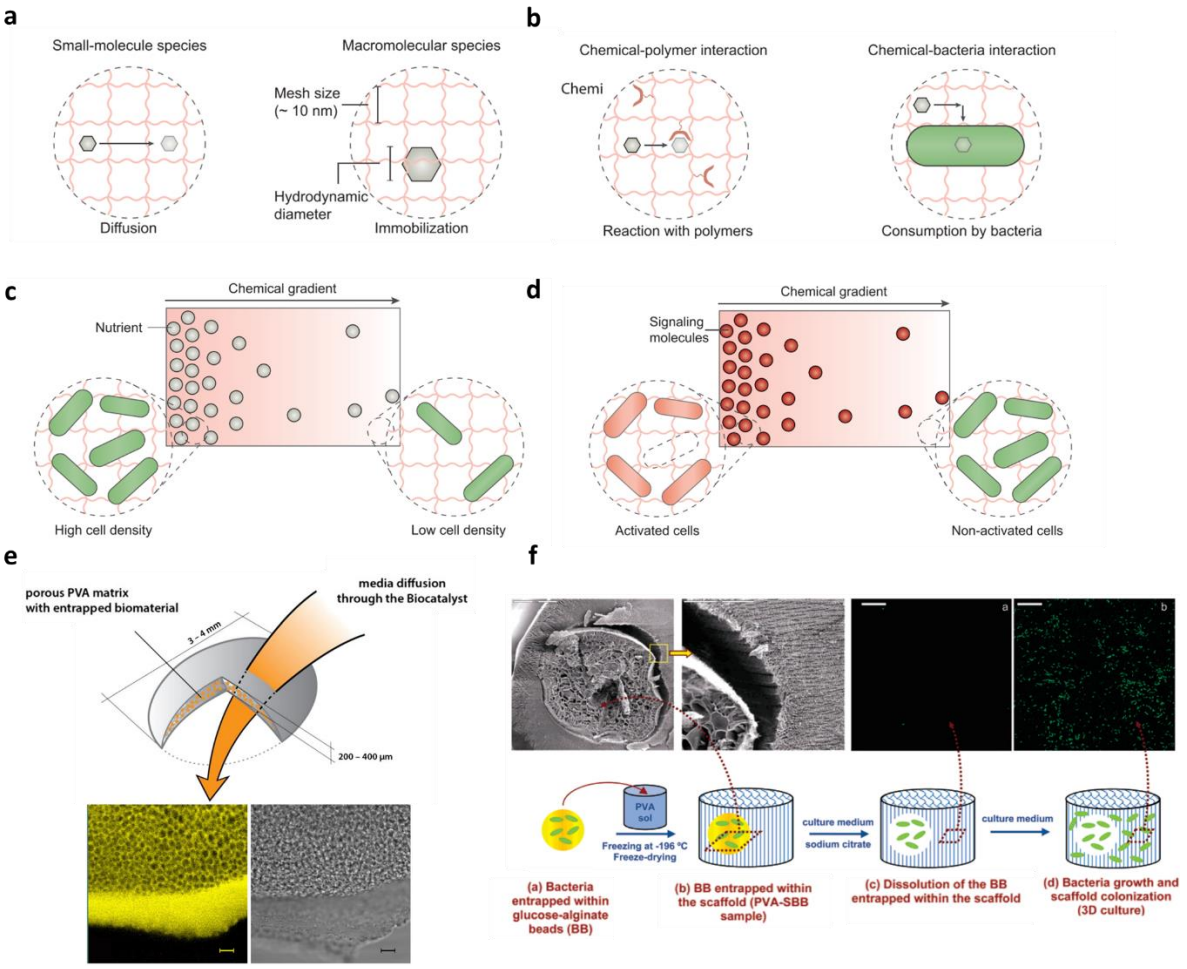

Figure 5: The porosity of the hydrogel matrix controls the diffusion of molecules through it. **a)** Molecules smaller than the mesh size can diffuse through the swollen polymer network whereas bigger aggregates are immobilized; **b)** Depending on the type of chemical species, the polymer network may interact with them, thus hindering diffusion; **c,d)** Gradients and heterogenous distribution of nutrients or signaling molecules lead to variable **c)** cell growth and **d)** cell phenotype;[20] Reprinted (adapted) with permission from ref[20]. Copyright © 2022 Wiley-VCH GmbH. **e)** Schematic representation of Lentikats® with the microporous inner structure and nanoporous outer shell (scale bar = 10 µm)[48][49]; Reprinted after permission from ref[48]. Copyright © 2014, Springer Nature. Reprinted after permission from ref[49].

Copyright © 2015, Springer Nature. **f)** Schematic representation of the PVA scaffolds with bacteria entrapped in alginate beads whose dissolution gives well defined macroporous structures suitable for bacterial proliferation (scale bar = 20 µm). Reprinted (adapted) with permission from ref[32]. Copyright © 2007, American Chemical Society.

2.2.1.2 Crosslinking and gelation mechanisms

The gelation mechanism of the hydrogel plays an essential role in the fabrication, storage and eventually, the viability and behavior of the encapsulated microbial cells.[50] Gelation can occur by physical or chemical crosslinking (**Figure 6**).[29][51] Physically crosslinked hydrogels are networks formed by molecular entanglements (eg. host-guest complexes like cyclodextrins[52]), ionic (eg. calcium alginate hydrogels[53]), hydrogen bonding or hydrophobic interactions (eg. coiled-coil peptides like leucine zipper domains[54]) which are reversible in nature.[55] On the other hand, chemically crosslinked hydrogels like polyacrylamide (PAAM), polyethylene glycol diacrylate (PEGDA) etc., are characterized by the presence of permanent, covalent bonds.[55] Hence, chemically crosslinked hydrogels are more stable compared to physically crosslinked networks. An intermediate case between physical and chemical crosslinks are dynamic crosslinks formed by covalent bonds that can be broken and formed reversibly. Dynamic crosslinks (eg. reversible hydrazone bond) confer hydrogels properties like shear thinning and self-healing.[55][56] The bond kinetics at the microscale influences the mechanical properties of the material at the macro scale and also influences the behavior of the encapsulated cells.[55]

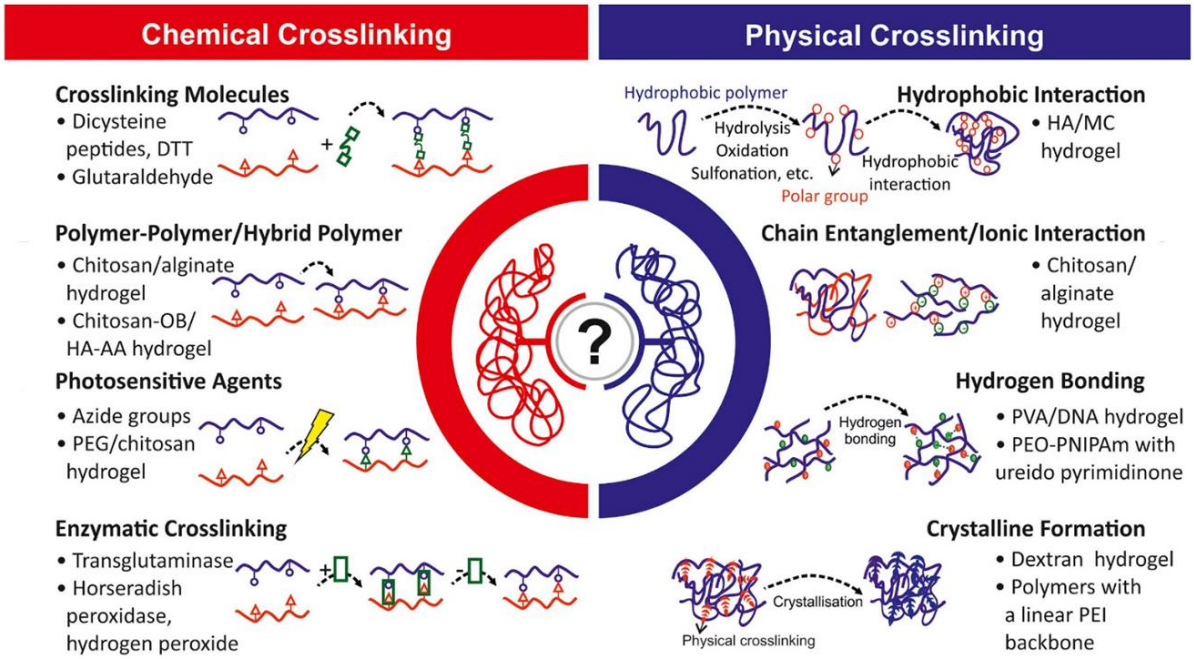

Figure 6: Examples of chemical and physical crosslinking systems that can be used in the production of hydrogels.[57]

Examples of covalently crosslinked hydrogels are polyacrylamide (PAAM) networks which were used to encapsulate *E. coli* for drug delivery applications.[16] PAAM hydrogels did not support active bacterial population long term, but they supported growth of yeast *Saccharomyces cerevisiae,* which was used to induce shape changes in the ELM.[12] Ionically crosslinked (Ca^{2+}) crosslinked alginate hydrogels have been used as physically crosslinked hydrogels in ELMs.[36] The gelation rate can be controlled by using buffer solutions containing phosphate which retards the gelation and widens the working time for the alginate gels.[53] Agarose, another common hydrogel used in ELMs, is a thermoreversible, physical hydrogel and the gelation temperature depends on its molecular weight.[58] Hydrogels with two or more crosslinking mechanisms have also been developed[55] and used for ELM applications. For example, Pluronic physical hydrogels with additional chemically crosslinkable end-chain functional groups are thermoreversible hydrogels with the possibility of dual crosslinking mechanism.[35][59] Interpenetrated networks formed by covalently crosslinked PAAM and physically crosslinked alginate hydrogel hybrids have also been explored for ELM fabrication.[60]

2.2.1.3 Mechanical properties

The mechanical properties of the hydrogel matrix influence the growth patterns and behavior of the encapsulated cells.[20][61] The stiffness of the matrix influences the bacterial behavior within the matrix.[62][63] As the encapsulated cells grow, they stretch the polymer network which can result in the buildup of a compressive stress on the cells (**Figure 7a and 7b**).[20] Hydrogel matrices that are physically crosslinked exhibit viscoelasticity in many cases, that is, they can dissipate mechanical energy like viscous liquids and they show elastic recovery like elastic solids.[64][65] The crosslinks within the physically crosslinked networks can unbind, reorganize upon application of external stress or strain and rebind again upon its cessation, leading to their viscoelastic behavior.[61] The reorganization of the network can dissipate the applied cell forces. By tuning the concentration of physical and covalent crosslinks, viscoelasticity within hydrogel matrices can be modulated.[61][66] PVA hydrogels crosslinked by physical and covalent bonds, showed differences in their mechanical behavior.[67] Bacterial biofilms are viscoelastic in nature and have been studied extensively to study the effect on the behavior of cells under confinement.[68][69] Viscoelastic parameters like creep compliance and stress relaxation of the surrounding matrices influence the cells growing within, as has been seen in case of naturally occurring biofilms (**Figure 7c and 7d**).[70]

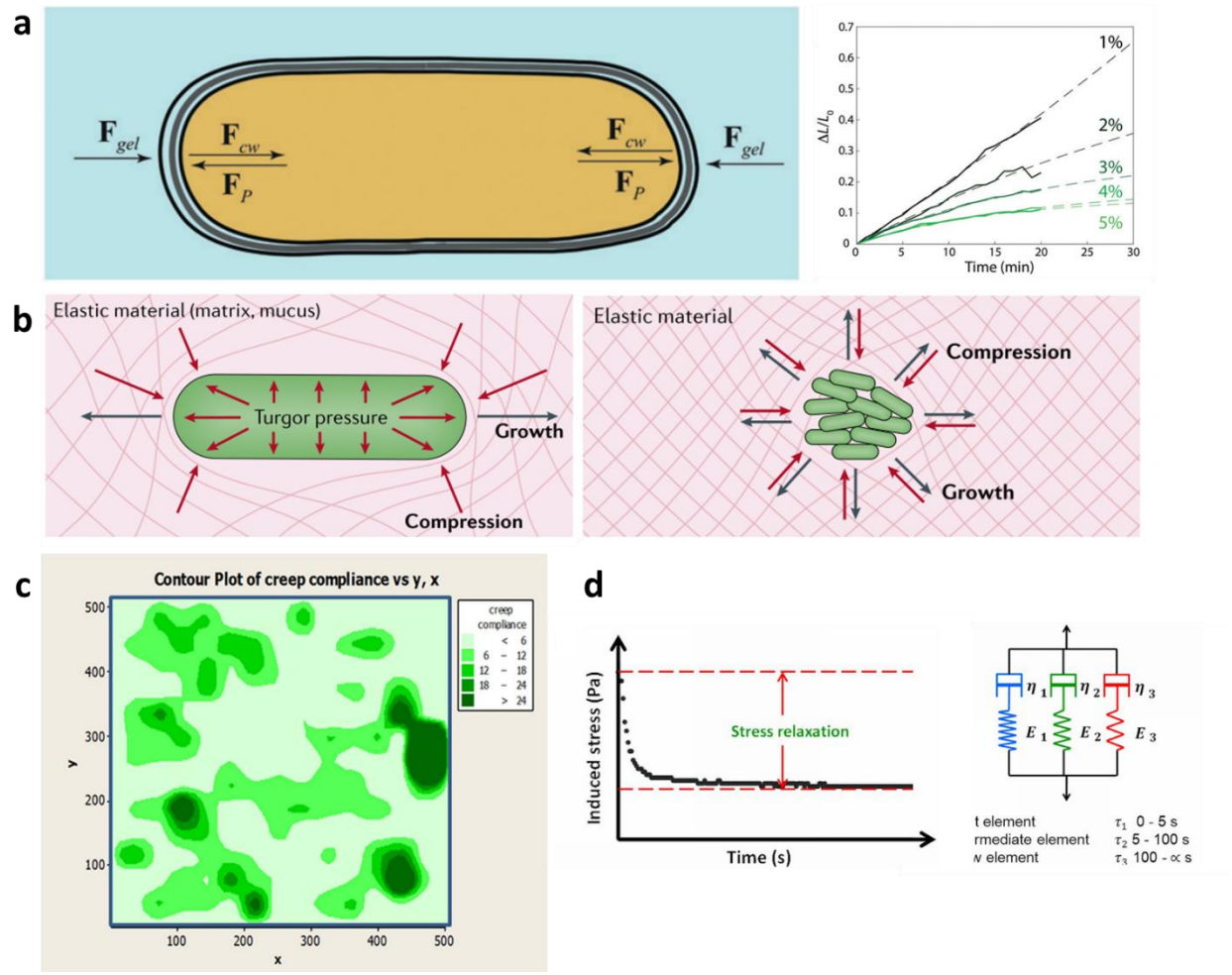

Figure 7: The mechanical forces in hydrogels impact the cellular growth. **a)** Bacterial growth within agarose hydrogel (at different concentrations) is shown to depend upon the cell wall stiffness, turgor pressure within the cell and the compressive forces of the surrounding gel[63]; Reprinted (adapted) with permission from ref[20]. Copyright © 2012, John Wiley and Sons. **b)** Schematic showing the growth of the encapsulated microorganisms can be limited at individual as well as population level. The size of the microbial colony saturates when it cannot push the surrounding polymeric network anymore. Reprinted after permission from ref[62]. Copyright © 2015, Springer Nature. **c)** XY mapping of creep compliance (Pa^{-1}) of *Pseudomonas fluorescens* biofilm using fluorescent bead-tracking highlighting the viscoelastic nature of biofilms which affect their behavior[68] and **d)** Stress relaxation profile (left) of a compressed dental biofilm and a three element Maxwell model (right) used to identify the relaxation time constants (τ).[69]

2.2.1.4 Stability and degradation rate

The stability of the matrix determines the functional lifetime of the ELM. Hydrogel networks can undergo hydrolytic or enzymatic degradation depending on their composition. Controlled degradation could help in sustained and controlled delivery of bacteria for treating gastrointestinal diseases.[71] *E. coli* containing alginate gels were coated with polydopamine, chitosan and poly-L-lysine polymer shells for longer term stability but could only reduce but not eliminate the leakage of bacteria.[72] The encapsulated microbes could also trigger chemical degradation of hydrogel matrices.[20] Bacterial cellulose based hydrogels have been shown to degrade in presence of cellobiohydrolases which could tune the mechanical properties of the ELMs.[26] As an alternate strategy, hydrogels were used along with elastomers for maintaining their mechanical and structural integrity.[20] PEG-PVA based biosensors where poly(ethyleneterephthalate) (PET) carrier material was used as a substrate for adding support and stability.[73]

2.2.1.5 Barrier properties: Protection from other microbes, isolation from immune system

Encapsulation or organisms within stable hydrogel matrices can prevent leaking of the organism to the environment. Encapsulation also prevents the microorganisms from external insults[15] and keeps organisms isolated from the immune system in case of therapeutic applications.[74] Probiotics, microorganisms which are known to be beneficial for gut health, are protected against low pH and bile present in the gastrointestinal tract due to encapsulation in polymeric matrices.[1][75] Such polymer encapsulations increase the shelf life of the probiotics.[1]

2.2.2 Encapsulated microorganisms

2.2.2.1 Bacteria

Bacteria, especially *E. coli*, are the workhorses for synthetic biology and the most used organisms in ELM demonstrations.[7][2] *E. coli* are robust, adaptable to many genetic modules and strains and have a protein overexpression capability.[40] Many probiotic bacteria from the genera of *Lactobacillus*, *Faecalibacterium*, *Roseburia* etc. are explored for clinical applications.[76] A summary of the growing reliance on the bacteria-based delivery systems[77] and the emerging trends and advances in diagnosis and therapy is shown in **Figure 8**.[71] Bacterial sensing systems, typically using natural or synthetically constructed pathways to

sense their surroundings, are able to detect molecules that are related to health, disease, environmental pollution or physiological stimuli like temperature.[78]

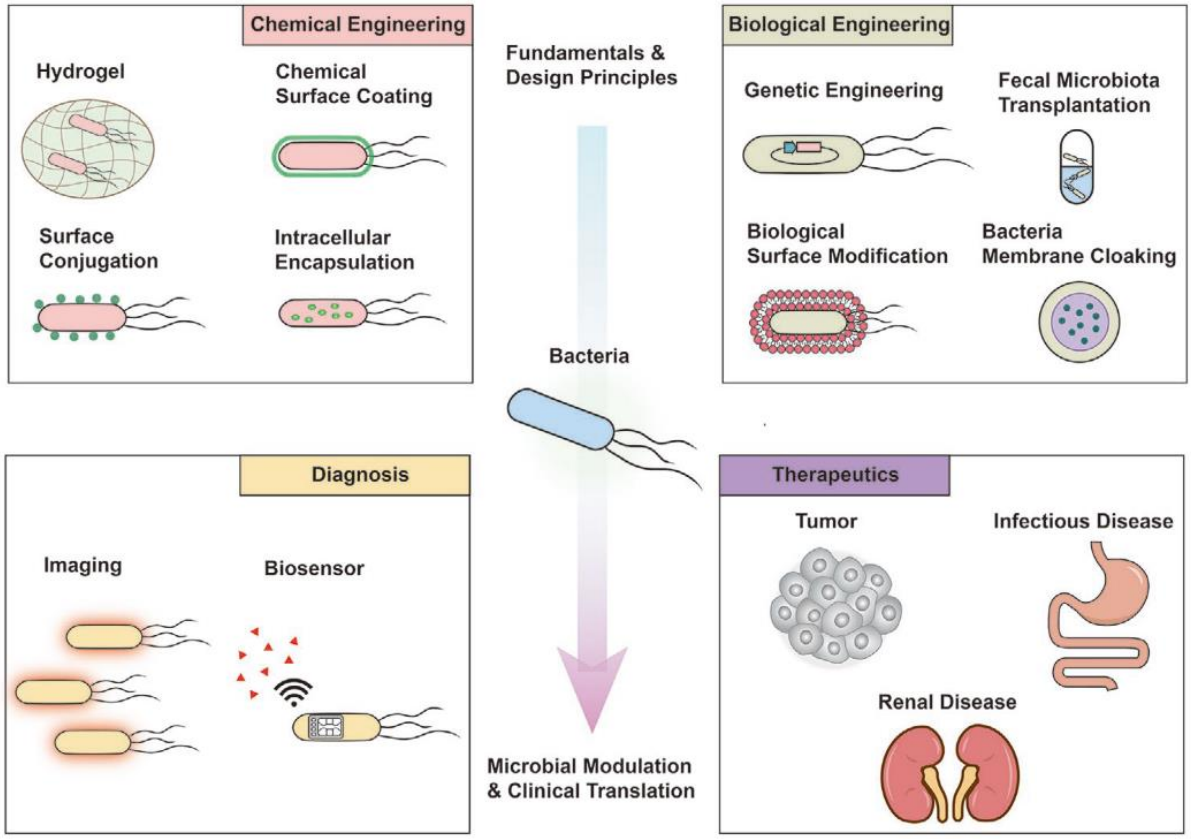

Figure 8: Chemical and biological engineering approaches have been demonstrated to use bacteria for diagnosis and therapeutic applications. Some of these approaches are in clinical translation. Reprinted (adapted) with permission from ref [71]. Copyright © 2021 WILEY-VCH Verlag GmbH & Co. KGaA, Weinheim.

Challenges of engineered bacteria for applications in ELMs are : (i) the stability during processing, (ii) their genetic stability over long time-scales, (iii) their scaled-up manufacturing, and (iv) their biocontainment.[71] The hydrogel properties influence the viability and functionality of the embedded bacteria. Most applications require ample access to nutrients for continuous functioning. Endospores which can survive extreme conditions like high temperature, acid and alkaline solutions, high pressures, can be employed for ELM fabrication.[79] Access to oxygen is essential for the growth of the embedded bacteria. Bacteria can be aerobes, anaerobes, or even facultative anaerobes, which can thus determine their performance and utilization in an ELM based on the material, design and fabrication techniques employed.[80]

Gram-positive bacteria like *Bacillus subtilis* as antifungal agents[5], *Micrococcus luteus* for gold sequestration[13], *Lactobacillus rhamnosus* for generation of structural and cellular materials[81], probiotic *Lactobacillus rhamnosus*[75] etc. while gram-negative bacteria like *Komagataeibacter rhaeticus* for cellulose-production[26], *E. coli* strain Nissle 1917 for secretion of curli nanofibers for surface adhesion in mucosal healing[24], *Caulobacter crescentus* for autonomous formation of synthetic protein matrix[18] have been programmed and used in ELMs.

2.2.2.2 Yeast and fungi

The yeast strain *Saccharomyces cerevisiae* has been used in different ELM applications. Encapsulated in alginate matrix, *Saccharomyces cerevisiae* has been shown to produce ethanol at 1.8 times higher rate.[36] Saha et al. used *Saccharomyces cerevisiae* yeast laden Pluronic hydrogel to print 3D scaffolds for continuous ethanol fermentation.[4] A symbiotic co-culture of genetically modified yeast *Saccharomyces cerevisiae* and bacteria *Komagataeibacter rhaeticus* was used by Gilbert et al. for production of bacterial cellulose-based materials for biosensing and biocatalysis applications.[26] Release of antibiotics and killing of gram-positive bacteria for days was demonstrated by Gerber et al. *in vitro* by encapsulation of penicillin producing fungi *Penicillium chrysogenum* in agar matrices.[38] In the field of construction materials, mycelium has been used to fabricate environmental friendly packaging and building materials.[2]

2.3 Processing methods for the fabrication of ELMs

The processability of the matrix at conditions compatible with living organisms is an important consideration in the design of an ELM. If a temperature-based processing technology is used, the living cells should survive the processing temperature. If a freeze- or freeze-drying process is used to fabricate the ELM, for example in poly(vinyl alcohol) based matrices, the use of cryoprotectants is necessary.[32] In case of UV crosslinkable hydrogel systems, the exposure dose should not alter the genetic content of the living component. If processing involves shear forces, like in extrusion-based processing technologies, the cells should be able to survive the shear forces generated. Thus, the combination of matrix, microbes and fabrication technique are important factors to considered in the development of a functional ELM.

The type of embedding matrix along with the fabrication method can impact on the viability of the encapsulated living organisms. Various encapsulation techniques have been used to fabricate functional ELMs[2], including 3D printing[35], electrospinning[82][83] or microfluidics[84] to name a few.

2.3.1 3D printing

3D printing, also termed as additive manufacturing, involves layer by layer deposition of materials into customized and complex 3D structures with a high degree of control over the architecture.[85] Different 3D printing techniques based on extrusion, stereolithography, powder bed fusion, selective laser sintering etc. exist which differ in their material requirements, costs, and resolution of the printed structures.[85] 3D printing of biologically relevant hydrogels, embedded with cells or bioactive cues, is termed as bioprinting while the biomimetic cell laden ink is known as a bioink.[59][86] Bioprinting enables mimicking complex structures found in nature and allows for precise positioning of the cell-loaded living bioinks in designs relevant for the applications. Mainly extrusion-based techniques, where a bioink is extruded through a nozzle using a mechanical piston, pneumatic or microfluidic based system[87], have been explored for ELMs. It allows organization of one or multiple types of cells within a supporting matrix or scaffolds with resolution of millimeter to micrometer scale.[17][79] The control over the architecture and design can be used to aid the compartmentalization of co-cultures systems[88] and distribution of other chemicals, influencing the diffusion properties within the scaffold and making the living material customizable and consistent.[17][4] Such control can help in developing biofilm mimics or even fabricate functional devices of desired shapes and sizes. **Figure 9** highlights some of the examples of 3D printed ELMs fabricated in

the recent past. Liu et al. showed the possibility of multi-material printing using pluronic-based bioinks with resolution of nearly 30 µm for their use in wearable devices (**Figure 9a**).[17] Balasubramanian et al. made use of calcium-alginate-based hydrogel system to bioprint microalgae onto agar and bacterial cellulose substrates (**Figure 9b**).[9] They were able to attain millimeter-scale resolution and showed potential for up-scaling (70 × 20 cm^2) it to produce photosynthetic bio-garments.[9] González et al. printed *Bacillus subtilis* spores encapsulated in agarose gels of 6 × 6 × 25 mm^3 blocks using extrusion based printing (**Figure 9c)**.[31] Sub-millimeter 3D printed structures with immobilized bacteria were obtained by tuning the rheological properties of a bioink called 'Flink' consisting of non-toxic biopolymers hyaluronic acid, κ-carrageenan together with fumed silica (**Figure 9d**).[41] Connell et al. used laser-writing approach based on multiphoton lithography to fabricate chambers of micrometer range to study interactions of different bacterial species (**Figure 9e**).[50]

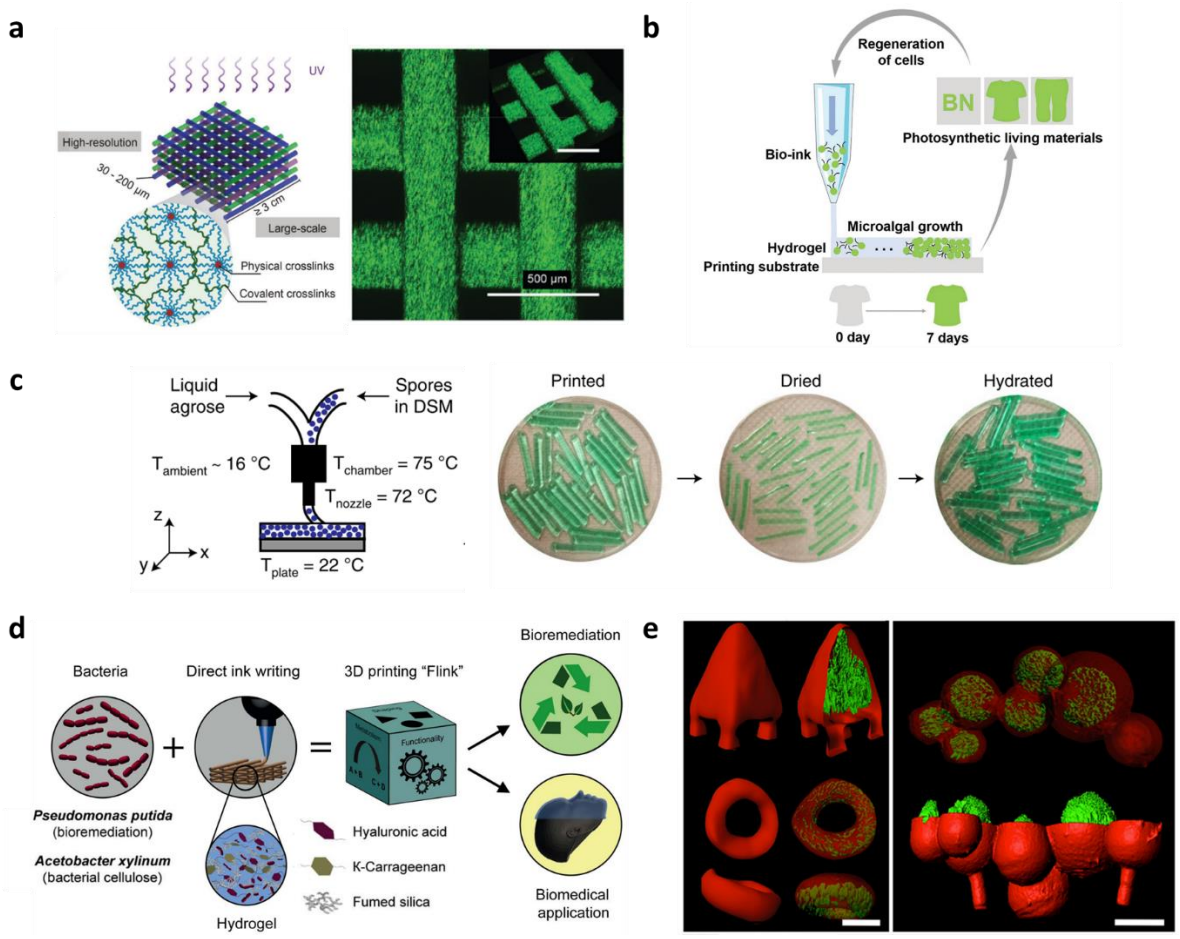

Figure 9: a) 3D printing of multi-ink and high resolution UV crosslinkable pluronic diacrylate and *E. coli* based constructs (scale bar = 500 µm). Reprinted (adapted) with permission from ref. [17] Copyright © 2017 WILEY-VCH Verlag GmbH & Co. KGaA, Weinheim. **b)** Bioprinting of

photosnthetic biogarments using sodium alginate and microalgae based bioink[9]; **c)** Agarose and *B. subtillis* spores (blue dots) based bioink printed using a printhead with controlled nozzle and plate temperatures used to print millimeter scale rods which could be dried and rehydrated without loss of shape or function. Reprinted after permission from ref[31]. Copyright © 2019, Springer Nature; **d)** Bioprinting of Flink - a hyaluronic acid, κ-carrageenan and fumed silica based bioink with bacteria specific for bioremediation or biomedical applications[41] and **e)** Gelatin based micro 3D printing isolating colonies of Pseudomonas aerunginosa in pyramid, torus and spheroid shaped chambers (scale bar = 20 μm)[50].

2.3.2 Microfluidic encapsulation

Microfluidic extrusion-based droplet generation devices can give microbeads of defined sizes and geometries with a controlled number of cells encapsulated within.[1] The compartmentalization of cells in the small microbeads allows faster diffusion of nutrients and metabolites compared to cells encapsulated in bulk hydrogels[89] *Gluconacetobacter xylinus*, a gram-negative, rod-shaped and non-pathogenic bacterium which secretes cellulose, was encapsulated within sacrificial alginate-agarose core-shell microspheres to form hollow bacterial cellulose microspheres as porous scaffolds for wound healing applications.[84] The micromorphology was controlled using droplet-based microfluidics technique with diameters ranging from 20 to 50 μm.[84] Zhao et al. encapsulated probiotic *Lactobacillus* and *Bacillus subtilis* into separate compartments within alginate microbeads using microfluidics.[90] One strain was encapsulated within microspheres with diameter ranging from 60 to 170 μm which served as cores for a second microencapsulation process using a coaxial capillary microfluidic chip integrated in an electrospray setup. These dual-core microbeads helped in correcting the gut disorders in mice and were explored for treating metabolic-related disorders.[90]

2.3.3 Electrospinning

Polymer fibres fabricated using electrospinning can be used to encapsulate microbes.[91] The fibers are typically in the sub-micrometer scale. The porosity of the electrospun scaffold can be tuned by varying the concentration of the polymer solution and the electrispinning parameters. The fibrous structures lead to high surface to volume ratio enabling efficient transport of molecules in and out of the encapsulation matrix for maintaining a functional and viable population.[83] Environmental and food biotechnology has widely made use of non-toxic and biocompatible polymers for the encapsulation of probiotic bacteria.[91] Lactobacillus plantarum 423, a probiotic bacteria strain, was encapsulated within polyethylene oxide

nanofibers.[92] Letnik et al. coaxially electrospun embedded yeast *Candida tropicalis* in the core of polyvinylpyrrolidone and a biodegradable shell of poly vinylidene fluoride-co-hexafluoropropylene and polyethylene glycol with average diameter of 10 µm and pore size of 40 nm.[93] Eroglu et al. immobilized microalgal cells within chitosan nanofibers mats with the fiber diameter ranging from 50-180 nm.[94] The swelling of the chitosan matrix increased the porosity of the mats and supported the *Chlorella vulgaris* cells (diameter of 3-4 µm), facilitating efficient diffusion of nutrients and waste products.[94]

2.3.4 Core-shell designs for preventing leakage

One of the major challenges for the reliable and safe function of an ELM device is the avoidance of escape of the living microorganisms out of the encapsulation matrix.[14][15] Uncontrolled leaking of the microbes may hamper the function of the device, especially in case of therapeutic ELM devices and sensing applications which may lead to incorrect inferences. Also, ELM devices may contain genetically engineered cells, hence, it is important to acknowledge and prevent the environmental risk associated with their interaction and release into the environment or in the body.[1] Fabrication of core-shell constructs has been realized as a biocontainment strategy for ELMs. Strategies involving use of coaxially electrospun polycaprolactone (PCL) and polyethylene glycol (PEG) shell with a polyethylene oxide (PEO) core to encapsulate *Pseudomonas ADP, E. coli*, and *Pseudomonas putida* for bioremediation applications was demonstrated by Klein et al.[91] The bacteria grew within a tubular space of an average diameter of 3.5 µm inside a non-degradable shell.[95] Tang et al. prevented the inadvertent escape of environmental sensing bacteria using an alginate core and a multilayered wrapping of polyacrylamide hard shell.[14] The shell is tough and resistant to fracture while it allows permeation to small molecules.[14] This core-shell construct enabled zero escape of the bacteria for over 72 h under rigorous shaking conditions at 37 °C.[14]

2.4 Biotechnological and biomedical applications of ELM

2.4.1 Whole-cell biosensors

Whole-cell biosensors use living cells for detection, amplification and response to external stimuli.[39][96] The output signal can be production or change of color, fluorescence, luminescence, or electrical current that can be measured.[73][97] Such sensors are interesting for fields such as biotechnology production, pharmacology, toxicology or environmental monitoring.[7][96][97][98] Many systems are useful for detecting important metabolites for mammalian cell culture such as sugars, amino acids, and metabolic waste products.[99] Whole-cell biosensors can be made not only from microorganisms like bacteria and fungi but also from plant and mammalian cells.[99] With the advent of synthetic biology techniques, it has become possible to engineer reliable sensors sensing specific compounds of interest ranging from heavy metals to biomolecules.[99] Thus, incorporating the genetically modified whole-cells into biocompatible scaffolding materials, hybrid living whole-cell biosensors can be built. One of the key advantages of the whole-cell biosensors is their exceptional sensitivity, allowing detection of compounds at extremely low concentrations (micromolar or nanomolar range).[99] Their self-renewing properties and ability to eliminate the need for enzyme purification lowers the cost.[99] Compared to traditional cell-free sensing techniques, the manipulation of whole-cell biosensors is rather easy and does not require specialized equipment or personnel.[7] Continuous monitoring or on-site signal readout are some of the advantages of using whole-cell biosensors.

Fesenko et al. developed a polyacrylamide-based hydrogel microchip encapsulating *E. coli* cells for detection of arsenite using a bioluminescent reporter.[100] However, the technique was limited to only a certain number of strains due to the potential toxicity of polyacrylamide monomers.[100] Schulz-Schönhagen et al. demonstrated the sensing capabilities of a PVA based biosensor platform encapsulating *Bacillus subtilis* spores to quantify isopropyl-β-d-thiogalactopyranoside (IPTG) (**Figure 10a**).[73] The quantification was possible using a smartphone-based device for up to a month after storage. Moya-Ramírez et al. encapsulated a lactate sensing *E. coli* strain within alginate gels coated with polydopamine, chitosan and poly-L-lysine polymer shells (**Figure 10b**).[72] Named as LAMPS, these whole-cell biosensors were evaluated for potential use in small bioreactors and other biomanufacturing processes. The LAMPS could be cryo-preserved for up to 10 days but the coatings showed susceptibility to failure when used in different culture mediums.[72] Liu et al. reported the use of stretchable

hydrogel-elastomer hybrid biosensors encapsulating *E. coli* cells which could produce green fluorescence protein (GFP) to detect multiple small molecules like diacetylphloroglucinol (DAPG), N-acyl homoserine lactone (AHL), IPTG, rhamnose, and anhydrotetracycline (aTc).[60] They showed the possibility of integrating these biosensors with interactive genetic circuits onto a glove fingertip (**Figure 10c**)[60] or as a living patch on the skin (**Figure 10d**)[17]. Gilbert et al. came up with a strategy to use a symbiotic culture of *Komagataeibacter rhaeticus* bacteria and *Saccharomyces cerevisiae* yeast to fabricate a living biosensor called synthetic SCOBY.[26] The yeast strain acted as the biosensor generating a strong GFP signal when exposed to β-oestradiol, an environmental pollutant, while the bacteria strain produced supporting matrix made up of bacterial cellulose (**Figure 10e**). Atkinson et al. demonstrated the use of genetically modified *E. coli* to produce electric current in response to thiosulfate as the inducer.[97] They used alginate embedded bacteria and wrapped it around with an agarose layer whose thickness varied from 1-2 mm (**Figure 10f**).

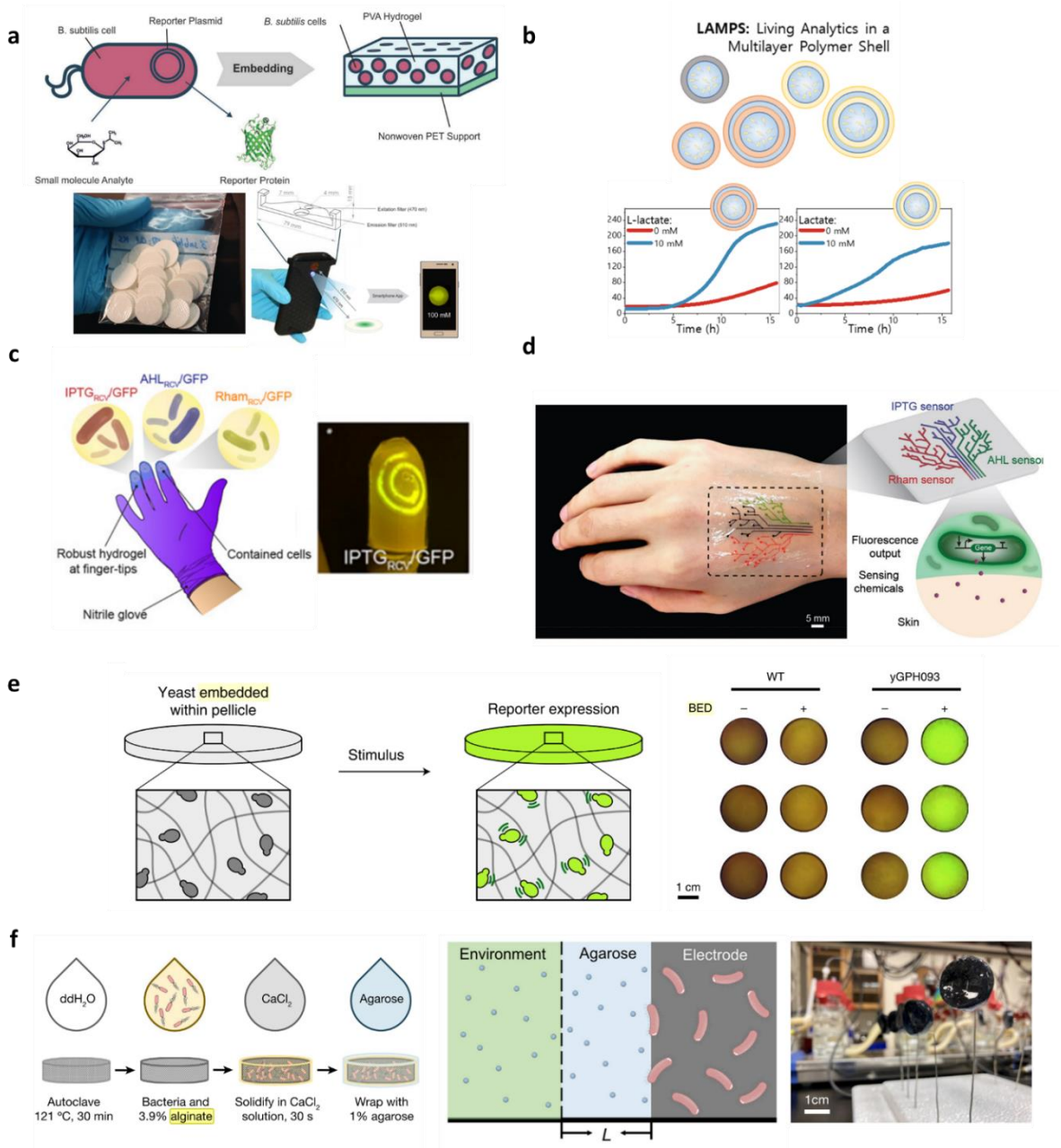

Figure 10: Examples of whole-cell biosensors. **a)** Genetically modified Bacillus subtilis embedded biosensor construct detecting IPTG using a smartphone-based facile method. Reprinted (adapted) with permission from ref[73]. Copyright © 2019 WILEY-VCH Verlag GmbH & Co. KGaA, Weinheim; **b)** LAMPS biosensor composed of alginate core with bacteria and chitosan or poly-L-lysine shells to detect lactate in the surrounding medium[72]; **c)** Schematic of a living wearable glove chemical detectors at the fingertips; **d)** Design of the living tattoo biosensor able to detect IPTG, rham or AHL. Reprinted (adapted) with permission from ref. [17] Copyright © 2017 WILEY-VCH Verlag GmbH & Co. KGaA, Weinheim; **e)** Bacterial cellulose producing bacteria co-cultured with yeast strain which is able to detect environmental pollutants like β-oestradiol (BED). Reprinted after permission from ref[26] Copyright © 2021,

Springer Nature Limited and f) Bioelectronic sensing using genetically modified *E. coli* strain embedded in alginate gels with an encapsulation layer of agarose. The thickness of agarose of nearly 1-2 mm dictated the diffusion of small molecules from the environment across to the bacteria. Reprinted after permission from ref.[97] Copyright © 2022, Springer Nature Limited.

As the detection sensitivity and operational range of the sensor are determined mainly by the cells used, the usage of the whole-cell biosensors is limited by the life of the living cells within.[96] They might require an expensive cold chain to maintain a viable cell population, lack of which limits the shelf-life of the biosensor.[73] While long-term use can be challenging, even the speed of sensing can be affected by factors such as the rate of protein expression, the detection methods used, and the efficiency of transport of molecules through the encapsulating layers.[97] Signal transmission can also be attenuated due to the thickness of the encapsulation matrix. Variability in the agarose matrix with thickness of 1-2 mm affected the diffusional timescales and impacted the response times of alginate embedded *E. coli* bioelectric sensors.[97] Moreover, potential inadvertent release of engineered microbes has been forewarned about and efforts for efficient biocontainment strategies are necessary to meet regulatory requirements.[101] This is even more critical for their use for clinical applications to prevent unintended side effects like horizontal gene transfers into native host microbiota. Strategies for developing bacterial sensors which are found in the human gut, like *Bacteroides* or *Lactobacillus*, need to be developed which will mitigate the risks involved.[101] The sensitivity and range of whole-cell biosensors can be improved by manipulating the strength of genetic promoters, controlling post-translational degradation, and getting rid of high levels of leaky expression.[7]

2.4.2 Drug eluting implants

Microbial cells - both native and genetically modified - are utilized in biotechnology plants for their ability to produce large quantities of complex drugs for therapeutic purposes.[6] The integration of these microbes into materials or implants has led to the development of living therapeutic materials (LTMs). The vision is that these materials could enable sustained, long-term treatments for chronic diseases through the controlled, point-of-use and on-demand production of essential drugs,[7][16] while improving the cost-effectiveness of treatments.[3] By maintaining a viable and functional population, these biohybrids can act as self-replenishing drug reservoirs that can be activated as needed.

Lufton et al. used a pluronic based formulation consisting of *Bacillus subtilis* that continually produces antifungal molecules and delivers them to the skin (**Figure 11a**).[5] Light regulated drug secretion using genetically modified *E. coli* bacteria encapsulated within agarose hydrogels was demonstrated by Sankaran et al. (**Figure 11b**).[16] The optogenetic metabolic pathways helped in using light, which can be easily tuned and delivered remotely, as an external trigger for release of deoxyviolacein (dVio) drug. Another example showed the use of penicillin-producing fungi encapsulated in an agar-based hydrogel (**Figure 11c**).[38] The living material was able to release the antibiotic for several days and was successful in killing gram-positive bacteria *in vitro.* Rivera-Tarazona et al. explored shape-morphing ability of polyacrylamide-based constructs embedded with yeast probiotics to deliver model drugs.[102] Varying the proliferation conditions (presence of specific amino acids or nucleotides) for the genetically programmed yeasts, the swelling behavior of the material was controlled thus dictating its shape morphing and drug delivery characteristics (**Figure 11d**). Another drug eluting ELMs was developed by Xie et al. where they encapsulated probiotic bacteria, *Escherichia coli* strain Nissle 1917 (licensed as a medication to treat acute diarrhea and has shown potential as anticancer bacteria) as a model microbe encapsulated within coaxially electrospun fibres of poly(ethylene glycol)-polylactide.[103]

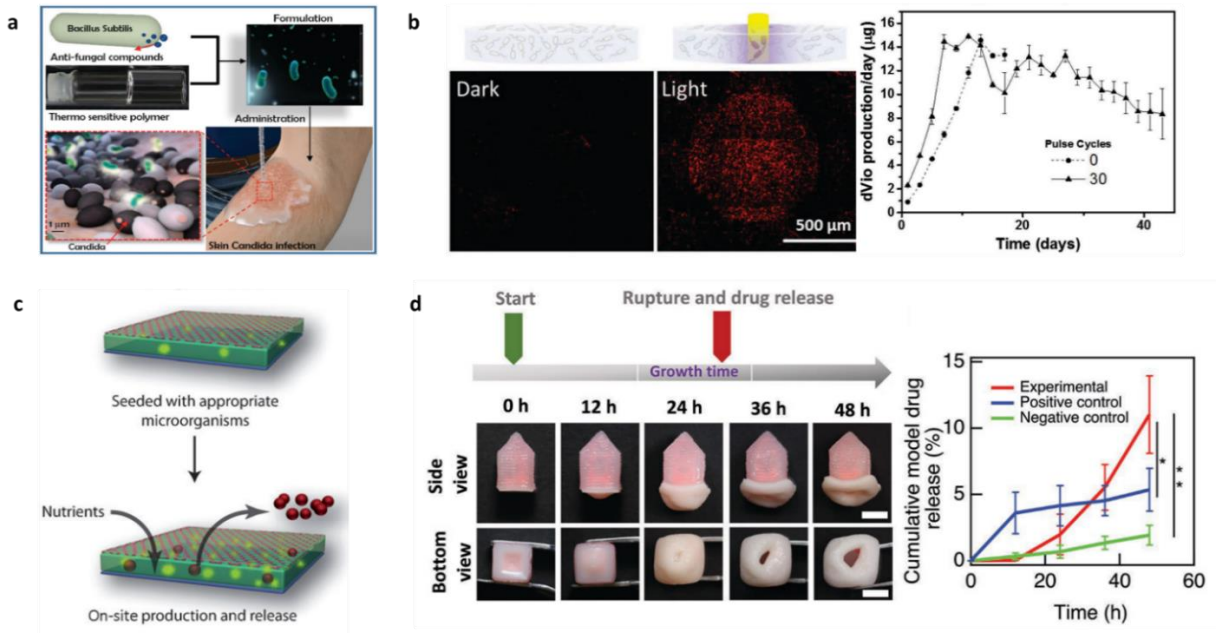

Figure 11: Examples of drug-eluting ELMs: **a)** *Bacillus subtilis* incorporated within pluronic hydrogel and producing antifungal agents applied to skin for treatment. Reprinted (adapted) with permission from ref[5] Copyright © 2018 WILEY-VCH Verlag GmbH & Co. KGaA, Weinheim; **b)** Light regulated, localized and long term release of deoxyviolacein (dVio) through

an agarose hydrogel encapsulating genetically engineered *E. coli* cells. Reprinted (adapted) with permission from ref[16] Copyright © 2018 WILEY-VCH Verlag GmbH & Co. KGaA, Weinheim; **c)** Schematic of agar hydrogels which are sandwiched between a porous membrane and elastomeric substrate and encapsulating penicillin producing fungi. Reprinted (adapted) with permission from ref[38] Copyright © 2012 WILEY-VCH Verlag GmbH & Co. KGaA, Weinheim and **d)** 4D printed ELM drug delivery device acting as a capsule drug reservoir which ruptures at the base upon external biochemical trigger. Reprinted (adapted) with permission from ref[102] Copyright © 2021 Wiley-VCH GmbH

Current limitations of LTMs for drug production include the requirement of a hours to days' timescale for production of therapeutically relevant doses.[1] Further research and optimization in the design of genetic circuits and the encapsulating matrix properties is essential. Biocontainment in LTMs is of the utmost importance as leaking devices leading to freely flowing microbes can overwhelm the immune system of the body. Development of genetic modules including kill switches can be implemented to prevent the inadvertent growth of microbes outside of the targeted region.[1][14] Evaluation of biocompatibility and safety in suitable animal models particularly in terms of immune responses[1][7] is necessary for translating them *in vivo* and furthering them up the technology readiness levels for clinical use.

2.5 Pluronic hydrogels

Pluronics (also known as poloxamers) are block copolymers with a central polypropylene oxide (PPO) block and poly (ethylene oxide) (PEO) blocks on the flanks, PEO_m-PPO_n-PEO_m. This structure confers amphiphilic properties to the polymers. Pluronic solutions are thermosensitive and form physical hydrogels above a certain temperature. Pluronics are shown to be non-toxic and non-irritant and are approved for clinical use. They find biomedical application as matrices for drug delivery for topical and systemic administration, replacements for synovial fluid, and also used in personal care products.[104][105][106][107][108] The first use of pluronics is reported in detergent development, agriculture, food, and paint industries.[104]

Various types of pluronics are differentiated based on the number PPO and PEO chain lengths which dictate the interactions forming the physical gel in aqueous conditions**. Table 1** summarizes the different pluronics and their properties like the PEO chain content, average molecular weight, and viscosity. The nomenclature of the different pluronics is based on their appearance where L stands for liquid, P stands for paste and F stands for flake. The letter is followed by one or two numbers referring to the molecular weight (×300) of the PPO blocks while the last number is the weight fraction in percentage (×10) of the PEO blocks.[104][109]

Table 1: Properties of the common pluronic or poloxamer polymers.[104]

Pluronic	Poloxamer	PEO %	Average Molecular Weight (Da)	Viscosity (Pa.s)
L35	P105	50	1900	0.375
F38	P108	80	4700	0.26
L42	P122	20	1630	0.28
L43	P123	30	1850	0.31
L44	P124	40	2200	0.44
L62	P182	20	2500	0.45
L63	P183	30	2650	0.49
L64	P184	40	2900	0.85
P65	P185	50	3400	0.18
F68	P188	80	8400	1

Pluronic	Poloxamer	PEO %	Average Molecular Weight (Da)	Viscosity (Pa.s)
L72	P212	20	2750	0.51
P75	P215	50	4150	0.25
F77	P217	70	6600	0.48
P84	P234	40	4200	0.28
P85	P235	50	4600	0.31
F87	P237	70	7700	0.7
F88	P238	80	11,400	2.3
F98	P288	80	13,000	2.7
P103	P333	30	4950	0.285
P104	P334	40	5900	0.39
P105	P335	50	6500	0.75
F108	P338	80	14,600	2.8
L122	P402	20	5000	1.75
P123	P403	30	5750	0.35
F127	P407	70	12600	3.1

Thermo-sensitive hydrogels undergo gelation either by cooling below the upper critical gelation temperature (UCGT) or by heating above the lower critical gelation temperature (LCGT).[104][110] Pluronic or poloxamers are thermo-reversible hydrogels with a LCGT. The gelation temperature depends on the concentration of the pluronic solutions. In temperature sensitive hydrogel systems, the physical crosslinks are due to hydrogen bonding and hydrophobic interactions. In aqueous environments, most pluronics form ordered self-assembled aggregates like spherical, rod-like or disc shaped micelles.[105][109] They exhibit macroscopic gelation upon heating due to the physical interactions of the micellar polymers. Micelles are formed with the hydrophilic PEO corona and hydrophobic PPO core above critical temperature and concentration.[111] The increase in the temperature causes an increase in the hydrophobicity of the PPO block which causes micellar formation.[112] The micelles arrange themselves in aggregates of cubic crystalline order with increase in the polymer concentration and temperature.[111][113]

2.5.1 Pluronic F127

Pluronic F127 is a specific member of the pluronic family where x=106 and y=70 in the PEO_x-PPO_y-PEO_x block composition.[113][114] It has got a lot of interest from researchers, as shown in **Figure 12** from the increasing trend of number of publications with Pluronic F127, especially for drug delivery and cell encapsulation applications, in the last two decades. The growing interest is mainly because of its gelation properties as its gelation temperature falls within the physiologically acceptable range at certain concentrations.[105][115] At moderate concentrations (15-30 wt. %), it is a liquid solution at low temperatures, and it forms a soft gel at physiological temperatures.[105][116]

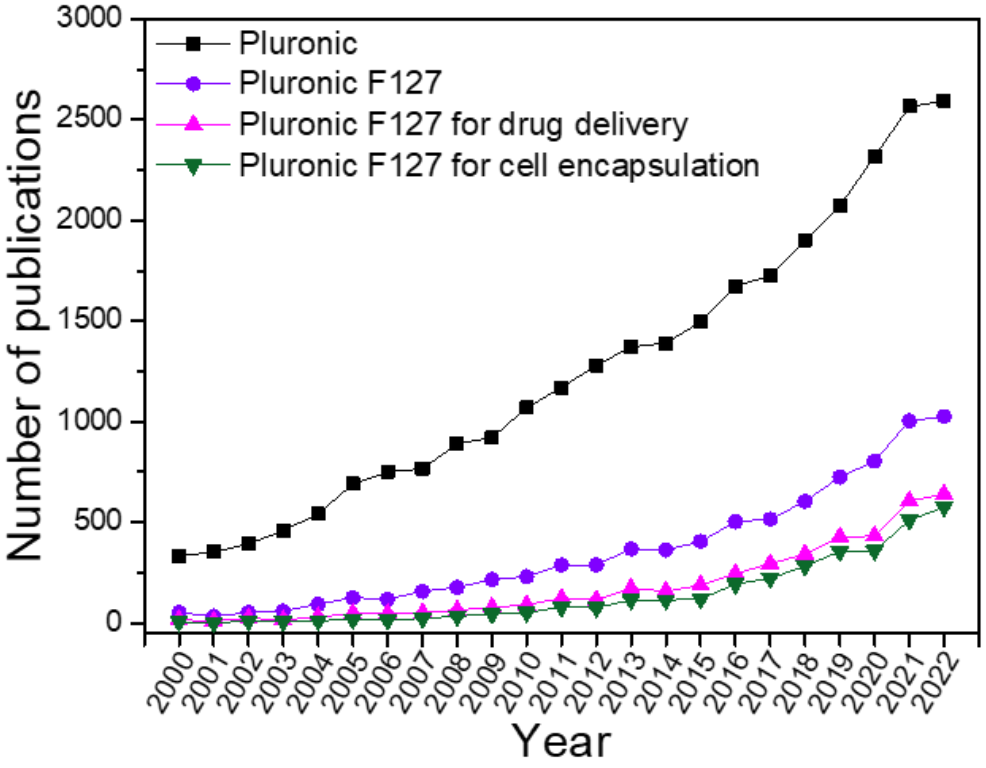

Figure 12: The increasing trends showing the number of publications with keywords 'Pluronic', 'Pluronic F127', 'Pluronic F127for drug delivery' and 'Pluronic F127for cell encapsulation' in Science Direct database during the past two decades (year 2000-2022).

2.5.2 Pluronic F127 micellar microstructure

Amphiphilic block copolymers can self-assemble their individual block copolymer molecules, also known as unimers, into micelles in aqueous solutions.[117] Various studies have been carried out to determine the conditions of micellization and gelation in water or buffer

solutions of Pluronic F127, for example dynamic light scattering (DLS), shear rheology, small angle X-ray scattering (SAXS), small angle neutron scattering (SANS), etc.[105][111] Molecular dynamics simulations have also been used to study the molecular, structural and mechanical properties of the micellar conformations.[118] Pluronic F127 has a micellar state at concentrations above 1 wt. % in water and a critical micellar concentration (CMC) of 0.1 wt. % at temperatures >30 °C.[105] At temperatures below 25 °C and concentrations too low to yield gels, each micelle can have up to 10 polymers while this number, also termed as aggregation number, increases with increasing temperature.[105][113][115] In the gel-like region, the aggregation number of nearly 60-65 and the micellar core radius of 4-5 nm are not sensitive to changes in concentration or temperature.[119] Mortensen et al. used cryogenic transmission electron microscopy to report that the core of the micelles in a 11.7 wt. % solution is nearly 5-7 nm in diameter.[120] Using SANS measurements, Prud'homme et al. determined the hydrodynamic diameter of a micelle in a 19.4 wt. % solution as nearly 22 nm.[121] Individual micelle diameter was calculated by Wu et al. using X-ray scattering study as 17.6 nm in a 28.8 wt. % gel and Li et al. reported it to be nearly 14.6 nm in a 30 wt. % gel using cryogenic transmission electron microscopy.[107] With increasing polymer concentration, the number of micelles increases and the material undergoes phase transition as the micelles organize themselves into face centred cubic structure characterized by some overlap between coronae of neighbouring micelles, as shown by Wu et al.[112] The intermicellar distance was nearly 20 nm for a 20 wt. % concentration gel above 20 °C, according to the SANS measurements by Gjerde et al.[122] The intermicellar distance reduces with increase in concentration. The intermicellar distance at 26 °C went from 21.3 nm to 19.5 nm for a change of concentration from 20 t. % to 30 wt. %.[123] The micellar density thus increases enhancing the interactions between PEO chains from adjacent micelles.[123]

2.5.3 Covalently crosslinked Pluronic F127

Due to the lack of covalent crosslinks, the micellar aggregates in physical Pluronic hydrogels swell, disentangle and dissolve in fluid flow environments.[105][124] Different strategies are employed to stabilize the micelles of the Pluronic F127 gels while maintaining their thermo-reversibility. The terminal hydroxyl groups of Pluronic F127 can be modified with covalently crosslinkable groups to improve the stability of the micelles and the resulting gel network.[108] Lin et al. used the hydroxyl groups of folic acid conjugated Pluronic F127 micelles to chemically crosslink with polyacrylic acid-bound iron oxides Fe_3O_4 nanoparticles. This resulted in stable

magnetic nanoparticles which were used as efficient drug carriers for cancer therapy applications.[125] Zhang et al. developed folic acid functionalized Pluronic F127 and Pluronic P123 mixed micelles. After activation by carbonyldiimidazole, amino-terminated micelles were synthesized and reacted with folic acid, to give stable carriers for increasing drug bioavailability *in vivo*.[108] Mawad et al. used bisacrylate ester-modified Pluronic F127 hydrogels and crosslinked using Ammonium persulfate (APS) and N,N,N',N'-tetramethylethylene diamine (TEMED) for long term drug delivery.[124] Pluronic with dimethacrylate functionalization was synthesized by Saha et al. for incorporating yeast cells for over 2 weeks.[4]

Pluronic diacrylate (PluDA) is another such macromer with end-chain polymerizable acrylate groups which can covalently crosslink the micelles to keep the structure of the gel intact.[114][126] López-Barrón et al. showed that PluDA can form a photo-crosslinked gel in presence of a photoinitiator and has notably enhanced viscoelasticity and stability.[113] They also highlighted that the addition of the acrylic end groups did not affect the crystalline microstructure of the gels significantly. They hypothesized that the covalent crosslinks formed are intra-micellar crosslinks at the micellar corona and inter-micellar crosslinks between neighboring micelles or bridged by block copolymer chains in the solution.[113] Di Biase et al. suggested that the acrylic groups are predominantly involved in intramicellar crosslinking, giving a colloidal template to the final morphology.[105] No differences were seen in the micellar radius, sol-gel transition and the volume fraction of the lattice before and after photocuring of the PluDA gels.[113] The aggregation number, which has been shown previously to increase with temperature in case of uncrosslinked samples, remains fixed in case of crosslinked samples.[113]

2.5.4 Properties of covalently crosslinked Pluronic F127

2.5.4.1 Swelling and degradation/stability

The equilibrium swelling of a hydrogel balances the capacity to uptake water with the elastic forces of the stretched crosslinked network.[28] The swelling degree depends upon the hydrophilicity of the polymer network as well as crosslinking density.[23] The extent of swelling can also influence the pore size of the hydrogel.[44] In chemically crosslinked Pluronic hydrogels, the concentration of polymer, the temperature and the degree of end-functionalization of the Pluronic macromers which can covalently crosslink, impact the

swelling of the hydrogels.[127] The swelling ratio of PluDA hydrogels showed a monotonic decline with increasing temperature.[127][128] As the temperature increases, a more compact pluronic micellar structure is observed due to the hydrophobic interactions of the PPO segments.[128] This reduces the swelling ratio with increasing temperatures. Variation in the surrounding aqueous environment with changing pH or ionic strength did not show much impact on the swelling behavior of the neutral polymeric network of PluDA gels without any charged groups.[127] Hydrolysis of the ester linkages in water however affects the swelling of the hydrogels.[128]

The swelling capacity of pluronic hydrogels was used in the design of a self-healing concrete. Pluronic containing bacterial spores were incorporated in the mortar. Upon water uptake, the encapsulated bacteria[11] help in precipitation of calcium carbonate in the crack.[129] Hydrogels formed with a 17:3 mixture of 20 % pluronic and PluDA tested for cell encapsulation showed an initial burst release and a steady release for more than three days.[59] The initial burst is associated with the loss of non-covalently crosslinked Pluronic chains from the hydrogel. Feng et al. tuned the swelling ratio of PluDA hydrogels from 1082 % to 759 % by increasing the concentration from 23.1 to 33.3 wt %.[130] 25 wt. % PluDA hydrogels degraded upto 50 % in dry weight after 5 weeks in PBS at 37 °C.[128] Higher swelling was observed in PluDA gels of 15 wt. % at lower pH beyond 3 weeks duration due to hydrolysis of the ester linkages.[127] Vandenhaute et al. used pluronic bismethacrylate to study long term degradation profiles of covalently crosslinked pluronic hydrogels.[129] They highlighted the degradation profiles of 25 and 30 wt. % hydrogels in wet and dry conditions at different temperatures.[129]

2.5.4.2 Optical properties

Matrix transparency is important for microscopic studies of encapsulated cells. A clear and optical transparent hydrogel also enables the use of light as a trigger for inducing the genetic circuits within the encapsulated living microbes. This also aids its potential use in optical biosensor systems. Pluronic solutions are clear and optically transparent at a range of compositions. [106][113] Optical transparency of pluronic hydrogels also enables efficient light penetration depth when used with photo-crosslinkers which affects the fidelity and resolution in case of 3D printed constructs.[85] Real time drug diffusion and release through the pluronic hydrogels was possible as at 20 wt. % it is transparent to UV light.[123] However, PluDA hydrogels (23-33 wt. %) were reported to be transparent in the visible range, whereas below

wavelength of 450 nm, the micellar structures accounted for strong absorbance.[130] The refractive index of PluDA hydrogels under 50 wt. % was less than 1.4.[130] These properties have enabled PluDA to be used in optical waveguides.[130][131] Such pluronic based optical waveguides can be further complemented with encapsulation of light-inducible microorganisms to open new vistas in therapeutic or biosensing ELM applications.

2.5.4.3 Mechanical properties

Hydrogel matrix for ELM based applications must hold and maintain its shape and integrity. Covalently crosslinked Pluronic hydrogels show a Young's modulus 3 times higher than physical crosslinked hydrogels with the same composition.[130] Young's Modulus of PluDA hydrogels with concentrations between 23.1 and 33.1 wt. %, range from 71 to 151 kPa.[130] 15 wt. % PluDA hydrogels can elongate over 11 times their original length without rupture, post equilibration at 37 °C in phosphate buffered saline (PBS), with a failure stress of nearly 300 kPa.[127] PluDA hydrogels with a shear modulus of 50 kPa and toughness of 77 Jm^{-2} at 27 wt. %,[17] were shown to effectively encapsulate microbial cells maintaining their viability and functioning post UV crosslinking.[17] Covalently crosslinked Pluronic based hydrogels with viscoelastic properties altered the colony sizes of encapsulated yeast cells.[35]

2.5.4.4 Shear thinning behavior

The shear-thinning behavior of pluronic hydrogels makes it an attractive option for injectable or extrusion-based 3D printing strategies to encapsulate microorganisms for ELM applications. Hydrogels are said to have shear thinning property when they start to flow, due to reduced viscosity, upon application of external shear and retain their shape upon its removal.[132] Such a behavior is essential for 3D printing applications where the hydrogel ink should reduce its viscosity to be able to pass through a thin nozzle and recover quickly upon its exit through the nozzle. The shear thinning behavior in pluronic hydrogels is due to the a reduced layer stacking of two-dimensional hexagonal close-packed (HCP) micelles according to Jiang et al.[119] Shriky et al. focused on a wide range of concentrations (1 to 35 wt. %) of pluronic F127 and found that concentrations above 15 % led to shear thinning physical gels.[133]

2.5.5 3D printing and other fabrication techniques used for pluronic based ELMs

The biocompatibility, thermosensitivity, and shear thinning properties of Pluronic hydrogels make them interesting materials for the bioprinting of ELMs.[110] Saha et al. used pluronic dimethacrylate for 3D printing yeast-laden ELMs and examined the decreasing shear viscosity

upon increasing shear rate followed by a rapid recovery under relaxed conditions.[4] PluDA also shows this shear thinning behavior, exploited for 3D printing of viable microbial cells by Liu et al.[17] Chemical crosslinking of these pluronic hydrogels enabled them to maintain their shape post printing and aided their long term stability.[4] 3D printed structures of 10 × 3 × 3.5 mm^3 were fabricated to immobilize yeast in pluronic based shear-thinning hydrogels using direct-write extrusion printing.[35] Pluronic F127 bis-urethane methacrylate and pluronic F127 dimethacrylate were the bioinks used to effect printing reproducibility and stable long term metabolic activity of the encapsulated yeast cells.[35][80] Liu et al. made use of pluronic F127 methacrylate blended with polyethylene oxide to electrospin *Pseudomonas fluorescens*, *Zymomonas mobilis* and *E. coli* to make fibrous meshes which were viable for 2 months when stored at -70 °C.[83] The fiber diameters were between 1 to 2 µm, slightly larger than the average size of the microbes used, effecting a thin polymeric coating over the cells.[83]

2.6 Rheological properties of hydrogels

Hydrogels used for cell encapsulation typically show viscoelastic properties, i.e. they have a combination of both, viscous and elastic behavior.[132] Rheology is a technique used to evaluate the viscoelastic properties of the hydrogels.[134] This section describes different rheological experiments and the information that can be extracted about the properties of the hydrogel.

2.6.1 Flow curves

Flow curves measure the viscosity of a hydrogel at increasing shear rate.[135] Physical hydrogels are generally non-Newtonian fluids and exhibit shear thinning behavior, i.e. a reduction of viscosity above a critical shear rate.[135] This property is important for processing by injection molding or extrusion printing.

2.6.2 Small amplitude oscillatory shear

Small deformation rheological tests, also termed as small amplitude oscillatory shear (SAOS), measure the material's response to small strains or stresses within the linear viscoelastic range (LVR), where the measured properties are independent of the magnitude of stress or strain.[136] In these measurements, the complex shear modulus G* is monitored against time, frequency, and strain.[136] G* comprises of two components, given by:

$G^* = G' + iG''$

where G', known as storage modulus, is the real component representing the elastic contribution and G'', known as loss modulus, is the imaginary component representing the viscous contribution during the shear process. [136] The loss factor, tan δ, is defined as the ratio of the loss modulus and storage modulus (G''/G').[64][136] For a fluid state, when viscous behavior dominates the elastic one, $G' < G''$ and $\tan \delta > 1$ whereas for a gel-like or solid state, when elastic behavior dominates the viscous one, $G' > G''$ and $\tan \delta < 1$.[132]

SAOS is used extensively to monitor the behavior of hydrogel systems, as a function of time (time sweep) or temperature (temperature sweep).[134] The time sweep test is used to determine changes in G' and G'' of a hydrogel over a specific time period.[135] In case of photocrosslinking pluronic hydrogels, the increase in the moduli with time can be monitored (**Figure 13a**). Similarly, the changes with respect to temperature can be monitored using temperature sweep tests.[135] This is particularly useful to determine the gelation temperatures for thermosensitive Pluronic hydrogels (**Figure 13b)**. The sol-gel transition point

(gel point) is characterized by tan δ = 1 i.e. G'=G''. Strain sweep test involves increasing oscillatory strain amplitude and determining its effect on G' and G'' at a constant frequency.[135] At lower amplitudes, both moduli display constant plateau values within the LVR. At a critical stress physical hydrogels reach their yield point and fluidize (**Figure 13c**).[135] A frequency sweep test examines the variation of G' and G'' with the oscillation frequency at a constant strain amplitude (**Figure 13d**).[135] It helps in assessing the behavior of the hydrogels at short and long time scales.

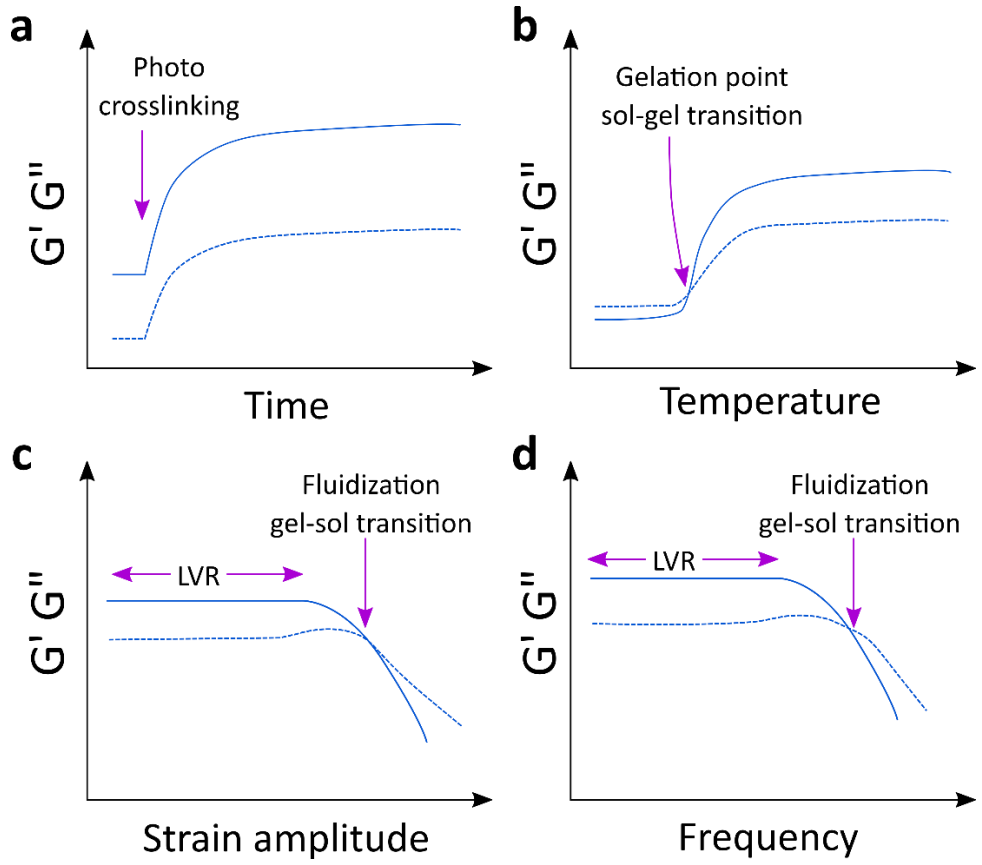

Figure 13: Schematic representations of different rheological tests for determining the response of moduli (G' – solid curve, G" – dashed curve) of Pluronic hydrogels with changing parameters of applied shear and surrounding conditions.[135] **a)** Time sweep experiment indicating evolution of moduli of physically crosslinked pluronic hydrogels before and after photocrosslinking; **b)** Temperature sweep experiment indicating the gelation temperature where G'=G" (sol-gel transition); **c)** Strain sweep experiment showing the LVR and fluidization point (gel-sol transition) and **d)** Frequency sweep experiment highlighting the LVR and crossover frequency point G'=G" (sol-gel transition).

2.6.3 Stress relaxation

Viscoelastic materials exhibit stress relaxation, i.e. a drop in the resistance to deformation over time, when subjected to a constant deformation or strain.[64] Elastic materials, on the other hand, maintain a constant stress under a constant deformation.[64] The stress per unit strain to maintain the constant deformation is defined as relaxation modulus.[137] In hydrogels consisting of reversible crosslinks, the stress relaxation is attributed to the unbinding of the crosslinks and flow of the hydrogel.[138] Thus, by studying the rate of stress relaxation, which corresponds to the rate of viscous energy dissipation in the material per unit time, the viscoelastic properties of a material can be analyzed.[64]

2.6.4 Creep recovery

The creep recovery test evaluates the time-dependent deformation of a hydrogel under a constant static load, a property also known as compliance.[135] This is done by applying a constant stress to hydrogel sample causing an increase in strain. After a certain period of time, the applied stress is removed, and the sample's recovery is measured over a set time duration.[132] Comparatively, hydrogels which undergo higher deformation are said to be more compliant, while those which show lesser deformation are said to be less compliant.

2.6.5 Mathematical models describing viscoelastic behavior

In order to mathematically describe the behavior of materials using rheological experiments, homogenous shear conditions are assumed throughout the shear gap. This allows for a constant shear rate or shear deformation to occur during the shear and removal of the load which enables to exhibit viscous, viscoelastic, or elastic behavior.[132] Viscoelastic behavior can be described mathematically using analog models comprising combination of springs (for the elastic components) and dashpots (for the viscous components).

Ideal elastic deformation behavior is presented by Hooke's law:

$$\tau = G \cdot \gamma$$

where τ is the shear stress γ is the shear strain/deformation and G is the shear modulus.

Ideal viscous flow behavior is presented by Newton's law:

$$\tau = \eta \cdot \dot{\gamma}$$

where τ is the shear stress, $\dot{\gamma}$ is the corresponding shear rate and η is the shear viscosity.

Some of the commonly used models to describe the rheological properties of viscoelastic materials are discussed in the further sections and highlighted in **Figure 14**.

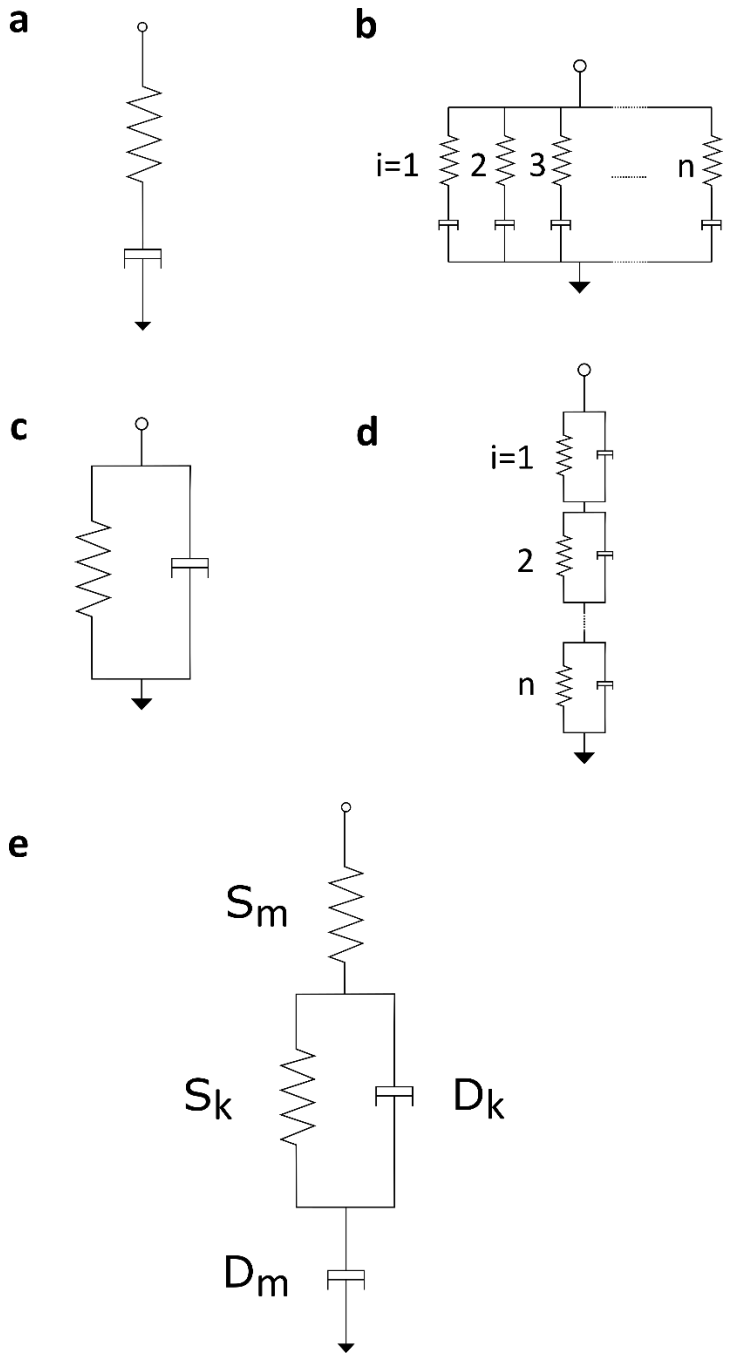

Figure 14: The deformation of viscoelastic materials can be mathematically described using models comprising springs and dashpots units. **a)** Maxwell model with a spring and a dashpot in series; **b)** Generalized Maxwell model with 'n' number of Maxwell elements connected in parallel; **c)** Kelvin-Voigt model with a spring a dashpot in parallel; **d)** Generalized Kelvin-Voigt model with 'n' number of Kelvin-Voigt elements connected in series and **e)** Burgers model with Maxwell and Kelvin-Voigt elements connected in series where S_m is Maxwell spring, D_m is Maxwell dashpot, S_k is Kelvin-Voigt spring and D_k is Kelvin-Voigt dashpot.

2.6.5.1 Maxwell model and generalized Maxwell model

The Maxwell model consists of a spring and a dashpot connected in series (**Figure 14a**). The spring and the dashpot are deflected independently of each other when subjected to an external load. When the material is subjected to a constant force, the spring immediately deforms and eventually reaches a constant deflection value. The dashpot also begins to move, but at a slower rate. After a certain time period, both the spring and the dashpot reach a certain extent of deformation. When the force is removed, the spring returns to its original shape, but the dashpot does not. The extent of the material's permanent deformation represents its viscous portion, while the extent of its recovery represents its elastic portion. These materials behave like liquids due to the irreversible deformation observed and are referred to as viscoelastic liquids or Maxwell fluids.[132]

The total deformation is the sum of individual deformations of the spring and the dashpot connected in series given by ('e' and 'v' in the subscript denote elastic and viscous portion, respectively):

$\gamma = \gamma_e + \gamma_v$

while same shear is acting on the components:

$\tau = \tau_e = \tau_v$

Therefore, the differential equation used to define the sum of shear rates according to the Maxwell elements is given by:

$$\dot{\gamma} = \dot{\tau}/G + \tau/\eta$$

The solution of the differential equation thus gives the time-dependent exponential function, usually used to describe stress relaxation behavior (as follows)[132]:

$$\tau(t) = \gamma_0 \cdot G \cdot exp\left(\frac{-t}{\lambda}\right)$$

where γ_0 is the preset shear strain and λ is the relaxation time when performing stress relaxation tests.

The generalized Maxwell model, which contains several Maxwell elements connected in parallel, can be used to analyze stress relaxation behavior of real-world viscoelastic materials like polymers (**Figure 14b**).[132] As polymers have a spectrum of molar mass distribution, the Generalized Maxwell model gives a spectrum of relaxation time constants and hence, a better estimate of the relaxation behavior.

The total stress value is given by[132]:

$\tau(t) = \gamma_0 \cdot \sum_i Gi \cdot exp\left(\frac{-t}{\lambda i}\right)$

where i denotes the number of Maxwell elements.

2.6.5.2 Kelvin-Voigt model and generalized Kelvin-Voigt model

The Kelvin-Voigt model comprises of a spring and dashpot in parallel (**Figure 14c**). When a constant loading force is applied, both components are deformed simultaneously and to the same extent. The deformation process can be given by time-dependent exponential function. When the loading force is removed, the spring immediately tries to return to its initial shape, however the dashpot delays this causing both components to return to their initial positions after a certain period of time. This reformation process is also given by time-dependent exponential function. The materials return to their initial state or original shape after the removal of the load, that is, it shows reversible deformation. Thus, these materials are referred to as viscoelastic solids.[132]

The total shear stress applied is the sum of shear stress applied on two individual spring and the dashpot connected in parallel given by ('e' and 'v' in the subscript denote elastic and viscous portion, respectively):

$\tau = \tau_e + \tau_v$

while both components deform to the same extent, thus the shear rate is given by:

$\dot{\gamma} = \dot{\gamma}_e = \dot{\gamma}_v$

Therefore, the differential equation used to define the behavior according to the Kelvin-Voigt elements is given by:

$\tau = G \cdot \gamma + \eta \cdot \dot{\gamma}$

The solution of the differential equation thus gives the time-dependent exponential function, usually used to describe behavior during creep tests to determine the deformation (as follows)[132]:

$\gamma(t) = (\tau/G) \cdot \left(1 - exp\left(\frac{-t}{\lambda}\right)\right)$

where λ is the retardation time defined as the delayed response to an applied stress when performing creep tests.

Generalized Kelvin-Voigt model, which contains several Kelvin-Voigt elements connected in series, can be used to analyze creep recovery behavior (**Figure 14d**).[132] The total sum of individual Kelvin-Voigt elements is given by[132]:

$$\gamma\,(t) = \sum_{i} (\tau 0/\,Gi) \cdot \left(1 - exp\left(\frac{-t}{\lambda_i}\right)\right)$$

where τ0 is the preset shear stress and i denotes the number of Kelvin-Voigt elements.

2.6.5.3 Burgers Model

The Burgers model, usually used to describe the creep behavior[139][140], comprises of a Maxwell element and a Kelvin-Voigt element in series (**Figure 14e**). The Maxwell spring is termed as S_m, the Maxwell dashpot is termed as D_m, the Kelvin-Voigt spring is termed as S_k while the Kelvin-Voigt dashpot is termed as D_k. During the creep phase, when a force is applied, an immediate deformation is seen in S_m, a delayed deformation is seen in S_k and D_k and a continuously increasing deformation is seen for D_m. After a sufficiently longer period of time, all the springs and dashpots deflect to a certain extent depending on the constant stress applied and its duration. In the creep recovery phase, when the force is removed, there is an immediate reformation of S_m, a delayed reformation of S_k and D_k while D_m remains deflected.[132]

For the creep phase, the deformation at time 't' is given by:

$$\gamma_{creep} = \frac{\tau}{G_m} + \frac{\tau}{G_k}\left(1 - exp\left(\frac{-t}{\lambda}\right)\right) + \frac{\tau}{\eta_m}t$$

For the recovery phase, the deformation at time 't' is given by:

$$\gamma_{\,recovery} = \gamma_{max} - \frac{\tau}{G_m} - \frac{\tau}{G_k}\left(1 - exp\left(\frac{-t}{\lambda}\right)\right)$$

τ is the fixed applied shear stress, t denotes the time after loading, G_m denotes the spring constant (shear modulus) of the spring and and η_m denotes the viscosity of the dashpot in the Maxwell element. G_k is the spring constant (shear modulus) of the spring and η_k is the viscosity of the dashpot in the Kelvin-Voigt element. λ is the retardation time taken to produce 63.2% of the total deformation in the Kelvin-Voigt unit and γ_{max} is the deformation at the end of the creep phase.

2.6.5.4 Stretched exponential function

The stretched exponential function, also termed as Weibull distribution function or Kohlrausch–Williams–Watts (KWW) function, is another commonly used model for the analysis of the viscoelastic behavior. It has been used for analyzing the recovery phase of the creep recovery tests[140], given by:

$$\gamma_{rec} = \gamma_k \{\exp\left[-\left(\frac{t - t_0}{\eta_r}\right)^{\beta}\right]\} + \gamma_p$$

where γ_{rec} is the deformation after the instantaneous strain recovery, γ_k denotes the delayed viscoelastic strain recovery (Kelvin-Voigt element), η_r is the characteristic life parameter and β the shape factor. Time t_0 is the time of the start of the recovery phase and γ_p is the permanent irreversible strain.

It is also used to describe the stress relaxation behavior[141][142], where the relaxation modulus at time t is given by:

$$G(t) = G_0 \exp\left(-\left(\frac{t}{\tau}\right)^{\beta}\right)$$

where G_0 is the shear modulus at time zero, τ is the relaxation time, and β is the stretching exponent ($0 < \beta < 1$). The value of β less than 1 indicates relaxation time distribution which can depict behavior in viscoelastic materials.

3 CUMULATIVE DESCRIPTION OF RESULTS OF THE RESEARCH PAPERS

The integration of cells as living components of functional materials and devices in application scenarios is not trivial from a technical and an environmental point of view. Numerous questions need to be answered, like: Which material properties can support the viability and function of embedded microbial populations at the application conditions? Which processing conditions and technologies are compatible with living cells? What strategies are needed to contain the growth of microorganisms at the application site and guarantee safe use? How do encapsulated microorganisms interact with other living cells in the confined environment? Addressing these questions at a fundamental level using model systems can contribute to accelerating the translation of ELMs into real products.

The selection of a suitable model hydrogel system is the first step in addressing the aforementioned questions. Hydrogels that combine elastic and dissipative components are useful for encasing mammalian cells in 3D culture models and tissue engineering. These hydrogels' mechanical properties affect the proliferation, migration, and differentiation of embedded cells.[64] The hydrogel systems with modifiable viscoelastic properties through crosslinks have especially helped in understanding the cells' mechanosensitivity range and responses.[56] Such hydrogels also have provided inspiration for encapsulating other cell types, such as bacteria or yeast, for applications in the ELM field. It is important, however, to regulate the growth and metabolic production of the embedded living biofactories to control pharmacokinetics and ensure safety by avoiding their inadvertent release. Studies indicate that bacteria or yeast embedded in hydrogels grow at a slower rate than in suspension because of the spatial confinement. The change in the matrix properties like increasing the stiffness of the hydrogel network has been shown to hinder extension of the bacterial cell wall and in effect reduce bacterial growth.[63][35] Bacteria behavior within biofilms have also been explained in terms of the viscoelastic properties. These viscoelastic properties are dependent on the spatial architecture as well as breakage of bonds, crosslinks, and entanglements between the extracellular polymeric matrix components within biofilms.[143] Tuning the viscoelasticity of the surrounding environment and the bacterial density influences the biofilm properties.[144] Therefore, by drawing inspiration from the field of tissue engineering and utilizing it as a guide for the choice of our hydrogel system that can both easily tune its viscoelastic properties and safely encapsulate bacteria, we explored the possibility of using Pluronic based hydrogels.

The triblock copolymer Pluronic F127 (Plu) chains form micelles above a critical concentration and temperature, and these micelles aggregate to form physically crosslinked hydrogels with LCST behavior. The sol-gel transition in Plu solutions occurs at concentrations > 5 wt. % and temperatures > 14 °C. As a result, Plu can be processed at low temperatures and used in applications at body temperature (37°C). The physical character of the network, with reversible crosslinks, confers Pluronic hydrogels a dynamic nature with the possibility for micellar aggregates to rearrange under stress and for the material to flow above a critical shear rate (shear thinning).[59][17] The shear thinning behavior and thermosensitivity allows Plu hydrogels to be easily processed, mixed with payloads, and injected for application in drug delivery and for replacing biological fluids.[133] Physical Plu hydrogels swell and dissociate into individual micelles when immersed in aqueous environments, affecting their long term stability.[59] Plu chains modified with acrylate terminal groups (PluDA) can be used to mechanically stabilize the hydrogels by photocrosslinking. These covalently crosslinked hydrogels have long-term shape fidelity and ideal properties for incorporating viable and functional populations of genetically modified microorganisms. They have also been utilized for encapsulation of bacteria in reported literature on ELMs for biosensing and drug delivery.[17] Similarly, other covalently crosslinked pluronic hydrogel systems have also been utilized to encapsulate bacteria (*Escherichia coli*) and yeast (*Saccharomyces cerevisiae*) while maintaining their viability for months and impacting their cellular phenotypes.[35] In this Thesis, by simply varying the fraction of Plu and PluDA, hydrogels with different mechanical properties were obtained. This was a consequence of the change in the nature of the crosslinking points of the network: from purely physical and reversible to a mixture of physical and covalent, i.e., permanent network points. This variability was exploited to quantify and understand the influence of the viscoelastic properties of the embedding microenvironment in the biological response of microbes.

The selection of the living component is crucial depending on the intended application. Given the robustness, versatility in protein overexpression, and the ability to incorporate a wide range of genetic modules and strains[145], *E. coli* was selected as the living component in this work. Most used *E. coli* lab strains are incompatible for medical purposes due to their endotoxic outer membranes.[40] Hence, we used a commercially available endotoxin-free strain called ClearColi for most parts in this work.

30% w/v hydrogels containing variable fractions of Plu and PluDA (named DA X hydrogels, where X is the percentage fraction of PluDA in the mixture) were prepared and characterized. DA X hydrogels with variable degree of covalent crosslinking were obtained as the X increased from 0 to 100. The hydrogels showed variable mechanical properties with changing X. An increase in the shear storage modulus from 18 to 43 kPa was quantified indicating that the covalent bonds reinforced the stability of the DA X hydrogels (Section 6.1). This was also reflected in an increase of the fluidization strain values from the strain sweep rheological experiments (Section 6.2).

Further investigations into the viscoelastic properties of DA X hydrogels were carried out by performing stress relaxation and creep recovery experiments. When varying the applied strain (0.5 to 30 %) in a step strain stress relaxation experiment (Section 6.2), the maximum induced stress within the physical DA 0 hydrogel networks reached a plateau at lower strains compared to DA 100. This highlighted that the DA 0 hydrogel could dissipate the stress easily because of the lack of covalent crosslinks. At a constant applied strain of 1% (within the linear viscoelastic range), DA X hydrogels with higher X values showed a lower percentage of relaxation at the end of the test, that is, less stress was dissipated in hydrogels with higher covalent crosslinking. Two modes of relaxation were visible at this strain and the corresponding relaxation times obtained by fitting the experimental curves with a linear combination of exponential functions were τ_1 (<1 s) and τ_2 (>1 min). The fast relaxation time constant became faster and more prominent with increasing X. This relaxation was associated with structural rearrangements at macroscopic, network scale which require cooperative motion of micelles. The slow relaxation time constant became slower with increasing X and was associated to relaxation modes at microscopic scale, such as the breaking of physical bonds between micelles within clusters. Creep recovery experiments at constant applied stress of 100 Pa revealed the higher compliance of hydrogels with lower X. The experimental curves fitted to the Burgers model and shorter retardation times were obtained with increasing X values suggesting that the covalent crosslinking between the micelles accelerates the sliding of micelles and the deformation of the hydrogel. In Section 6.1, recovery curves after reaching a strain value of 1 % under different applied stresses for different DA X hydrogels were analysed. In Section 6.2, recovery curves after reaching different strain values under a constant applied stress of 100 Pa were analysed. From the recovery curves, the elastic, viscoelastic and plastic contribution to deformation under the applied stress were calculated. An increasing elastic

and decreasing non-elastic contribution were observed in the hydrogels with increasing X in both experimental conditions.

The rheological studies of DA X hydrogels in Sections 6.1 and 6.2 together allowed a detailed quantification of the correlation between mechanical response and compositional changes, i.e., covalent crosslinking degree. But do bacteria within these hydrogels respond to these differences in the viscoelastic properties? And how? To answer these questions, *E. coli* bacteria (ClearColi) were encapsulated within DA X hydrogels at low density (Section 6.1). The growth of bacteria inside the hydrogels was studied within microchannels by brightfield microscopy image analysis. Bacteria grew inside all hydrogels to an extent which was dependent on the composition of the hydrogel and the availability of nutrients. Within the DA 0 network, bacteria grew at a faster rate and formed elongated and larger colonies than in hydrogels with higher X. The colonies became rounded when the fraction of covalent crosslinks increased. In the constrained hydrogel environment, bacteria growth deviated from the typical chain-like growth seen in liquid cultures. Such a phenomenon, also called verticalization when observed in biofilms, is due to the stresses generated by the neighboring cells and the network in a confined environment.[146] The growing chain buckled, at earlier time points for DA X hydrogels with higher X, resulting in rounded colony shapes. The differences in growth and morphology were evaluated by quantifying the volume of the individual colonies and their sphericity in microwells using confocal microscopy image analysis. Smaller volumes and higher sphericity were obtained for bacterial colonies growing in hydrogels with higher covalent crosslinking, confirming the observations described before. Also, control experiments with higher nutrient concentration showed similar trends and confirmed that the observed effects as function of X were related to the properties of the encapsulating matrix and not to differences in the availability of nutrients.

The production of protein within living cells is closely linked to both external conditions and internal requirements.[147] The question was whether the metabolic activity of the encapsulated bacteria influenced by the mechanical constraints of the hydrogel network as well? Using a light-inducible red fluorescent protein (RFP)-producing strain of ClearColi, the highest protein production rate was observed in DA X hydrogels with X=50 (Section 6.1). This suggested that the slower growing colonies in hydrogels with higher chemical crosslinking were more efficient in RFP production compared to colonies growing faster in physical

hydrogels. However, beyond a certain level of restriction, the growth is suppressed to such an extent that the overall protein production is reduced.

Reported studies in mechanobiology using bacteria biofilms indicate that bacteria - either individually or as a collective - can detect and respond to the mechanical properties of the embedding microenvironment.[146] Studies of bacteria growth within channels also indicate that bacteria sense crowding during colony growth by mechanosensory elements.[62] It seems therefore logical to associate the differences in bacteria behavior observed in Section 6.1 of this Thesis with the differences in the mechanical properties of DA X hydrogels with different compositions. This correlation shows an inverse linear dependence of colony volume with the storage modulus and the critical stress for fluidization for the DA X hydrogels from the rheology experiments. The increase in colony sphericity with increasing X correlated with the increase in the elastic contribution to deformation in the creep recovery experiments, although we observed a deviation at lower X values. In summary, the data from Sections 6.1 and 11.2 demonstrate that hydrogel design can be exploited to control and regulate bacterial growth and metabolic activity, just by simple changes in the type and degree of crosslinking.

The acquired knowledge in the behavior of *E. coli* within Pluronic-based networks was used to design an ELM that could support bacteria function long term and avoid bacteria outgrowth as discussed in detail in Sections 6.3 and 6.4. These two properties are fundamental for the safe application of ELMs. A bilayer hydrogel in the form of a thin film on silanized glass substrates was conceived for a safe ELM. A thin enveloping layer of DA 100 could prevent leakage of the bacteria embedded in different DA X core hydrogels, when immersed in nutrient medium. In these conditions, different extent of swelling degrees was observed for the DA X hydrogels. The swelling is also accompanied by elution of non-diacrylated Pluronic from the bilayer cores into surrounding.[59] This phenomenon could help to increase the porosity of the hydrogel after film formation and swelling, favoring diffusion of nutrients and cell viability. Although non-homogenous distribution of the bacterial colonies was seen for DA X hydrogel cores with X≤25. Also, the DA 50 core layer displayed the highest rate of RFP production (5.1 ± 0.1 au/h), whereas DA 0 (DA 0 = 3.1 ± 0.1 au/h) and DA 100 (4.0 ± 0.1 au/h) had significantly lower rates. The rates of RFP production at DA 25 and DA 75 were only slightly lower than those for DA 50. Thus, even in environments where a continuous nutrient supply is present, similar bacterial behavior to that observed previously (in Section 6.1) could still be

observed. As a result, thin films with bacterial core layer of DA 50 were chosen for further testing to assess the safety of encapsulating bacteria in the thin films and to evaluate the long-term activity of the bacterial bilayers.

Protein production could be monitored for over two weeks using simple spectrometric measurements at different time points. RFP was not just continuously produced but also secreted outside of the DA 50 bacterial gels and through the encapsulating DA 100 layer to the surroundings for over two weeks without leakage of bacteria. Exchange of fresh nutrient medium every two days, however, led to loss of adhesion of the encapsulating layer with the glass substrate for nearly half of the samples. Thus, the stability of the thin film is not constrained by the degradation of the outer hydrogel but rather by the design of the interface between the glass and hydrogel.

The bilayer thin films containing bacteria were tested as whole-cell biosensors and their ability to sense the presence of a small molecule (lactate) in the incubation medium was quantified (Section 6.3). A bacterial strain of *E. coli*, able to sense L-lactate and respond by producing a fluorescent protein, CreiLOV, as reporter, was encapsulated in the DA 50 core layer for these studies. This protein allowed quantification of production over time by fluorescence measurements when lactate (at concentrations of 0, 1 and 10 mM) was added to the surrounding medium. When the induction coincided with the starting point of growth of bacterial colonies (at 0 h), a higher fluorescence intensity was observed for films with higher lactate in the incubation medium. However, these fluorescence signals exhibited prolonged response times of 9 h for 1 mM and 6 h for 10 mM. Whereas, when induced after allowing the bacterial colonies to grow for 6 h, a faster fluorescence response time (within 2 h) was observed. This corroborated our previous results that protein production was growth dependent. To evaluate its robustness in an application scenario, the performance of the sensor was tested after storage. The bacteria in the hydrogels were allowed to grow for a day and the thin film biosensors were stored in phosphate buffered saline (PBS) at room temperature for 2 days or 3 weeks. Thin films were then transferred to cell-culture medium containing lactate at different concentrations. Shorter response times (between 2-4 h), compared to the earlier conditions, were observed for thin films in medium with 10 mM L-lactate. However, high levels of leaky expression of proteins in the absence of L-lactate was observed, affecting the sensitivity of the biosensor. This level of leaky expression overlapped

with the response to 1 mM L-lactate for nearly 8 h. The long-term usage of living biosensors has been limited by factors such as the viability, function, and safe containment of the living cells within the device.[100][14] Our results show that the bilayer thin films could support viable and functional bacterial colonies without leaking the bacteria to the surrounding even after storage for three weeks. The thin encapsulating layer of ca. 100–150 µm allowed efficient transport of small molecules minimizing signal attenuation. Also, the flat and transparent nature of the thin film enabled microscopy and spectroscopy-based analyses for continuous monitoring. Addressing the current limitations with regards to the leaky expression of proteins in the lactate sensing genetic circuit could improve their performance further.

The design of a safe ELM construct, able to confine microorganisms for at least two weeks, allows performing experiments to quantify the biocompatibility of such living materials to be applied in a therapeutic context. For this purpose, it is important to first quantify the bacteria density in the thin film during the time of the assay. Fluorescence and confocal microscopy image analysis of the DA 50 inner bacterial gels showed a mixed population of live and dead bacteria within the inner core layer after 1 day (Section 6.3) as well as after 3 and 7 days (Section 6.4). An assay was established to quantify the release of extracellular ATP to the incubation medium as an indicator of metabolically active cells (Section 6.4). In a liquid bacteria culture, extracellular ATP peaks during the early log phase and decreases in the stationary phase.[148] In the incubation medium of the thin film bilayers with ClearColi, a similar bell-shaped curve was observed. After a 6 h lag period, nearly 0.15 nM/h ATP was detected for the next 18 h, followed by a progressive drop. This meant that the bacteria in hydrogels are in the log phase within the first 6 to 24 h of encapsulation, whereas they reach the stationary phase at 48 and 72 h.

In cooperation with the School of Medicine at Saarland University (Homburg), ClearColi containing thin films were prepared to test the biocompatibility in cultures with primary immune cells (Section 6.4). Since bacteria in the thin film are not in direct contact with the immune cells, the possible responses from immune cells would be associated with secreted substances, bacteria debris, or properties of the encapsulating hydrogel. Studies in the Medical School in co-cultures of the living thin films with human peripheral blood mononuclear cells (PBMCs) from donors and analysis of cytokine release showed that the ClearColi hydrogels did not elicit severe immune responses in cells from healthy donors. This

positive result indicates that Pluronic thin films prepared in this Thesis are suitable candidates for *in vivo* animal testing aimed to further develop the ELMs for therapeutic and clinical application.

The studies in this Thesis contribute to the advancement of ELMs through the development of materials and device designs that maintain and optimize the function and performance of the encapsulated organisms. This research has shown that Plu/PluDA hydrogels, with their tunable mechanics and processability, are valuable materials for gaining fundamental insights into bacteria-matrix interactions in confined environments. Through quantification of the elastic, viscoelastic, and plastic responses of physical Pluronic hydrogels with varying degrees of covalent crosslinking, correlations between material parameters and cell responses in model encapsulated systems could be established. The information in these model systems can aid in the understanding of bacteria behavior in natural cases of bacterial encapsulations, like biofilms in infected sites. Additionally, a secure bacterial encapsulation format was developed using Pluronic F127-based hydrogels for creating ELMs, with the ultimate goal of improving the performance and safety of these materials for a wide range of applications, like drug delivery and biosensing. The cooperative work in this thesis has further revealed that the bacterial hydrogels generate a low immunogenic response and could be suitable prototypes for further *in vitro* and possibly *in vivo* testing of ELM designs for drug delivery in animal experiments.

4 CONCLUSIONS AND OUTLOOK

In this doctoral thesis, the interactions and interplay between the hydrogels made using a clinically approved material for drug delivery, Pluronic F127, and genetically modified *E. coli* bacteria encapsulated in it were studied within the context of ELMs' development for therapeutic and sensing applications. The main areas of investigation in this study, as highlighted in **Figure 15**, were: 1) quantification of the growth and biological function of encapsulated *E. Coli* within the Pluronic hydrogel networks of different compositions, 2) characterization of the viscoelastic behavior of the hydrogels and correlation of mechanical response with the behavior of the organisms within the network, and 3) development of a stable and safe ELM device design that allows evaluation of biosensing performance, *in vitro* immune response studies and demonstration of how materials design can provide safe ELMs in the future.

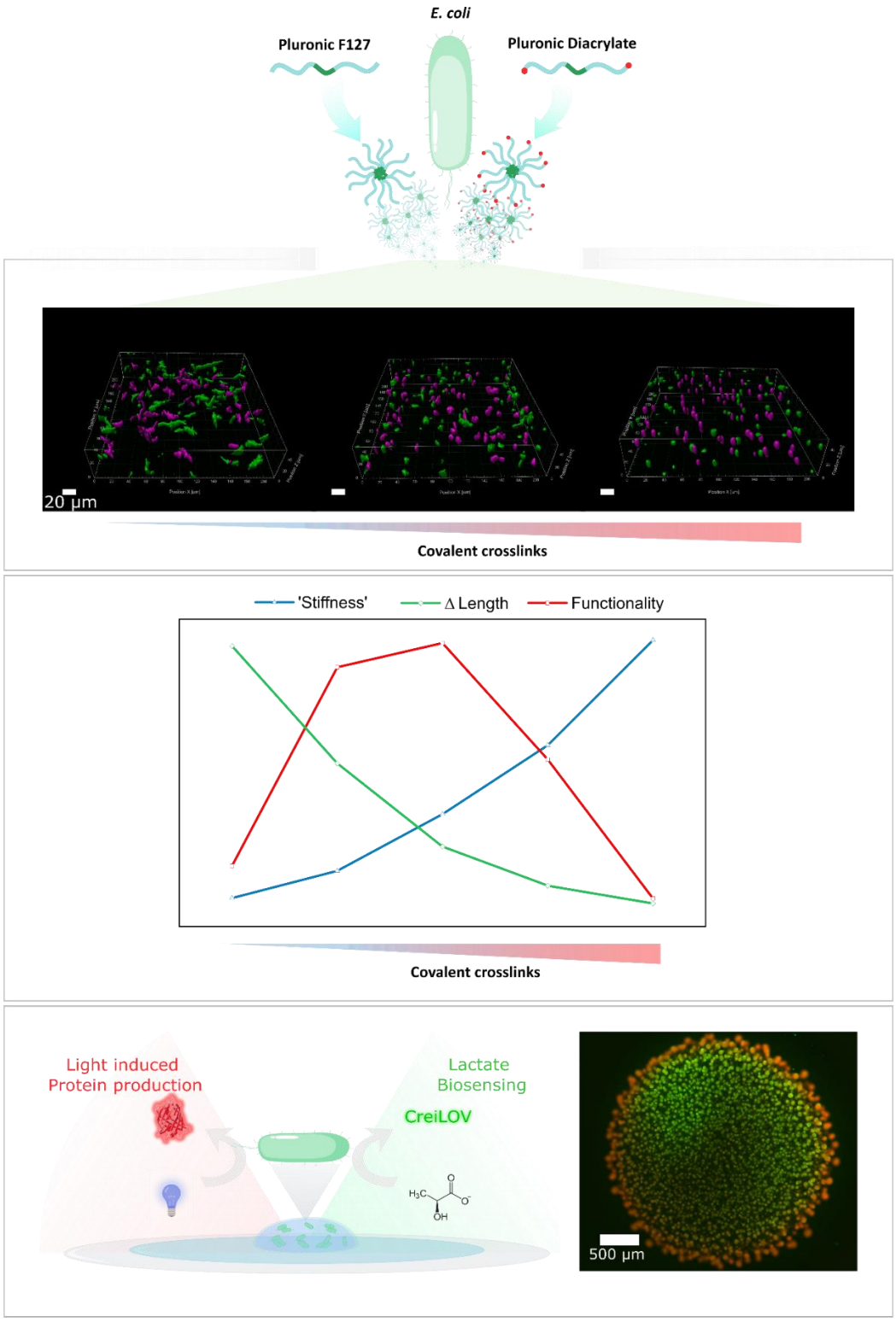

Figure 15: Graphical summary of the present work. Encapsulation of genetically modified *E. coli* bacteria within a tunable Plu/PluDA hydrogel, growth behavior of bacteria as function of encapsulation material (scale = 20 µm), relationship between the mechanical properties of Pluronic hydrogel and bacterial behavior, and protein-eluting or biosensor ELM design that is stable and functional for 3 weeks (scale = 500 µm).

The most important conclusions of this work are:

- Pluronic (Plu) and pluronic diacrylate (PluDA) based DA X hydrogels (where X is the percentage fraction of PluDA in the mixture) securely encapsulate the bacteria within its covalently crosslinked micellar network.
- DA X hydrogels show increasing storage modulus (from 18 to 43 kPa) and decreasing percentage relaxation with increasing X. Under external shear load, the covalent bonds introduced by higher PluDA fraction confer increasing elasticity and reduce viscoelasticity and plasticity.
- Higher covalent crosslinking degree of the DA X matrix decelerates the bacterial growth, reduces their colony size, and leads to more rounded colony morphologies. The volume fraction of the bacteria within the gels increases with time and nearly halves at 24 h with X content increasing from 0 to 100.
- Metabolic activity (light-induced protein production) of bacteria within DA X hydrogels increases with X for X≤50. However, for X>50, the growth is suppressed to such an extent that the overall protein production reduces.
- A bilayer thin film with DA X inner hydrogel layer and DA 100 outer hydrogel layer can encapsulate bacteria in the core for up to 2 weeks without leaking.
- The bacterial bilayer thin films show potential as protein/drug eluting and biosensing units with cheap room temperature storage options for 3 weeks.
- Immune response studies demonstrate that bacterial bilayer thin films do not elicit severe immune responses in cells from healthy donors and show potential to be promising platforms for future *in vivo* examinations.

The field of ELMs is still in its early stages of development and poised for many newer avenues and innovations. There are numerous opportunities to continue the development of ELMs based on the results of this Thesis and plenty of open questions that remain to be addressed by the ELM community.

On the materials front, pluronic based hydrogels with different crosslinking chemistries and at different concentrations could be explored. These studies could widen the window for tuning viscoelastic properties and diffusion of macromolecules within the hydrogels.

The core-shell design could be transferred to 3D printing methodologies (**Figure 16**) to fabricate customized geometries[149] and increase the biomass of the encapsulated bacteria.[1] It could also allow co-culturing of different strains of microbes for cell-cell communication or cross-species interaction studies.[150]

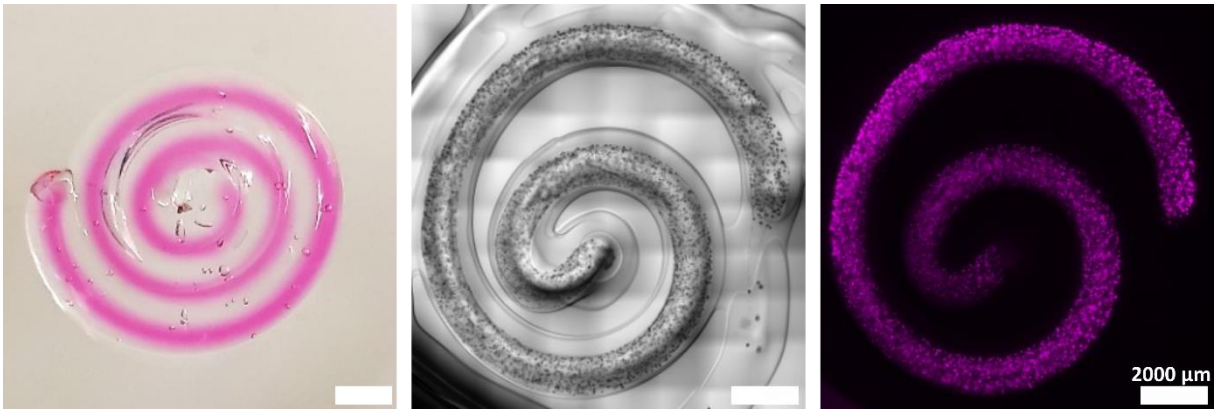

Figure 16: Photograph and microscopy images of 3D printed core-shell living therapeutic fibers containing light responsive violet colored deoxyviolacein (dVio), an anti-bacterial and anti-tumoral drug (scale = 2000 µm).

The design of living biosensors, which often have a high degree of noise and error[7], can be improved by enabling the use of genetically encoded logic functions with complex biosensing competencies in specific patterns. Optimizations through the use of artificial intelligence, machine learning, and automation in the design and testing process to could help further.[7]

While research has been conducted using well-studied model systems, as more genetic tools become available, different organisms with high engineering feasibility will become the focus.[7] The variability in the cellular behavior at the microscale provides a significant challenge for accurately linking them with the macroscale hydrogel properties. Thus, analysis of the mechanical properties at the microscale, using techniques like traction force microscopy[62] or atomic force microscopy[10], could provide estimate of the stresses generated and felt by micron-sized bacterial colonies and help in using better design strategies.

Another challenge is to visualize individual bacterium within a larger colony inside a 3D hydrogel. With the use of these thin film platforms and higher resolution microscopy techniques, precise positioning of individual bacterium can be known. This information along

with the mechanical properties of the hydrogels can aid in developing predictive computational models to precisely estimate the cellular responses.

Thus, seamless integration of biotic and abiotic components with a focus of scalability and automation with relevant safety and regulations will further push the ELM devices towards translation.

5 REFERENCES

[1] A. Rodrigo-Navarro, S. Sankaran, M. J. Dalby, A. del Campo, M. Salmeron-Sanchez, *Nature Reviews Materials* **2021**, *6*, 1175.

[2] P. Q. Nguyen, N. M. D. Courchesne, A. Duraj-Thatte, P. Praveschotinunt, N. S. Joshi, *Advanced Materials* **2018**, *30*, DOI 10.1002/adma.201704847.

[3] R. S. H. Smith, C. Bader, S. Sharma, D. Kolb, T. C. Tang, A. Hosny, F. Moser, J. C. Weaver, C. A. Voigt, N. Oxman, *Advanced Functional Materials* **2020**, *30*, 1.

[4] A. Saha, T. G. Johnston, R. T. Shafranek, C. J. Goodman, J. G. Zalatan, D. W. Storti, M. A. Ganter, A. Nelson, *ACS Applied Materials and Interfaces* **2018**, *10*, 13373.

[5] M. Lufton, O. Bustan, B. hen Eylon, E. Shtifman-Segal, T. Croitoru-Sadger, A. Shagan, A. Shabtay-Orbach, E. Corem-Salkmon, J. Berman, A. Nyska, B. Mizrahi, *Advanced Functional Materials* **2018**, *28*, 1801581.

[6] A. Maxmen, *Nature Medicine* **2017**, *23*, 5.

[7] T. C. Tang, B. An, Y. Huang, S. Vasikaran, Y. Wang, X. Jiang, T. K. Lu, C. Zhong, *Nature Reviews Materials* **2021**, *6*, 332.

[8] B. An, Y. Wang, Y. Huang, X. Wang, Y. Liu, D. Xun, G. M. Church, Z. Dai, X. Yi, T. Tang, C. Zhong, *Chemical Reviews* **2022**, DOI 10.1021/acs.chemrev.2c00512.

[9] S. Balasubramanian, K. Yu, A. S. Meyer, E. Karana, M. E. Aubin-Tam, *Advanced Functional Materials* **2021**, *31*, 2011162.

[10] W. Wang, L. Yao, C. Y. Cheng, T. Zhang, H. Atsumi, L. Wang, G. Wang, O. Anilionyte, H. Steiner, J. Ou, K. Zhou, C. Wawrousek, K. Petrecca, A. M. Belcher, R. Karnik, X. Zhao, D. I. C. Wang, H. Ishii, *Science Advances* **2017**, *3*, 1.

[11] J. Y. Wang, D. Snoeck, S. Van Vlierberghe, W. Verstraete, N. De Belie, *Construction and Building Materials* **2014**, *68*, 110.

[12] L. K. Rivera-Tarazona, V. D. Bhat, H. Kim, Z. T. Campbell, T. H. Ware, *Science Advances* **2020**, *6*, eaax8582.

[13] C. Knierim, M. Enzeroth, P. Kaiser, C. Dams, D. Nette, A. Seubert, A. Klingl, C. L.

Greenblatt, V. Jérôme, S. Agarwal, R. Freitag, A. Greiner, *Macromolecular Bioscience* **2015**, *15*, 1052.

[14] T. C. Tang, E. Tham, X. Liu, K. Yehl, A. J. Rovner, H. Yuk, C. de la Fuente-Nunez, F. J. Isaacs, X. Zhao, T. K. Lu, *Nature Chemical Biology* **2021**, *17*, 724.

[15] Z. Bayat, M. Hassanshahian, S. Cappello, *The open microbiology journal* **2015**, *9*, 48.

[16] S. Sankaran, J. Becker, C. Wittmann, A. Campo, *Small* **2019**, *15*, 1804717.

[17] X. Liu, H. Yuk, S. Lin, G. A. Parada, T. C. Tang, E. Tham, C. de la Fuente-Nunez, T. K. Lu, X. Zhao, *Advanced Materials* **2018**, *30*, 1704821.

[18] S. Molinari, R. F. Tesoriero, D. Li, S. Sridhar, R. Cai, J. Soman, K. R. Ryan, P. D. Ashby, C. M. Ajo-Franklin, *Nature Communications* **2022**, *13*, DOI 10.1038/s41467-022-33191-2.

[19] A. D. Lantada, J. G. Korvink, M. Islam, *Cell Reports Physical Science* **2022**, *3*, DOI 10.1016/j.xcrp.2022.100807.

[20] X. Liu, M. E. Inda, Y. Lai, T. K. Lu, X. Zhao, *Advanced Materials* **2022**, *34*, 1.

[21] D. E. Moormeier, J. L. Endres, E. E. Mann, M. R. Sadykov, A. R. Horswill, K. C. Rice, P. D. Fey, K. W. Bayles, *Applied and Environmental Microbiology* **2013**, *79*, 3413.

[22] J. M. Chem, M. L. Japas, S. A. Bilmes, **2011**, 4546.

[23] S. R. Caliari, J. A. Burdick, *Nature Methods* **2016**, *13*, 405.

[24] P. Praveschotinunt, A. M. Duraj-Thatte, I. Gelfat, F. Bahl, D. B. Chou, N. S. Joshi, *Nature Communications* **2019**, *10*, DOI 10.1038/s41467-019-13336-6.

[25] C. Gilbert, T. Ellis, *ACS Synthetic Biology* **2019**, *8*, 1.

[26] C. Gilbert, T. C. Tang, W. Ott, B. A. Dorr, W. M. Shaw, G. L. Sun, T. K. Lu, T. Ellis, *Nature Materials* **2021**, *20*, 691.

[27] V. Hagel, T. Haraszti, H. Boehm, *Biointerphases* **2013**, *8*, 1.

[28] R. M. Ottenbrite, K. Park, T. Okano, *Biomedical Applications of Hydrogels Handbook*, Springer, New York, **2010**.

[29] S. Rathore, P. M. Desai, C. V. Liew, L. W. Chan, P. Wan, S. Heng, *Journal of Food Engineering* **2013**, *116*, 369.

[30] N. Kandemir, W. Vollmer, N. S. Jakubovics, J. Chen, *Scientific Reports* **2018**, *8*, 10893.

[31] L. M. González, N. Mukhitov, C. A. Voigt, *Nature Chemical Biology* **2020**, *16*, 126.

[32] M. C. Gutierrez, Z. Y. Garcia-Carvajal, M. Jobbagy, L. Yuste, F. Rojo, C. Abrusci, F. Catalina, F. del Monte, M. L. Ferrer, *Chemistry of Materials* **2007**, *19*, 1968.

[33] A. M. Jonas, K. Glinel, A. Behrens, A. C. Anselmo, R. S. Langer, A. Jaklenec, *ACS Applied Materials & Interfaces* **2018**, *10*, 16250.

[34] S. Guo, E. Dubuc, Y. Rave, M. Verhagen, S. A. E. Twisk, T. Van Der Hek, G. J. M. Oerlemans, M. C. M. Van Den Oetelaar, L. S. Van Hazendonk, M. Brüls, B. V. Eijkens, P. L. Joostens, S. R. Keij, W. Xing, M. Nijs, J. Stalpers, M. Sharma, M. Gerth, R. J. E. A. Boonen, K. Verduin, M. Merkx, I. K. Voets, T. F. A. De Greef, *ACS Synthetic Biology* **2020**, *9*, 475.

[35] H. Priks, T. Butelmann, A. Illarionov, T. G. Johnston, C. Fellin, T. Tamm, A. Nelson, R. Kumar, P. J. Lahtvee, *ACS Applied Bio Materials* **2020**, *3*, 4273.

[36] J. K. Park, H. N. Chang, *Biotechnology Advances* **2000**, *18*, 303.

[37] I. Jung, H. Bin Seo, J. eun Lee, B. Chan Kim, M. B. Gu, *Analyst* **2014**, *139*, 4696.

[38] L. C. Gerber, F. M. Koehler, R. N. Grass, W. J. Stark, *Angewandte Chemie* **2012**, *124*, 11455.

[39] C. A. Mora, A. F. Herzog, R. A. Raso, W. J. Stark, *Biomaterials* **2015**, *61*, 1.

[40] S. Sankaran, A. Campo, *Advanced Biosystems* **2019**, *3*, 1800312.

[41] M. Schaffner, P. A. Rühs, F. Coulter, S. Kilcher, A. R. Studart, *Science Advances* **2017**, *3*, DOI 10.1126/sciadv.aao6804.

[42] C. M. Heveran, S. L. Williams, J. Qiu, J. Artier, M. H. Hubler, S. M. Cook, J. C. Cameron, W. V. Srubar, *Matter* **2020**, *2*, 481.

[43] L. Ionov, *Materials Today* **2014**, *17*.

[44] J. Liu, F. Cheng, H. Grénman, S. Spoljaric, J. Seppälä, J. E. Eriksson, S. Willför, C. Xu, *Carbohydrate Polymers* **2016**, *148*, 259.

[45] M. S. Rehmann, K. M. Skeens, P. M. Kharkar, E. M. Ford, E. Maverakis, K. H. Lee, A. M. Kloxin, *Biomacromolecules* **2017**, *18*, 3131.

[46] N. Lorén, M. Nydén, A. M. Hermansson, *Advances in Colloid and Interface Science* **2009**, *150*, 5.

[47] S. Shen, R. Zhou, Y. Li, B. Liu, G. Pan, Q. Liu, Q. Xiong, X. Wang, X. Xia, J. Tu, *Small Methods* **2019**, *3*, 1.

[48] A. Schenkmayerová, M. Bu, P. Gemeiner, *Applied Biochemistry and Biotechnology* **2014**, *174*, 1834.

[49] V. Kras, R. Stloukal, M. Rosenberg, M. Rebro, *Applied Microbiology and Biotechnology* **2016**, *100*, 2535.

[50] J. L. Connell, E. T. Ritschdorff, M. Whiteley, J. B. Shear, *Proceedings of the National Academy of Sciences of the United States of America* **2013**, *110*, 18380.

[51] I. Jeon, J. Cui, W. R. K. Illeperuma, J. Aizenberg, J. J. Vlassak, *Advanced Materials* **2016**, *28*, 4678.

[52] X. Chen, C. Dong, K. Wei, Y. Yao, Q. Feng, K. Zhang, F. Han, A. F. T. Mak, B. Li, L. Bian, *NPG Asia Materials* **2018**, *10*, 788.

[53] K. Yong, D. J. Mooney, *Progress in Polymer Science* **2012**, *37*, 106.

[54] S. Banta, I. R. Wheeldon, M. Blenner, *Annual Review of Biomedical Engineering* **2010**, *12*, 167.

[55] H. Wang, S. C. Heilshorn, *Advanced Materials* **2015**, *27*, 3717.

[56] M. Rizwan, A. E. G. Baker, M. S. Shoichet, *Advanced Healthcare Materials* **2021**, *10*, 2100234.

[57] J. George, C. C. Hsu, L. T. B. Nguyen, H. Ye, Z. Cui, *Biotechnology Advances* **2020**, *42*, DOI 10.1016/j.biotechadv.2019.03.009.

[58] V. Normand, D. L. Lootens, E. Amici, K. P. Plucknett, P. Aymard, *Biomacromolecules* **2000**, *1*, 730.

[59] M. Müller, J. Becher, M. Schnabelrauch, M. Zenobi-Wong, *Biofabrication* **2015**, *7*, 035006.

[60] X. Liu, T. Tang, E. Tham, H. Yuk, S. Lin, T. K. Lu, *PNAS* **2017**, *114*, DOI 10.1073/pnas.1618307114.

[61] O. Chaudhuri, *Biomaterials Science* **2017**, *5*, 1480.

[62] Y. F. Dufrêne, A. Persat, *Nature Reviews Microbiology* **2020**, *18*, 227.

[63] H. H. Tuson, G. K. Auer, L. D. Renner, M. Hasebe, C. Tropini, M. Salick, W. C. Crone, A. Gopinathan, K. C. Huang, D. B. Weibel, *Molecular Microbiology* **2012**, *84*, 874.

[64] D. Indana, P. Agarwal, N. Bhutani, O. Chaudhuri, *Advanced Materials* **2021**, *33*, 2101966.

[65] P. F. Lenne, V. Trivedi, *Nature Communications* **2022**, *13*, 1.

[66] K. H. Vining, A. Sta, D. J. Mooney, **2019**, *188*, 187.

[67] T. Narita, K. Mayumi, G. Ducouret, P. Hébraud, *Macromolecules* **2013**, *46*, 4174.

[68] H. Cao, O. Habimana, A. Safari, R. Heffernan, Y. Dai, E. Casey, *NPJ Biofilms and Microbiomes* **2016**, *2*, 1.

[69] Y. He, B. W. Peterson, M. A. Jongsma, Y. Ren, P. K. Sharma, H. J. Busscher, H. C. van der Mei, *PLoS ONE* **2013**, *8*, DOI 10.1371/journal.pone.0063750.

[70] E. J. Stewart, M. Ganesan, J. G. Younger, M. J. Solomon, *Scientific Reports* **2015**, *5*, 1.

[71] Z. Li, Y. Wang, J. Liu, P. Rawding, J. Bu, S. Hong, Q. Hu, *Advanced Materials* **2021**, *33*, 1.

[72] I. Moya-Ramírez, P. Kotidis, M. Marbiah, J. Kim, C. Kontoravdi, K. Polizzi, *ACS Synthetic Biology* **2021**, DOI 10.1021/acssynbio.1c00577.

[73] K. Schulz-Schönhagen, N. Lobsiger, W. J. Stark, *Advanced Materials Technologies* **2019**, *4*, 1900266.

[74] C. Knierim, C. L. Greenblatt, S. Agarwal, A. Greiner, *Macromolecular Bioscience* **2014**, *14*, 537.

[75] W. K. Ding, N. P. Shah, *Journal of Food Science* **2009**, *74*, DOI 10.1111/j.1750-3841.2009.01067.x.

[76] M. E. Sanders, D. J. Merenstein, G. Reid, G. R. Gibson, R. A. Rastall, *Nature Reviews Gastroenterology and Hepatology* **2019**, *16*, 605.

[77] S. B. Suh, A. Jo, M. A. Traore, Y. Zhan, S. L. Coutermarsh-Ott, V. M. Ringel-Scaia, I. C. Allen, R. M. Davis, B. Behkam, *Advanced Science* **2019**, *6*, DOI 10.1002/advs.201801309.

[78] D. T. Riglar, P. A. Silver, *Nature Reviews Microbiology* **2018**, *16*, 214.

[79] L. M. González, N. Mukhitov, C. A. Voigt, *Nature Chemical Biology* **2020**, *16*, DOI 10.1038/s41589-019-0412-5.

[80] T. Butelmann, H. Priks, Z. Parent, T. G. Johnston, T. Tamm, A. Nelson, P. J. Lahtvee, R. Kumar, *ACS Applied Bio Materials* **2021**, *4*, 7195−7203.

[81] A. Manjula-Basavanna, A. M. Duraj-Thatte, N. S. Joshi, *Advanced Functional Materials* **2021**, *31*, DOI 10.1002/adfm.202010784.

[82] M. Gensheimer, A. Brandis-heep, S. Agarwal, R. K. Thauer, A. Greiner, *Macromolecular Bioscience* **2011**, *11*, 333.

[83] Y. Liu, M. H. Rafailovich, R. Malal, D. Cohn, D. Chidambaram, *Proceedings of the National Academy of Sciences of the United States of America* **2009**, *106*, 14201.

[84] J. Yu, T. R. Huang, Z. H. Lim, R. Luo, R. R. Pasula, L. De Liao, S. Lim, C. H. Chen, *Advanced Healthcare Materials* **2016**, *5*, 2983.

[85] H. Tetsuka, S. R. Shin, *Journal of Materials Chemistry B* **2020**, DOI 10.1039/D0TB00034E.

[86] S. Hafeez, H. Ooi, F. Morgan, C. Mota, M. Dettin, C. van Blitterswijk, L. Moroni, M. Baker, *Gels* **2018**, *4*, 85.

[87] F. L. C. Morgan, L. Moroni, M. B. Baker, **2020**, *1901798*, DOI 10.1002/adhm.201901798.

[88] T. G. Johnston, S. F. Yuan, J. M. Wagner, X. Yi, A. Saha, P. Smith, A. Nelson, H. S. Alper, *Nature Communications* **2020**, *11*, 563.

[89] T. S. Kaminski, O. Scheler, P. Garstecki, *Lab on a Chip* **2016**, *16*, 2168.

[90] C. Zhao, Y. Zhu, B. Kong, Y. Huang, D. Yan, H. Tan, L. Shang, *ACS Applied Materials & Interfaces* **2020**, *12*, 42586.

[91] B. Balusamy, O. F. Sarioglu, A. Senthamizhan, T. Uyar, *ACS Applied Bio Materials* **2019**, DOI 10.1021/acsabm.9b00308.

[92] T. D. J. Heunis, M. Botes, L. M. T. Dicks, *Probiotics and Antimicrobial Proteins* **2010**, *2*, 46.

[93] I. Letnik, R. Avrahami, J. S. Rokem, A. Greiner, E. Zussman, C. Greenblatt, *Biomacromolecules* **2015**, *16*, 3322.

[94] E. Eroglu, V. Agarwal, M. Bradshaw, X. Chen, S. M. Smith, C. L. Raston, K. Swaminathan Iyer, *Green Chemistry* **2012**, *14*, 2682.

[95] S. Klein, J. Kuhn, R. Avrahami, S. Tarre, M. Beliavski, M. Green, E. Zussman, *Biomacromolecules* **2009**, *10*, 1751.

[96] L. Bousse, *Sensors and Actuators, B: Chemical* **1996**, *34*, 270.

[97] J. T. Atkinson, L. Su, X. Zhang, G. N. Bennett, *Nature* **2022**, DOI 10.1038/s41586-022-05356-y.

[98] T. Trantidou, L. Dekker, K. Polizzi, O. Ces, Y. Elani, *Interface Focus* **2018**, *8*, DOI 10.1098/rsfs.2018.0024.

[99] L. Goers, C. Ainsworth, C. H. Goey, C. Kontoravdi, P. S. Freemont, K. M. Polizzi, *Biotechnology and Bioengineering* **2017**, *114*, 1290.

[100] D. O. Fesenko, T. V Nasedkina, D. V Prokopenko, A. D. Mirzabekov, *Biosensors and Bioelectronics* **2005**, *20*, 1860.

[101] T. Tanna, R. Ramachanderan, R. J. Platt, *Current Opinion in Microbiology* **2021**, *59*, 24.

[102] L. K. Rivera-Tarazona, T. Shukla, K. A. Singh, A. K. Gaharwar, Z. T. Campbell, T. H. Ware, *Advanced Functional Materials* **2022**, *32*, DOI 10.1002/adfm.202106843.

[103] S. Xie, S. Tai, H. Song, X. Luo, H. Zhang, X. Li, *Journal of Materials Chemistry B* **2016**, *4*, 6820.

[104] E. Russo, C. Villa, *Pharmaceutics* **2019**, *11*, DOI 10.3390/pharmaceutics11120671.

[105] M. Di Biase, P. De Leonardis, V. Castelletto, I. W. Hamley, B. Derby, N. Tirelli, *Soft Matter* **2011**, *7*, 4928.

[106] M. Zhang, M. Djabourov, C. Bourgaux, K. Bouchemal, *International Journal of Pharmaceutics* **2013**, *454*, 599.

[107] J. Li, C. Marmorat, G. Vasilyev, J. Jiang, N. Koifman, Y. Guo, I. Talmon, E. Zussman, D. Gersappe, R. Davis, M. Rafailovich, *Acta Biomaterialia* **2019**, *96*, 295.

[108] W. Zhang, Y. Shi, Y. Chen, J. Ye, X. Sha, X. Fang, *Biomaterials* **2011**, *32*, 2894.

[109] K. Mortensen, *Polymers for Advanced Technologies* **2001**, *12*, 2.

[110] E. Gioffredi, M. Boffito, S. Calzone, S. M. Giannitelli, A. Rainer, M. Trombetta, P. Mozetic, V. Chiono, *Procedia CIRP* **2016**, *49*, 125.

[111] R. Basak, R. Bandyopadhyay, *Langmuir* **2013**, *29*, 4350.

[112] C. Wu, T. Liu, B. Chu, D. K. Schneider, V. Graziano, *Macromolecules* **1997**, *30*, 4574.

[113] C. R. López-Barrón, R. Chen, N. J. Wagner, P. J. Beltramo, *Macromolecules* **2016**, *49*, 5179.

[114] C. R. López-Barrón, R. Chen, N. J. Wagner, *ACS Macro Letters* **2016**, *5*, 1332.

[115] D. Attwood, J. H. Collett, C. J. Tait, *International Journal of Pharmaceutics* **1985**, *26*, 25.

[116] J. C. Gilbert, J. L. Richardson, M. C. Davies, K. J. Palin, J. Hadgraft, *Journal of Controlled Release* **1987**, *5*, 113.

[117] A. V Kabanov, E. V Batrakova, V. Yu, *Journal of Controlled Release* **2002**, *82*, 189.

[118] J. M. R. Albano, D. Grillo, J. C. Facelli, M. B. Ferraro, M. Pickholz, *Processes* **2019**, *7*, 1.

[119] J. Jiang, C. Burger, C. Li, J. Li, M. Y. Lin, R. H. Colby, M. H. Rafailovich, J. C. Sokolov, *Macromolecules* **2007**, *40*, 4016.

[120] K. Mortensen, Y. Talmon, *Macromolecules* **1995**, *28*, 8829.

[121] R. K. Prud'homme, G. Wu, D. K. Schneider, *Langmuir* **1996**, *12*, 4651.

[122] N. Gjerde, K. Zhu, K. D. Knudsen, B. Nyström, *European Polymer Journal* **2019**, *112*, 493.

[123] F. Ye, A. Yaghmur, H. Jensen, S. W. Larsen, C. Larsen, J. Østergaard, *European Journal of Pharmaceutical Sciences* **2011**, *43*, 236.

[124] D. Mawad, J. L. J. R. Foster, A. Lauto, *International Journal of Pharmaceutics* **2008**, *360*, 231.

[125] J. J. Lin, J. S. Chen, S. J. Huang, J. H. Ko, Y. M. Wang, T. L. Chen, L. F. Wang, *Biomaterials* **2009**, *30*, 5114.

[126] Y. Wang, Y. Miao, J. Zhang, J. Ping, T. Brett, J. Xu, D. Ma, W. Xue, *Materials Science & Engineering C* **2018**, *84*, 44.

[127] C. Shen, Y. Li, Y. Wang, Q. Meng, *Lab on a Chip* **2019**, *19*, 3962.

[128] J. B. Lee, J. J. Yoon, D. S. Lee, T. G. Park, *Journal of Biomaterials Science, Polymer Edition* **2004**, *15*, 1571.

[129] M. Vandenhaute, D. Snoeck, E. Vanderleyden, N. De Belie, S. Van Vlierberghe, P. Dubruel, *Polymer Degradation and Stability* **2017**, *146*, 201.

[130] J. Feng, Y. Zheng, Q. Jiang, M. K. Włodarczyk-Biegun, S. Pearson, A. del Campo, *Advanced Materials Technologies* **2022**, DOI 10.1002/admt.202101539.

[131] J. Feng, Y. Zheng, S. Bhusari, M. Villiou, S. Pearson, A. del Campo, *Advanced Functional Materials* **2020**, *30*, DOI 10.1002/adfm.202004327.

[132] T. G. Mezger, *The Rheology Handbook: For Users of Rotational and Oscillatory*

Rheometers, **2014**.

[133] B. Shriky, A. Kelly, M. Isreb, M. Babenko, N. Mahmoudi, S. Rogers, O. Shebanova, T. Snow, T. Gough, *Journal of Colloid and Interface Science* **2020**, *565*, 119.

[134] J. M. Zuidema, C. J. Rivet, R. J. Gilbert, F. A. Morrison, *Journal of Biomedical Materials Research Part B: Applied Biomaterials* **2014**, *102B*, 1063.

[135] G. Stojkov, Z. Niyazov, F. Picchioni, R. K. Bose, *Gels* **2021**, *7*, DOI 10.3390/gels7040255.

[136] C. Yan, D. J. Pochan, *Chemical Society Reviews* **2010**, *39*, 3528.

[137] A. V. Tobolsky, *Journal of Applied Physics* **1956**, *27*, 673.

[138] O. Chaudhuri, L. Gu, D. Klumpers, M. Darnell, S. A. Bencherif, J. C. Weaver, N. Huebsch, H. Lee, E. Lippens, G. N. Duda, D. J. Mooney, *Nature Materials* **2015**, DOI 10.1038/NMAT4489.

[139] X. Hong, J. P. Stegemann, C. X. Deng, *Biomaterials* **2016**, *88*, 12.

[140] D. Biswal, B. Anupriya, K. Uvanesh, A. Anis, I. Banerjee, K. Pal, *Journal of the Mechanical Behavior of Biomedical Materials* **2016**, *53*, 174.

[141] M. Zabet, S. Mishra, S. Kundu, *RSC Advances* **2015**, *5*, 83936.

[142] P. L. Drzal, K. R. Shull, *Macromolecules* **2003**, *36*, 2000.

[143] S. G. V. Charlton, M. A. White, S. Jana, L. E. Eland, P. G. Jayathilake, J. G. Burgess, J. Chen, A. Wipat, T. P. Curtis, *Journal of Bacteriology* **2019**, *201*, DOI 10.1128/JB.00101-19.

[144] S. Liu, S. Shankar, M. C. Marchetti, Y. Wu, *Nature* **2021**, *590*, 80.

[145] S. Sankaran, S. Zhao, C. Muth, J. Paez, *Advanced Science* **2018**, *1800383*, 1.

[146] J. Nijjer, C. Li, Q. Zhang, H. Lu, S. Zhang, J. Yan, *Nature Communications* **2021**, *12*, DOI 10.1038/s41467-021-26869-6.

[147] M. Kafri, E. Metzl-Raz, G. Jona, N. Barkai, *Cell Reports* **2016**, *14*, 22.

[148] R. Mempin, H. Tran, C. Chen, H. Gong, K. Kim Ho, S. Lu, *BMC Microbiology* **2013**, *13*, 1.

[149] L. M. González, N. Mukhitov, C. A. Voigt, *Nature Chemical Biology* **2020**, *16*, 126.

[150] J. L. Connell, E. T. Ritschdorff, M. Whiteley, J. B. Shear, *PNAS* **2013**, *110*, 18380.

[151] S. Bhusari, S. Sankaran, A. del Campo, *Advanced Science* **2022**, *2106026*, 1.

6 ANNEX: PEER REVIEWED RESEARCH PAPERS AND UNPUBLISHED PAPERS

This section contains the peer reviewed research articles and unpublished (submitted/soon to be submitted) articles with their corresponding supplementary information.

6.1 Regulating bacterial behavior within hydrogels of tunable viscoelasticity

Shardul Bhusari[1,2], Shrikrishnan Sankaran[1]*, Aránzazu del Campo[1,2]*

[1]INM – Leibniz Institute for New Materials, Campus D2 2, 66123 Saarbrücken, Germany

[2]Chemistry Department, Saarland University, 66123 Saarbrücken, Germany

*Corresponding authors

Email: shrikrishnan.sankaran@leibniz-inm.de, aranzazu.delcampo@leibniz-inm.de

Citation: Bhusari, S., Sankaran, S. and Del Campo, A., 2022. Regulating bacterial behavior within hydrogels of tunable viscoelasticity. *Advanced Science*, p.2106026.

Own Contribution: Methodology (all experiments including rheology and microscopy), Validation, Visualization, Formal analysis, Investigation, Writing (Original draft, review and editing).

Check for updates

RESEARCH ARTICLE

ADVANCED SCIENCE Open Access

www.advancedscience.com

Regulating Bacterial Behavior within Hydrogels of Tunable Viscoelasticity

Shardul Bhusari, Shrikrishnan Sankaran, and Aránzazu del Campo**

Engineered living materials (ELMs) are a new class of materials in which living organism incorporated into diffusive matrices uptake a fundamental role in material's composition and function. Understanding how the spatial confinement in 3D can regulate the behavior of the embedded cells is crucial to design and predict ELM's function, minimize their environmental impact and facilitate their translation into applied materials. This study investigates the growth and metabolic activity of bacteria within an associative hydrogel network (Pluronic-based) with mechanical properties that can be tuned by introducing a variable degree of acrylate crosslinks. Individual bacteria distributed in the hydrogel matrix at low density form functional colonies whose size is controlled by the extent of permanent crosslinks. With increasing stiffness and elastic response to deformation of the matrix, a decrease in colony volumes and an increase in their sphericity are observed. Protein production follows a different pattern with higher production yields occurring in networks with intermediate permanent crosslinking degrees. These results demonstrate that matrix design can be used to control and regulate the composition and function of ELMs containing microorganisms. Interestingly, design parameters for matrices to regulate bacteria behavior show similarities to those elucidated for 3D culture of mammalian cells.

1. Introduction

The combination of synthetic biology and materials science has given rise to the field of engineered living materials (ELMs), wherein live organisms (bacteria, yeast, algae, etc.) become active components of material's design and perform advanced functions.[1–3] Examples of ELMs include biofilters to sequester metals[4] or viruses,[5] bacterial hydrogels for biosensing,[6] shape-morphing composites,[7] self-healing adhesives,[8] photosynthetic biogarments[9] or self-regulated drug delivery devices.[10] A common feature in these constructs is the encapsulation of the organisms within matrices including natural polymers like agarose,[11,12] alginate,[13] and dextran,[14] synthetic polymers like polyvinyl alcohol[15] and Pluronic,[16,17] or inorganic matrices like porous silica.[18] Alternatively, proteinaceous[19] or cellulose[6] matrices produced by the organisms themselves, as in a biofilm, can serve as encapsulating networks. The matrix confers a protective environment for the cells while it allows the diffusion of nutrients and gases to maintain the viability and functionality of the entrapped organisms. It also confines and retains the organisms inside the material, which is a necessary requirement in the future application of ELMs containing genetically modified organisms.

Recent studies have highlighted that spatial confinement and matrix mechanical properties affect the growth and functionality of embedded bacteria in ELMs.[10,20,21] The current understanding, mainly from studies of bacteria or yeast embedded in hydrogels, indicate that the microbes grow inside the hydrogel network to form dense clusters at slower rates than in suspension.[20,22,23] Cell's response to the mechanical properties of their microenvironment is well known from 3D cultures of mammalian cells, whose proliferation, migration, or differentiation programs depend on the viscoelasticity[24] and the degradation kinetics of the hydrogel network.[25,26] Studies in engineered hydrogels with viscoelastic properties that can be modulated by the type of network crosslinks (reversible/dynamic vs permanent) and by the nature of the degradable sequences have helped to understand and quantify eukaryotic organism's mechanosensitivity range and response.[27] Preliminary studies from us[10] and others[21] on hydrogel-embedded bacteria have indicated that increasing stiffness of the hydrogel network hinders extension of the bacterial cell wall and thus reduces bacterial growth. Based on these observations, we hypothesized that the behavior of encapsulated bacterial colonies, e.g., growth rate or metabolic activity, might be regulated by tuning the viscoelastic properties of the embedding matrix. Hydrogels formed by the triblock copolymer Pluronic F127 (Plu, PEG_{106}-PPO_{70}-PEG_{106})[28] and chemically cross-linkable derivatives,[16,23,29] previously used for bacterial

S. Bhusari, S. Sankaran, A. del Campo
INM - Leibniz Institute for New Materials
Campus D2 2, 66123 Saarbrücken, Germany
E-mail: shrikrishnan.sankaran@leibniz-inm.de;
aranzazu.delcampo@leibniz-inm.de

S. Bhusari, A. del Campo
Chemistry Department
Saarland University
66123 Saarbrücken, Germany

The ORCID identification number(s) for the author(s) of this article can be found under https://doi.org/10.1002/advs.202106026

© 2022 The Authors. Advanced Science published by Wiley-VCH GmbH. This is an open access article under the terms of the Creative Commons Attribution License, which permits use, distribution and reproduction in any medium, provided the original work is properly cited.

DOI: 10.1002/advs.202106026

21983844, 2022, 17, Downloaded from https://onlinelibrary.wiley.com/doi/10.1002/advs.202106026 by Inm - Leibniz-Institut Für Neue Materialien, Wiley Online Library on [17/01/2023]. See the Terms and Conditions (https://onlinelibrary.wiley.com/terms-and-conditions) on Wiley Online Library for rules of use; OA articles are governed by the applicable Creative Commons License

ADVANCED SCIENCE NEWS
www.advancedsciencenews.com

ADVANCED SCIENCE Open Access
www.advancedscience.com

encapsulation in ELMs, seemed appropriate as a model system to test this hypothesis. Plu solutions above critical micellar concentration (0.725 wt% at 25 °C[30]) self-assemble in water and form micelles.[31] At concentrations >5 wt% and temperatures above 14 °C, micelles self-assemble through physical interactions and form an associative hydrogel (**Figure 1**a).[28,29,31] Such hydrogels swell and dissociate into individual micelles when immersed in water. When Plu is mixed with its diacrylated derivative (PluDA), similar hydrogels are formed but in this case they can be stabilized by covalent cross-linking of the acrylate end-groups. By varying the polymer concentration between 5 and 30 wt%, hydrogels with a storage modulus between 1 and 50 kPa can be obtained.[31]

In this work, we show that by varying the covalent cross-linking degree in Plu/PluDa hydrogels, we can tune their viscoelastic properties, which in turn influences the behavior of encapsulated *Escherichia coli*. We reveal fundamental insight on bacterial growth rate and metabolic function in response to material's mechanics. Our results provide guidance for the design of functional and safe ELMs, by which the function of the embedded organisms is supported, controlled, and improved.

2. Results

2.1. Physicochemical Properties of Pluronic F127/Pluronic F127–Diacrylate Mixtures

Pluronic F127-based hydrogels were formed at a polymer concentration of 30% w/v, commonly used in engineered living materials studies.[16,23,29] The Plu/PluDA mixed hydrogels were prepared by mixing 30% w/v solutions of Plu and PluDA in different ratios (0/100, 25/75, 50/50, 75/25, 100/0) at 4 °C. The 30% w/v Plu/PluDA mixtures formed hydrogels at temperatures above 14 °C (Figure S1g, Supporting Information). To covalently crosslink the hydrogels, a light exposure step was used to photoinitiate the radical polymerization of the acrylate groups. This process yielded transparent hydrogels with constant polymer content, similar organization of the physical network (as reflected by the values of the shear modulus before photopolymerization, Figure S1g, Supporting Information), and different degrees of covalent crosslinking.

The combination of physical (reversible) and chemical (permanent) crosslinks confers Plu/PluDA hydrogels (named DA 0 to DA 100 in the following text) viscoelastic properties that vary with PluDA concentration. The hydrogels showed increasing storage modulus (from 18 to 43 kPa) with increasing concentration of PluDA from 0% to 100% (Figure 1b, Table S1 and Figure S2, Supporting Information). Creep-recovery experiments were performed to estimate the elastic, viscoelastic, and plastic contributions to the mechanical response (Figure S3, Supporting Information). A stress to reach a peak strain of 1% after 3 min was applied to the different hydrogels, and the recovery was monitored for further 3 min. The hydrogels behaved as viscoelastic solids (Figure 1c). The stronger viscous response of hydrogels with high Plu concentration is a consequence of the dynamic nature of a physical network (Figure 1d). The polymer chains and the micelles are associated with reversible interactions and can

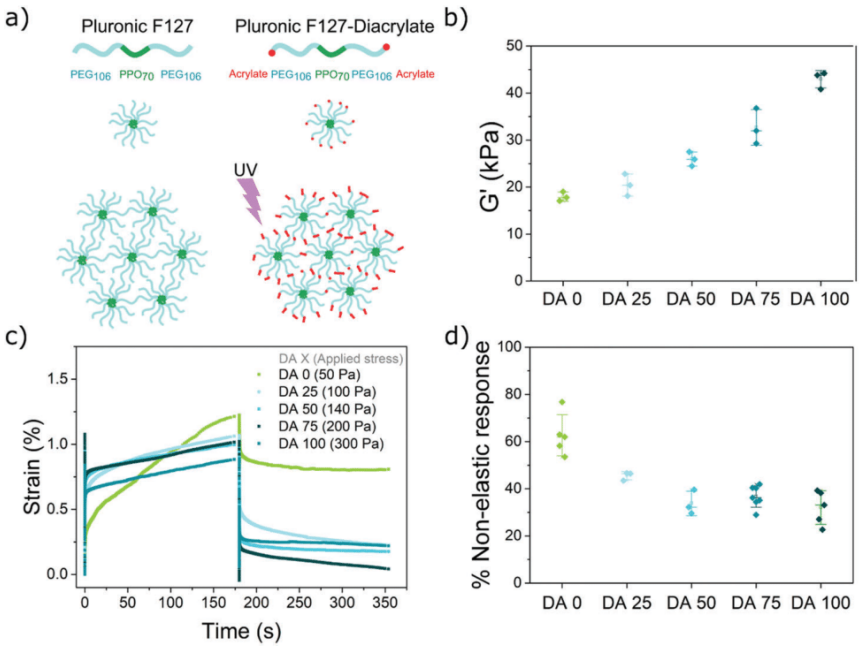

Figure 1. Structure and properties of Plu/PluDA hydrogels (DA 0-100). a) The amphiphilic Pluronic F127 chains form micellar assemblies above 14 °C. Acrylate terminated Pluronic-DA introduces covalent inter and intramicellar crosslinks after the photoinitiated radical polymerization step in the presence of Irgacure 2959. b) Storage modulus of Plu/PluDA hydrogels with increasing PluDA concentration after photoinitiated polymerization. c) Representative creep/recovery curves of Plu/PluDA hydrogels to reach a peak strain of ≈1% in 3 min. The stress applied to each hydrogel is indicated in the legend. d) Percentage of nonelastic response calculated from the creep experiment in c). ($N \geq 3$, whiskers indicate standard deviation values and horizontal line in the middle denote median).

 © 2022 The Authors. Advanced Science published by Wiley-VCH GmbH

21983844, 2022, 17, Downloaded from https://onlinelibrary.wiley.com/doi/10.1002/advs.202106026 by Inm - Leibniz-Institut Für Neue Materialien, Wiley Online Library on [17/01/2023]. See the Terms and Conditions (https://onlinelibrary.wiley.com/terms-and-conditions) on Wiley Online Library for rules of use; OA articles are governed by the applicable Creative Commons License

ADVANCED SCIENCE NEWS
www.advancedsciencenews.com

ADVANCED SCIENCE Open Access
www.advancedscience.com

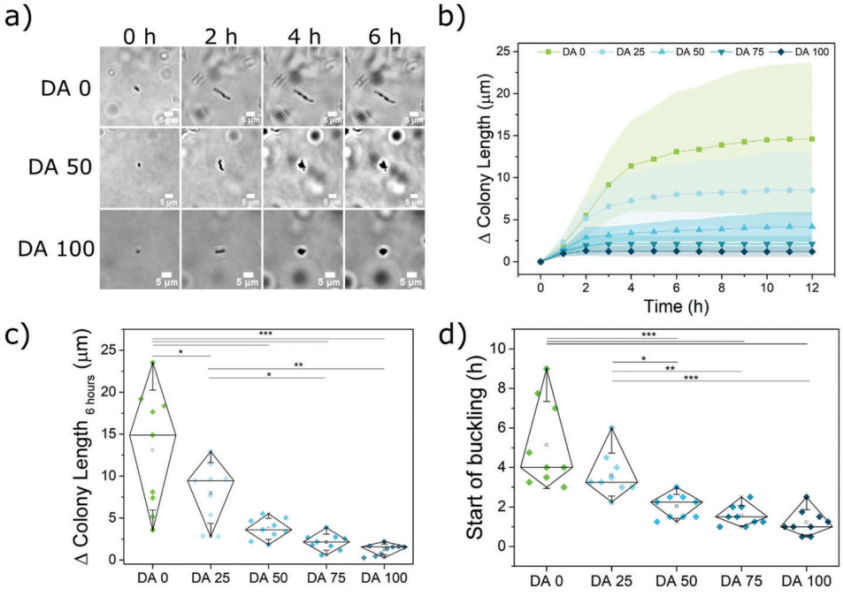

Figure 2. Bacterial growth inside DA 0-100 hydrogels inserted in microchannels, and quantification of geometrical and dimensional features of the growing colonies. a) Time lapse bright-field images of bacterial colonies within DA 0, DA 50, and DA 100 hydrogels (scale = 5 µm) representing the differences in the morphology of the growing colonies. b) Increase in the in plane length of the encapsulated bacterial colonies along the longitudinal axis of the first cell with time (mean ± standard deviation). c) Increase in the length of individual colonies at 6 h timepoint. d) Time point for the first buckling event along the longitudinal axis of a growing bacterial colony in the different hydrogels. $N = 9$ colonies from three independent experiments. (Diamond plots indicate 10 and 90 percentile values, whiskers indicate standard deviation values, p-values are calculated using one-way ANOVA with post hoc Tukey HSD test, * $p < 0.05$, ** $p < 0.01$, *** $p < 0.001$).

reorganize under the applied load.[32] With increasing PluDA ratio, the hydrogels required a higher load to reach the peak strain and showed higher elastic recovery. The covalent bonds introduced by PluDA fix the position of PluDA chains in a permanent crosslinked network and confer elastic properties to the hydrogel. This is reflected as a decline in the viscoelastic and plastic contributions to the mechanical response (Figure S3, Supporting Information), summed up as the nonelastic response in Figure 1d. In summary, the viscoelastic properties of the DA0-100 hydrogels can be tuned depending on the extent of covalent crosslinks incorporated.

2.2. Colony Growth and Metabolic Activity inside Pluronic Hydrogels with Different Ratios of Chemical Crosslinking

Plu/PluDA hydrogels loaded with bacteria in LB medium were injected in microchannels of a commercial microfluidics chip or formed as films in a microwell plate (Figure S4, Supporting Information). In both formats, bacteria were cultured under static conditions, i.e., no medium exchange. The bacteria-laden hydrogels were transparent to the eye and for microscopy. Bacteria encapsulated within microchannels were imaged by bright field microscopy. Right after encapsulation, isolated bacteria were homogeneously distributed across the hydrogel. Bacteria were not motile inside the hydrogels, presumably due to the physical confinement imposed by the hydrogel network. Bacteria divided inside the hydrogels and daughter cells remained bundled together in what we will hereafter refer to as a "colony." Initially, progeny cells arranged end-to-end, in a chain-like morphology (**Figure 2**a–c). As the length of the colony increased, buckling events occurred along the chain of growing cells, wherein 2 adjacent cells deviated from the linear chain and daughter cells emerging from them formed parallel or branched chains on continued growth (Figure 2a,d and Figure S5 and videos, Supporting Information). This was observed as an increase in the in-plane width (Figure S6b, Supporting Information) of the colonies (i.e., measured in the focal plane of imaging), or an increase in contrast when the buckled cells overlapped in the Z direction. Beyond 6 h, the colony size increased minimally. The rate and extent of colony elongation varied with the ratio of chemical crosslinking in the hydrogel. More pronounced and faster elongation was observed in hydrogels with lower chemical crosslinking ratio (Figure 2b). The overall in plane length reached by the colonies and the time before their first buckling event occurred decreased with increasing ratio of chemical crosslinking (Figure 2a–d). The mean colony length at 6 h dropped from 13.1 ± 7.1 µm for DA 0 to 1.2 ± 0.6 µm for DA 100 (Figure 2c). The first buckling event occurred at a mean time point of 5.1 ± 2.2 h for DA 0 and at 1.2 ± 0.6 h for DA 100 (Figure 2d and Figure S5 and videos, Supporting Information). This time point corresponded to the 4^{th} or 10^{th} division cycles in DA 25 or DA0 gels and to the 1^{st} or 2^{nd} division cycle in DA 100. The growing colonies in hydrogels with higher PluDA ratio showed a more rounded shape. This was reflected in the smaller in-plane aspect ratio of the colony (Figure 2a and Figure S6c,f, Supporting Information). DA 25, DA 50, and DA 75 showed intermediate behavior with regard to all the above-mentioned aspects. These results indicate that the covalent

 © 2022 The Authors. Advanced Science published by Wiley-VCH GmbH

21983844, 2022, 17, Downloaded from https://onlinelibrary.wiley.com/doi/10.1002/advs.202106026 by Inm - Leibniz-Institut Für Neue Materialien, Wiley Online Library on [17/01/2023]. See the Terms and Conditions (https://onlinelibrary.wiley.com/terms-and-conditions) on Wiley Online Library for rules of use; OA articles are governed by the applicable Creative Commons License

ADVANCED SCIENCE NEWS
www.advancedsciencenews.com

ADVANCED SCIENCE Open Access
www.advancedscience.com

21983844, 2022, 17, Downloaded from https://onlinelibrary.wiley.com/doi/10.1002/advs.202106026 by Inm - Leibniz-Institut Für Neue Materialien, Wiley Online Library on [17/01/2023]. See the Terms and Conditions (https://onlinelibrary.wiley.com/terms-and-conditions) on Wiley Online Library for rules of use; OA articles are governed by the applicable Creative Commons License

crosslinking of the hydrogel matrix impacts the growth behavior of the encapsulated bacteria in the 3D network. The higher the chemical crosslinking degree of the matrix, the slower the bacteria elongation rate, the smaller the size of the colonies (as measured within the focal plane), and the more rounded shape the colonies adopt. Interestingly, the distribution of the in-plane colony length values and of the buckling times narrowed as the ratio of chemical crosslinks in the hydrogel increased, i.e., the permanent crosslinks homogenized the morphology of the individual colonies.

A number of control experiments were performed to assess the impact of nutrients in the observed behavior of encapsulated bacteria. No differences in the diffusion rate of small molecules across the hydrogels with a different crosslinking degree were observed in FRAP experiments (Figure S7, Supporting Information). Growth experiments performed in hydrogels with a twofold nutrient concentration showed a similar shape of the growth curves and a higher in-plane growth length in DA0 and DA25 hydrogels (Figure S8, Supporting Information). These results suggest that confinement is the dominant factor regulating growth behavior of *E. coli* in hydrogels with higher chemical crosslinking degree (DA 50–100), whereas bacterial growth in hydrogels with lower chemical crosslinking degrees is also influenced by the nutrient concentration under our experimental conditions. Overall, our data confirm our hypothesis that bacterial growth in hydrogels can be regulated by tuning the design of the encapsulating network, more specifically through the type and degree of crosslinking.

To better investigate the morphology of the colonies in 3D and quantify colony volumes in the different conditions, we used confocal fluorescence microscopy to follow the colony growth. Experiments were performed in hydrogel films within a microwell plate sealed with silicone oil to prevent evaporation of water from the hydrogel while allowing O_2 diffusion. Since nuclear staining can cause genetic modifications in the bacteria and impact growth behavior, we opted to use a genetically engineered strain of *E. coli* that constitutively produces the fluorescent iLOV protein.[33] This strain grows only slightly slower than unmodified *E. coli* (Figure S9, Supporting Information), presumably as a consequence of the metabolic burden of expressing the protein. Z-stack images of the bacteria in the hydrogels were acquired at 0, 3, 6, and 24 h as shown in **Figure 3** and Figure S10 (Supporting Information). Under these conditions, isolated bacteria at 0 h grew into colonies of similar morphologies as observed with unmodified *E. coli* in the microchannels (Figure 2a). Bacteria in hydrogels with higher chemical crosslinking degrees formed smaller colonies, in agreement with our observations in the in-plane colony length extension analysis (Figure 2), with mean colony volumes ranging from 472 ± 439 μm^3 for DA 0 to 213 ± 94 μm^3 for DA 100 (Figure 3b). Higher chemical crosslinking degrees restricted the maximum size the colonies could reach. The volumes of the larger colonies (95th percentile) drop from 1115 μm^3 in DA 0 to 359 μm^3 in DA 100 (Figure 3b). Colony volume values were more homogenous (narrower distribution) in gels with higher degrees of chemical crosslinking (Figure 3b). At the whole culture level, the volume fraction of the bacteria within the gels increased with time and decreased with DA content (from 0.06% at the start to 2% for DA 0 and to 1.1% for DA 100 by 24 h) (Figure 3c, Figure S10, Supporting Information). The morphology of the colonies imaged in 3D was also different across the hydrogels. The sphericity of the colonies increased with the degree of chemical cross-linking (Figure 3d and Figure S11, Supporting Information), in agreement with the trends previously observed in the in-plane measurements and aspect ratio (Figure 2 and Figure S6c,f, Supporting Information). The distribution of bacterial volume fraction and colony sphericity was narrower in hydrogels with higher degree of covalent cross-linking (Figure 3c,d), also in line with the in-plane measurements (Figure 2). Additional experiments with iLOV producing bacteria in microchannels (Figure S12, Supporting Information) showed similar trends, indicating that the control mechanism of bacterial colony growth and morphologies imparted by the chemical crosslinks (i.e., by the mechanical constraint) is independent of metabolic variations.

We then explored whether the metabolic activity of the encapsulated bacteria was also influenced by the mechanical constraint of the hydrogel network. It is important to note that induced protein overexpression competes with metabolic resources needed for bacterial growth. Strategies to externally regulate these two processes are of utmost relevance in biotechnological production chains to maximize production yield.[34–36] For our analysis, we used a red fluorescent protein (RFP)-producing strain, which can be induced by light to drive overexpression of the protein.[12] Since our previous results indicated bacterial growth within the first few hours (Figure 2), induction was initiated right after encapsulation. RFP production was detected after 4–5 h and it increased linearly with time in all hydrogels up to 11–12 h, at which time the signal saturated (**Figure 4**b). Interestingly, the extent of protein production, quantified at 10 h, was higher in hydrogels with intermediate degrees of chemical cross-linking (DA25 and DA50) (Figure 4c). To check whether this behavior was driven by a confinement-dependent balance between metabolic activity and growth, a complementary experiment was performed in which encapsulated bacteria were first allowed to grow for 6 h (rapid growth phase) in the dark (no induction) after which protein production was induced by light. Under these conditions, the extent of RFP production did not vary appreciably across the different gel compositions (Figure S13, Supporting Information), even though the gels with higher cross-linking degrees would have a lower number of cells. This suggests that the slower growing colonies in hydrogels with higher chemical crosslinking were more efficient in RFP production compared to colonies growing faster in physical hydrogels. Thus, bacterial growth restrictions imposed by the mechanical properties of the Plu/PluDA hydrogel network regulated the metabolic activity of the encapsulated cells. We do not expect differences in the accessibility to nutrients or oxygen inside individual colonies because of their small size, typically diameter <30 μm. These results show that hydrogel networks combining reversible and permanent crosslinks can be used as external modulators of the growth and metabolic activity of cells in ELMs.

2.3. Correlation between Bacteria Behavior and Mechanical Properties of the Hydrogel

Figure 5 summarizes the trends observed in bacterial behavior and mechanics of Plu/PluDA hydrogels. The extent to which the colony volume grows correlates with the nonelastic component

 © 2022 The Authors. Advanced Science published by Wiley-VCH GmbH

ADVANCED SCIENCE NEWS
www.advancedsciencenews.com

ADVANCED SCIENCE Open Access
www.advancedscience.com

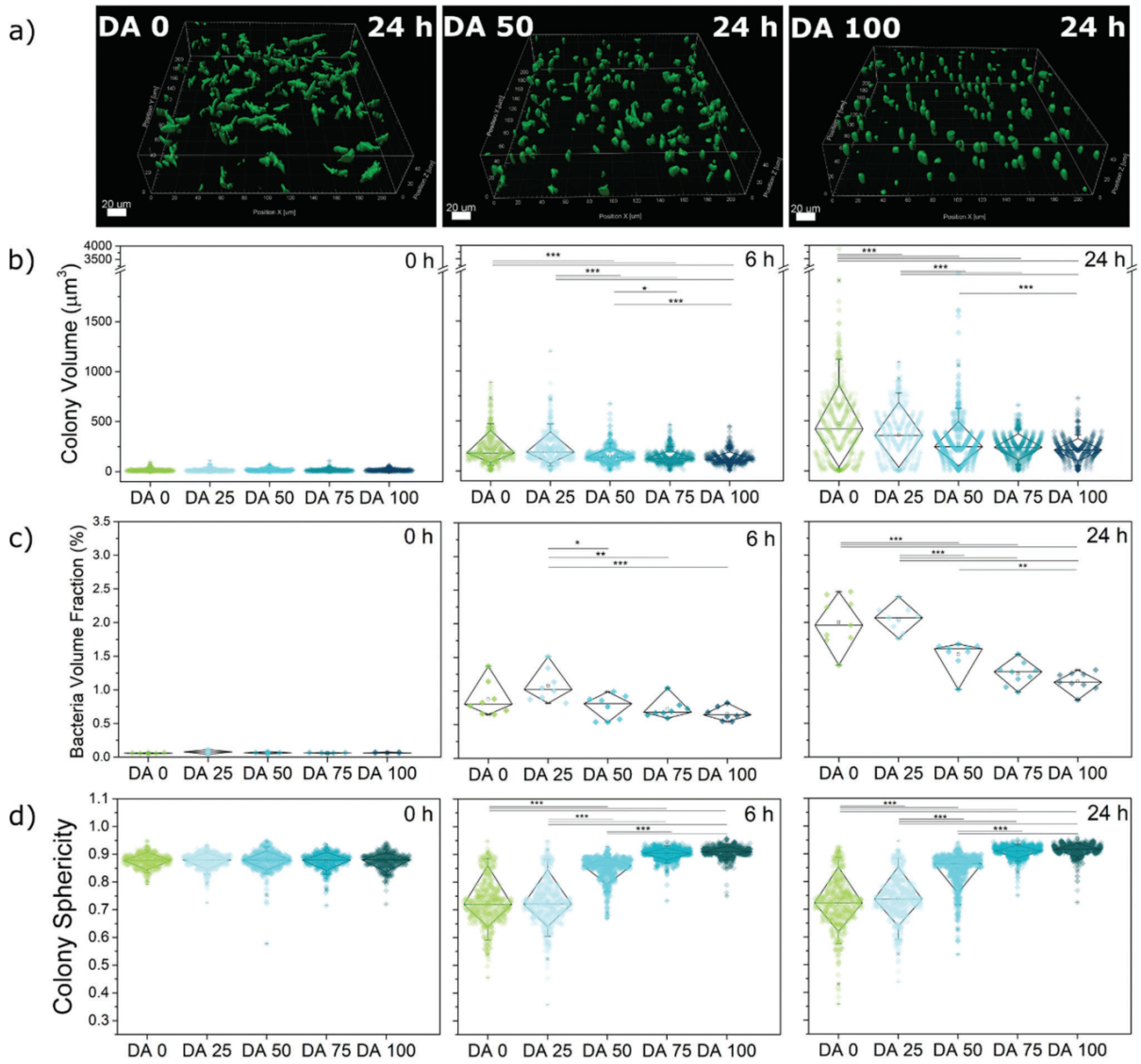

Figure 3. Quantification of bacterial growth in 3D within DA 0-100 matrices formed in microwells. a) Exemplary volumetric scan of iLOV producing bacterial colonies inside the hydrogels after 24 h. This visualization is presented using surface masks made with the IMARIS software (scale = 20 µm). b) Quantified colony volume within DA 0-100 hydrogels at 0, 6, and 24 h timepoints. c) Volume fraction of bacterial colonies within DA 0-100 hydrogels at 0, 6, and 24 h timepoints. d) Sphericity values for individual colonies within DA 0-100 hydrogels at 0, 6, and 24 h timepoints. (Diamond plots indicate median, 10 and 90 percentile values, whiskers indicate 5 and 95 percentile values, 338 ≥ Number of colonies ≥ 667 from 3 individual experiments, *p*-values are calculated using one-way ANOVA with post hoc Tukey HSD test, * $p < 0.05$, ** $p < 0.01$, *** $p < 0.001$).

of the mechanical response (Figure 5 and Figure S14, Supporting Information). Protein production showed a more complex dependence of the mechanical properties of the gel, with a biphasic behavior as a function of elasticity. Mechanical restriction seems to favor increased protein production rates, possibly by slowing down growth rates. Beyond a certain level of restriction, the growth is suppressed to such an extent that reduces the overall protein production. A recent report demonstrated that photosynthesis in cyanobacteria can also be regulated by mechanical confinement,[37] corroborating that confinement could be used as external factor to regulate metabolic processes in bacteria.

3. Discussion

During biofilm formation, soil homeostasis, or invasion of biological tissues, microorganisms grow within confined spaces and push against their natural surroundings to accommodate new cells and grow as colony. The resulting compressive forces on

 © 2022 The Authors. Advanced Science published by Wiley-VCH GmbH

21983844, 2022, 17, Downloaded from https://onlinelibrary.wiley.com/doi/10.1002/advs.202106026 by Inm - Leibniz-Institut Für Neue Materialien, Wiley Online Library on [17/01/2023]. See the Terms and Conditions (https://onlinelibrary.wiley.com/terms-and-conditions) on Wiley Online Library for rules of use; OA articles are governed by the applicable Creative Commons License

ADVANCED SCIENCE NEWS
www.advancedsciencenews.com

ADVANCED SCIENCE Open Access
www.advancedscience.com

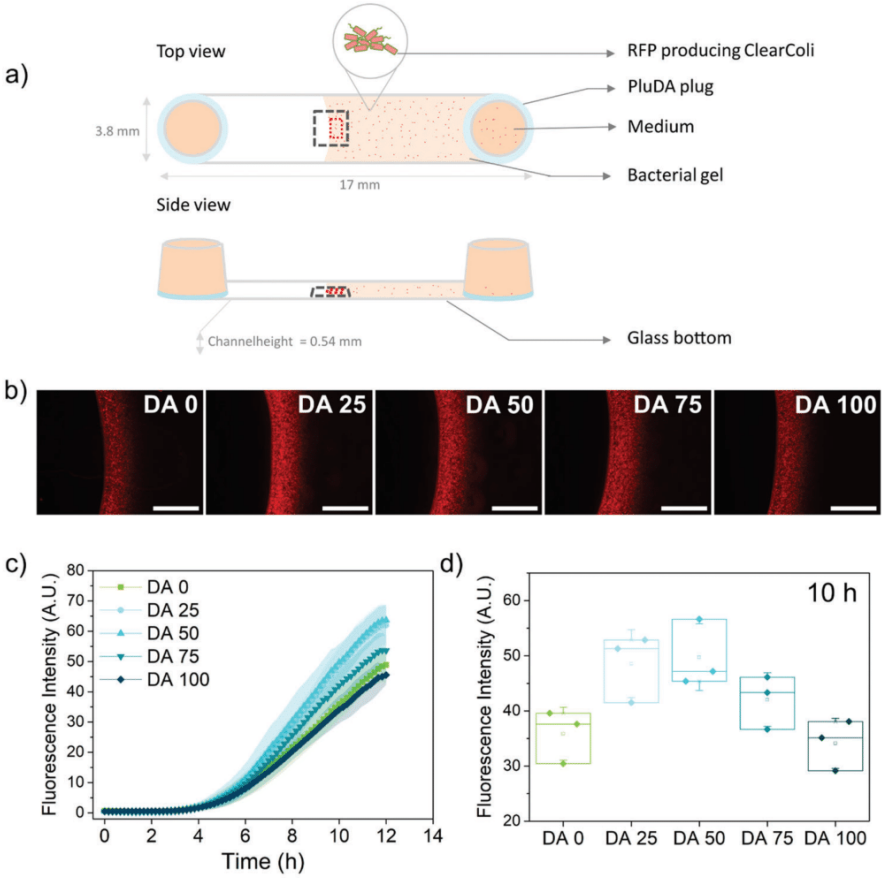

Figure 4. Quantification of protein production by bacteria encapsulated in DA 0-100 hydrogels. a) Schematic of the bacterial gels within the microchannels with an open end. The black dotted box (3636 × 2727 μm^2) represents the observed field of view in the microscope, taken at ≈ 0.27 mm height, and the red dotted box (200 × 600 μm^2) is the area considered for RFP intensity measurement. b) Fluorescence images of RFP producing bacterial gels indicating RFP expressed by the encapsulated bacterial colonies at 10 h (induction, i.e., blue light illumination started at 0 h, scale = 1000 μm). c) Quantification of fluorescence intensity indicating RFP production in the hydrogels during 12 h (mean ± standard deviation). d) RFP production values within different hydrogel compositions at 10 h ($N = 3$, box represents 25 and 75 percentile values, whiskers indicate standard deviation).

the cell population are dependent on the mechanical properties of the local microenvironment, cell–cell and cell–matrix interactions and mechanical instabilities at cellular scale,[38] and have been shown to influence cell size,[39] to limit cell growth[40,41] and to delay cell cycle[42] in studies with microorganisms in synthetic model systems.[43,44] Physical models under discussion consider self-driven jamming and build-up of large mechanical pressures as natural principles behind the collective growth and organization of a colony in 3D confinement.[42,45] Macromolecular crowding and slower diffusion inside the cell, as a consequence of confined growth, have been recently suggested as inherent biophysical feedback routes that can regulate the metabolic behavior of microorganisms in confinement.[46] Envelope proteins, motility regulators, and secreted extracellular matrix seem to play a role as sensors and triggers of cellular pathways that convert mechanical inputs in biochemical signals or vice versa.[41,47–50] Understanding how bacterial colonies can be regulated by the embedding natural microenvironment is relevant to combat infections or improve soil fertility, but also to improve the performance of biofilters, microbial fuel cells, and in general ELMs of any kind.[1–3]

Most biophysical studies of mechanomicrobiology in 3D spatial confinement have been performed in microchannels of different dimensions[42] or in microdroplets.[51] Hydrogel networks are alternative model systems for such studies.[21,52,53] In physical hydrogel networks (agarose,[12,21] alginate[13]) formed by reversible crosslinks that can rearrange dynamically and dissipate mechanical stress as bacteria push, bacteria grow into large colonies and eventually outgrow. In contrast, in hydrogels stabilized by covalent crosslinks (e.g., PEGDA,[52] polyacrylamide,[10] acrylate-modified Pluronic F127[16,29]), the bacteria grow as small colonies or remain as single cells over time, presumably as a consequence of increasing compressive forces due to the restricted ability of the surrounding material to dissipate growth-related stress. The DA 0-100 hydrogels used in our work contain physical and covalent (i.e., permanent) crosslinks at adjustable ratios and yield encapsulating materials with tunable viscoelasticity within a range that allows tuning the behavior of embedded growing

 © 2022 The Authors. Advanced Science published by Wiley-VCH GmbH

21983844, 2022, 17, Downloaded from https://onlinelibrary.wiley.com/doi/10.1002/advs.202106026 by Inm - Leibniz-Institut Für Neue Materialien, Wiley Online Library on [17/01/2023]. See the Terms and Conditions (https://onlinelibrary.wiley.com/terms-and-conditions) on Wiley Online Library for rules of use; OA articles are governed by the applicable Creative Commons License

ADVANCED SCIENCE NEWS
www.advancedsciencenews.com

ADVANCED SCIENCE Open Access
www.advancedscience.com

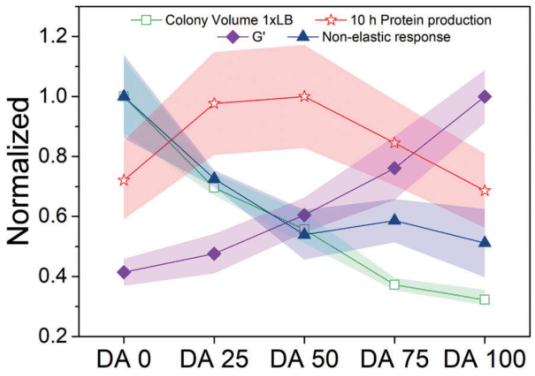

Figure 5. Comparative representation of normalized material's properties and bacterial response as a function of Plu/PluDA matrix composition. Normalized values of shear storage modulus *G'* and nonelastic response (from Figure 1), 95th percentile volumes of colonies after 24 h (from Figure 3), and protein production after 10 h (from Figure 4). The values were normalized with respect to the highest value in each category (Original values plotted in Figure S14, Supporting Information). The symbols and shaded regions of the normalized colony volume data indicate 95 ± 2 percentile value range, for all other data the symbols and shaded regions indicate mean ± SD.

E. coli populations from a non-restricted to a restricted mode. In these hydrogels, bacteria form compact, viable and metabolically active colonies of smaller sizes and at slower rates when the ratio of permanent crosslinks increases. Rod-shaped bacteria exert longitudinal forces during growth, contributed by their turgor pressure (30–300 kPa for *E. coli*) and limited by the rate of cell wall synthesis.[21] The stress applied to a surrounding hydrogel has been estimated around ≈10 kPa for *E. coli* at their ends.[54] Our results suggest that this stress is enough to deform the physically crosslinked matrix in Plu hydrogels, where bacteria form large colonies and can outgrow if nutrients are available.[28] However, Plu/PluDA hydrogels with PluDA fraction >25% restrict bacterial growth and colony size, independent of nutrient availability, in a way that seems to correlate with their higher mechanical resistance to deformation (Figure 5). The growth restriction in turn influences the metabolism of the bacteria, leading to faster-induced protein overexpression. Notably, the tunability of the 30% w/v Plu/PluDA hydrogels by varying only the ratio of the components affects both the elastic and viscoelastic response of the final gel, which limits the current study from unambiguously determining the influence of specific mechanical components on bacterial behavior. A possible strategy to overcome this limitation in the following studies will be to identify Plu/PluDA hydrogel compositions having different polymer concentrations[31] that yield the same storage moduli but have different viscoelastic properties based on the degree of permanent crosslinks.

The ability of hydrogels with permanent crosslinks to restrict the size of the bacterial colonies allows for biocontainment of the bacterial population inside the hydrogel matrix, a highly desired feature in ELMs and related devices.[55] 25–30 wt% Plu based hydrogels have been used to encapsulate bacteria (*Escherichia coli*)[29] and yeast (*Saccharomyces cerevisiae*)[16,17] in ELMs, and maintain bacteria viability for months.[16] Such Plu/PluDA based hydrogels are stable in vitro for days[23,56] to years[16] and in vivo for weeks[57] to months.[58] Although the specific mechanisms underlying bacterial mechano-regulation in our study remain to be elucidated, the Plu/PluDA compositions studied in this article can be used to optimize the functionality of bacteria-based ELMs.

4. Conclusion

This study explores the growth and protein production of encapsulated bacteria using DA0-100 hydrogels with tunable viscoelasticity. Our results indicate that bacterial functions like growth and metabolic production can be regulated by engineering the mechanical properties of the Plu/PluDA encapsulating matrix, independently of the access to nutrients. This is relevant for the design and performance optimization of ELMs containing functional organisms.

5. Experimental Section

Preparation of Precursors Solutions: Pluronic diacrylate (PluDA) was synthesized by reaction of Pluronic F127 (Plu) with acryloyl chloride in the presence of triethylamine according to a reported protocol.[31] 30% (w/v) Plu and PluDA stock solutions in Milli-Q water (for rheological measurements) or LB medium (for bacterial growth measurements) containing Irgacure 2959 photoinitiator at 0.2% w/v were prepared and stored at 4 °C and allowing them to form the gel at room temperature for 10 min.[59] The composition of DA0 and DA100 hydrogels corresponded to that of the stock solutions of Plu and PluDA, respectively. DA 25, DA 50, and DA 75 hydrogels were prepared by mixing of the stock solutions in ratios as shown in Table S1 (Supporting Information). For the photoinitiated crosslinking of the hydrogels, these were exposed to UV light (365 nm, 6 mW cm^{-2}) using a OmniCure Series 1500 lamp during 60 s (Milli Q water solutions) or 120 s (LB medium solutions).

Rheological Studies: The rheological properties were measured using a rotational rheometer (DHR3, TA Instruments) using a parallel plate geometry. A 20 mm Peltier plate/UV transparent plate was used as bottom plate and a smooth stainless steel 12 mm disk was used as top plate. The rheometer was equipped with a UV Source (OmniCure, Series 1500, 365 nm, 6 mW cm^{-2}) for illumination of the hydrogel samples between the rheometer plates. Experiments were performed at room temperature unless otherwise mentioned. To avoid drying of the sample by evaporation during testing, a solvent trap was used, and the sample was sealed with silicone oil. A volume of precursor solution of 35 µL and a gap between plates of 300 µm was used for the experiments. All tests were initiated 10 min after loading the sample on the rheometer.

Strain sweeps were conducted from 0.001% to 1000% at a frequency of 1 Hz. Frequency sweeps were conducted from 0.01 to 100 Hz at a constant strain of 0.1% with a controlled temperature of 23 °C. From these experiments, the linear viscoelastic region was identified (Figure S1a–f, Supporting Information). Temperature sweep experiments were carried out from 4 °C to 40 °C at a 5 °C min^{-1} ramp rate, 1 Hz frequency, and 0.1% strain value (found to be in the linear viscoelastic range). These experiments were used to characterize the gelation temperature of the solutions (Figure S1g, Supporting Information). The gelation point (defined as crossover point of *G'* and *G''*) in the temperature sweep experiment was 15.5 °C for 30% DA 0 solutions and 14 °C for DA 100. Time sweep experiments to monitor the changes in the mechanical properties of the hydrogels during crosslinking were performed. For this purpose, samples were irradiated at 365 nm (6 mW cm^{-2}) during 60 s at room temperature, and the changes in the shear moduli were recorded for a total of 7 min (Figure S2, Supporting Information). All time sweep experiments were performed at least in triplicate.

Creep Recovery Experiments: Creep-recovery experiments at peak strain of 1% after 3 min were performed for Plu/PluDA hydrogels. The applied shear stress was monitored during the creep phase and for further 3 min after removal of the shear stress (recovery phase). The contributions of the

 © 2022 The Authors. Advanced Science published by Wiley-VCH GmbH

21983844, 2022, 17, Downloaded from https://onlinelibrary.wiley.com/doi/10.1002/advs.202106026 by Inm - Leibniz-Institut Für Neue Materialien, Wiley Online Library on [17/01/2023]. See the Terms and Conditions (https://onlinelibrary.wiley.com/terms-and-conditions) on Wiley Online Library for rules of use; OA articles are governed by the applicable Creative Commons License

ADVANCED SCIENCE NEWS
www.advancedsciencenews.com

ADVANCED SCIENCE Open Access
www.advancedscience.com

elastic, viscoelastic and plastic phases were quantified from the recovery phase (Figure S3, Supporting Information).[60] The viscoelastic and plastic contributions are summed up as nonelastic contributions.

Bacteria Cultures: An endotoxin-free strain of *E. coli* (ClearColi BL21(DE3), BioCat)[12] was used for the bacterial growth studies. It was transformed with the plasmid pUC19 to enable Ampicillin resistance and minimize the risk of contamination in the culture. Bacterial cultures were grown for 16 h at 35 °C, 180 rpm in LB Miller medium supplemented with 50 μg mL^{-1} of Ampicillin to an optical density at 600 nm wavelength (OD600) value between 0.5 and 1. For the fluorescence-based experiments, we used a previously optogenetically engineered strain of ClearColi that produces red fluorescence protein (RFP) when illuminated with blue light,[12] and a ClearColi strain that constitutively produces iLOV protein. The iLOVf gene insert was amplified from the pET28-iLOVf plasmid (Addgene #63723) and assembled into the pLp-3050sNuc vector[61] (Addgene #122030) using Gibson Assembly. The iLOVf gene is under the constitutive expression of the P48 promoter.[62] The construct was sequence verified and subsequently transformed in the Clearcoli BL21 DE3 strain and maintained with the additional supplementation of 200 μg mL^{-1} Erythromycin. Since these bacteria grew slightly slower than the pUC19 harboring variants (Figure S9, Supporting Information), they were initially cultured for 16 h at 35 °C, 220 rpm in LB Miller medium until an optical density at 600 nm wavelength (OD600) value of 0.2–1 was reached. The RFP producing strain harbors the plasmid pDawn-RFP (pDnSR) that encodes blue-light activatable gene expression and provides kanamycin resistance. The red fluorescence signal was used to image bacterial growth inside the hydrogels and to quantify protein production in hydrogel-encapsulated bacterial populations. The bacteria were cultured for 16 h at 35 °C, 220 rpm in LB Miller medium supplemented with 50 μg mL^{-1} of Kanamycin to an optical density at 600 nm wavelength (OD600) value between 0.5 and 1.5. All procedures with the light-inducible bacterial strain were performed either in the dark or under a laminar hood with an orange film that cuts off blue light.

Bacterial Encapsulation in Hydrogels: Hydrogels with 30% (w/v) polymer concentration were prepared by mixing stock solutions of Plu and PluDA precursors in bacterial medium with bacterial suspensions (at OD_{600} of 0.5–4 × 10^7 cells mL^{-1}) at 9/1 (v/v) ratio to achieve a final OD600 of 0.05 within the gels. This concentration allowed individual bacteria to be homogeneously dispersed in the hydrogels and most to grow into individual bacterial colonies that did not coalescence during 24 h. This allowed quantification of individual colony dimensions and morphologies throughout the hydrogel. The solutions were stored in ice before and after mixing. At this temperature, Pluronic solutions are liquid and can be homogeneously mixed with the bacteria by pipetting at the start of the experiment.[45] Hydrogels were produced in two different formats: i) Inside channels using Ibidi μ-Slides VI 0.4 (17 × 3.8 × 0.4 mm^3) or Ibidi μ-Slide VI 0.5 Glass Bottom (17 × 3.8 × 0.54 mm^3) consisting of six parallel microfluidic channels and ii) inside ibidi μ-Slide angiogenesis microwells with polymer coverslip bottom (Figure S4, Supporting Information). For the in-plane colony length extension analysis (Figure 2a), Ibidi μ-Slides VI 0.4 were used. 30 μL of this pluronic/bacteria suspension was pipetted into the microchannel, placed on ice, filling the entire channel. For the high magnification confocal microscopy experiments to determine the colony volume, 30 μL of this pluronic/iLOV-producing bacteria suspension was pipetted into the Ibidi μ-Slide VI 0.5 Glass Bottom microchannel (Figure S12, Supporting Information). Experiments in Figure 3a were done with Pluronic/iLOV-producing bacteria suspensions (10 μL) pipetted into the micro-well of the μ-Slide angiogenesis dish. Measurements were done near the center of the wells and 50 μm from the bottom. Ibidi μ-Slides VI 0.5 with glass bottom were used for the experiments with pluronic/RFP-producing bacteria suspension (Figure 4). 20 μL suspension was pipetted into the microchannel and filled up to half the length of the channel, resulting in a sharp hydrogel-air interface (Figure 4), to enable oxygen availability required for folding of the RFP protein.[12] RFP production was measured 50 μm from the edge of the gel–air interface using a 200 × 600 $μm^2$ area as the region of interest. The reservoir at both the ends of the channel was plugged with 20 μL of DA 100 gel and 50 μL of medium to avoid drying of the hydrogel in the channel for all the experiments with channels. The microculture was kept at room temperature for 10 min for physically cross-linked gelation to occur and exposed for 120 s to a UV Lamp inside Alpha Innotech FluorChem Q system (Biozym, Oldendorf, Germany) (6 mW cm^{-2}) which was the illumination step used to initiate the photopolymerization of the acrylate groups and covalent crosslinking of the hydrogels. This illumination mildly affects bacterial growth rates and protein production (Figure S15, Supporting Information). All hydrogel compositions were illuminated with the same intensity and for the same period of time irrespective of the acrylate content. The bacterial gels in μ-Slide angiogenesis microwells were topped with 20 μL of silicone oil (350 cSt, Sigma-Aldrich) to prevent drying of the hydrogel during the experiment.

Imaging and Quantification of In-Plane Length Extension of Colonies inside the Channels: Brightfield microscopy analysis was performed using Nikon Ti-Eclipse (Nikon Instruments Europe B.V., Germany) microscope with 20 × S Plan Fluor objective with a numerical aperture of 0.45 and a working distance of 8 mm, Sola SE 365 II (Lumencor Inc., Beaverton, USA) solid-state illumination device and an Andor Clara (Andor Technology Ltd, Belfast, UK) CCD camera for detection. Ibidi μ-Slides VI loaded with the bacterial hydrogels were incubated at 37 °C and 5% CO_2 using an Okolab (Okolab SRL, Pozzuoli, Italy) incubation chamber coupled to the microscope. Imaging locations were selected near the middle of the channel length and about halfway between the bottom and top of the channel. Such a position was chosen to minimize the possibility of variations in material properties (swelling, dissolution) or nutrient variability that might occur due to diffusion of the medium at the reservoirs. Changes in material properties of the gel near the reservoirs were inferred from the movement of the bacterial gel in and out of the imaging field during the experiment. Time-lapse imaging was performed from 30 min to 1 h after introducing the bacterial gels in the channel slides and subsequently in the incubation chamber to ensure that the samples reach 37 °C. Time-lapse imaging was done with an interval of 15 min for 12 h. Each type of experiment was performed in triplicates.

Quantification of Colony Growth: The pluronic/iLOV-producing bacteria samples in the ibidi μ-Slide angiogenesis micro-wells were imaged by Zeiss LSM 880 confocal laser scanning microscopy (CLSM) at 0, 3, 6, and 24 h timepoints. Two-photon laser was used for imaging the iLOV protein producing bacterial colonies.[63] The exposure conditions were optimized for minimizing cell photodamage using the objective LD C-Apochromat 40×/1.1 W Korr M27, detection wavelength 499–624 nm, laser wavelength of 880 nm, and power of 5%. Z-stacks of 50.102 μm were taken in steps of 0.65 μm. Images of a size of (*xy*) 212.5 × 212.5 μm were acquired with a resolution 512 × 512 pixels, twofold line averaging, and using constant values for laser power (5%) and pixel dwell time of 2.06 μs. The digital gain value was 800 for 0, 3, and 6 h measurements and adjusted to 730 for 24 h measurements, as some pixels reached oversaturation. Imaris software (Version 9.0, Bitplane, Zurich, Switzerland) was used to process CLSM image z-stacks to create 3D images using the Imaris surface tool. The surfaces were generated with smooth function set to 0.5 μm, the background threshold to 10 μm and the minimum surface voxels limit to 10. The sphericity was quantified as the ratio between the volumes of the colony to its surface area (Imaris surface tool). Volume fraction of the bacterial colonies covering the hydrogel samples was calculated as the ratio of sum of all colony volumes and the volume of the observed hydrogel field of view. For calculation of single colony volumes, the colonies touching the edges of the field of view and those which coalesced together were avoided. Colonies below the volumes of 5 $μm^3$ (which was approximately the volume of single bacterium) were neglected.

Protein Production in the Hydrogels: Ibidi μ-Slide VI 0.5 Glass Bottom microfluidic channels loaded with bacterial hydrogels were used in these experiments. The culture was kept in static conditions at 37 °C using an incubation chamber coupled to a BZ-X800 (Keyence, Osaka, Japan) microscope. For fluorescence imaging to detect the RFP production, filter channel TRITC (BZ-X Filter OP-87764, excitation 545/25, emission 605/70) was used. RFP production was activated, at 0 h/6 h, by illuminating the channels with blue light (BZ-X Filter GFP OP-87763, excitation 470/40, emission 525/50) pulses of 500 ms every 10 min for 18 h using the 4× objective (Keyence Plan Apochromat, numerical aperture 0.20, working distance 20 mm) of the microscope. The light intensity and exposure settings were

 © 2022 The Authors. Advanced Science published by Wiley-VCH GmbH

21983844, 2022, 17, Downloaded from https://onlinelibrary.wiley.com/doi/10.1002/advs.202106026 by Inm - Leibniz-Institut Für Neue Materialien, Wiley Online Library on [17/01/2023]. See the Terms and Conditions (https://onlinelibrary.wiley.com/terms-and-conditions) on Wiley Online Library for rules of use; OA articles are governed by the applicable Creative Commons License

ADVANCED SCIENCE NEWS
www.advancedsciencenews.com

ADVANCED SCIENCE Open Access
www.advancedscience.com

optimized for detecting early time-point generation of fluorescence and following increase in intensity for several hours. Image processing and analyses were performed using Fiji edition of ImageJ (ImageJ Java 1.8.0). Quantification of the fluorescence intensities was done by determining the mean grey value, at a height of ≈0.27 mm (mid-point of channel thickness) and 50 µm away from the edge (as larger colonies were observed near edge, owing to possible differences in the mechanical properties at the interface with air[20,21]) within a 200 × 600 µm^2 area of the gel and subtracting the mean grey value of the background.

Statistical Analyses: One-way analysis of variance (ANOVA) with post hoc Tukey HSD test was performed with results involving more than three data points. Differences were considered statistically significant at * $p < 0.05$, ** $p < 0.01$, *** $p < 0.001$. Analyses were performed with Origin Pro 9.1 software. Concrete parameters used for the different types of analyses performed have been described in the sections and figure captions of the related experiments.

Supporting Information

Supporting Information is available from the Wiley Online Library or from the author.

Acknowledgements

The authors acknowledge support from the Deutsche Forschungsgemeinschaft's Collaborative Research Centre, SFB 1027, and the Leibniz Science Campus on Living Therapeutic Materials, LifeMat. pET28-iLOVf plasmid was a gift from Prof. Brian Smith, Addgene #63723. pLp-3050sNuc vector was a gift from Prof. Geir Mathiesen, Addgene #122030. The authors also thank Dr. Mitchell Han for his valuable insights in image analysis and Sourik Dey for iLOV plasmid transformation.

Open Access funding enabled and organized by Projekt DEAL.

Conflict of Interest

The authors declare no conflict of interest.

Data Availability Statement

The data that support the findings of this study are available from the corresponding author upon reasonable request.

Keywords

bacterial hydrogel, bacterial–materials interactions, cell encapsulation, dynamic hydrogel, engineered living material

Received: December 27, 2021
Revised: March 18, 2022
Published online: April 11, 2022

[1] A. Rodrigo-Navarro, S. Sankaran, M. J. Dalby, A. del Campo, M. Salmeron-Sanchez, *Nat. Rev. Mater.* **2021**, *6*, 1175.
[2] L. Xu, X. Wang, F. Sun, Y. Cao, C. Zhong, W.-B. Zhang, *Curr. Opin. Solid State Mater. Sci.* **2021**, *5*, 105.
[3] T. C. Tang, B. An, Y. Huang, S. Vasikaran, Y. Wang, X. Jiang, T. K. Lu, C. Zhong, *Nat. Rev. Mater.* **2021**, *6*, 332.
[4] C. Knierim, M. Enzeroth, P. Kaiser, C. Dams, D. Nette, A. Seubert, A. Klingl, C. L. Greenblatt, V. Jérôme, S. Agarwal, R. Freitag, A. Greiner, *Macromol. Biosci.* **2015**, *15*, 1052.
[5] J. Pu, Y. Liu, J. Zhang, B. An, Y. Li, X. Wang, K. Din, C. Qin, K. Li, M. Cui, S. Liu, Y. Huang, Y. Wang, Y. Lv, J. Huang, Z. Cui, S. Zhao, C. Zhong, *Adv. Sci.* **2020**, *7*, 1903558.
[6] C. Gilbert, T. C. Tang, W. Ott, B. A. Dorr, W. M. Shaw, G. L. Sun, T. K. Lu, T. Ellis, *Nat. Mater.* **2021**, *20*, 691.
[7] L. K. Rivera-Tarazona, V. D. Bhat, H. Kim, Z. T. Campbell, T. H. Ware, *Sci. Adv.* **2020**, *6*, eaax8582.
[8] B. An, Y. Wang, X. Jiang, C. Ma, M. Mimee, F. Moser, K. Li, X. Wang, T. C. Tang, Y. Huang, Y. Liu, T. K. Lu, C. Zhong, *Matter* **2020**, *3*, 2080.
[9] S. Balasubramanian, K. Yu, A. S. Meyer, E. Karana, M. E. Aubin-Tam, *Adv. Funct. Mater.* **2021**, *31*, 2011162.
[10] S. Sankaran, J. Becker, C. Wittmann, A. Campo, *Small* **2019**, *15*, 1804717.
[11] L. M. González, N. Mukhitov, C. A. Voigt, *Nat. Chem. Biol.* **2020**, *16*, 126.
[12] S. Sankaran, A. Campo, *Adv. Biosyst.* **2019**, *3*, 1800312.
[13] K. Witte, A. Rodrigo-Navarro, M. Salmeron-Sanchez, *Mater. Today Bio* **2019**, *2*, 100011.
[14] S. Guo, E. Dubuc, Y. Rave, M. Verhagen, S. A. E. Twisk, T. Van Der Hek, G. J. M. Oerlemans, M. C. M. Van Den Oetelaar, L. S. Van Hazendonk, M. Brüls, B. V. Eijkens, P. L. Joostens, S. R. Keij, W. Xing, M. Nijs, J. Stalpers, M. Sharma, M. Gerth, R. J. E. A. Boonen, K. Verduin, M. Merkx, I. K. Voets, T. F. A. De Greef, *ACS Synth. Biol.* **2020**, *9*, 475.
[15] K. Schulz-Schönhagen, N. Lobsiger, W. J. Stark, *Adv. Mater. Technol.* **2019**, *4*, 1900266.
[16] T. G. Johnston, S. F. Yuan, J. M. Wagner, X. Yi, A. Saha, P. Smith, A. Nelson, H. S. Alper, *Nat. Commun.* **2020**, *11*, 563.
[17] A. Saha, T. G. Johnston, R. T. Shafranek, C. J. Goodman, J. G. Zalatan, D. W. Storti, M. A. Ganter, A. Nelson, *ACS Appl. Mater. Interfaces* **2018**, *10*, 13373.
[18] M. Perullini, M. Amoura, C. Roux, T. Coradin, J. Livage, M. L. Japas, M. Jobbágy, S. A. Bilmes, *J. Mater. Chem.* **2011**, *21*, 4546.
[19] A. M. Duraj-Thatte, A. Manjula-Basavanna, N. M. D. Courchesne, G. I. Cannici, A. Sánchez-Ferrer, B. P. Frank, L. van't Hag, S. K. Cotts, D. H. Fairbrother, R. Mezzenga, N. S. Joshi, *Nat. Chem. Biol.* **2021**, *17*, 732.
[20] B. Pabst, B. Pitts, E. Lauchnor, P. S. Stewart, *Antimicrob. Agents Chemother.* **2016**, *60*, 6294.
[21] H. H. Tuson, G. K. Auer, L. D. Renner, M. Hasebe, C. Tropini, M. Salick, W. C. Crone, A. Gopinathan, K. C. Huang, D. B. Weibel, *Mol. Microbiol.* **2012**, *84*, 874.
[22] M. Werthén, L. Henriksson, P. Ø. Jensen, C. Sternberg, M. Givskov, T. Bjarnsholt, *APMIS* **2010**, *118*, 156.
[23] H. Priks, T. Butelmann, A. Illarionov, T. G. Johnston, C. Fellin, T. Tamm, A. Nelson, R. Kumar, P. J. Lahtvee, *ACS Appl. Bio Mater.* **2020**, *3*, 4273.
[24] D. Indana, P. Agarwal, N. Bhutani, O. Chaudhuri, *Adv. Mater.* **2021**, *33*, 2101966.
[25] S. R. Caliari, J. A. Burdick, *Nat. Methods* **2016**, *13*, 405.
[26] C. M. Madl, L. M. Katz, S. C. Heilshorn, *ACS Macro Lett.* **2018**, *7*, 1302.
[27] M. Rizwan, A. E. G. Baker, M. S. Shoichet, *Adv. Healthcare Mater.* **2021**, *10*, 2100234.
[28] M. Lufton, O. Bustan, B. hen Eylon, E. Shtifman-Segal, T. Croitoru-Sadger, A. Shagan, A. Shabtay-Orbach, E. Corem-Salkmon, J. Berman, A. Nyska, B. Mizrahi, *Adv. Funct. Mater.* **2018**, *28*, 1801581.
[29] X. Liu, H. Yuk, S. Lin, G. A. Parada, T. C. Tang, E. Tham, C. de la Fuente-Nunez, T. K. Lu, X. Zhao, *Adv. Mater.* **2018**, *30*, 1704821.
[30] R. Basak, R. Bandyopadhyay, *Langmuir* **2013**, *29*, 4350.
[31] M. Di Biase, P. De Leonardis, V. Castelletto, I. W. Hamley, B. Derby, N. Tirelli, *Soft Matter* **2011**, *7*, 4928.

 © 2022 The Authors. Advanced Science published by Wiley-VCH GmbH

21983844, 2022, 17, Downloaded from https://onlinelibrary.wiley.com/doi/10.1002/advs.202106026 by Inm - Leibniz-Institut Für Neue Materialien, Wiley Online Library on [17/01/2023]. See the Terms and Conditions (https://onlinelibrary.wiley.com/terms-and-conditions) on Wiley Online Library for rules of use; OA articles are governed by the applicable Creative Commons License

[32] H. Li, F. Liu, Z. Li, S. Wang, R. Jin, C. Liu, Y. Chen, *ACS Appl. Mater. Interfaces* **2019**, *11*, 17925.
[33] T. Drepper, T. Eggert, F. Circolone, A. Heck, U. Krauß, J. K. Guterl, M. Wendorff, A. Losi, W. Gärtner, K. E. Jaeger, *Nat. Biotechnol.* **2007**, *25*, 443.
[34] A. Milias-Argeitis, M. Rullan, S. K. Aoki, P. Buchmann, M. Khammash, *Nat. Commun.* **2016**, *7*, 12546.
[35] M. Pasini, A. Fernández-Castané, A. Jaramillo, C. de Mas, G. Caminal, P. Ferrer, *New Biotechnol.* **2016**, *33*, 78.
[36] O. Borkowski, C. Bricio, M. Murgiano, B. Rothschild-Mancinelli, G. B. Stan, T. Ellis, *Nat. Commun.* **2018**, *9*, 1457.
[37] K. A. Moore, S. Altus, J. W. Tay, J. B. Meehl, E. B. Johnson, D. M. Bortz, J. C. Cameron, *Nat. Microbiol.* **2020**, *5*, 757.
[38] F. Beroz, J. Yan, Y. Meir, B. Sabass, H. A. Stone, B. L. Bassler, N. S. Wingreen, *Nat. Phys.* **2018**, *14*, 954.
[39] J. Männik, R. Driessen, P. Galajda, J. E. Keymer, C. Dekker, *Proc. Natl. Acad. Sci. USA* **2009**, *106*, 14861.
[40] D. Yang, A. D. Jennings, E. Borrego, S. T. Retterer, J. Männik, *Front. Microbiol.* **2018**, *9*, 871.
[41] Welker, M. H., N. Bender, T. Cronenberg, G. Schneider, B. Maier, *Biophys. J.* **2021**, *120*, 3418.
[42] M. Delarue, J. Hartung, C. Schreck, P. Gniewek, L. Hu, S. Herminghaus, O. Hallatschek, *Nat. Phys.* **2016**, *12*, 762.
[43] H. Du, W. Xu, Z. Zhang, X. Han, *Front. Cell Dev. Biol.* **2021**, *9*, 524.
[44] N. Kandemir, W. Vollmer, N. S. Jakubovics, J. Chen, *Sci. Rep.* **2018**, *8*, 10893.
[45] P. F. Lenne, V. Trivedi, *Nat. Commun.* **2022**, *13*, 664.
[46] B. Alric, C. Formosa-Dague, E. Dague, L. J. Holt, M. Delarue, *Nat. Phys.* **2022**, *12*, 762.
[47] R. Hartmann, P. K. Singh, P. Pearce, R. Mok, B. Song, F. Díaz-Pascual, J. Dunkel, K. Drescher, *Nat. Phys.* **2019**, *15*, 251.
[48] R. Mishra, N. Minc, M. Peter, *Trends Microbiol.* **2022**, https://doi.org/10.1016/j.tim.2021.11.006.
[49] B. T. Larson, T. Ruiz-Herrero, S. Lee, S. Kumar, L. Mahadevan, N. King, *Proc. Natl. Acad. Sci. USA* **2020**, *117*, 1303.
[50] R. Chawla, R. Gupta, T. P. Lele, P. P. Lele, *J. Mol. Biol.* **2020**, *432*, 523.
[51] T. S. Kaminski, O. Scheler, P. Garstecki, *Lab Chip* **2016**, *16*, 2168.
[52] K. G. Lee, T. J. Park, S. Y. Soo, K. W. Wang, B. I. Kim, J. H. Park, C. S. Lee, D. H. Kim, S. J. Lee, *Biotechnol. Bioeng.* **2010**, *107*, 747.
[53] M. C. Duvernoy, T. Mora, M. Ardré, V. Croquette, D. Bensimon, C. Quilliet, J. M. Ghigo, M. Balland, C. Beloin, S. Lecuyer, N. Desprat, *Nat. Commun.* **2018**, *9*, 1120.
[54] Y. F. Dufrêne, A. Persat, *Nat. Rev. Microbiol.* **2020**, *18*, 227.
[55] T. C. Tang, E. Tham, X. Liu, K. Yehl, A. J. Rovner, H. Yuk, C. de la Fuente-Nunez, F. J. Isaacs, X. Zhao, T. K. Lu, *Nat. Chem. Biol.* **2021**, *17*, 724.
[56] J. Jiang, C. Li, J. Lombardi, R. H. Colby, B. Rigas, M. H. Rafailovich, J. C. Sokolov, *Polymer* **2008**, *49*, 3561.
[57] P. Ren, H. Zhang, Z. Dai, F. Ren, Y. Wu, R. Hou, Y. Zhu, J. Fu, *J. Mater. Chem. B* **2019**, *7*, 5490.
[58] J. Li, C. Marmorat, G. Vasilyev, J. Jiang, N. Koifman, Y. Guo, I. Talmon, E. Zussman, D. Gersappe, R. Davis, M. Rafailovich, *Acta Biomater.* **2019**, *96*, 295.
[59] M. Müller, J. Becher, M. Schnabelrauch, M. Zenobi-Wong, *Biofabrication* **2015**, *7*, 035006.
[60] S. Nam, J. Lee, D. G. Brownfield, O. Chaudhuri, *Biophys. J.* **2016**, *111*, 2296.
[61] G. Mathiesen, A. Sveen, M. B. Brurberg, L. Fredriksen, L. Axelsson, V. G. H. Eijsink, *BMC Genomics* **2009**, *10*, 425.
[62] I. Rud, P. R. Jensen, K. Naterstad, L. Axelsson, *Microbiology* **2006**, *152*, 1011.
[63] R. J. Homans, R. U. Khan, M. B. Andrews, A. E. Kjeldsen, L. S. Natrajan, S. Marsden, E. A. McKenzie, J. M. Christie, A. R. Jones, *Phys. Chem. Chem. Phys.* **2018**, *20*, 16949.

 © 2022 The Authors. Advanced Science published by Wiley-VCH GmbH

21983844, 2022, 17, Downloaded from https://onlinelibrary.wiley.com/doi/10.1002/advs.202106026 by Inm - Leibniz-Institut Für Neue Materialien, Wiley Online Library on [17/01/2023]. See the Terms and Conditions (https://onlinelibrary.wiley.com/terms-and-conditions) on Wiley Online Library for rules of use; OA articles are governed by the applicable Creative Commons License

ADVANCED SCIENCE
Open Access

Supporting Information

for *Adv. Sci.*, DOI 10.1002/advs.202106026

Regulating Bacterial Behavior within Hydrogels of Tunable Viscoelasticity

Shardul Bhusari, Shrikrishnan Sankaran and Aránzazu del Campo**

WILEY-VCH

Supporting Information

Regulating bacterial behavior within hydrogels of tunable viscoelasticity

Shardul Bhusari, Shrikrishnan Sankaran, Aránzazu del Campo**

Synthesis of Pluronic diacrylate (Plu-DA)

Dry Plu-DA (20 g, 1.59 mmol) and triethylamine (0.55 ml, 3.98 mmol) dissolved in 200 ml of dichloromethane were charged in a 500-ml round-bottomed flask. Acryloyl chloride (0.25 ml, 6.36 mmol) was added dropwise. The reaction mixture was stirred at 4 °C for 12 h and then at room temperature for 12 h. A white precipitate formed and was filtered. The solution was concentrated and filtered again. Precipitation in diethylether and drying in vacuum for 1 day rendered 18 g of Pluronic-DA. The chemical structure of Plu-DA and the extent of acrylation were determined by ^{1}H-NMR. The acrylation degree was determined by the ratio of the terminal acrylic protons (5.98-6.52 ppm) to the methylene groups of the backbone (1.05-1.28 ppm). Plu-DA with substitution degree of 70% was obtained.

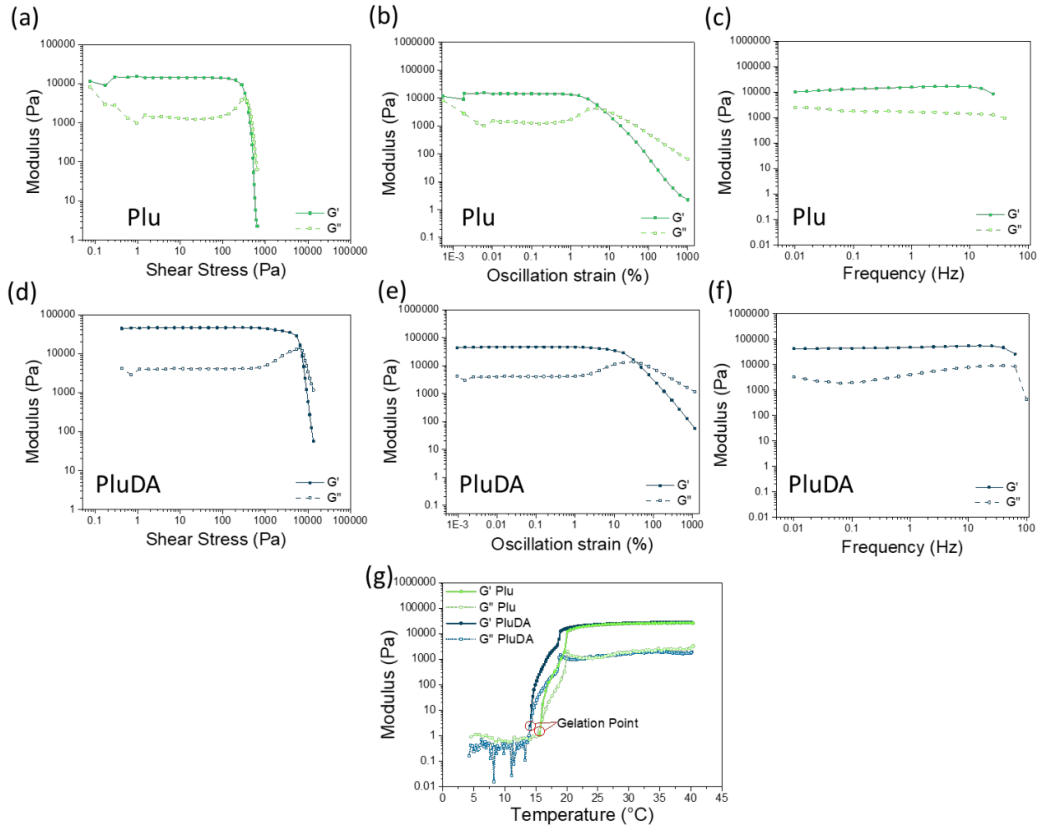

Figure S1. Rheological measurements of Plu and PluDA hydrogels at 30% w/v polymer concentration. **a)** Strain sweep experiment to identify the yield stress value of Plu hydrogel, **b)** Strain sweep and **c)** frequency sweep experiments to determine the linear viscoelasticity region of Plu hydrogel. **d)** Strain sweep experiment to identify the yield stress value of PluDA hydrogel, **e)** Strain sweep and **f)** frequency sweep rheograms to determine the linear viscoelasticity region of PluDA hydrogel after UV irradiation. **a-f**: All measurements were performed at room temperature. **g)** Temperature sweep measurement to determine the gelation point (G'= G'') of Plu and PluDA without UV irradiation.

Table S1. Mechanical properties of DA 0-100 hydrogels with different compositions obtained from rheology: shear storage modulus (G') of the crosslinked hydrogels (Figure 1b, t = 420 s), applied stress in the creep experiment to reach 1% deformation in 3 min (Figure 1c), and the residual deformation (irreversible strain) after recovery (Figure 1c, t = 360 s).

Hydrogel	**Composition Plu : PluDA**	**Shear storage modulus [kPa]**	**Applied stress in creep experiment (Pa)**	**Irreversible strain [%]**
DA 0	100 : 0	17.8 ± 1.4	50	0.47 ± 0.22
DA 25	75 : 25	20.4 ± 2.4	100	0.22 ± 0.01
DA 50	50 : 50	25.9 ± 1.5	140	0.18 ± 0.05
DA 75	25 : 75	32.7± 3.8	200	0.29 ± 0.06
DA 100	0 : 100	42.9 ± 1.9	300	0.20 ± 0.13

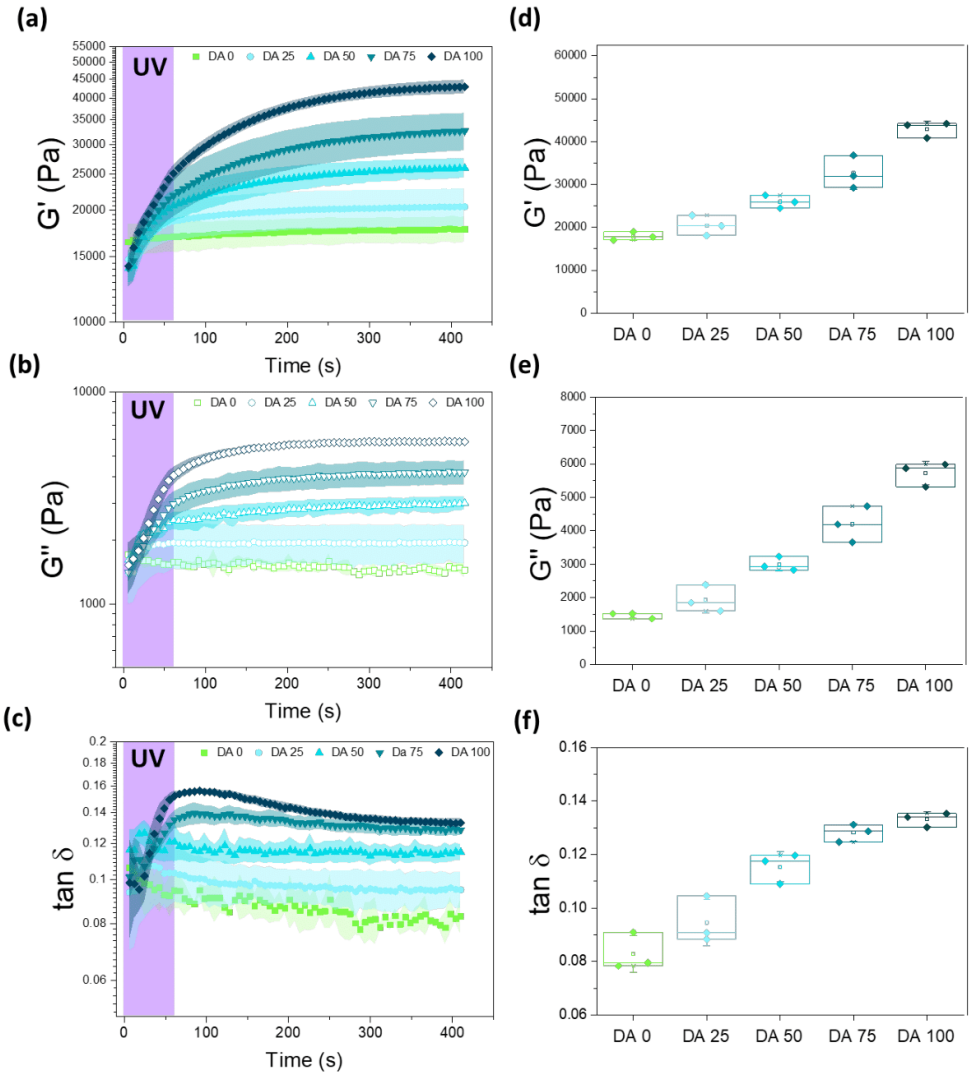

Figure S2. Rheological properties of Plu/PluDA (DA 0-100) hydrogels. **a-c)** Evolution of the **a)** shear storage modulus, **b)** shear loss modulus and **c)** tan δ values after physical gel formation (t=0 s), during photoinitiated crosslinking (t=0-60 s) and afterwards (t=60-400 s). The curves show post-exposure polymerization characteristic of crosslinking processes as a consequence of the hindered mobility of the initiated radicals that slows down the polymerization and termination reactions.[1] **d-e)** Values of **d)** shear storage modulus, **e)** shear loss modulus and **e)** tan δ at t = 420 s from the rheological curves in **a-c**. (N = 3, box represents 25 and 75 percentile values and whiskers indicate standard deviation.)

WILEY-VCH

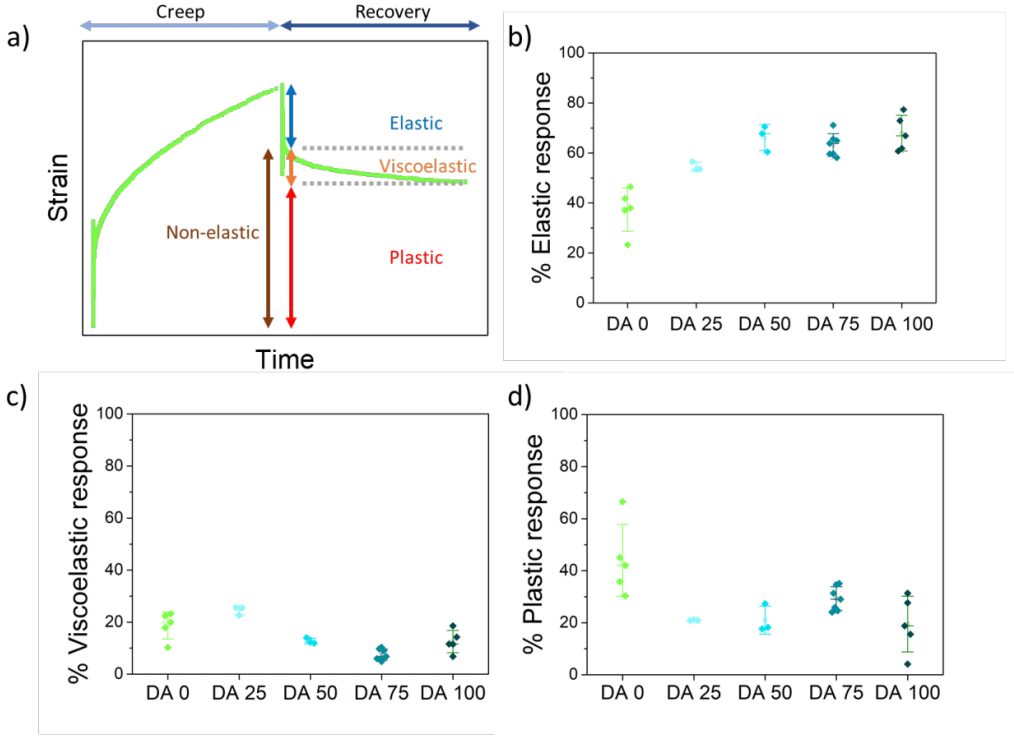

Figure S3. a) The representative creep-recovery curve highlights the basic features of the material response to a constant stress. When a constant stress is applied, the material exhibits instantaneous elastic response and its strain gradually increases over time. A peak strain value is reached at the end of the creep test. After release of the constant stress, the material undergoes elastic and viscoelastic recovery leaving residual or irreversibe strain. b) % Elastic, c) % Viscoelastic and d) % Plastic response of the curves represented in Figure 1c were calculated.

...

WILEY-VCH

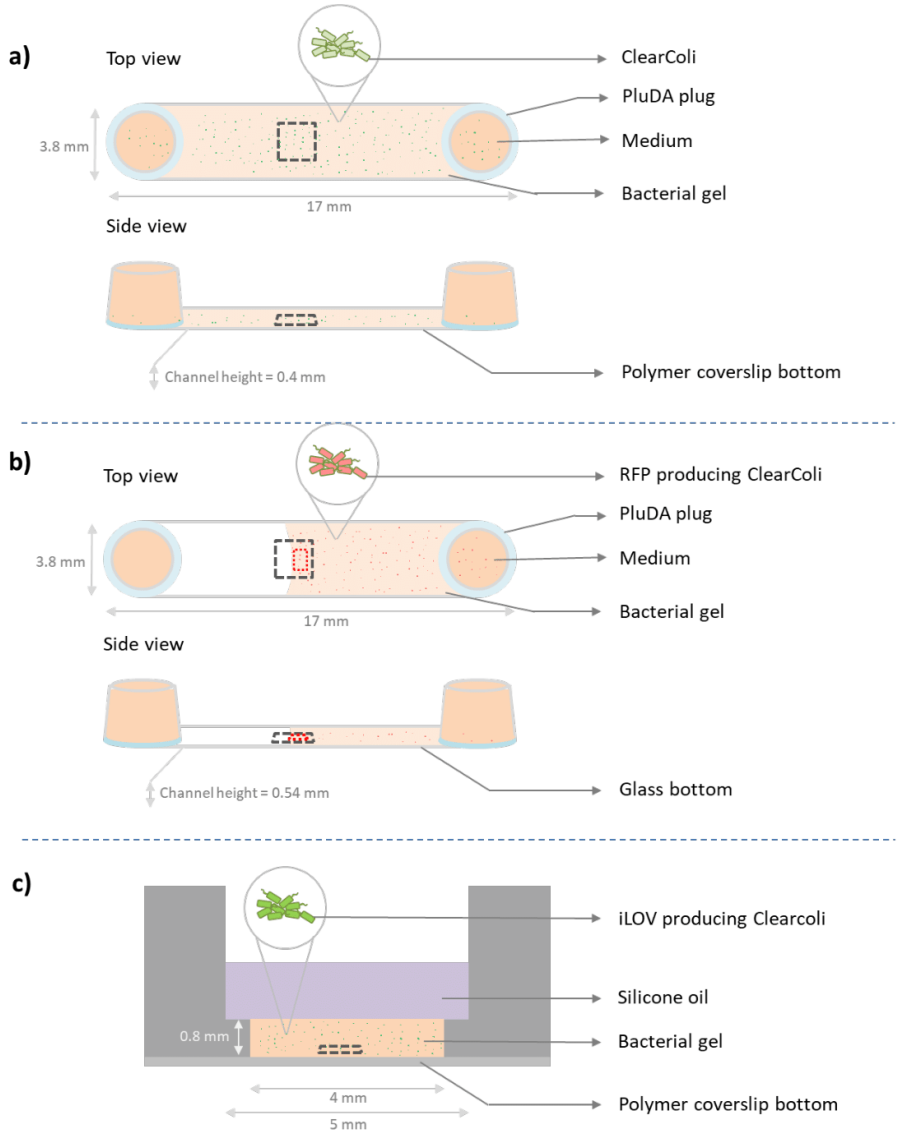

Figure S4. Design of experimental platforms used to quantify bacterial behavior inside the hydrogels. **a)** Microchannels in Ibidi µ-Slides VI 0.4 (17 x 3.8 x 0.4 mm^3). Volume of bacterial hydrogel used to fill the channel was 30 µL, imaging locations (black dotted box of 449 x 335 um^2) were selected near the middle of the channel length and nearly 150-250 µm from the bottom of the channel; **b)** Microchannel in Ibidi µ-Slide VI 0.5 Glass Bottom (17 x 3.8 x 0.54 mm^3). Volume of bacterial hydrogel used to fill the channel was 20 µL, imaging location (black dotted box of 3636 x 2727 μm^2) representing the observed field of view in the microscope was selected at the hydrogel-air interface at a height of ca. 0.27 mm (mid-point of channel thickness) and quantification of the fluorescence intensities was done 50 µm away from the edge within a 200 × 600 μm^2 area (red dotted box); **c)** Microwell in Ibidi µ- Slide angiogenesis. Volume of bacterial hydrogel used to fill the well was 10 µL, measurement at 50 µm from the bottom (black dotted box of 212.5 × 212.5 × 50.102 μm^3). **a-c**) The grey square indicates the region of interest (ROI) of the hydrogel used for imaging, and the red square indicates the region used for quantification of RFP intensity.

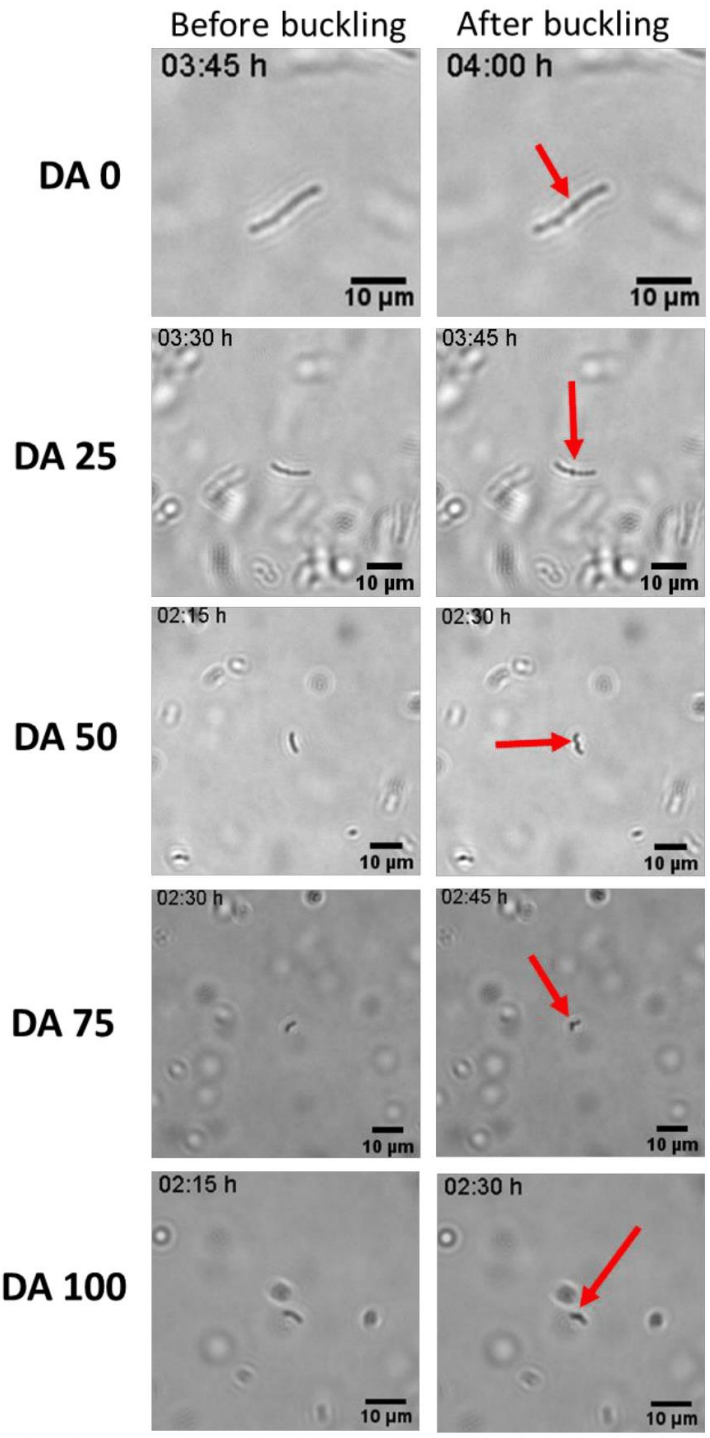

Figure S5. Bacteria colony growth and buckling inside DA0-100 hydrogels in microchannels. Bright field, snap shot images from time lapse video in 1x LB medium. Buckling starts at 4 h in DA0, as appreciated from change in contrast in the middle of the growing bacterial chain (highlighted by red arrows) which is associated to grow in the z plane. Similar phenomena are visible at 2:30 h in DA 100.

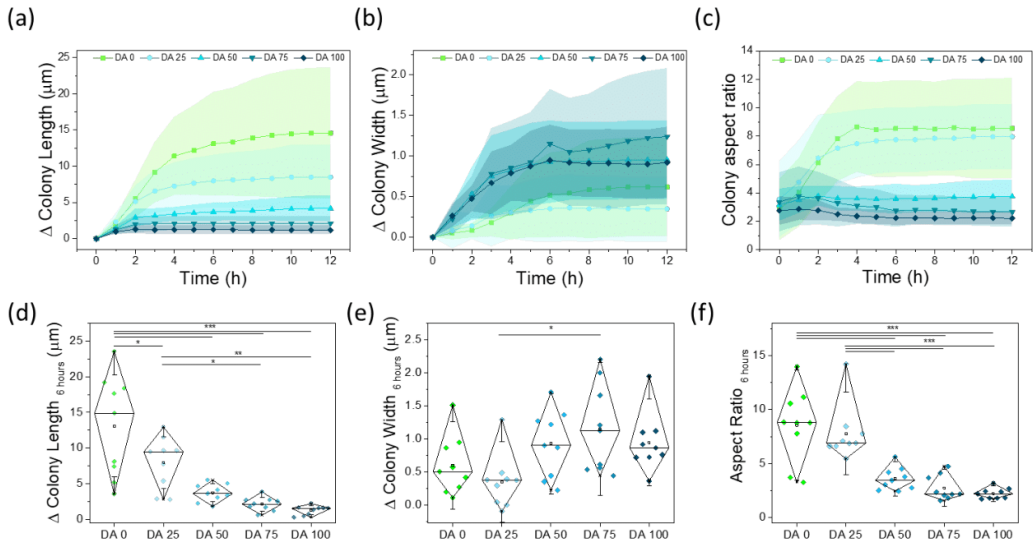

Figure S6. In-plane quantification of dimensional changes of bacterial colonies encapsulated in DA 0-100 hydrogels in microchannels (Figure S4a) with 1x concentration LB medium. **a-c)** Evolution of the length, width and aspect ratio of individual colonies within 12 h of culture (mean ± SD). **d-f)** Comparative values of changes in colony length, width and aspect ratio after 6 hours in the different hydrogels. (Diamond plots indicate 10 and 90 percentile values, whiskers indicate standard deviation values, number of colonies = 9, p-values are calculated using one-way ANOVA with post hoc Tukey HSD test, * $p < 0.05$, ** $p < 0.01$, *** $p < 0.001$)

Fluorescence recovery after photobleaching (FRAP) in the hydrogels

For all of the FRAP measurements, a fluorescent small molecule erythrosin B was used[2] and observed under a confocal laser-scanning microscope (LSM 880) equipped with an Airyscan detector (Zeiss, Germany). The gels, within the microchannel constructs as shown in Figure S4a, were visualized under an air immersion objective (EC Plan-Neofluar 10x/0.30 Ph1 M27), and images were acquired with a 514 nm laser diode, detection wavelength 519-653 nm, dwell time of 0.42 µs per pixel and 0.1% laser power. For bleaching, a circular region of interest with a diameter of 26 µm was illuminated using a 405-nm laser diode at 30% laser power with a dwell time of 131 µs per pixel. The total acquisition length was 261.9 s, with a frame rate of 2 fps.

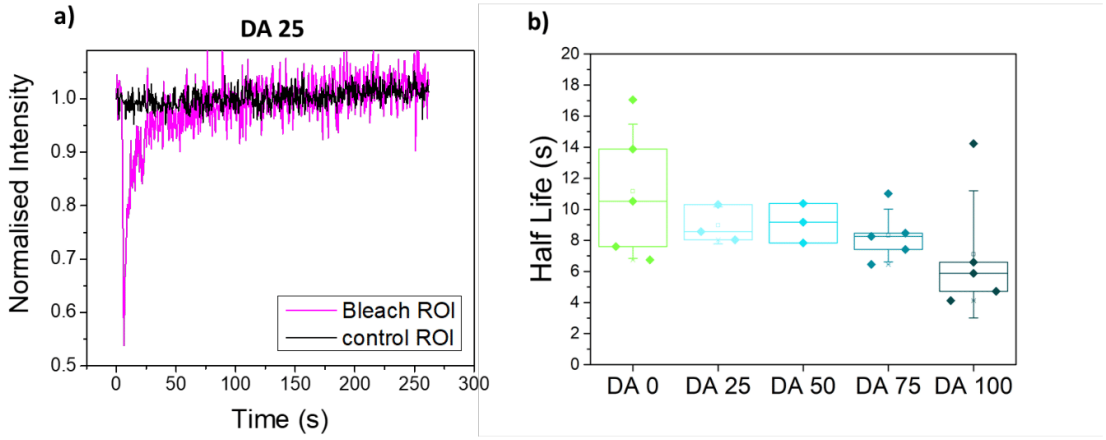

Figure S7. FRAP assay comparison of molecular diffusion rates inside DA 0-100 hydrogels. **a)** Normalized FRAP curve of Erythrosin B dye in DA 25 hydrogel. **b)** Quantified recovery time values, τ ½, of FRAP in the DA 0-100 hydrogels. The obtained τ ½ were close to 10 seconds for all hydrogel compositions with no significant differences. This indicates that the diffusion rate of nutrients within the hydrogels are expected to be similar. (N ≥ 3, box represents 25 and 75 percentile values and whiskers indicate standard deviation.)

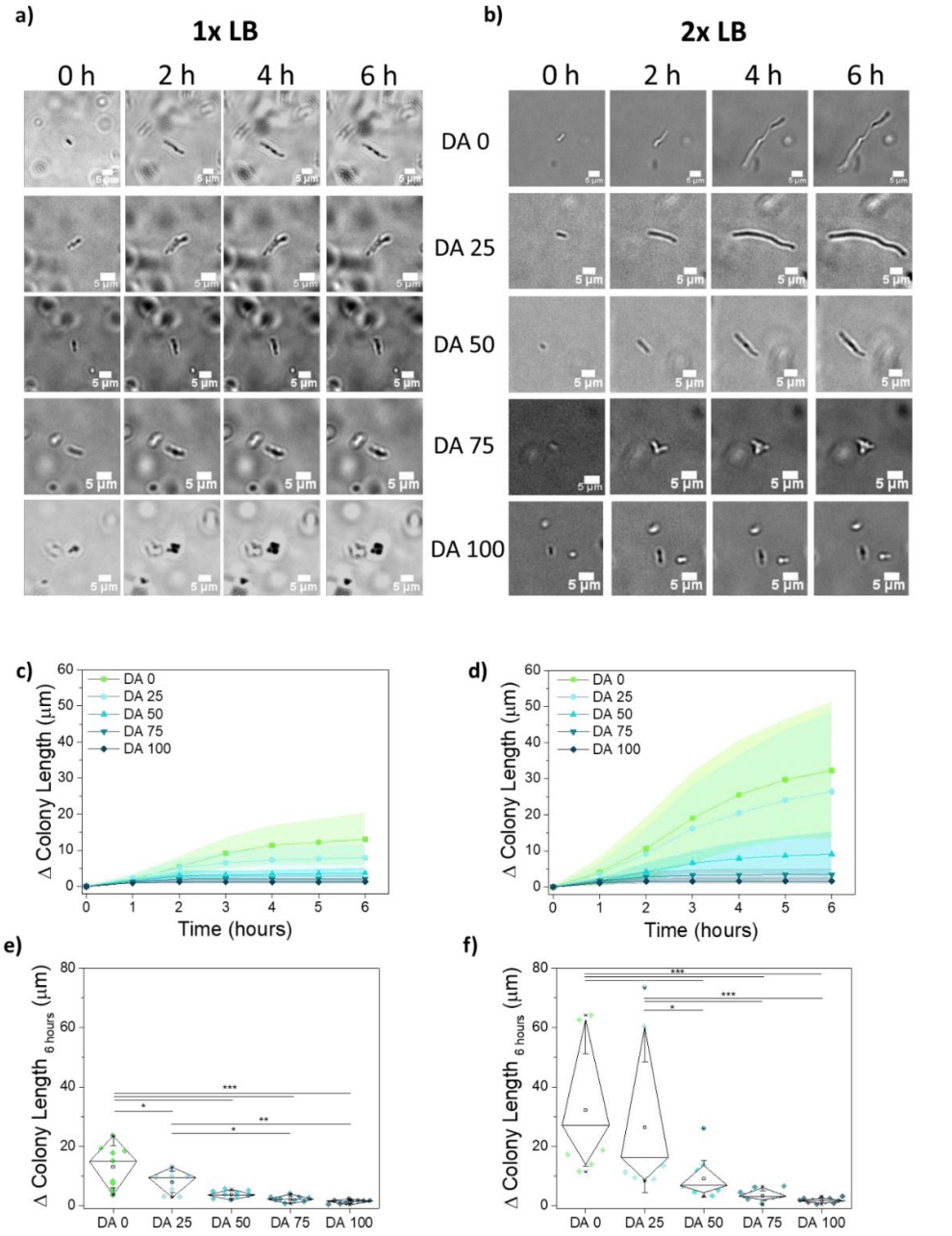

Figure S8. Bacteria colony growth inside hydrogels in microchannels (Figure S4a). **a)** Time lapse bright-field images of bacterial colonies within Da 0-100 hydrogels in 1x LB medium. Scale bar corresponds to 5 µm. **b)** Time lapse bright-field images of bacterial colonies within DA0-100 hydrogels in 2x LB medium. Scale bar corresponds to 5 µm. **c-d)** Quantification of the extension of bacteria colony length within the hydrogels with **c)** 1x and **d)** 2x LB concentration with increasing time; **e,f)** Bacterial length extension values at 6 h with **e)** 1x and **f)** 2x LB concentration. (Diamond plots indicate 10 and 90 percentile values, whiskers

indicate standard deviation values, 9 ≥ Number of colonies ≥ 13, p-values are calculated using one-way ANOVA with post hoc Tukey HSD test, * $p < 0.05$, ** $p < 0.01$, *** $p < 0.001$)

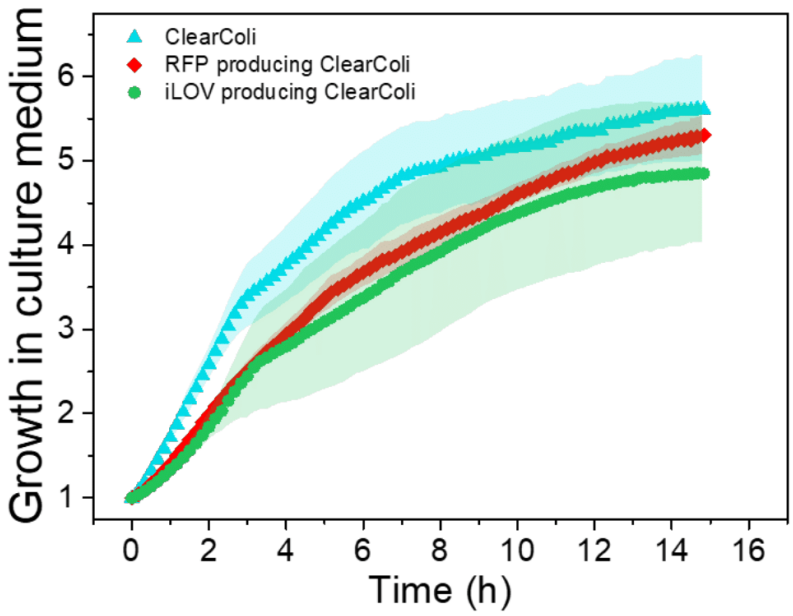

Figure S9. Growth rate of ClearColi, genetically modified RFP producing ClearColi and genetically modified iLOV producing ClearColi bacteria in culture medium determined by OD 600 measurements in a microplate reader (TECAN Infinite 200 Pro) at 37°C with shaking. The y axis indicates the multiplication factor of the growing bacteria population compared to the starting OD 600 of ~ 0.1. The RFP producing ClearColi were pre-irradiated for 5 h under a white lamp before measurement and not further induced during the time course of the experiment. (Symbols – mean, shaded regions – SD, N=3)

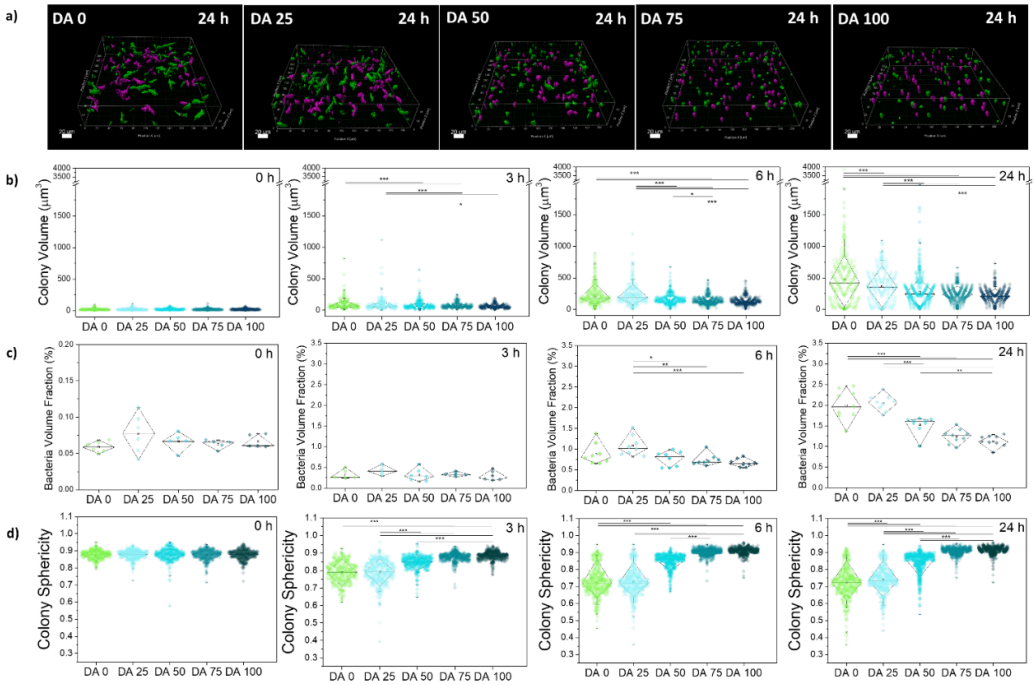

Figure S10. Bacteria colony growth inside hydrogels in microwells (Figure S4c). **a)** Fluorescence image of 212.5 × 212.5 × 50.102 µm^3 volumes of bacterial hydrogels producing iLOV after 24 h culture. The magenta-colored colonies do not touch the edges of the ROI, while the green colored colonies do. The magenta and green colored colonies were used for the quantification of the bacteria volume fraction **(b).** Only magenta-colored colonies were considered for the quantification of the volume **(c)** and sphericity **(d)** of individual colonies. For visualization surface masks obtained by IMARIS software were used. The scale bar corresponds to 20 µm. **b)** Volume of individual colonies in DA 0-100 hydrogels quantified at 0, 3, 6 and 24 h timepoints; **c)** Bacteria volume fraction in DA 0-100 hydrogels quantified at 0, 3, 6 and 24 h timepoints; and **d)** Sphericity of bacteria colonies quantified in DA 0-100 hydrogels. (Diamond plots indicate 10 and 90 percentile values, whiskers indicate 5 and 95 percentile values, 338 ≥ Number of colonies ≥ 667, p-values are calculated using one-way ANOVA with post hoc Tukey HSD test, * $p < 0.05$, ** $p < 0.01$, *** $p < 0.001$)

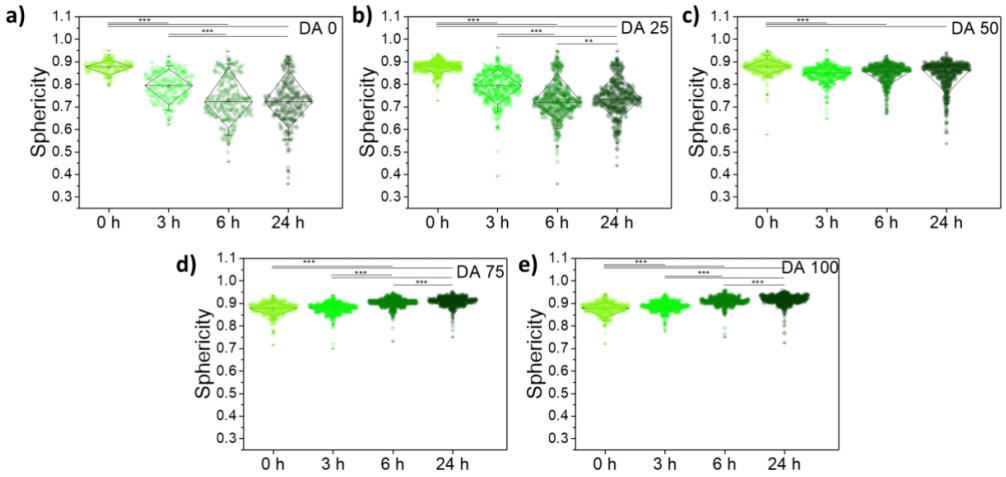

Figure S11. Quantification of the sphericity of iLOV producing ClearColi colonies within DA 0-100 hydrogels, a) DA 0, b) DA 25, c) DA 50, d) DA 75 and e) DA 100 in microwells (Figure S4c) as function of culture time. (Diamond plots indicate 10 and 90 percentile values, whiskers indicate 5 and 95 percentile values, 338 ≥ number of colonies ≥ 667, p-values are calculated using one-way ANOVA with post hoc Tukey HSD test, * $p < 0.05$, ** $p < 0.01$, *** $p < 0.001$)

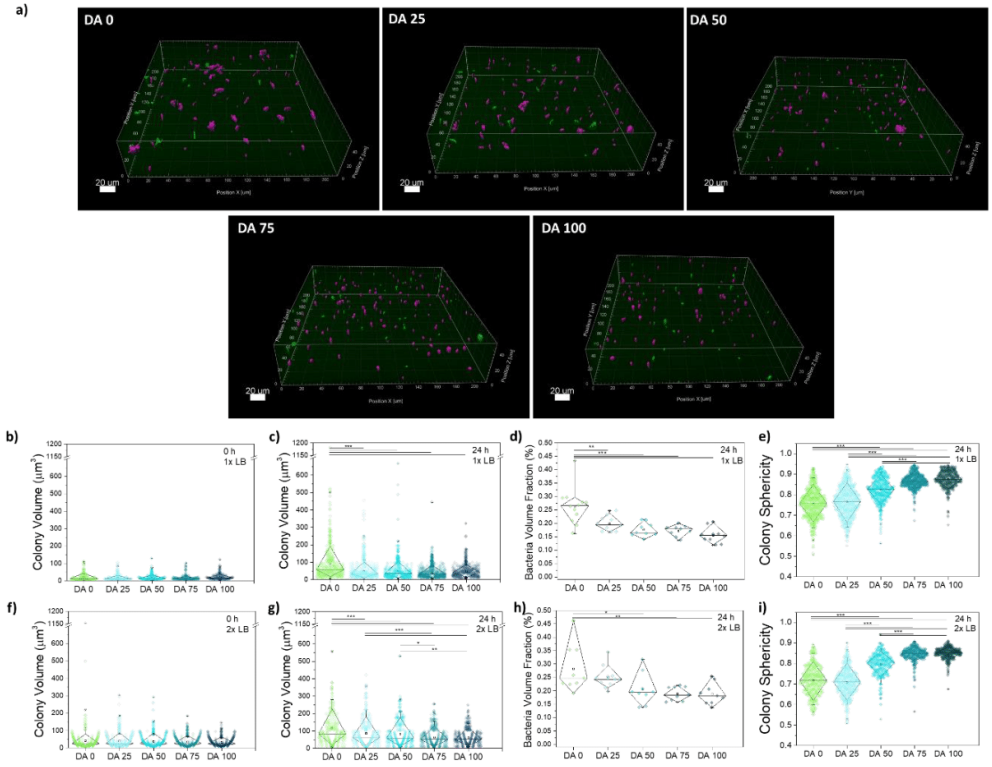

Figure S12. Bacteria colony growth inside hydrogels in microchannels (Figure S4b microchannel, filled with bacterial gel volume of 30 ul). a) Fluorescence image of 212.5 × 212.5 × 50.102 µm^3 volumes of 1x LB concentration bacterial hydrogels producing iLOV after 24 h culture. The magenta-colored colonies do not touch the edges of the ROI, while the green colored colonies do. The magenta and green colored colonies were used for the quantification of the bacteria volume fraction (d,h). Only magenta-colored colonies were considered for the quantification of the volume (b,c,f,g) and sphericity (e,i) of individual colonies. For visualization surface masks obtained by IMARIS software were used. The scale bar corresponds to 20 µm; b) Colony volume distribution within different hydrogels of 1x LB concentration at 0 h and c) 24 h; d) Volume fraction of bacteria colonies within different hydrogels of 1x LB concentration at 24 h timepoint; e) The sphericity of the colonies within different hydrogels of 1x LB concentration at 24 h timepoint and f) Colony volume distribution within different hydrogels of 2x LB concentration at 0 h and g) 24 h; h) Volume fraction of bacteria colonies within different hydrogels of 2x LB concentration at 24 h timepoint and i) The sphericity of the colonies within different hydrogels of 2x LB concentration. (Diamond plots indicating 10 and 90 percentile values, whiskers indicating 5 and 95 percentile values, p-values are calculated using one-way ANOVA with post hoc Tukey HSD test, * $p < 0.05$, ** $p < 0.01$, *** $p < 0.001$)

WILEY-VCH

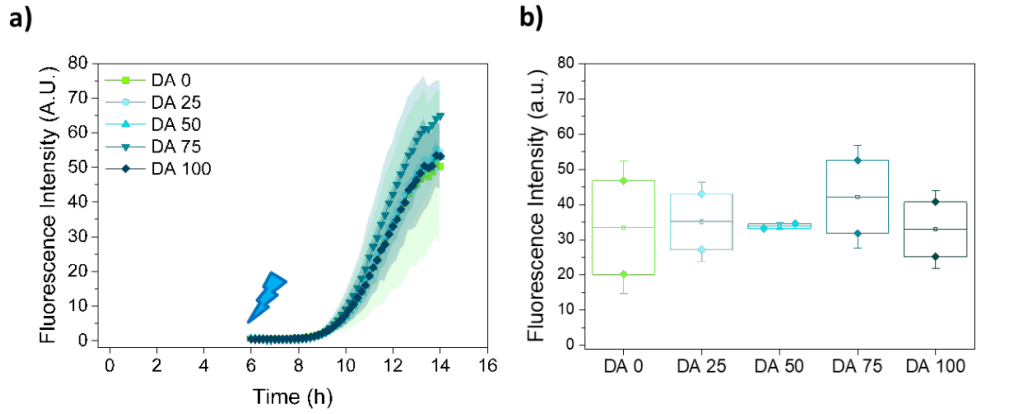

Figure S13. RFP production analysis. **a)** Normalized fluorescence intensity (mean ± standard deviation) associated to RFP production measured in bacteria loaded DA 0-100 hydrogels in microchannels (Figure S4b). The hydrogels were cultured for 6 h and then irradiated to induce protein production. **b)** Fluorescence intensity measured in the hydrogels at 12 h (6 h after the onset of irradiation). (N = 2, box represents 25 and 75 percentile values, whiskers indicate standard deviation)

Different formats lead to different metabolic conditions but result in similar bacterial behavioral trends

When the gel-encapsulated bacteria were allowed to grow in micro-channels, confocal imaging at 0 h and 24 h timepoints indicated that colony volumes increased over time but were smaller (5 – 8x on average) compared to colony volumes in the micro-well format. The trend of colony volumes decreasing and sphericity increasing with increase in chemical cross-linking degree was still observed and was more pronounced when using medium with 2x concentration of nutrients, indicating that the hydrogels were imparting the same type of mechanical constraints in both microwell and micro-channel formats. Another notable aspect was that the fluorescence intensities within the cells were sufficient for quantification at 0 h and 24 h timepoints but not at earlier timepoints (3 h, 6 h), during which the highest rates of bacterial growth are expected to be occurring based on the data from Figure 3.

When RFP-expressing bacteria were encapsulated within the different types of gels and formed within the microchannels with one interface accessible to air, fluorescence appeared only to a depth of ~ 1mm from that interface (**Figure S16**). This indicated that oxygen, which

is required for RFP fluorophore formation, does not diffuse deeper into the gel, causing the bacteria to switch to anaerobic metabolic pathways for growth and sustenance, leading to smaller colony volumes and weaker protein production, as found by previous reports.[3] Such oxygen diffusion limitations are not expected in the hydrogel films in the microwell since the silicone covering film is permeable to oxygen (Figure 3). Nevertheless, even under these conditions, trends of decreasing colony volumes, increasing sphericity and narrowing of distributions for both with increasing chemical cross-linking degrees were similar to the trends observed in the micro-well format. This indicated that the mechanical constraints imparted by the chemical cross-links influenced colony morphologies independent of metabolic variations.

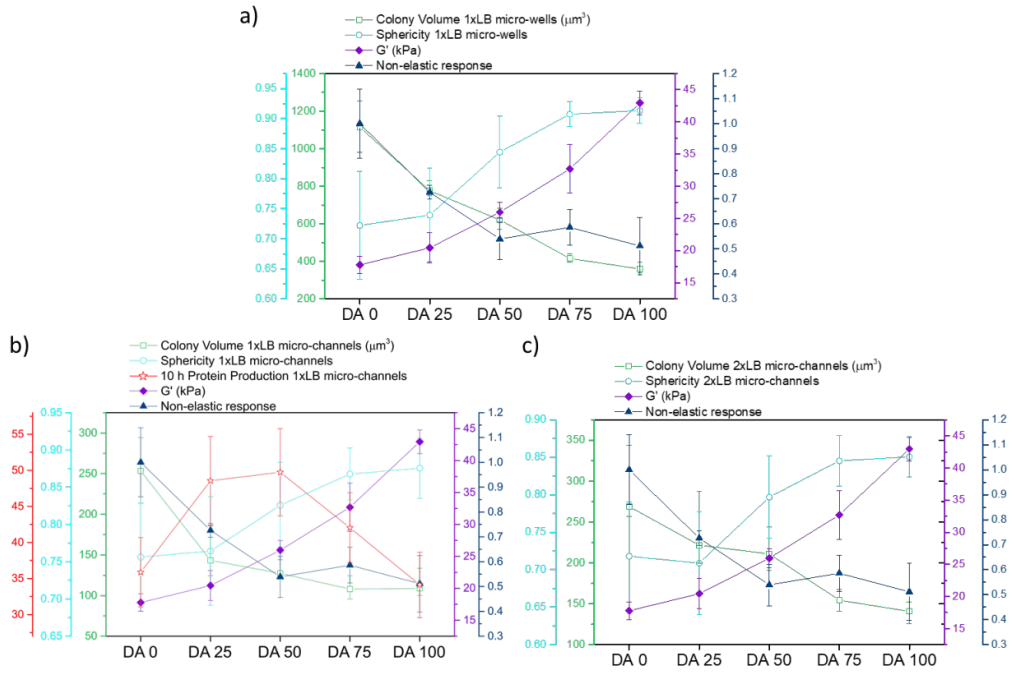

Figure S14. Comparative representation of hydrogel mechanical properties and the behavior of embedded bacteria colonies in DA 0-100 hydrogels in 3 different formats – (a) in micro-wells with 1x nutrient concentration, (b) in micro-channels with 1x nutrient concentration and (c) in micro-channels with 2x nutrient concentration. Mean value of shear storage modulus (from Figure 1b) and proportion of non-elastic response from the creep recovery experiment (from Figure 1d), 95th percentile of colony volume values and mean sphericity after 24 h, and mean protein production after 10 h (from Figure 4d) within the indicated constructs were

plotted. The error bars indicate the 93rd-97th percentile value range for the colony volume data, for the rest, the error bars indicate standard deviation.

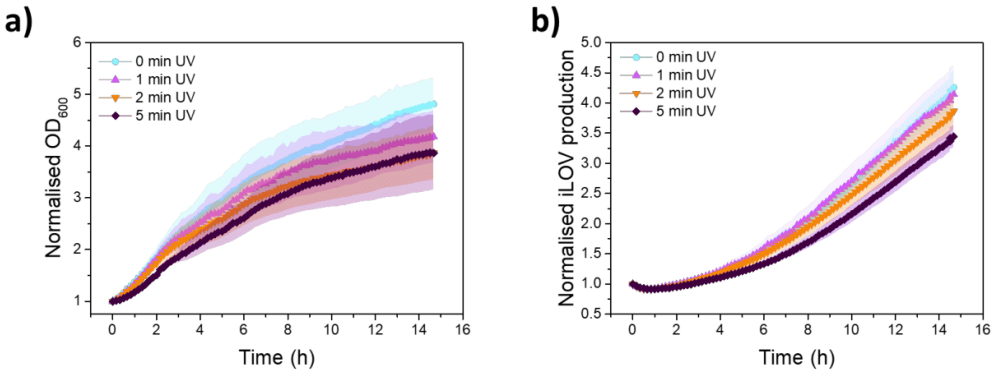

Figure S15. a) Growth rate (OD 600) and **b)** protein production of genetically modified iLOV producing ClearColi in culture medium after UV irradiation (0, 1, 2 and 5 min) determined by OD 600 measurements in a microplate reader (TECAN Infinite 200 Pro, excitation wavelength 447 nm, emission wavelength 497 nm, with gain regulation) at 37°C with shaking. The y axis indicates the multiplication factor of the growing bacteria population compared to the starting OD 600 of ~ 0.1. (Symbols – mean, shaded regions – SD, N ≥ 6).

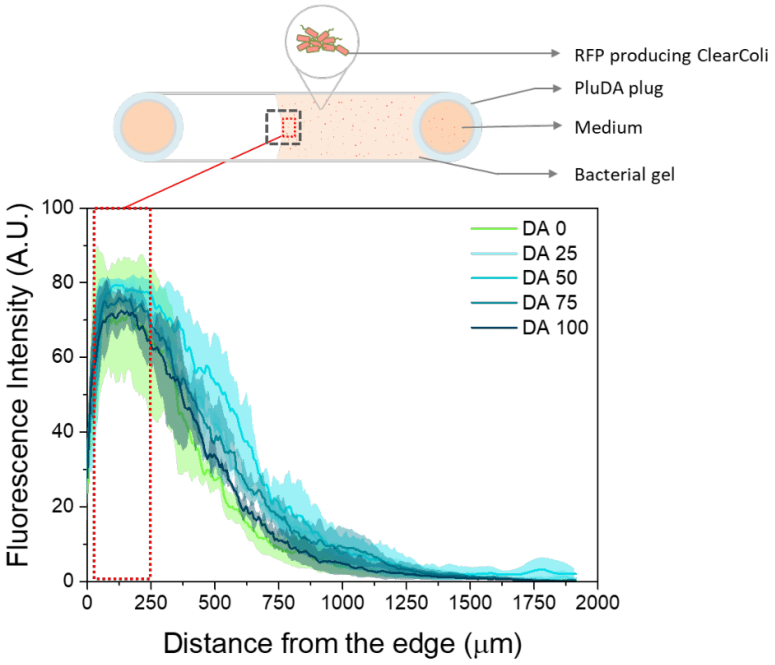

Figure S16. Fluorescence intensity profile in RFP producing bacteria hydrogels inside microchannels (Figure S4b) at t = 18 h. The fluorescence was measured from the edge of the hydrogel to the end of the channel along the channel longitudinal axes. The highlighted dotted

box (200 × 600 μm^3) indicates the region of the bacterial hydrogel considered for RFP fluorescence intensity measurement (Figure 4). (mean ± SD, N=3)

Supplementary video 1 "DA 0_10x video": Bacteria colony growth and buckling inside DA 0 hydrogel in a microchannel.

Supplementary video 2 "DA 25_10x video": Bacteria colony growth and buckling inside DA 25 hydrogel in a microchannel.

Supplementary video 3 "DA 50_10x video": Bacteria colony growth and buckling inside DA 50 hydrogel in a microchannel.

Supplementary video 4 "DA 75_10x video": Bacteria colony growth and buckling inside DA 75 hydrogel in a microchannel.

Supplementary video 5 "DA 100_10x video": Bacteria colony growth and buckling inside DA 100 hydrogel in a microchannel.

References (Supporting Information)

[1] E. Andrzejewska, *Free Radical Photopolymerization of Multifunctional Monomers*, Elsevier Inc., **2016**.

[2] N. B. Hatzigrigoriou, C. D. Papaspyrides, C. Joly, P. Dole, *J. Agric. Food. Chem.* **2010**, *58*, 8667.

[3] J. Von Wulffen, RecogNice-Team, O. Sawodny, R. Feuer, *PLoS ONE* **2016**, *11*, e0158711.

6.2 Rheological behavior of Pluronic/Pluronic diacrylate hydrogel matrices used for bacteria encapsulation

Shardul Bhusari[1,2], Maxi Hoffmann[3], Petra Herbeck-Engel[1], Shrikrishnan Sankaran[1], Manfred Wilhelm[3], Aránzazu del Campo[1,2]*

[1] INM - Leibniz Institute for New Materials, Saarbrücken, Germany

[2] Chemistry Department, Saarland University, 66123 Saarbrücken, Germany

[3] Institute of Chemical Technology and Polymer Chemistry, Karlsruhe Institute of Technology (KIT), Karlsruhe, Germany

*Corresponding author

Email: aranzazu.delcampo@leibniz-inm.de

Unpublished original work

Own Contribution: Methodology (all experiments - rheology, curve fitting), Validation, Visualization, Formal analysis, Investigation, Writing (Original draft – shared with A.d.C., review and editing).

Rheological behavior of Pluronic/Pluronic diacrylate hydrogel matrices used for bacteria encapsulation

Abstract

The physical and architectural cues of the surrounding matrix play a critical role in regulating bacterial behavior like growth and metabolic activity. Pluronic based hydrogels have been shown to regulate bacterial behavior by tuning the fraction of covalent crosslinks present in the network. Here we investigate viscoelastic properties of this tunable pluronic-based hydrogel system, which forms inter- and intra-micellar covalent crosslinks. We report that higher stresses (a difference of up to two orders of magnitude) are required to fluidize the network with increasing covalent crosslinks within the network. The hydrogel network exhibits two distinct processes in stress relaxation: faster relaxation mode (occuring under 1 s) that accelerates with increasing covalent crosslinks and another slower one (occuring beyond 1 min) that slows down with increasing covalent crosslinks. Creep recovery experiments reveal the higher contribution of elastic components with increasing covalent crosslinks when acted upon by constant strain values. Trends of these viscoelastic parameters and bacterial growth and morphology were compared to elucidate the complex interplay between the cell-matrix interactions which can prove beneficial for the development of engineered living materials.

Introduction

Soft hydrogel networks with combined physical (dynamic) and covalent (permanent) crosslinks are interesting materials for the encapsulation and controlled expansion of cells.[1] The inherent reorganization capability of the dynamic crosslinks allows cells to deform the surrounding material as they proliferate, and accommodate daughter cells. In parallel, the elastic network imposes increasing compressive forces on the cell population as it grows.[2] The magnitude of the compressive forceregulates the size and morphology of the cellular aggregates and depends on the viscoelastic properties of the hydrogel network (**Scheme 1**).[3]

Hydrogels featuring elastic and dissipative components [1]have been used to encapsulate bacteria and yeast for the fabrication of Engineered Living Materials for the delivery of therapeutics.[4][5] In these applications, the regulation of the growth and the metabolic production of the embedded biofactories is relevant to control pharmacokinetics and ensure

safe use.[6] Pluronic (PEO_x-PPO_y-PEO_x) hydrogels have been adopted as model hydrogels to embed bacteria[7] or yeast[8] in living therapeutic devices[9][10]. Pluronic (Plu) hydrogels are physical networks stabilized by reversible interactions. By mixing with Pluronic diacrylate (PluDA), covalent crosslinks can be introduced in the network structure without disturbing the physical crosslinks. We recently reported that the growth rate and colony size of *E. coli* strains embedded in Plu/PluDA hydrogels decrease as the degree of covalent crosslinks in the network increase. This behavior is independent of nutrient availability and is attributed to the mechanical properties of the embedding hydrogel network.[5] Although the trend has been seen by other authors and in other systems,[11] the details on the interplay between hydrogel mechanics and colony growth remain to be clarified.[12]

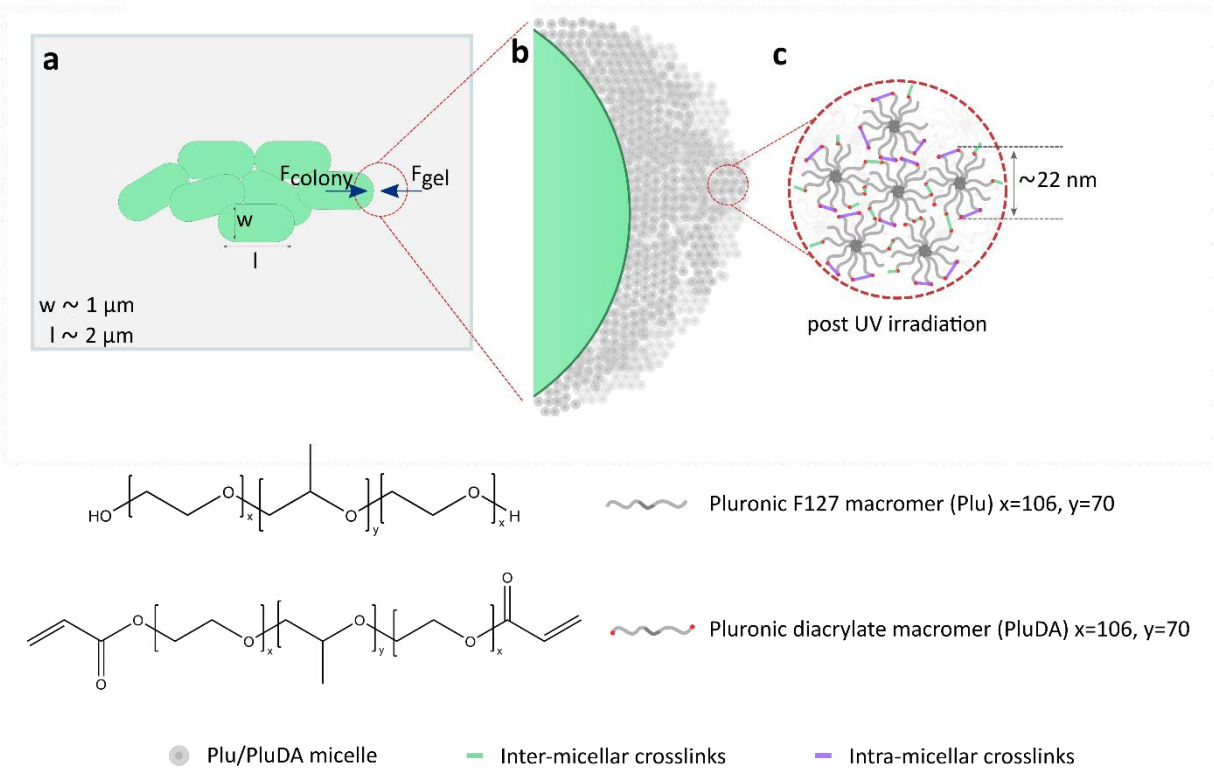

Scheme 1: **a)** Representation of a growing bacteria colony embedded in Pluronic/Pluronic diacrylate hydrogel; **b)** Micellar structure of the Plu/PluDA hydrogel above the sol-gel transition temperature. The micelles have a diameter of ca. 22 nm and build aggregates that form a network and **c)** Micellar structure representing the organization of the PEOx-PPOy-PEOx triblock copolymer chains in the micelles and the inter- and intra-micellar covalent crosslinks between PluDA chains.

Physical Pluronic hydrogels are formed by aggregation of the Pluronic micelles into clusters stabilized through the interactions between the PEO corona of neighboring micelles (**Scheme 1**). Above the transition temperature, the micellar clusters grow and build a 3D network.[13][14] For Pluronic F127 (PEO_{106}-PPO_{70}-PEO_{106}), which will be used in the experiments in this article, the critical micellar concentration (cmc) is at 0.725 wt. % in water at 25 °C[15], and the sol-gel transition occurs at polymer concentrations > 5 wt. % and temperatures above 14 °C. The assembly of Pluronic F127 chains in 3D networks has been studied by scattering methods like dynamic light scattering (DLS) and small angle neutron scattering (SANS).[16][17] The order of the micelles in the clusters depends on external conditions (i.e., temperature, salt concentration, shear forces)[18][17] and ranges from perfect face-centered cubic (FCC) or hexagonally close packed (HCP) structures to random stackings. As associative physical networks, Pluronic hydrogels show elastic properties in the quiescent state and undergo yielding, i.e. fracture and flow, when the stress surpasses the interparticle forces.[19] The shear thinning behavior and the thermosensitivity makes Pluronic gels interesting from a biomedical perspective. It allows them to be easily processed, mixed with payloads, and injected for application in drug delivery and for replacing biological fluids.[20][21]

Physical Pluronic hydrogels swell and dissociate into individual micelles when immersed in water. The introduction of polymerizable acrylate functionalities as end-groups of the Pluronic chains provides the possibility to stabilize the micellar hydrogel via the formation of permanent, covalent bonds between the micelles.[8][14] Covalent crosslinking affects the mechanical behavior of the hydrogel. By varying the PluDA fraction in Plu/PluDA hydrogels the density of chemical crosslinks in the hydrogel and the resulting mechanical properties can be tuned. 30 wt. % Plu/PluDA hydrogels show increasing elastic response (G') (from 17.8 ± 1.4 to 42.9 ± 1.9 kPa) and decreasing non-elastic response (from creep-recovery curves) when the PluDA fraction in the mixture increased from 0 to 100%.[5]

Here, we present a detailed study of the time-dependent rheological behavior of Plu/PluDA hydrogels as a function of PluDA ratio. We use 30 wt. % Plu/PluDA hydrogels since similar compositions have been used for bacteria growth cultures in ELMs by different groups. [7][8][22] We discuss the observed responses together with previous observations of bacteria growth in hydrogels of similar composition and correlate the behavior of the living organisms with the mechanics of the surrounding matrix.[5] The results of this work are relevant for the wide

Engineered Living Materials community using Pluronic-based hydrogels for the functional encapsulation of microorganisms in living devices for different applications.[7][9][10][22][23]

Results

30 wt. % Plu/PluDA hydrogels were prepared by mixing defined volumes of 30 wt. % solutions of Plu and PluDA polymers.[5] Hydrogels were named DA X**,** with X being the fraction of PluDA in the Plu/PluDA mixture, between 0 and 100 % (**Table 1**).

1. Rheological behavior of Plu and PluDA physical hydrogels

30 wt. % solutions of Pluronic F127 (Plu) in water form physical hydrogels at temperature >15.5°C.[5] At room temperature (22°C) and shear strain amplitudes (γ_0) below 1 %, the Plu hydrogel behaves as a linear viscoelastic solid (**Figure 1a**) with a strain amplitude independent shear modulus G' of 15.3 ± 1.6 kPa (**Figure 1b**). At higher strain amplitudes (>1%), Plu hydrogels show strain-induced yielding, gradual fluidization and overshoot in the shear loss modulus (**Figure 1a**). This behavior is characteristic of colloidal or granular hydrogels,[24] in which particles aggregate through reversible interparticle interactions to form an interconnected, percolated 3D network structure that yields when the applied stress exceeds the interparticle attractive forces.[25] The critical strain for yielding mainly depends on the particle content and the strength of the interparticle interactions including interparticle (electrostatic, van der Waals, steric, depletion) and hydrodynamic forces.[26]

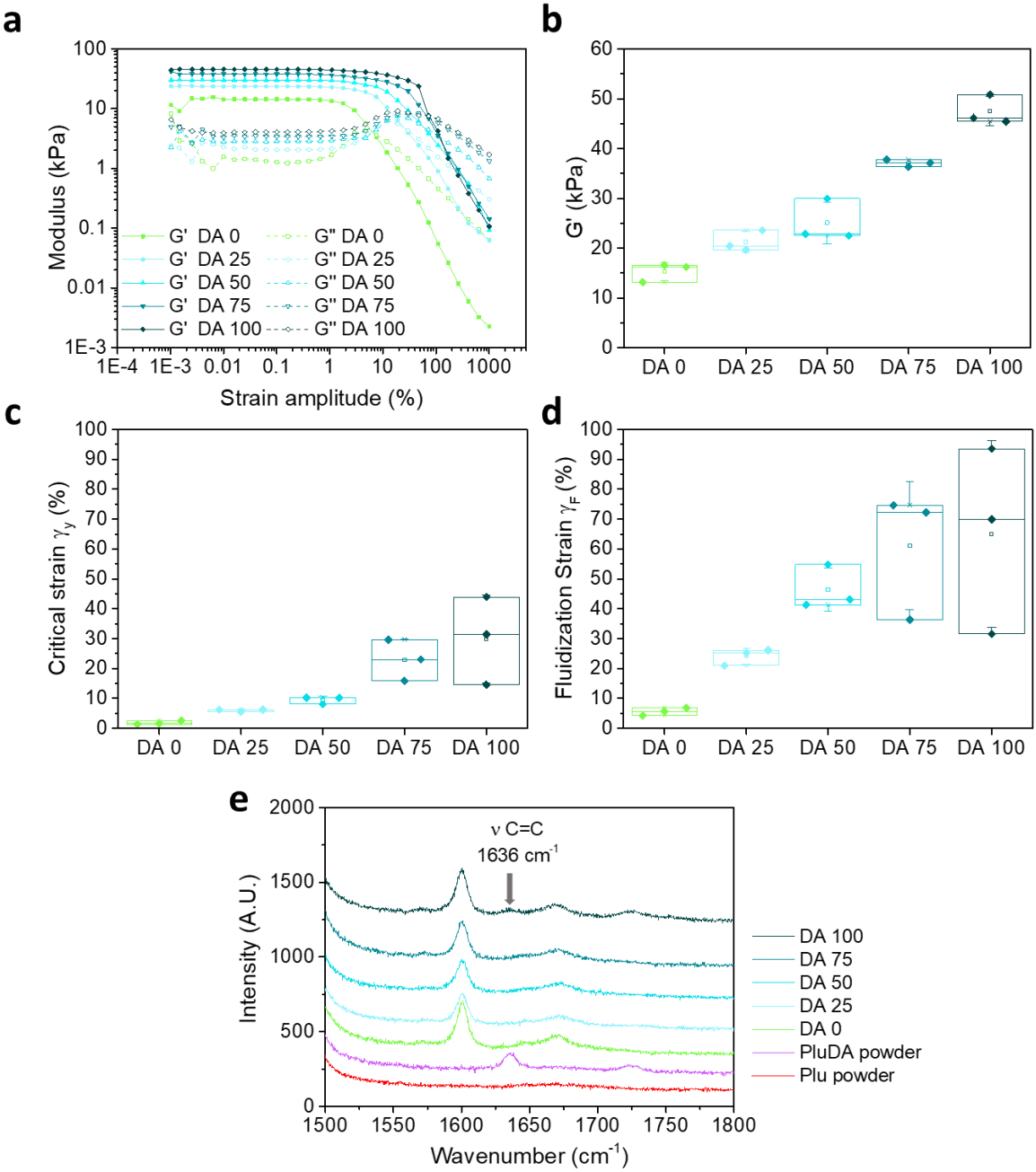

Figure 1. **a**) Representative strain amplitude sweeps of DA X hydrogels measured at a frequency of 1 Hz; **b)** G' values of DA X hydrogels from (a) at 0.1 % strain amplitude at a frequency of 1 Hz; **c)** Values of critical yield strain amplitude, γ_y, and **d)** strain amplitude at fluidization point, γ_F, of DA X hydrogels as function of X obtained from the strain amplitude sweep experiment in **a**) and **e)** Raman spectra (vertically shifted for clarity) of Plu and PluDA powders and DA X hydrogels. PluDA powder shows the C=C stretching mode (ν) at 1636 cm^{-1}. The band at 1600 cm^{-1} corresponds to the -OH bending mode of water molecules, which is absent in the powders.

Table 1: Composition and mechanical parameters of DA X hydrogels. Note that the end-group functionalization degree of PluDA component is 70% and, therefore, the real fraction of covalent fixed chains differs for each composition and reaches 70% as maximum value in DA 100.

Hydrogel name (DA X)	Plu:PluDA ratio	Real % of diacrylated chains[1]	Shear storage modulus[2] G' (kPa)	Critical strain amplitude[3] γ_y (%)	Fluidization strain amplitude[3] γ_F (%)	Critical stress τ_y (kPa)[4]	Fluidization stress τ_F (kPa)[5]
DA 0	100 : 0	0	15.3 ± 1.9	1.8 ± 0.6	5.5 ± 1.3	0.2 ± 0.0	0.2 ± 0.0
DA 25	75 : 25	17.5	21.2 ± 2.1	6.0 ± 0.4	24.1 ± 2.8	0.9 ± 0.0	1.7 ± 0.0
DA 50	50 : 50	35	25.1 ± 4.2	9.5 ± 1.2	46.4 ± 7.3	1.7 ± 0.3	3.9 ± 0.2
DA 75	25 : 75	52.5	37.1 ± 0.7	22.8 ± 6.9	61.1 ± 21.4	5.2 ± 0.8	6.7 ± 0.6
DA 100	0 : 100	70	47.5 ± 2.9	30.0 ± 14.7	65.0 ± 31.3	8.3 ± 3.1	9.9 ± 0.9

[1] *calculated taking into account 70% end-group functionalization of PluDA*

[2] *from strain amplitude sweep, values at* $\gamma_0 = 0.1$ *% (from* ***Figure 1a****)*

[3] *obtained from* ***Figure 1a***

[4] *corresponding stress values of* γ_y

[5] *corresponding stress values of* γ_F

30 wt. % solutions of diacrylated Pluronic F127 (PluDA, 70 % end-group functionalization) also form physical hydrogels at a slightly lower temperature of 14°C.[5] The substitution of the terminal –OH groups by less polar acrylic functionalities in the outer surface of the PEO shell of Pluronic micelles enhances micellar aggregation and gel formation.[14] The resulting physical PluDA hydrogels show a similar G' in the linear viscoelastic region (**Figure S1a**) and a two-fold higher critical strain amplitude for yielding in the strain sweep experiment (**Figure S1b**) compared to Plu hydrogels, confirming stronger inter-micellar interactions in the gels with acrylate end-groups.

The strain sweep curves show an overshoot in G'' at intermediate strain amplitudes between the linear viscoelastic and the fluidization regions. This overshoot is referred to as the Payne effect and is related to the fact that yielding is a gradual transition, occurring to an increased extent as the deformation increases.[27] Strain-dependent breakdown of the internal structure, length scale-dependent rearrangements or forced stress relaxation are believed to contribute to the overshoot of G''.[27]

1. Rheological behavior of **only** physically *vs.* physically **and** covalently crosslinked PluDA hydrogel

Covalently crosslinked PluDA hydrogels were prepared from 30 wt. % PluDA solutions containing 0.2 wt. % Irgacure 2959 (photoinitiator). The solution was left to form a physical gel between the rheometer plates, and it was covalently crosslinked subsequently by exposure to 365 nm light through the UV transparent bottom plate. The degree of conversion of the acrylate groups after polymerization was evaluated by Raman spectroscopy. The characteristic band for the stretching of the C=C bond, observed at 1635 cm^{-1} in the spectrum of PluDA powder, diminished in Plu powder and in the PluDA hydrogel after UV irradiation (**Figure 1e**). This indicates nearly full conversion of the acrylate groups in the photo-crosslinking step.

The polymerization of the acrylate groups influenced the rheological response of the PluDA hydrogel. The covalently crosslinked hydrogel showed a broader linear viscoelastic range than the exclusively physically crosslinked PluDA, with strain amplitude independent moduli up to γ_0 =10% (**Figure S1a**). At higher strain amplitudes, a continuous drop in G' was observed. This strain induced yielding and gradual fluidization suggests that the micellar network in the covalent crosslinked PluDA hydrogel can undergo major reorganization and stress dissipation in spite of 70% of the endgroups of the polymeric chains being covalently crosslinked. This behavior can be understood considering that acrylate groups at the PluDA chain terminals can form inter- and intra-micellar crosslinks during the photoinduced polymerization reaction.[14] Micellar clusters which are covalently crosslinked are expected to contribute to the elasticity of the hydrogel and be the reason for the higher G' and higher critical yielding strain of the covalently crosslinked PluDA hydrogel compared to the physically crosslinked PluDA hydrogel (30 ± 14.7 v*s.* 4.2 ± 0.8 %, **Figure 1c, S1b**). Intra-micellar crosslinks stabilize the micelles and form loops in the chains. These crosslinks do not interfere with the inherent ability of physical micellar aggregates to flow above the critical strain. Note that the average residence time of a Pluronic molecule in a physical micellar aggregate has been estimated to be several hours.[28] Therefore, crosslinking during photopolymerization (1 min time scale) can mainly occur between chain ends located in close proximity. The observed strain-induced yielding and fluidization (**Figure 1d**) above a critical yield stress in our PluDA hydrogels suggests that a significant fraction of the covalent crosslinks are intra-micellar. This has been previously suggested by other authors based on gel permeation chromatography (GPC) and

light scattering analysis of the sol phase after crosslinking and cooling below the transition temperature.[14]

2. Rheological behavior of covalently crosslinked Plu/PluDA hydrogels with variable PluDA content

We analysed the rheological response of Plu/PluDA covalent hydrogels as a function of the degree of covalent crosslinking. Near full conversion after the photo-crosslinking step was confirmed by Raman spectroscopy (**Figure 1e**).

Covalently crosslinked DA X hydrogels showed an increasing trend of G', γ_Y and γ_F values from Plu (=DA 0) to PluDA (=DA 100) hydrogels. The strain amplitude sweep curves showed a linear viscoelastic and a fluidization region. The storage modulus G' at 0.1 % strain amplitude increased from 15.3 ± 1.8 to 47.5 ± 2.9 kPa as the PluDA content increased from 0 to 100 % (**Figure 1c**). The critical strain for yielding, γ_y, also increased from 1.7 ± 0.4 to 29.7 ± 15.2 % (**Figure 1d, Table 1**) from DA 0 to DA 100. The strain amplitude needed to reach the fluidization point (crossover of G'' and G', as opposite to gelation point), γ_F, increased from 5.5 ± 1.2 to 65.0 ± 31.3 % (**Figure 1e**) and the corresponding stress values at the fluidization point ranged from 0.2 ± 0.0 to 9.9 ± 0.9 kPa (**Figure S2, Table 1**). The increase in the density of covalent links between neighboring micelles (inter-micellar) with increasing X hinders the viscous deformation of the hydrogel and higher mechanical stability and elasticity under the applied strain.

3. Stress relaxation of DA X hydrogels

Figure 2a-c shows the stress induced in DA 0, DA 50 and DA 100 hydrogels during a stress relaxation experiment with step-strain increase from 0.5 to 30 % (300 s) and strain raise time of 200 ms. The stress relaxation curves are normalized with respect to the maximum stress values attained post the strain raise time of 200 ms for better visualization. In DA 0 hydrogels, the maximum induced stress increased from 78 ± 17 to 231 ± 55 Pa with the applied strain of 0.5 to 5 %, and it plateaued for larger deformations (**Figure 2d**). In contrast, the maximum induced stress in covalently crosslinked DA 100 increased linearly with the strain up to 15 % and reached values up to 5708 ± 246 Pa (**Figure 2d**), denoting a primarily elastic behavior within this strain range. DA 50 showed an intermediate behavior. These differences are in agreement with the observations from the strain sweep experiment (**Figure 1c**), where γ_Y of

physical DA 0 hydrogel was 1.8 ± 0.6% while that for covalently crosslinked DA 100 hydrogel was 30.0 ± 14.7 %.

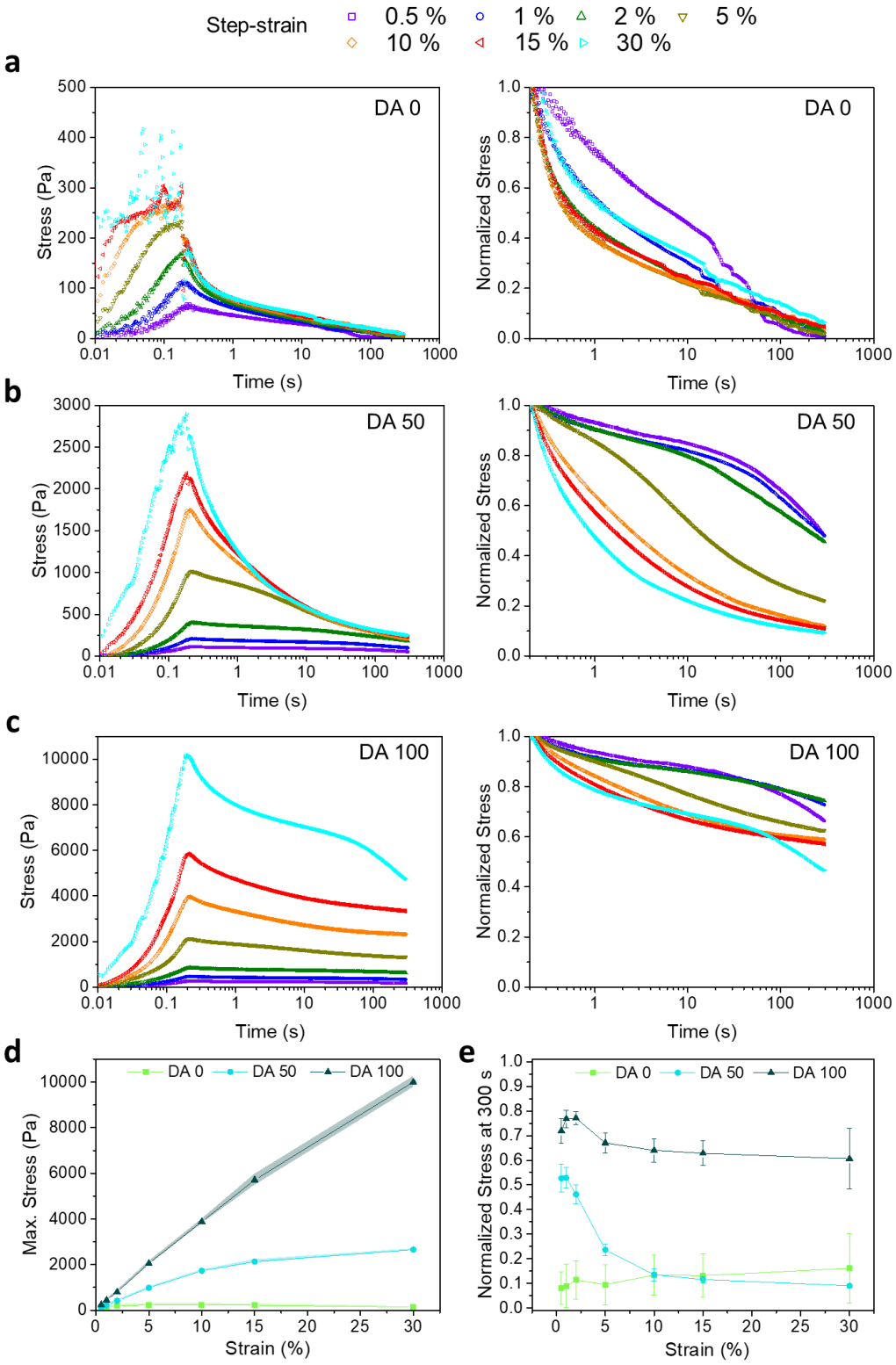

Figure 2: Representative step-strain stress relaxation curves as a function of increasing applied strain values from 0.5 to 30 % on **a)** DA 0, **b)** DA 50 and **c)** DA 100 hydrogels (left) with their corresponding normalized stress values (right); **d)** Mean maximum stress values at 200 ms

(strain raise time) and **e)** Normalized stress values at the end of the stress relaxation test (300 s). Error bars indicate standard deviation, N=2 for DA 0 and DA 50 at 30 % applied strain, N=3 for all the rest.

The strain-dependent stress relaxation curves of DA X hydrogels were also dependent on the amount of X (**Figure 2a**). Whereas DA 0 was able to relax the induced stress almost completely within 300 s at all strain values, DA 100 retained at least 60% of the stress, in agreement with its elastic nature (**Figure 2e**). DA 50 showed an intermediate behavior with up to 50% relaxation for strains <2%, whereas it relaxed >70% for larger strain values. For all hydrogels, the stress was dissipated faster at higher strains, when the γ_F range was reached (**Figure 2e**).

Relaxation modulus is used to describe the stress relaxation of viscoelastic materials with respect to time.[29] The comparative relaxation behavior of DA X hydrogels (for X = 0, 25, 50, 75 and 100) at 1 % strain, i.e., within the linear viscoelastic regime, is shown in **Figure 3**. The shape of the curves indicates that stress is dissipated by two different relaxations processes with different time scales: a fast first one (<1 s) and a slower second one (>1 min). To analyze the relaxation mechanisms behind the two processes, the stress relaxation curves were fitted to a linear combination of two exponential functions **(Eq. 1)**[30]:

$$G = G_0 \left\{ \left(A \times \exp\left[-\left(\frac{t}{\tau_1} \right)^{\beta_1} \right] \right) + (1 - A) \times \exp\left[-\left(\frac{t}{\tau_2} \right)^{\beta_2} \right] \right\} + G_e \qquad \text{.....(1)}$$

where G_0 is the relaxation modulus linearly extrapolated to zero time, τ_1 and τ_2 are the viscoelastic relaxation times for the two processes, β_1 and β_2 are stretching exponents for the two processes ($0 < \beta \leq 1$), A is the fractional contribution of the fast relaxation to the whole relaxation process ($0 < A$) and G_e is the equilibrium relaxation shear modulus. This function fitted well with the experimental data with $r^2 > 0.99$ (**Figure 3c**). The values of G_0, G_e, A, τ_1, τ_2, β_1, and β_2 and are represented in **Figure 3 d-j** as a function of the hydrogel composition. The two relaxation times τ_1 (<1 s) and τ_2 (>1 min) differed in more than two orders of magnitude and showed an opposite dependence on the degree of the covalent crosslinking of the hydrogels. τ_1 decreased from 0.25 s to 0.01 s as X increased from 0 to 100 (**Figure 3g**), i.e. the relaxation became faster as the covalent crosslinking degree increased. The relative contribution of this relaxation mode to stress dissipation (A parameter, **Figure 3f**) increased with the covalent crosslinking of the hydrogel. The shape parameter β_1, which reflects the width of the relaxation time distribution, did not show significant changes with the hydrogel

composition and is around 0.3-0.4 (**Figure 3g**). The relaxation process at longer time scales became slower in hydrogels with increasing covalent crosslinking (mean τ_2 increased from nearly 100 s to 560 s for DA 0 to DA 100, **Figure 3h**) and the strength of this relaxation decreased with X. The possible mechanisms behind these relaxations are weighed up further in the discussion section.

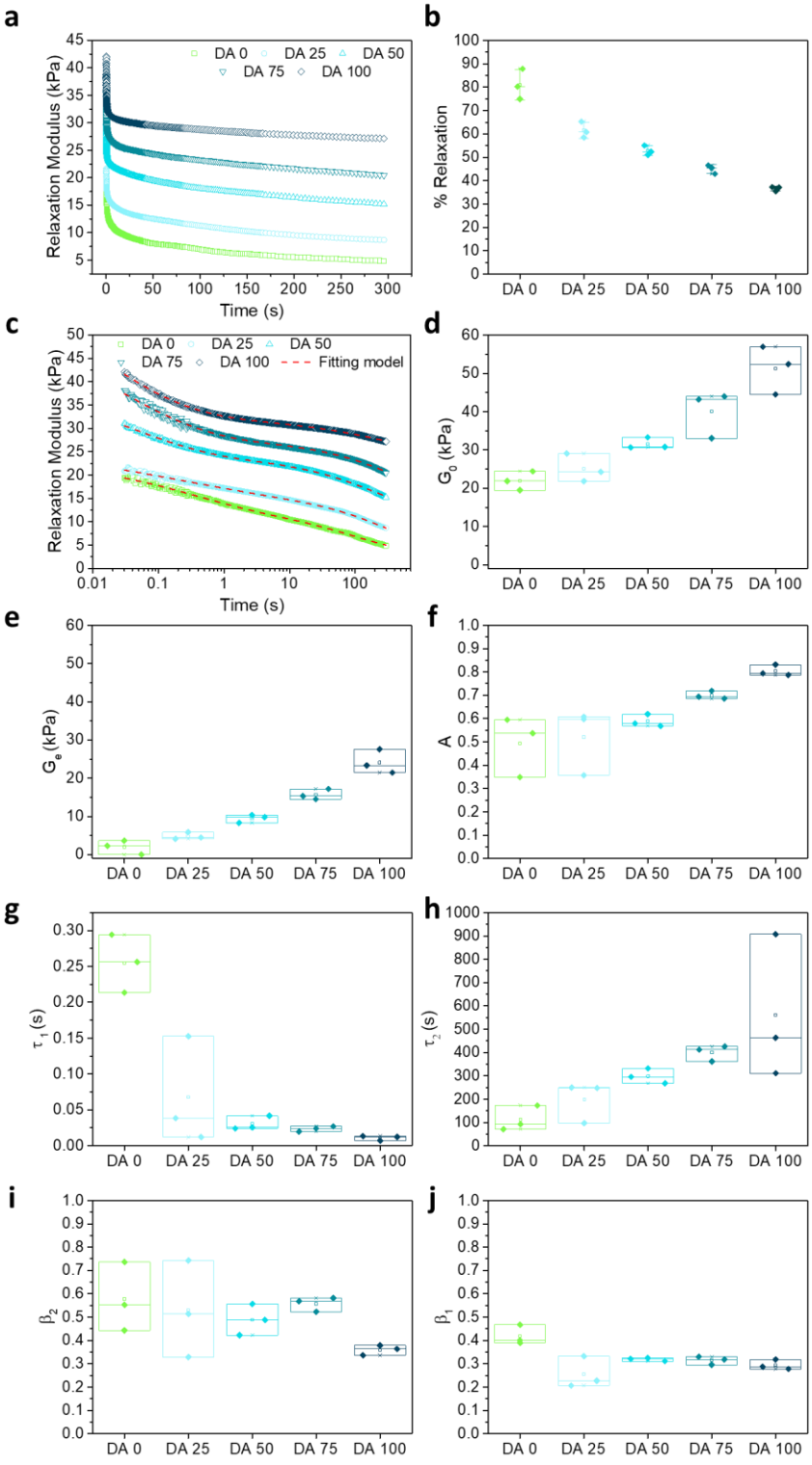

Figure 3: a) Representative stress relaxation curves of crosslinked DA X hydrogels at a constant applied strain of 1 %. **b)** Calculated normalized drop of relaxation modulus in DA X hydrogels from experiment in a) at time = 300 s (see details in experimental section). **c)** Stress relaxation curves from a) represented with a logarithmic scale and the fits with a double stretched exponential function (red dashed lines). Data below 30 ms were not considered for the fitting since this time was required by the equipment to reach a stable strain value of 1 %; **d)** G_0 values as function of X that were extrapolated linearly from stress relaxation curves in a) to time zero. **e-j)** Fitted parameters as a function of X: **e)** G_e; **f)** A (fractional contribution of relaxation 1, fast relaxation process); **g)** τ_1 ; **h)** τ_2 ; **i)** β_1 and **j)** β_2. The experimental curves of three consecutive measurements are shown in **Figure S3**. All measurements were performed at room temperature.

4. Creep-recovery of DA X hydrogels

Figure 4a shows a creep-recovery experiment with DA X hydrogels at a constant stress of 100 Pa. In DA 25-75 hydrogels an instantaneous deformation was observed, followed by a slower deformation (creep). The instantaneous deformation was more pronounced in hydrogels with higher covalent crosslinking, while the creep process was more pronounced in hydrogels with lower PluDA concentration. DA 100 reached the plateau right after the initial deformation. DA 0 was the farthest from reaching a plateau deformation value during the 180 s of creep. When the 100 Pa stress ceased, an instantaneous and a time-dependent strain recovery was observed for all samples. DA 50-100 almost instantaneously fully recovered to their initial state, which is in agreement with their predominant elastic character as consequence of the covalent crosslinks. In comparison to that, DA 25 and DA 0 retained a residual deformation (**Figure 4a**), in agreement with their predominant physical gel character.

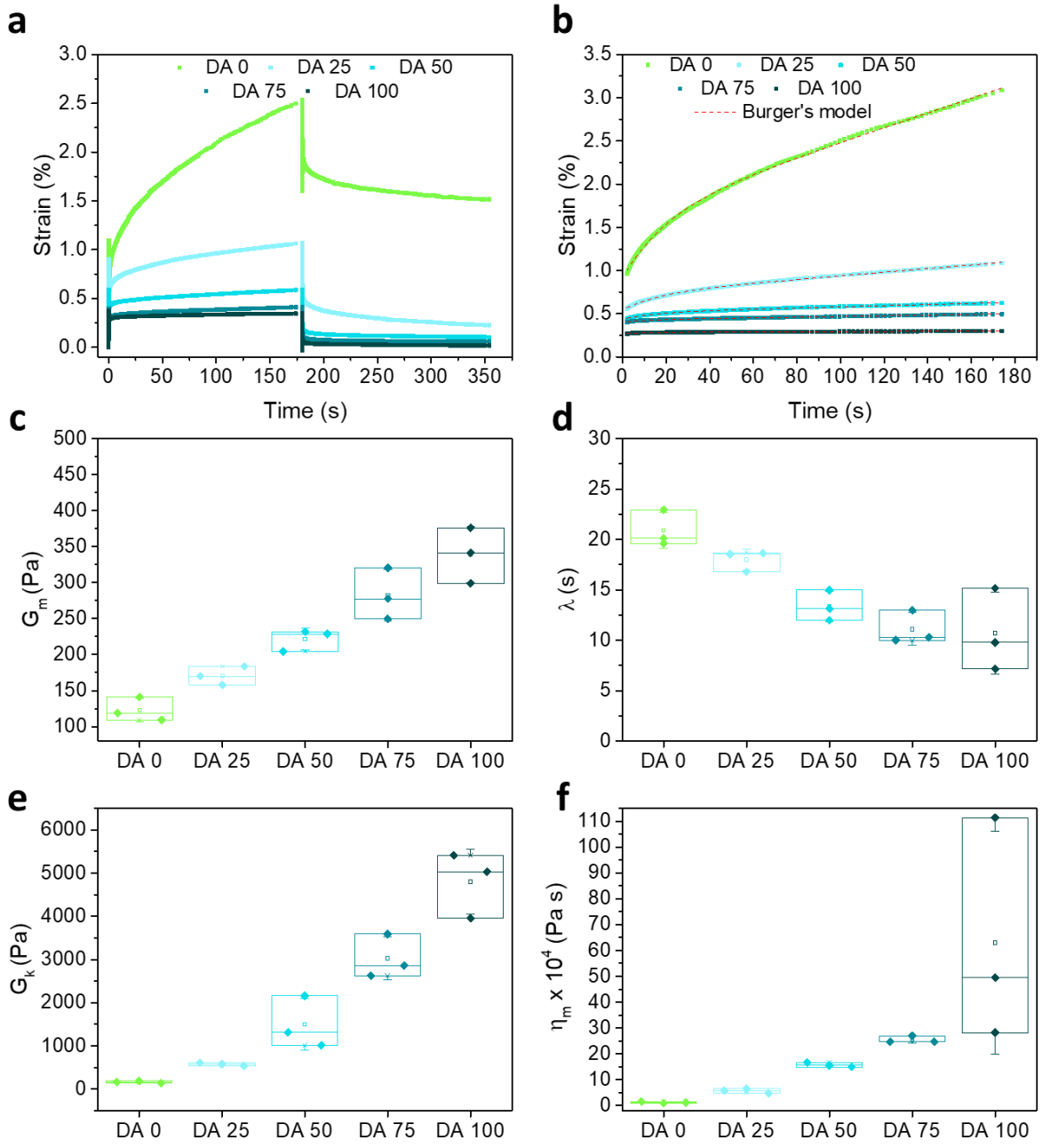

Figure 4: **a)** Representative creep/recovery curves of DA X hydrogels at an applied stress of 100 Pa for 180 s. The strain was monitored during stress application and also during the recovery phase for an additional 180 s. **Figures S4 and S5** show all experimental curves. **b)** Creep curves and fittings to the Burgers model (Eq. 3, red dotted lines), **c-f)** parameters of the Burgers fitting represented as a function of X. G_m and η_m denote the spring constant of the spring and the viscosity of the dashpot in the Maxwell element, G_k is the spring constant of the dashpot in the Kelvin element and λ is the retardation time.

The creep curves were fitted to a four-elements Burgers model[31][32][33], consisting of Maxwell and Kelvin-Voigt elements.[34][35] In this model, the strain during creep, γ_{creep} , is expressed as:

$$\gamma_{creep} = \frac{\tau}{G_m} + \frac{\tau}{G_k}\left(1\text{-}e^{\frac{-t}{\lambda}}\right) + \frac{\tau}{\eta_m}t \quad \text{......(2)}$$

where τ is the applied shear stress (100 Pa), t denotes the time after loading, G_m denotes the spring constant of the spring , η_m denotes the viscosity of the dashpot in the Maxwell element, G_k is the spring constant of the dashpot in the Kelvin element, and λ is the retardation time (η_k/G_k) needed to achieve 63.2% of the total deformation in the Kelvin unit (where η_k is the viscosity of the dashpot in the Kelvin element). The Burgers model fit was applied to the experimental data (red dashed lines in **Figure 3c**) and obtained fitting parameters as function of the hydrogel composition are represented in **Figure 3d-j**. The elastic constants G_m and G_k increased in DA X hydrogels with increasing X, and therefore an increased elasticity is observed due to a higher number of crosslinks. The reorganization of covalently linked micelles and clusters requires additional work, which causes an increment in the opposition to deformation. This higher resistance capacity contributes to elasticity. In the Burgers model, the retardation time λ is connected to the viscoelastic solid material behavior. In the micellar hydrogel model described before, the viscoelastic response is expected to depend on the intermolecular forces between micelles connected by inter-micellar covalent bonds. The shorter retardation times observed with increasing X indicate that the covalent connection between the micelles accelerates the sliding of micelles and the deformation of the hydrogel. Furthermore, η_m increases with X and reflects the increasing resistance, and thus lesser deformation due to the viscous component. We associate this with sliding of micelles and clusters connected by physical interactions.

The recovery part of the creep experiment was fitted using a Weibull distribution equation. The strain $\gamma_{recovery}$ is expressed as[31]:

$$\gamma_{recovery} = \gamma_k \{\exp\left[-\left(\frac{t-t_0}{\eta_r}\right)^{\beta}\right]\} + \gamma_p \quad \text{...... (3)}$$

where γ_k denotes the delayed viscoelastic strain recovery (Kelvin-Voigt element), η_r is the characteristic life parameter, β the shape factor, t_0 the time when the stress is removed, and γ_p the permanent irreversible strain. The Weibull equation fitted the experimental data (**Figure 5a**). The delayed viscoelastic strain recovery γ_k decreased with increasing covalent

crosslinking in DA X hydrogels, reflecting that the presence of permanent crosslinks hinders viscoelastic deformation. The permanent irreversible strain γ_p was 10 times higher for DA 0 than for the other hydrogels as consequence of the absence of covalent bonds that provide elasticity.

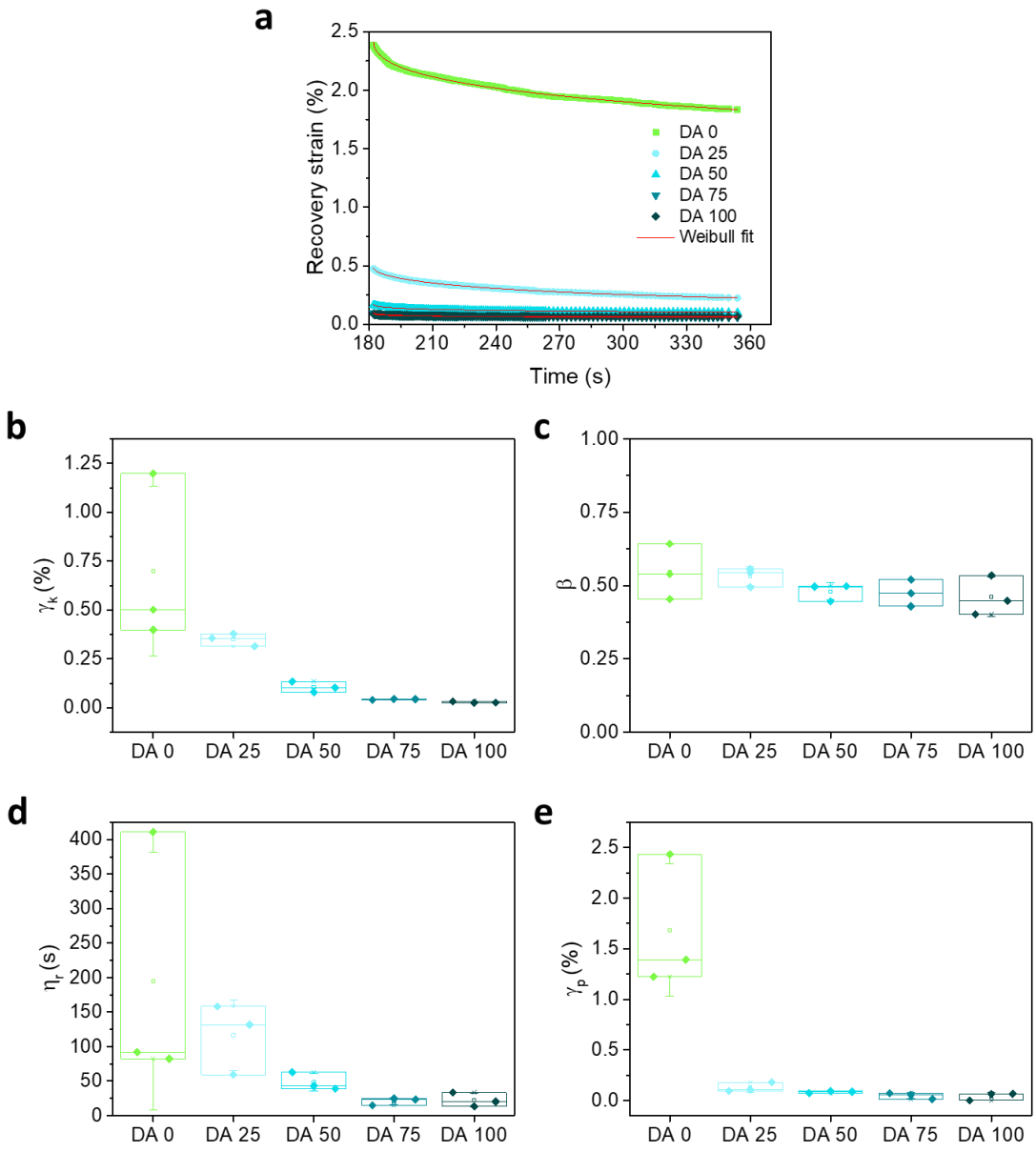

Figure 5: **a)** Recovery curves including fittings to the Weibull distribution function and **b-e)** parameters of the Weibull fitting as function of DA X composition.

The elastic, viscoelastic and plastic contributions to the deformation extracted from the Weibull model are represented in F**igure 6**.[31] The elastic recovery corresponds to the

instantaneous recovered deformation and is represented by the Maxwell spring in the Weibull model. $\gamma_{maxwell\ spring}$ was calculated as:

$$\gamma_{maxwell\ spring} = \gamma_{ms} = \gamma_{Maximum} - (\gamma_k + \gamma_p) \quad \text{.....(4)}$$

where $\gamma_{maximum}$ is the strain at the end of the creep test. At an applied stress of 100 Pa, hydrogels DA 25-100 showed increasing elastic and decreasing viscoelastic responses with increasing covalent crosslinking, and a small plastic response with little dependence on X. DA 0 hydrogels showed a strong plastic response and a comparatively much lower elastic and viscoelastic contributions.

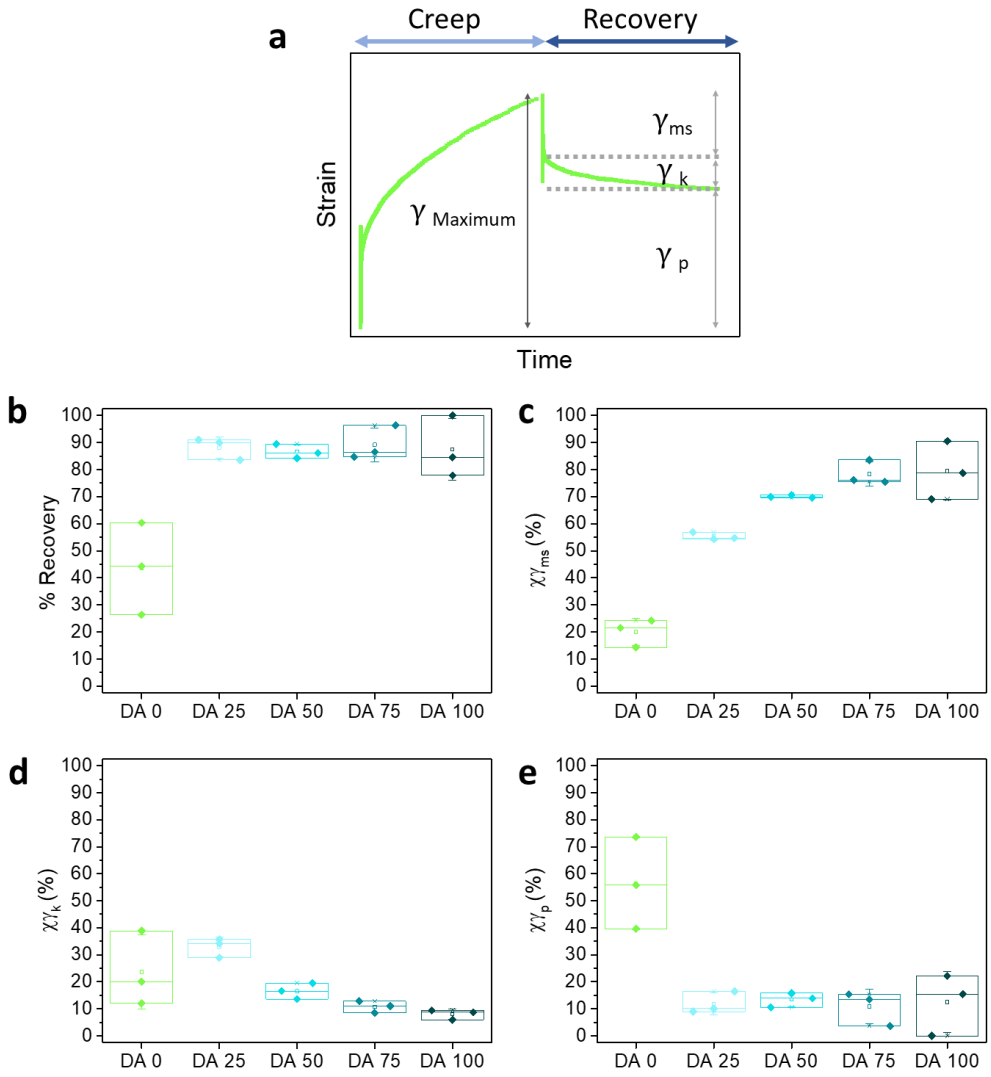

Figure 6: a) Elastic, viscoelastic and plastic contributions obtained from the creep-recovery experiment. The curve corresponds to DA 0 at an applied stress of 100 Pa; **b)** Recovery (%)

calculated from recovery curves at 180 s after 100 Pa applied stress; **c-e)** Contributions of elastic, **d)** viscoelastic and **e)** plastic deformation.

Discussion

The rheological properties of micellar DA X hydrogels are discussed here within the framework of a granular gel.[36][37] The internal structure of granular gels depends on the particle volume fraction and the strength of inter-particle interactions.[38] At high particle volume fractions and weak interaction forces, gelation occurs as a consequence of the dynamical arrest of a phase separation process.[39] In the particle-rich domains, particles aggregate and form clusters that grow until their dynamics is arrested within the 3D network.[40] Clusters act as rigid, load bearing units and have been postulated to be the origin of elasticity in colloidal gel networks. The reversibility of the interactions between particles allows shear-induced rearrangement of the aggregates and particles by breaking reversible bonds. As a consequence, granular hydrogels show shear thinning behavior. The observed behavior of physical Pluronic hydrogels is in agreement with this picture. The inter-micellar covalent bonds introduced after physical gelation in DA X hydrogels reinforce the stability of the clusters and contribute to a stronger elastic character of the material.[37]

Previous literature has discussed the behavior of Pluronic F127 hydrogels under shear.[17][41] Micelles are considered hard spheres and their aggregates can undergo phase transitions (melting, recrystallization) or reorientation as function of shear conditions (shear stress, rate or direction).[17][41] Inter-micellar covalent bonds in DA X hydrogels internally stabilize micellar clusters and affect the rearrangement mechanisms. We expect that the time scale of these rearrangements relates to the observed experimental time scales for stress relaxation. Our fitting method for the stress relaxation curves of DA X hydrogels indicated two different relaxation processes with relaxation times τ_1 (<1 s) and τ_2 (>1 min) that depend on DA content. The fast relaxation process became faster and more prominent with increasing covalent crosslinking. We associate this relaxation to structural rearrangements at macroscopic, network scale which require cooperative motion of micelles.[42][43] In contrast, the slow relaxation process could be associated to relaxation modes at microscopic scale, such as the breaking of physical bonds between micelles within clusters, which becomes slower with increasing number of covalent crosslinks.[42][44] A recent article has studied the deformation mechanisms of 24 wt% PluDA hydrogel in an ionic liquid using rheology and SANS.[45] The

authors highlighted the possible contribution of free inter-micellar PluDA chains to elasticity by forming covalent inter-micellar bridges. Under tensile stress, the bridging chains would store mechanical energy during stretching and pull micelles back into their original positions after deformation. Although this model could explain our results, the range of stress applied was three orders of magnitude larger than the stress applied in our experiments and, therefore, the deformation mechanisms might differ.

DA X hydrogels have been used as matrices to encapsulate and control the proliferation of bacteria and yeast in examples of engineered living materials.[7][46] With strain sweep, stress relaxation and creep-recovery experiments and their fitted parameters, we correlated the rheological properties of the DA X hydrogels to the bacterial behavior quantified in our previous work.[5] Our studies of *E. coli* within DA 0-75 hydrogels showed bacteria growing into colonies up to a steady size that decreased almost linearly with the degree of covalent crosslinking (**Figure 7**).[5] This trend was independent of nutrient or oxygen availability and could only be explained in terms of bacteria's mechanosensing and mechanoresponse, i.e. the ability of the bacteria - either individually or collectively - to detect and react to the differences in the mechanical properties of the embedding microenvironment.[12] The inverse linear dependence of colony volume with X for DA 0-75 hydrogels correlates with the trends observed for the storage modulus (**Figure 1c**) and the critical stress for fluidization τ_F (**Figure S2c**) with X in the rheology experiments. Bacteria embedded in DA 100 hydrogels showed similar growth volumes as in DA 75, indicating that the mechanical parameters regulating bacteria growth do not vary significantly between these two hydrogels. The elastic contribution to deformation $X\gamma_{ms}$ (**Figure 6c**) in our creep-recovery experiments was similar for DA 75 and DA 100, whose trend coincides with the bacterial colony sphericity values at X≥50. The deviation between the trends for lower X (0 and 25) can be attributed to the limited nutrients available for the bacteria within the constructs. However, the available data is not yet enough to make statements about the direct correlation between the mechanical response and rates of bacteria growth.

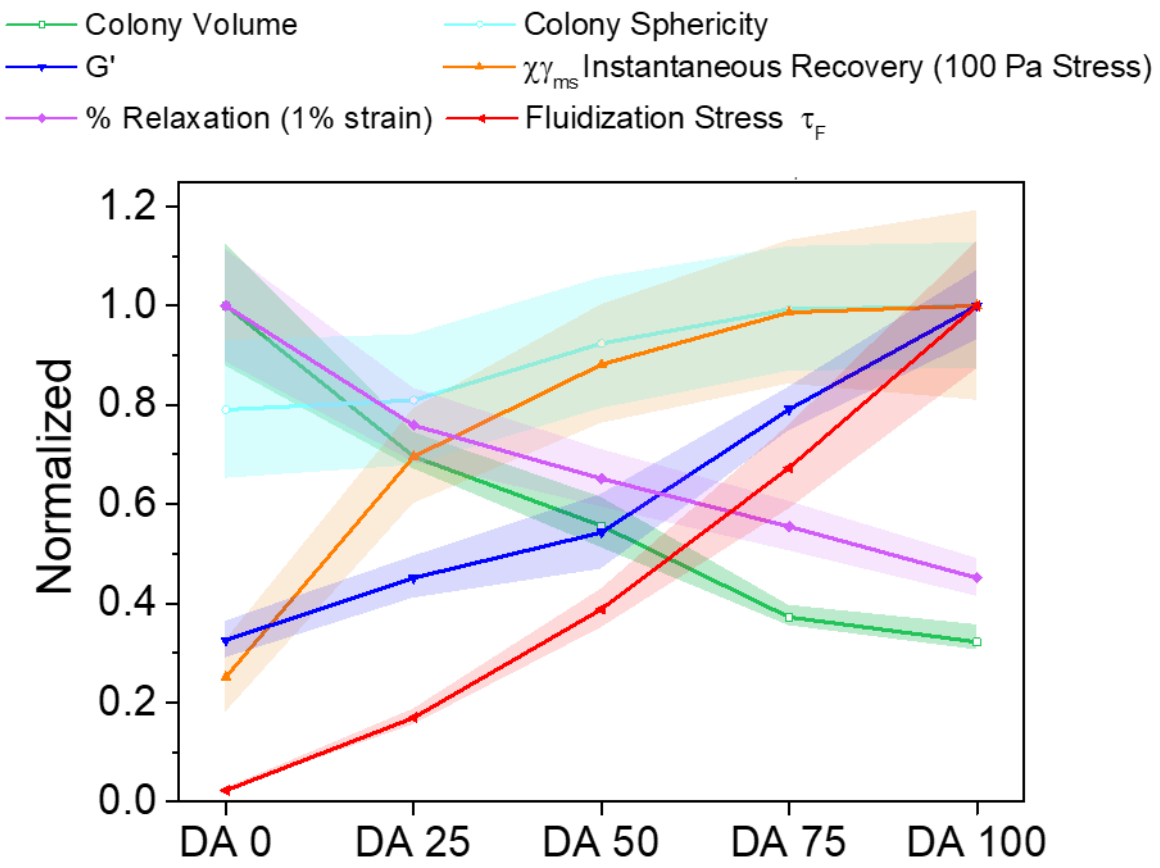

Figure 7: Comparing trends of normalized parameters calculated from fitted data for material rheological properties and bacterial growth. 95th percentile volumes of colonies after 24 h and mean sphericity of colonies[5], shear storage modulus G', fluidization stress τ_F, contribution of the Maxwell spring γ_{ms} from the creep-recovery test (applied stress of 100 Pa) and % relaxation post stress relaxation test with 1 % constant strain applied. The values were normalized with respect to the highest value in each category. The symbols and shaded regions of the normalized colony volume data indicate 95 ± 2 percentile value range, for all other data the symbols and shaded regions indicate mean ± SD.

Like other bacteria, *E. coli* exerts forces on the surrounding matrix as it grows as consequence of its internal turgor pressure. Turgor pressure depends on the bacteria strain and is estimated as 30-300 kPa for *E. coli*.[12] As bacteria grow into colonies, collective pushing forces resulting from the combination of single-cell forces in the colony lead to a build-up of mechanical pressure within populations as a self-driven jamming mechanism.[47] The growth rate of *E coli* in suspension and in the presence of nutrients is >20 minutes. According to our rheological results (**Figure 1a and S2**), a hypothetical stress of 10 kPa at a time scale of 20 minutes applied

by growing *E. coli* to a surrounding DA X matrix would deform the hydrogel beyond the yield point. Therefore, a correlation between bacteria growth and the elastic/viscoelastic properties of the matrix that would determine the residual stress at long relaxation times, seems reasonable as a first approximation.

Rheological experiments probe mechanical responses at macroscale although bacteria probe the mechanics of their microenvironment at microscopic or eventually molecular scale.[12] The extent to which rheological data can be correlated with cellular responses is an issue of active debate in the mechanobiology community.[12][33] Future quantification of the stress applied at single bacterium and at bacterial colony level through traction force microscopy studies could provide some clarity. This question remains also open in mechanobiology studies with mammalian cells, despite extensive research efforts in the field during the last two decades.[1][48] Hydrogels with granular structure at the microscale, like Pluronic, might present additional particularities and advantages over other hydrogel systems. A recent study of 3D cultures of endothelial cells embedded in granular gelatin gels with different strengths of inter-particle interactions showed different morphologies during vessel growth, either as restricted networks or as extended and interconnected networks.[49] These results suggest that tuning the internal morphology of Pluronic hydrogels by means of end-group functionalization or gelation conditions could also affect mechanics and help to regulate bacteria responses.

Conclusions

In this article, we present the rheological behavior of Pluronic/Pluronic diacrylate hydrogels with compositions relevant for embedding and culturing bacteria within the context of living material systems. We quantified the elastic, viscoelastic and plastic responses of physical DA X hydrogels with varying degree of covalent crosslinking. We identified mechanical parameters of the network that correlate with cell growth and which could be used to control and eventually predict the dynamics of a bacteria population in engineered living materials constructs based on Pluronic hydrogels. Physical confinement of an expanding bacteria colony and the mechanical resistance of the environment to the colony growth are proven to be important factors in triggering biofilm development, also in infection scenarios.[50] The results from the current and future work provide correlations between material parameters and cell responses in model encapsulated systems that could help to understand the natural cases.

Materials and Methods

Sample preparation

Pluronic diacrylate (PluDA) was synthesized by reaction of Pluronic F127 (Plu) with acryloyl chloride in the presence of triethylamine according to a reported protocol.[31] Acrylation degrees of 70% were typically obtained. The conditions for DA X gel preparation were taken from a previous report.[5] In short, 30 wt. % Plu and PluDA stock solutions (named DA 0 and DA 100, respectively) were prepared in milliQ water and contained 0.2% w/v Irgacure 2959 as photoinitiator. Solutions were stored at 4 °C. DA 25, DA 50 and DA 75 hydrogels were prepared by mixing DA 0 and DA 100 stock solutions in the following ratios- 3:1 (DA 25), 1:1 (DA 50) and 1:3 (DA 75) (**Table 1**). After mixing, the DA X hydrogels were allowed to form at room temperature for 10 minutes.[47] For the photoinitiated crosslinking, hydrogels were exposed to UV light (365 nm, 6 mW/cm^2) using a OmniCure Series 1500 lamp for 60 s through a UV transparent bottom plate for rheology.

Raman spectroscopy of Plu/PluDA powders and DA 0-100 hydrogels

Raman investigations were carried out at ambient conditions on a LabRAM HR Evolution HORIBA Jobin Yvon A Raman microscope (Longmujeau, France) using a 633 nm He–Ne laser (Melles Griot, IDEX Optics and Photonics, Albuquerque, NM, USA) equipped with 1800 lines per mm grating.

Rheological measurements

The rheological properties were measured with a stress-controlled rheometer (DHR3, TA Instruments) using a parallel plate geometry. A 20 mm Peltier plate/ UV transparent plate was used as bottom plate and a smooth stainless steel 12 mm disk was used as top plate. The rheometer was equipped with a UV Source (OmniCure, Series 1500, 365 nm, 6 mW/cm^2) for illumination of the hydrogel samples in between the rheometer plates. Experiments were performed at room temperature (22-23°C). To avoid drying of the sample by evaporation during testing a solvent trap was used and the sample was sealed with silicone oil.

30 wt. % DA X hydrogels were prepared by pipetting 35 µL of a freshly prepared 30 wt. % DA X precursors solution on the rheometer plate, and allowing the gel to form between the plates (diameter 12 mm, gap 300 µm) during 10 min. The polymerization of the acrylate groups was

initiated by exposure to 365 nm (6 mW/cm^2) through the UV transparent bottom plate. Strain sweeps were conducted from 0.001% to 1000% at a frequency of 1 Hz. In the strain amplitude sweep curves, a line was fit to the plateau region (linear) and the drop-off region (non-linear). The intersection is taken as the critical strain value (γ_y).[25][51] Fluidization strain (γ_F) was taken as the value at the intersection of G' and G'', i.e., at G' = G'').[51] The corresponding stress values were used as critical stress (τ_y) and fluidization stress (τ_F) values. The experimental conditions for the rheological experiments were taken from our previous work.[5]

Stress relaxation measurements

In the experiment shown in **Figure 2** (step-strain experiment), strains of 0.5, 1, 2, 5, 10, 15 and 30 % were applied to the same sample (DA 0, 50 and 100, n=3) for 300 s with a strain raise time of 0.2 s. To avoid cumulative stress buildup and shear history effects, the strain was reversed (negative strain, equivalent to the positive strain) after each run to reach rheometer stress = 0 Pa, and the next run was started after 10 min equilibration time.

In the experiment shown in **Figure 3 and S3**, a constant strain of 1% was applied to the sample (strain raise time 0.01 s) and the stress was monitored for 300 s. Each experiment was repeated three times.

The percentage of relaxation was defined as the drop in the relaxation modulus from the start (30 ms) to the end (300 s) of the experiment normalized by the starting relaxation modulus[52].

The relaxation curves in **Figure 3 and S3** were fitted to a linear combination of two exponential or Kohlrausch–Williams–Watts (KWW) functions,[30]

$$G = G_0 \left\{ \left(A \times \exp\left[-\left(\frac{t}{\tau_1} \right)^{\beta_1} \right] \right) + (1 - A) \times \exp\left[-\left(\frac{t}{\tau_2} \right)^{\beta_2} \right] \right\} + G_e \qquad \text{.....(1)}$$

where G_0 is relaxation modulus linearly extrapolated to zero time, τ_1 and τ_2 are viscoelastic relaxation time for the two processes ($0 < \tau$), β_1 and β_2 are stretching exponent for the two processes ($0 < \beta \leq 1$), A is fractional contribution of the fast relaxation to the whole relaxation process ($0 < A$) and G_e is the equilibrium relaxation shear modulus.

Creep recovery measurements

A shear stress of 100 Pa was applied for 180 s to the hydrogel sample in the rheometer. The shear strain was monitored during this time (creep phase), and for a further 180 s after

removal of the shear stress (recovery phase). Creep ringing phenomenon was observed at short time scales (2 s) in the creep and recovery experiments.[53]

Creep deformation, γ_{creep}, was fitted to a Burgers model:[31][32][33]

$$\gamma_{creep} = \frac{\tau}{G_m} + \frac{\tau}{G_k}\left(1-e^{\frac{-t}{\lambda}}\right) + \frac{\tau}{\eta_m}t \quad \ldots\ldots(2)$$

where, τ is the applied shear stress (fixed to 100 Pa), t denotes the time after loading, G_m denotes the shear modulus (or spring constant) of the spring and and η_m denotes the viscosity of the dashpot in the Maxwell element. G_k denotes the shear modulus (or spring constant) and η_k denotes the viscosity of the dashpot in the Kelvin element and λ is the retardation time taken to produce 63.2% of the total deformation in the Kelvin unit. The non-linear curve fit function of the OriginPro 9.1 software was used for the fitting and four parameters (G_m, G_k, η_m and τ) were defined. Creep ringing phenomenon was observed at short time scales. Therefore only data at $t > 2$ s were considered in the fitting.[53]

Recovery data was fitted to a Weibull distribution function.[31][34]

$$\gamma_{rec} = \gamma_k \{\exp\left[-\left(\frac{t-t_0}{\eta_r}\right)^{\beta}\right]\} + \gamma_p \quad \ldots\ldots (3)$$

where where γ_{rec} denotes the deformation after the instantaneous strain recovery, γ_k denotes the delayed viscoelastic strain recovery (Kelvin-Voigt element), η_r is the characteristic life parameter and β the shape factor. The stress is removed at time t_0 (180 s) and γ_p is the permanent irreversible strain. Ringing phenomenon was observed again at short time scales as in creep data. Therefore $t_0 = 182$ s was considered for the fitting.

References

[1] M. Rizwan, A. E. G. Baker, M. S. Shoichet, *Advanced Healthcare Materials* **2021**, *10*, 2100234.

[2] X. Liu, M. E. Inda, Y. Lai, T. K. Lu, X. Zhao, *Advanced Materials* **2022**, *34*, 1.

[3] D. Indana, P. Agarwal, N. Bhutani, O. Chaudhuri, *Advanced Materials* **2021**, *33*, 2101966.

[4] A. Rodrigo-Navarro, S. Sankaran, M. J. Dalby, A. del Campo, M. Salmeron-Sanchez, *Nature Reviews Materials* **2021**, *6*, 1175.

[5] S. Bhusari, S. Sankaran, A. del Campo, *Advanced Science* **2022**, *2106026*, 1.

[6] S. Sankaran, J. Becker, C. Wittmann, A. Campo, *Small* **2019**, *15*, 1804717.

[7] X. Liu, H. Yuk, S. Lin, G. A. Parada, T. C. Tang, E. Tham, C. de la Fuente-Nunez, T. K. Lu, X. Zhao, *Advanced Materials* **2018**, *30*, 1704821.

[8] T. G. Johnston, S. F. Yuan, J. M. Wagner, X. Yi, A. Saha, P. Smith, A. Nelson, H. S. Alper, *Nature Communications* **2020**, *11*, 563.

[9] T. Butelmann, H. Priks, Z. Parent, T. G. Johnston, T. Tamm, A. Nelson, P. J. Lahtvee, R. Kumar, *ACS Applied Bio Materials* **2021**, *4*, 7195−7203.

[10] A. Saha, T. G. Johnston, R. T. Shafranek, C. J. Goodman, J. G. Zalatan, D. W. Storti, M. A. Ganter, A. Nelson, *ACS Applied Materials and Interfaces* **2018**, *10*, 13373.

[11] H. H. Tuson, G. K. Auer, L. D. Renner, M. Hasebe, C. Tropini, M. Salick, W. C. Crone, A. Gopinathan, K. C. Huang, D. B. Weibel, *Molecular Microbiology* **2012**, *84*, 874.

[12] Y. F. Dufrêne, A. Persat, *Nature Reviews Microbiology* **2020**, *18*, 227.

[13] D. Attwood, *International Journal of Pharmaceutics* **1985**, *26*, 25.

[14] M. Di Biase, P. De Leonardis, V. Castelletto, I. W. Hamley, B. Derby, N. Tirelli, *Soft Matter* **2011**, *7*, 4928.

[15] R. Basak, R. Bandyopadhyay, *Langmuir* **2013**, *29*, 4350.

[16] J. Dey, S. Kumar, S. Nath, R. Ganguly, V. K. Aswal, K. Ismail, *Journal of Colloid and*

Interface Science **2014**, *415*, 95.

[17] J. Jiang, C. Burger, C. Li, J. Li, M. Y. Lin, R. H. Colby, M. H. Rafailovich, J. C. Sokolov, *Macromolecules* **2007**, *40*, 4016.

[18] P. Alexandridis, T. Alan Hatton, *Colloids and Surfaces A: Physicochemical and Engineering Aspects* **1995**, *96*, 1.

[19] J. Goodwin, R. Hughes, *Rheology for Chemists: An Introduction*, Royal Society Of Chemistry, **2008**.

[20] W. Zhang, Y. Shi, Y. Chen, J. Ye, X. Sha, X. Fang, *Biomaterials* **2011**, *32*, 2894.

[21] C. Wu, A. K. Gaharwar, B. K. Chan, G. Schmidt, *Macromolecules* **2011**, *44*, 8215.

[22] H. Priks, T. Butelmann, A. Illarionov, T. G. Johnston, C. Fellin, T. Tamm, A. Nelson, R. Kumar, P. J. Lahtvee, *ACS Applied Bio Materials* **2020**, *3*, 4273.

[23] M. Lufton, O. Bustan, B. hen Eylon, E. Shtifman-Segal, T. Croitoru-Sadger, A. Shagan, A. Shabtay-Orbach, E. Corem-Salkmon, J. Berman, A. Nyska, B. Mizrahi, *Advanced Functional Materials* **2018**, *28*, 1801581.

[24] T. H. Qazi, V. G. Muir, J. A. Burdick, *ACS Biomaterials Science and Engineering* **2022**, *8*, 1427.

[25] P. Bertsch, L. Andrée, N. H. Besheli, S. C. G. Leeuwenburgh, *Acta Biomaterialia* **2022**, *138*, 124.

[26] E. Dickinson, *Advances in Colloid and Interface Science* **2013**, *199–200*, 114.

[27] G. J. Donley, P. K. Singh, A. Shetty, S. A. Rogers, *PNAS* **2020**, *117*, 21945.

[28] M. Malmeten, B. Lindman, *Macromolecules* **1992**, *25*, 5440.

[29] T.-C. Tang, Towards Engineering Living Functional Materials, **2021**.

[30] T. Iyo, Y. Maki, N. Sasaki, M. Nakata, *Journal of Biomechanics* **2004**, *37*, 1433.

[31] Y. Jia, K. Peng, X. L. Gong, Z. Zhang, *International Journal of Plasticity* **2011**, *27*, 1239.

[32] S. Nam, J. Lee, D. G. Brownfield, O. Chaudhuri, *Biophysical Journal* **2016**, *111*, 2296.

[33] X. Hong, J. P. Stegemann, C. X. Deng, *Biomaterials* **2016**, *88*, 12.

[34] H. L. Ornaghi, J. H. S. Almeida, F. M. Monticeli, R. M. Neves, *Composites Part C: Open Access* **2020**, *3*, 100051.

[35] K. S. Fancey, *Journal of Materials Science* **2005**, *40*, 4827.

[36] H. Tsurusawa, M. Leocmach, J. Russo, H. Tanaka, *Science Advances* **2019**, *5*, 1.

[37] L. C. Hsiao, R. S. Newman, S. C. Glotzer, M. J. Solomon, *Proceedings of the National Academy of Sciences of the United States of America* **2012**, *109*, 16029.

[38] M. Y. Lin, H. M. Lindsay, D. A. Weitz, R. C. Ball, R. Klein, P. Meakin, *Nature* **1989**, *339*, 360.

[39] H. Tsurusawa, S. Arai, H. Tanaka, *Science Advances* **2020**, *6*, 1.

[40] K. A. Whitaker, Z. Varga, L. C. Hsiao, M. J. Solomon, J. W. Swan, E. M. Furst, *Nature Communications* **2019**, *10*, DOI 10.1038/s41467-019-10039-w.

[41] C. R. López-Barrón, N. J. Wagner, L. Porcar, *Journal of Rheology* **2015**, *59*, 793.

[42] B. Nyström, H. Walderhaug, F. K. Hansen, *Faraday Discussions* **1995**, *101*, 335.

[43] L. Mohan, M. Cloitre, R. T. Bonnecaze, *Journal of Rheology* **2015**, *59*, 63.

[44] T. Murakami, T. Kawamori, J. D. Gopez, A. J. McGrath, D. Klinger, K. Saito, *Journal of Polymer Science, Part A: Polymer Chemistry* **2018**, *56*, 1033.

[45] C. R. López-Barrón, R. Chen, N. J. Wagner, P. J. Beltramo, *Macromolecules* **2016**, *49*, 5179.

[46] S. Bhusari, J. Kim, K. Polizzi, S. Sankaran, A. Campo, *bioRxiv* **2022**, DOI https://doi.org/10.1101/2022.09.29.510162.

[47] M. Delarue, J. Hartung, C. Schreck, P. Gniewek, L. Hu, S. Herminghaus, O. Hallatschek, *Nature Physics* **2016**, *12*, 762.

[48] X. Hong, J. P. Stegemann, C. X. Deng, *Biomaterials* **2016**, *88*, 12.

[49] S. K. Nair, S. Basu, B. Sen, M. H. Lin, A. N. Kumar, Y. Yuan, P. J. Cullen, D. Sarkar, *Scientific Reports* **2019**, *9*, 1.

[50] E. K. Chu, O. Kilic, H. Cho, A. Groisman, A. Levchenko, *Nature Communications* **2018**, *9*, DOI 10.1038/s41467-018-06552-z.

[51] M. Dinkgreve, J. Paredes, M. M. Denn, D. Bonn, *Journal of Non-Newtonian Fluid Mechanics* **2016**, *238*, 233.

[52] S. S. Sagiri, V. K. Singh, S. Kulanthaivel, I. Banerjee, P. Basak, M. K. Battachrya, K. Pal, *Journal of the Mechanical Behavior of Biomedical Materials* **2015**, *43*, 1.

[53] M. Zabet, S. Mishra, S. Kundu, *RSC Advances* **2015**, *5*, 83936.

Supporting Information

Rheological behavior of Pluronic/Pluronic diacrylate hydrogel matrices used for bacteria encapsulation

Shardul Bhusari[1,2], Maxi Hoffmann[3], Petra Herbeck-Engel[1], Shrikrishnan Sankaran[1], Manfred Wilhelm[3], Aránzazu del Campo[1,2]*

[1] INM - Leibniz Institute for New Materials, Saarbrücken, Germany

[2] Chemistry Department, Saarland University, 66123 Saarbrücken, Germany

[3] Institute of Chemical Technology and Polymer Chemistry, Karlsruhe Institute of Technology (KIT), Karlsruhe, Germany

*Corresponding author

Email: aranzazu.delcampo@leibniz-inm.de

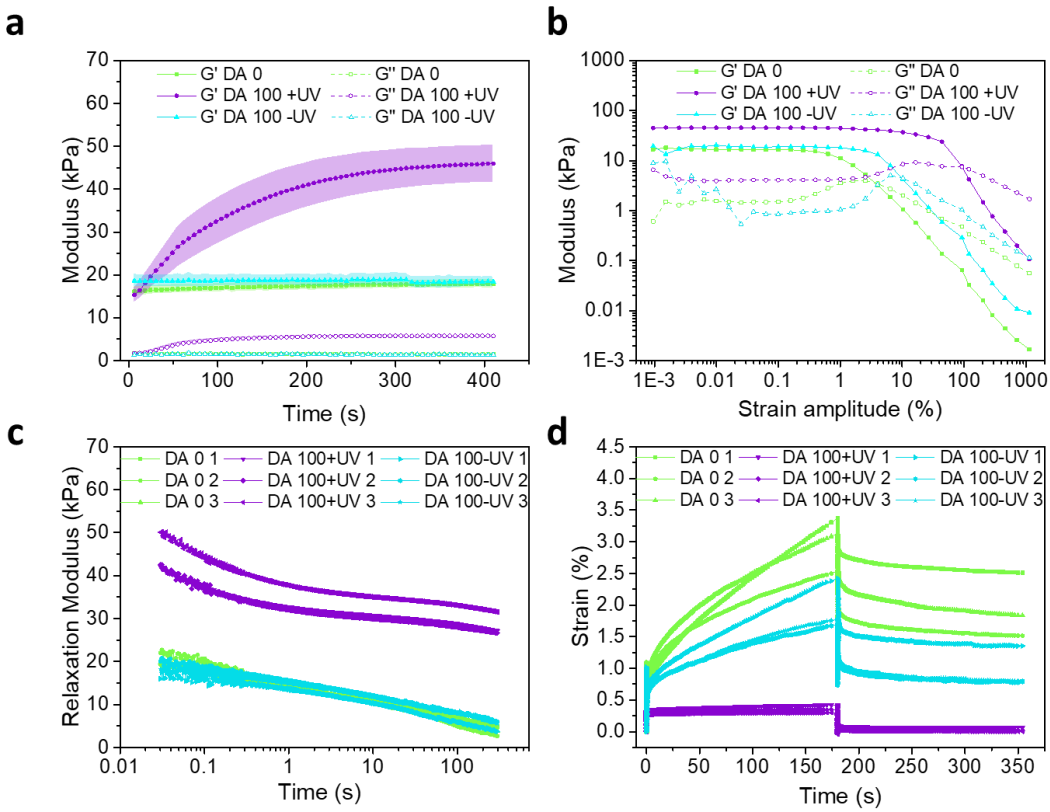

Figure S1: Rheological properties of DA 0 and DA 100 hydrogels before and after UV exposure and polymerization **a)** Evolution of the G' and G'' (shaded regions around the data points indicate mean ± standard deviation) at room temperature; **b)** Representative strain amplitude sweep of DA X hydrogels measured at a frequency of 1 Hz; **c)** Creep/recovery curves at an

applied stress of 100 Pa (Stress was applied for 180 s and then removed to measure the recovery over the next 180 s), and **d)** Stress relaxation curves at 1 % strain.

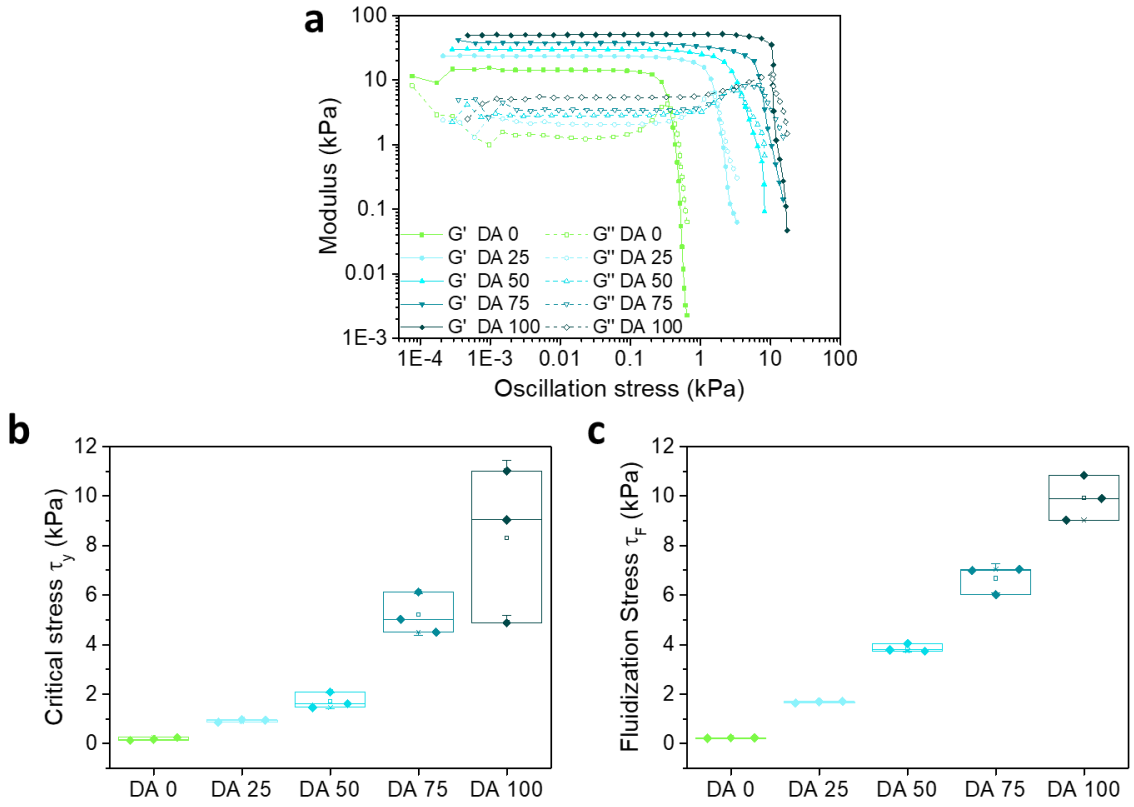

Figure S2. a) Representative stress sweeps and the corresponding **b)** yield stress, τ_y, and **c)** stress at fluidization point, τ_F with increasing DA content in the hydrogels.

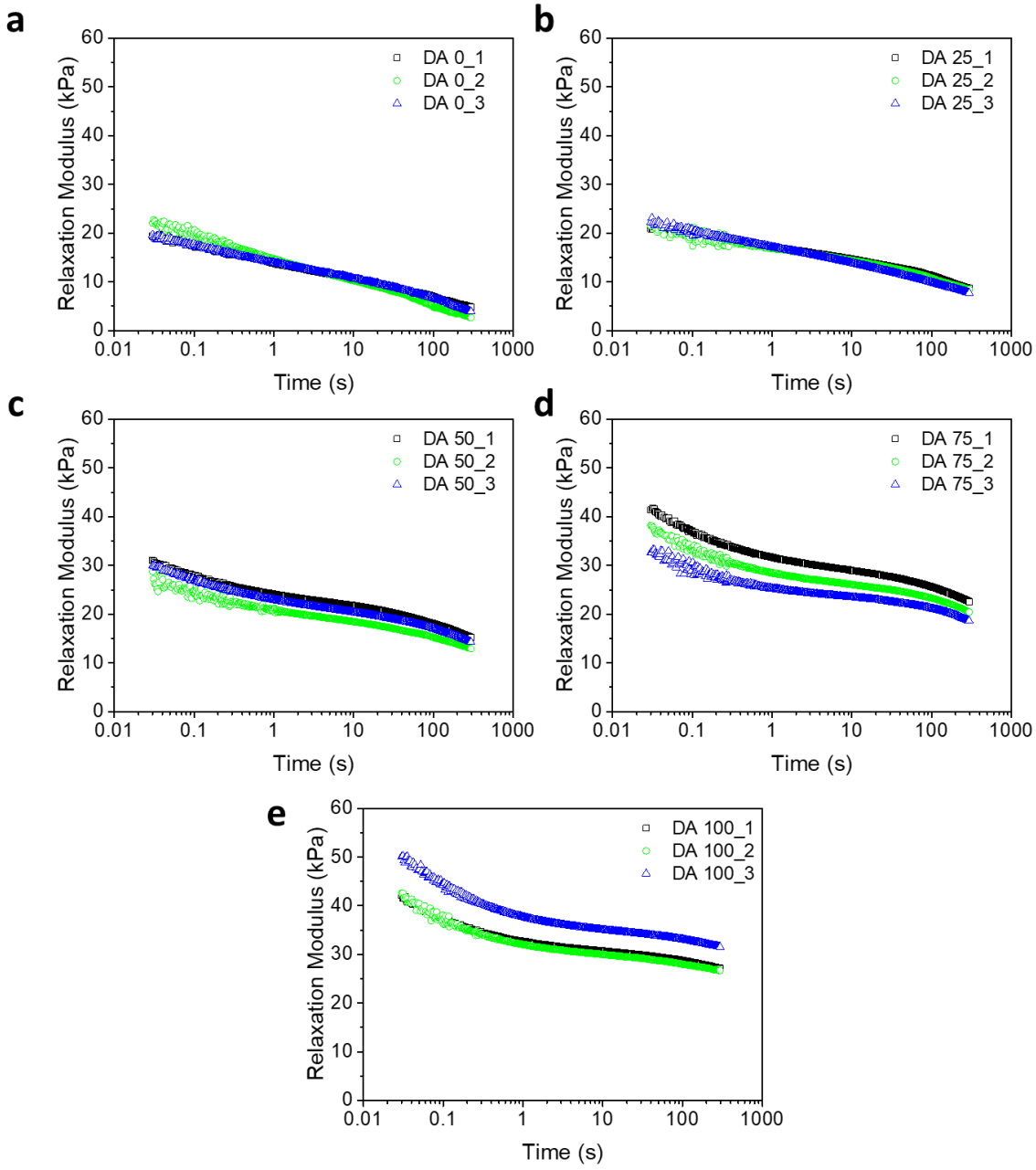

Figure S3: Stress relaxation curves of the DA 0-100 hydrogels at strain of 1% from three consecutive experiments used for the fitting in **Figure 3**. We note a higher variability in the experimental data from DA 75 and DA 100 hydrogels for which we do not have an explanation.

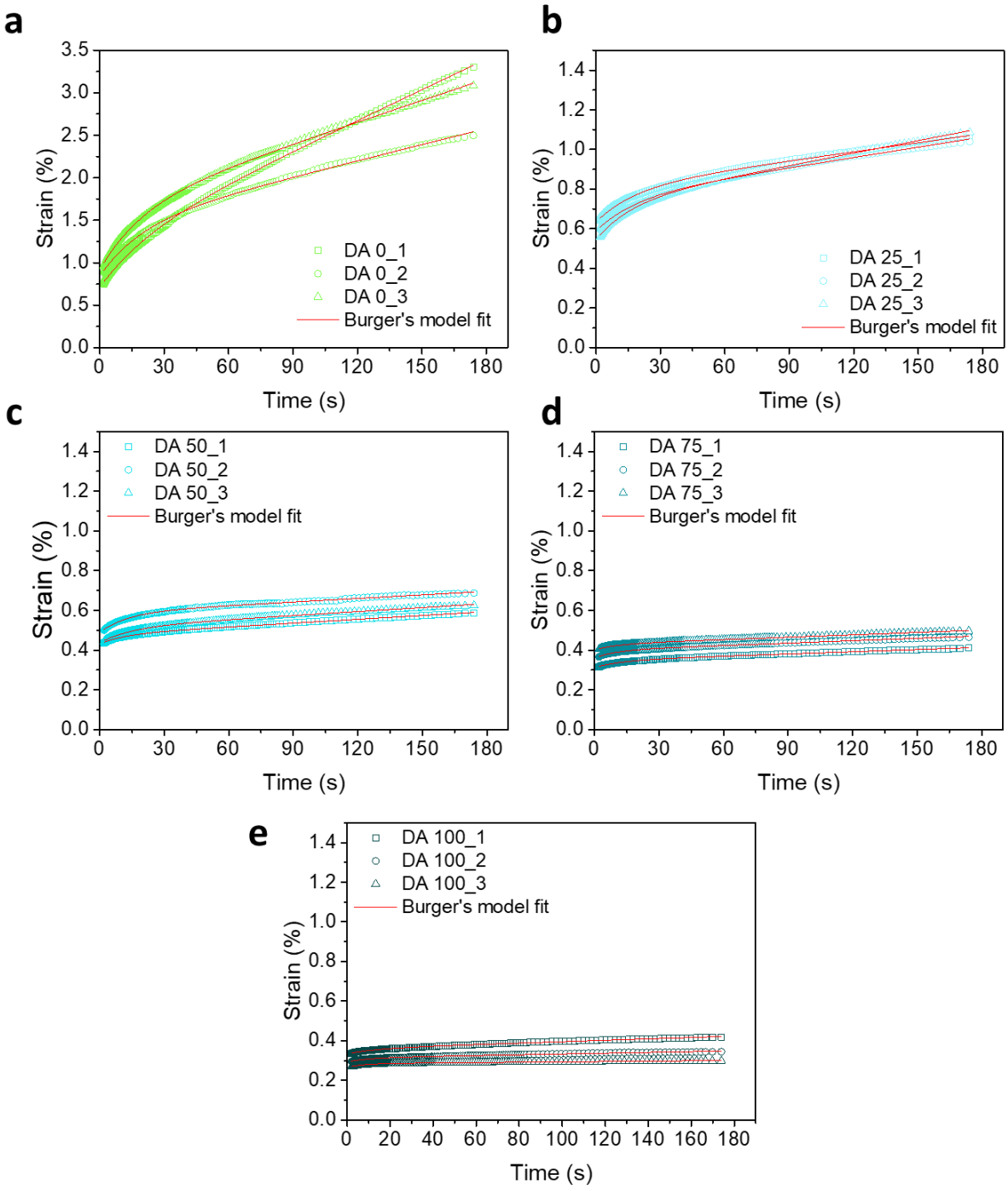

Figure S4: Creep strain and corresponding burgers model (Eq. 3) fits for the DA 0-100 hydrogels.

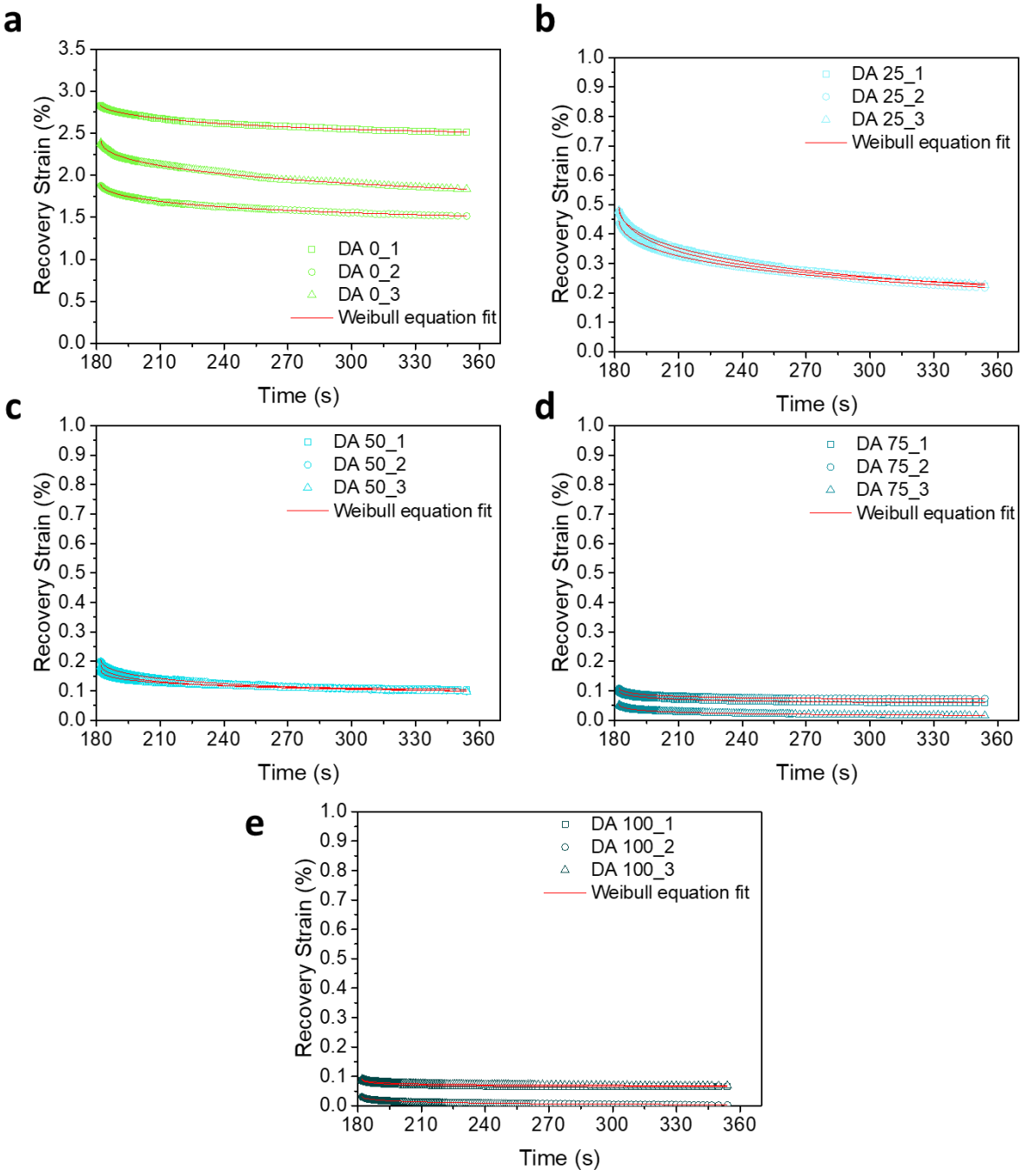

Figure S5: Recovery strain and corresponding fits to the Weibull equation (Eq. 4) for DA 0-100 hydrogels.

6.3 Encapsulation of bacteria in bilayer Pluronic thin film hydrogels: A safe format for engineered living materials

Shardul Bhusari[1,2], Juhyun Kim[3,4,5], Karen Polizzi[3,4], Shrikrishnan Sankaran[1]*, Aránzazu del Campo[1,2]*

[1] INM - Leibniz Institute for New Materials, Saarbrücken, Germany

[2] Chemistry Department, Saarland University, 66123 Saarbrücken, Germany

[3] Department of Chemical Engineering, Imperial College London, London SW7 2AZ, United Kingdom

[4] Imperial College Centre for Synthetic Biology, Imperial College London, London SW7 2AZ, United Kingdom

[5] Current affiliation - School of Life Sciences, BK21 FOUR KNU Creative BioResearch Group, Kyungpook National University, Daegu 41566, Republic of Korea

*Corresponding authors

Email: shrikrishnan.sankaran@leibniz-inm.de, aranzazu.delcampo@leibniz-inm.de

Citation: Bhusari, S., Kim, J., Polizzi, K., Sankaran, S. and Del Campo, A., 2022. Encapsulation of bacteria in bilayer Pluronic thin film hydrogels: a safe format for engineered living materials. *Biomaterials Advances*, p.213240.

Own Contribution: Methodology (all experiments - fabrication, imaging), Validation, Visualization, Formal analysis, Investigation, Writing (Original draft – shared with S.S. and A.d.C., review and editing).

145 (2023) 213240

Contents lists available at ScienceDirect

Biomaterials Advances

journal homepage: www.journals.elsevier.com/materials-science-and-engineering-c

Encapsulation of bacteria in bilayer Pluronic thin film hydrogels: A safe format for engineered living materials

Shardul Bhusari [a,b], Juhyun Kim [c,d,e], Karen Polizzi [c,d], Shrikrishnan Sankaran [a,*], Aránzazu del Campo [a,b,*]

[a] INM - Leibniz Institute for New Materials, Saarbrücken, Germany
[b] Chemistry Department, Saarland University, 66123 Saarbrücken, Germany
[c] Department of Chemical Engineering, Imperial College London, London SW7 2AZ, United Kingdom
[d] Imperial College Centre for Synthetic Biology, Imperial College London, London SW7 2AZ, United Kingdom
[e] Current affiliation - School of Life Sciences, BK21 FOUR KNU Creative BioResearch Group, Kyungpook National University, Daegu 41566, Republic of Korea

ARTICLE INFO

Keywords:
Engineered living material
Bacterial hydrogel
Biosensor
Bacteria-materials interactions
Living therapeutics
Biocontainment

ABSTRACT

In engineered living materials (ELMs) non-living matrices encapsulate microorganisms to acquire capabilities like sensing or biosynthesis. The confinement of the organisms to the matrix and the prevention of overgrowth and escape during the lifetime of the material is necessary for the application of ELMs into real devices. In this study, a bilayer thin film hydrogel of Pluronic F127 and Pluronic F127 acrylate polymers supported on a solid substrate is introduced. The inner hydrogel layer contains genetically engineered bacteria and supports their growth, while the outer layer acts as an envelope and does not allow leakage of the living organisms outside of the film for at least 15 days. Due to the flat and transparent nature of the construct, the thin layer is suited for microscopy and spectroscopy-based analyses. The composition and properties of the inner and outer layer are adjusted independently to fulfil viability and confinement requirements. We demonstrate that bacterial growth and light-induced protein production are possible in the inner layer and their extent is influenced by the crosslinking degree of the used hydrogel. Bacteria inside the hydrogel are viable long term, they can act as lactate-sensors and remain active after storage in phosphate buffer at room temperature for at least 3 weeks. The versatility of bilayer bacteria thin-films is attractive for fundamental studies and for the development of application-oriented ELMs.

1. Introduction

Engineered living materials (ELMs) are composites containing microorganisms programmed to perform specific functions. In ELMs for biosensing or drug delivery [1,2], the organisms -typically bacteria- are encapsulated within hydrogels. These matrices need to support the growth and activity of the organisms, but also biocontainment by preventing the organisms from escaping to the surroundings [3,4].

The growth and the metabolic activity of bacteria embedded in hydrogels depends on the composition and physical properties of the hydrogel matrix [3,5]. In physically crosslinked hydrogels, like agarose or alginate, bacteria grow slower than in free suspension and eventually grow out of the hydrogel (i.e. into the surrounding medium) if there are enough nutrients available [6]. In chemically crosslinked hydrogels, like poly(ethyleneglycol diacrylate) or poly(acrylamide), bacterial growth is restricted to small colonies, independent of the nutrient concentration [7]. Previous studies have demonstrated that Pluronic-based hydrogels are good matrices to encapsulate bacteria [3,5,8,9]. 30 wt% mixtures of Pluronic F127 and Pluronic F127 diacrylate at different concentrations (named DA X, where X represents the fraction of diacrylated Pluronic in the mixture) formed stable hydrogels after covalent crosslinking by photoinitiated radical polymerization of the acrylate groups. The variation of the diacrylate content in the mixture lead to hydrogels with different mechanical properties in terms of elastic moduli (Table S1) and viscoelasticity as consequence of the introduction of covalent crosslinks into the physical network [5]. *E. coli* encapsulated in these hydrogels proliferated and kept their metabolic function to an extent which was dependent on the concentration of acrylate groups, i.e. the degree of covalent crosslinks in the hydrogel. In particular, bacteria in DA X hydrogels with X > 50 grew in the form of small, spherical colonies and

* Correspondence to: A. del Campo or S. Sankaran, INM - Leibniz Institute for New Materials, Campus D2 2, 66123 Saarbrücken, Germany.
E-mail addresses: shrikrishnan.sankaran@leibniz-inm.de (S. Sankaran), aranzazu.delcampo@leibniz-inm.de (A. del Campo).

https://doi.org/10.1016/j.bioadv.2022.213240
Received 6 October 2022; Received in revised form 4 December 2022; Accepted 8 December 2022
Available online 20 December 2022
2772-9508/© 2022 Elsevier B.V. All rights reserved.

did not overgrow out of the material [5], suggesting that these could be appropriate materials for a confinement layer. In DA X hydrogels with X < 50, bacterial growth was found to be significantly less restricted and controlled [5]. Interestingly, highest rates of inducible protein production were observed in the gels with intermediate degrees of chemical cross-linking (DA X, 25 < X < 75), indicating that encapsulation influences both growth and metabolic activity of the bacteria in potentially different manner.

While most ELM examples demonstrate bacterial function inside the material, many of them do not address the need for containment [9,10]. This limits the transfer of ELMs into applicable technological solutions. The simplest approach to meet growth and containment requirements for ELMs is a bilayer design, for example core-shell particles or compartments [10]. Tang et al. used Ca^{2+} crosslinked alginate as core material and alginate/poly(acrylamide) double network in the shell to encapsulate *E. coli* in beads which retained the organisms for at least 14 days. Liu et al. encapsulated liquid cultures of genetically modified *E. coli* in poly(acrylamide)-alginate compartments covered by a polydimethylsiloxane (PDMS) elastomer layer [11]. The resulting living sensor prevented escape of the bacteria for at least 3 days. Connell et al. reported compartments made of photo-crosslinked gelatin shells and viscous gelatin cores where bacteria like *Staphylococcus aureus* and *Pseudomonas aeruginosa* could grow and molecularly interact with those in neighboring compartments [12]. Liu et al. *f*abricated tattoos using *E. coli* encapsulated in Pluronic hydrogels with a Sylgard 184 (Dow Corning) and Silgel 613 (Wacker) elastomer second layer and demonstrated bacterial retention and function over 8 h [13]. Knierim et al. encapsulated *Micrococcus luteus* for gold sequestration and *Nitrobacter winogradskyi* for bioremediation of nitrite in poly(vinylalcohol) fibres and coated it with a poly(p-xylylene) shell by chemical vapor deposition [14]. The shell reduced bacterial escape as a function of the thickness. These examples demonstrate the capabilities and versatility of core-shell designs for bacterial containment in ELMs. In this study, we leverage this design principle to establish a bilayer thin-film platform with which material properties that are optimal for bacterial functions can be investigated while preventing bacterial escape.

The design is based on Pluronic F127 hydrogels. This polymer exhibits a thermo-responsive sol-gel transition at temperatures >14 °C at 30 wt% concentration which results in physically assembled gels. This enables easy fabrication of hydrogel structures involving mixing of the polymer solution with the living organisms at 4 °C and the fast gelation at room temperature. In this work, we demonstrate that the combination of a DA X core and a DA 100 shell to generate a bilayer thin film is useful for making ELMs wherein bacterial behavior can be tuned by varying the composition of the core while the shell ensures long-term (at least 15 days) biocontainment. The combination of acrylated and non-acrylated polymer allows the design of core and shell out of the same backbone. The use of this format to fabricate live biosensors has been evaluated using engineered L-lactate sensing bacteria relevant for the biotech and biopharma industries [15–17].

2. Results and discussion

Bilayer thin films in this work are composed of an inner functional layer containing bacteria embedded in 30 wt% DA X hydrogel, which is sandwiched between a containment layer of 30 wt% DA 100 and a glass slide (Fig. 1). The bilayers were fabricated manually by pipetting the solutions at 0 °C onto the glass slide (functional layer) and onto a releasable parafilm (containment layer), allowing the physical gel to form at room temperature, and photopolymerizing the acrylate end-groups in both layers in a single exposure step (Fig. 1a). The initial volumes of the inner and outer layers were 2 and 30 μL. The outer diameter of the thin film was ca. 11 mm and the inner diameter was 2–3 mm. Bilayers with different DA X compositions of the inner layer were

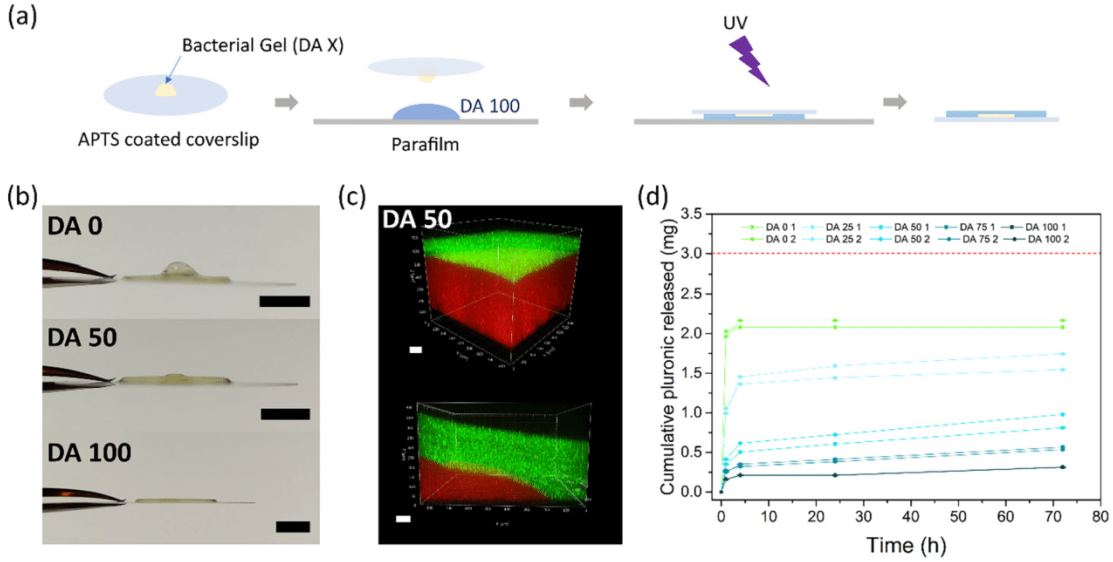

Fig. 1. Bilayer thin films prepared with DA X inner layers and a DA 100 outer layer. a) Fabrication steps to obtain the bilayer thin films. A drop of DA X/bacteria mixture is placed on an acryl-terminated coverslip and pressed onto a larger DA 100 drop on a parafilm. The drops are pipetted from solutions on ice and the bilayer is left at room temperature to form the physical gel. UV exposure activates the covalent crosslinking of the two layers; b) Side view images of a DA 0, DA 50 and DA 100 bilayer thin films with bacterial inner gels at 24 h showing the central protrusion as consequence of higher swelling in the inner gel (Scale = 5 mm); c) Confocal microscopy imaging of a swollen bilayer thin film with DA 50 inner core. *Z*-stack images were taken in the middle of the inner gel and at the edge of the inner-outer layer interface after swelling for 24 h. DA 50 inner gel contains red fluorescent beads and DA 100 outer gel contains green fluorescent beads (Scale = 100 μm) and d) Cumulative release profile of Pluronic molecules from DA X hydrogel discs during 3 days in water as calculated from gel permeation chromatography (GPC) measurements ($N = 2$ and $n \geq 3$, whiskers indicate mean ± standard deviation). The maximum theoretical Pluronic concentration that can be released from the films according to the mass of the thin film is 3 mg (dotted red line). (For interpretation of the references to colour in this figure legend, the reader is referred to the web version of this article.)

prepared in order to identify the best possible combination that maximizes the metabolic activity of the bacteria. The thin films were transparent and allowed microscopy imaging of the bacteria in the inner gel.

When immersed in water or buffer solutions, DA 0 hydrogels swell and dissolve since they are only held by physical interactions. Müller et al. showed a 382 % swelling degree for DA 15 discs [18]. The swelling degree of DA X films in our study decreases with increasing X value (i.e. increasing covalent crosslinking, Fig. S1) in films with X ≥ 25. The DA X films retain their format after swelling. In the case of the bilayers, swelling results in a protrusion in the middle of the bilayer as consequence of the higher swelling of the DA 0–75 inner layers with lower crosslinking degree than the outer DA 100 shell (Figs. 1b-c, S2). The thickness of the outer layer after swelling is ca. 100–150 μm (measured on the top of the protrusion, Fig. 1c).

Swelling of the Pluronic hydrogels is accompanied by leakage of non-diacrylated Pluronic from the bilayer into the water phase. This could be an advantageous feature for bilayer-based ELMs, since it increases the porosity of the hydrogel after film formation and swelling, and this can favor diffusion of nutrients and cell viability [18]. We tested the release of Pluronic molecules from DA X hydrogel films after immersing them in water for up to 72 h by GPC analysis of the supernatant. Pluronic was released to the medium from all DA X hydrogels within 1–2 h (Figs. 1d, S3). At longer time scales, slow release was observed in DA 25–75 hydrogels and no release in DA 100. The molar mass distribution of the released polymer corresponded to that of the Pluronic precursor, indicating that only molecules that are not crosslinked were able to diffuse out of the hydrogel. The amount of pluronic released into the supernatant decreased with increasing PluDA content, from ca. 55 % of the film mass in DA 25 to ca. 10 % of the film mass in DA 100 after 72 h. Note that the degree of substitution of PluDA was 70 %, meaning that all hydrogels contain at least 30 % of Pluronic chains with only one or no acrylated chains. Although DA 0 samples dissolved completely, the amount of Pluronic detected in the supernatant was lower than the expected polymer mass in the film (represented by the red dotted line). This could be due to (i) adsorption of Pluronic molecules on the surface of the wells and pipettes or (ii) micellar association of Pluronic molecules in the solution.

To assess the behavior of encapsulated bacteria, we fabricated bilayer thin films containing *E. coli* in inner layer hydrogels made with different DA X compositions. Brightfield and fluorescence microscopy images of live/dead stained bacteria after 24 h revealed that bacteria grew in all the inner gels, although with different morphologies in the different composition (Fig. 2). In DA 0, i.e. inner layer with no chemical crosslinking, the bacteria grew as a uniform biomass, suggesting that the gel network did not constrain the growth of the organisms. Despite swelling of the inner layer causing the outer DA 100 layer to expand, bacterial containment was not compromised within the timescale of the experiment. In all other compositions, bacteria formed colonies with individual, elongated (DA 25) or rounded (DA 50 – DA 100) geometries visible under the microscope. Such morphologies are in line with the results of bacteria growth within DA X hydrogels within closed microchannels from our previous report [5]. In DA 25 hydrogels colonies showed an elongated morphology in the vertical direction, towards the supernatant. This could be a consequence of mechanical effects during swelling. Note that in thin films the hydrogels are exposed to medium and there is a release of Pluronic during the first hours. This indicates that the covalently cross-linked DA X network restricts growth also after swelling and loss of polymer fraction. No bacterial motility was observed in the inner gel for all constructs except for DA 0. The staining further revealed that most of the bacteria were alive, suggesting that the bilayer sustains bacteria function.

In ELMs developed as biosensors or therapeutic devices, function is often associated to production of a protein in response to an external stimulus or inducer molecule. Inducible protein production in our thin films was tested using an optogenetically engineered *E. coli* strain that expresses a red fluorescent protein (RFP) in response to blue light [5,6].

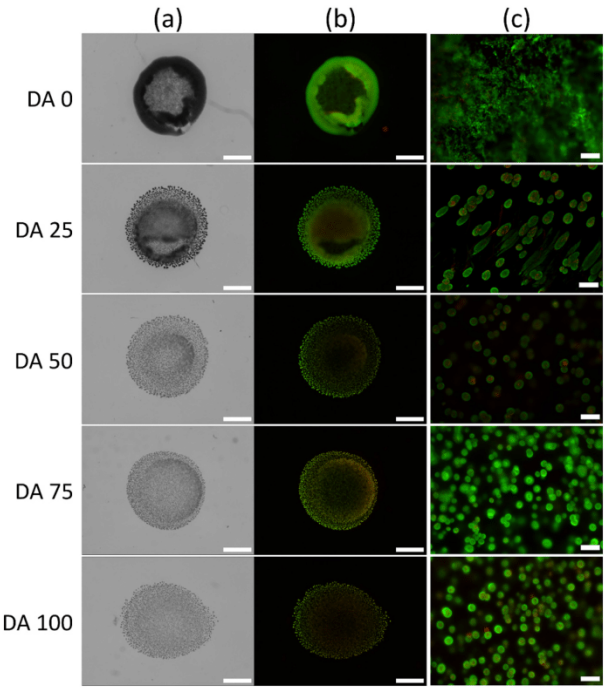

Fig. 2. Viability of bacterial populations within the bilayer thin films. a) Brightfield and b) fluorescence microscopy images showing *E. coli* growth within bilayer thin films with different DA X inner layer. Images were taken near the bottom of the inner gel. (scale bar = 1000 μm); c) Representative images of bacterial colonies at a higher magnification after 24 h. (scale = 50 μm) Samples were stained with SYTO 9 (green = live) and Propidium Iodide (red = dead) after 24 h of incubation. (For interpretation of the references to colour in this figure legend, the reader is referred to the web version of this article.)

With pulsed light irradiation (470 nm, 500 ms ON, 10 min OFF), fluorescence was detectable in the inner film within 4 h, although it was not homogeneous through the film. Higher fluorescence intensity was observed at the outer edge of the inner layer (Fig. 3a). This could be a consequence of a higher nutrient concentration, which would lead to a higher bacterial density [19]. We estimated the overall kinetics of protein production across the film by quantifying the total fluorescence intensity for 18 h. An increase in fluorescence was observed during the first 4–10 h (Fig. 3b) and a plateau value was reached at longer times. The plateau was reached when fluorescence intensity exceeded the fluorescence saturation level of the microscope required to observe the early stage of RFP production. Therefore, it does not reflect the real RFP concentration in the film at longer time scales. We analyzed the slope of the linear part or the fluorescence curves for an estimation of the kinetics of RFP expression in the different systems. The result of this analysis is shown in Fig. 3c and reveals faster RFP production in DA 50 (5.1 ± 0.1 au/h) compared to the other compositions (DA 0 = 3.1 ± 0.1 au/h, DA 25 = 4.8 ± 0.1 au/h, DA 75 = 4.8 ± 0.1 au/h, DA 100 = 4.0 ± 0.1 au/h). RFP production in DA 50 inner layers also showed the smallest deviation across the whole period of the experiment. The higher rate of protein expression in DA 50 hydrogels is in agreement with our previous observations of RFP production in bacterial DA X hydrogels within closed microchannels [5].

We selected DA 50 as inner hydrogel for the next experiments and tested the safe encapsulation of the bacteria in the film and the activity of the bacterial bilayers over longer periods of time (Fig. 3d). Bilayer thin films were cultured for over two weeks. No outgrowth of bacteria was detected in the biofilms incubated for over 10 days (Fig. S4),

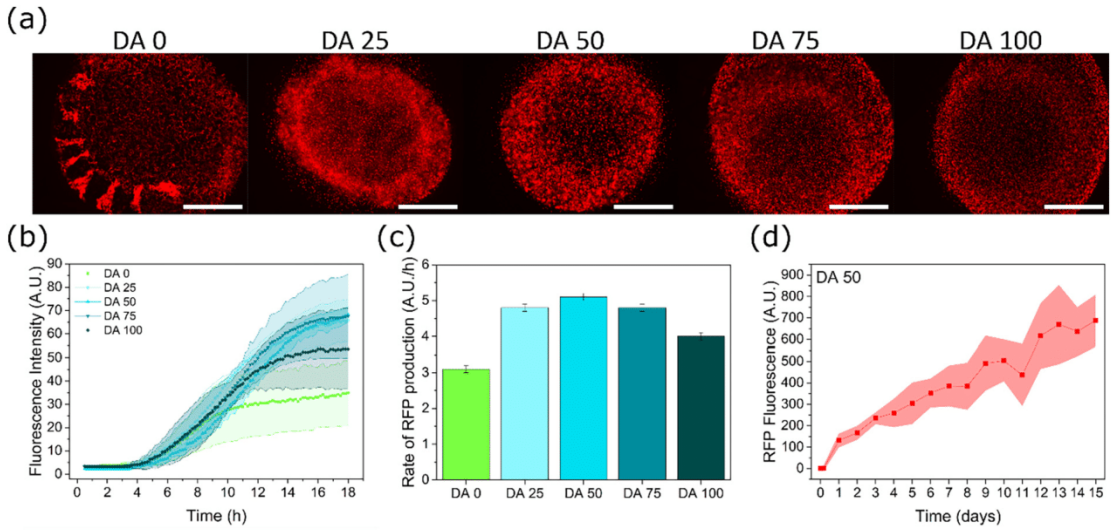

Fig. 3. RFP production within the bilayer thin films: a) Fluorescence images of RFP producing bacterial gels indicating RFP expressed by the encapsulated bacterial colonies at 12 h (scale = 1000 μm); b) Quantification of total fluorescence intensity of the bilayer thin films during 24 h from fluorescence microscope images in (a) ($N = 3$, mean ± standard deviation); c) Rate of RFP production in bilayers with different DA X layer compositions estimated from the slope of the linear part of the fluorescence intensity curves in (b) (mean ± standard deviation) and d) Quantification of fluorescence intensity within DA 50 bacterial gel thin films for 15 days using the plate reader ($N = 8$ until day 12, $N = 4$ until day 15, mean ± standard deviation, medium was changed every 2 days).

demonstrating the capability of bilayer hydrogels with DA 50 inner layer and DA 100 outer layer to safely support activity while confining bacteria colonies. Beyond 15 days, loss of adhesion between the gel and the glass substrate was observed in half of the samples, indicating that the stability of the thin film is not limited by the stability of the enveloping/outer hydrogel, but rather by the design of the glass-hydrogel interface. Optimization of the glass treatment step could be a simple solution for longer studies. The overall fluorescence signal of the bilayer increased during 15 days. Note that this quantification was done using a microplate reader that provided a larger dynamic range for measuring fluorescence intensity than the microscope images in Fig. 3a. Analysis of the supernatant indicated that RFP was released from the bilayer hydrogels already on day 2, and at a higher concentration on day 8 (Fig. S5) [6]. In this experiment the medium was changed every two days. Since the bacterial colonies are not expected to considerably increase in number or size beyond 1 day (Fig. S6), the increase in fluorescence suggests that the protein is continuously secreted and accumulates within the network.

We then tested the suitability of the bilayer hydrogels for biosensing by encapsulating bacteria engineered as L-lactate biosensors. Lactate biosensors are used to monitor the health of mammalian cell cultures, for which secure encapsulation would be a fundamental requirement [17]. This metabolite is a waste product in mammalian cell cultures formed as a byproduct of glycolysis. High concentration of lactate causes acidification of the medium and impacts growth and productivity in the culture [20]. Current lactate monitoring is done by HPLC or electrochemical analysis methods, which have limits in terms of cost, sensitivity, and robustness. Industry standard instruments (eg. Bioprofile Analyzer) and kits for lactate sensing based on enzymatic reactions have high costs associated with the purified enzymes. To address these issues, bacterial biosensors able to sense lactate in mammalian cell culture medium and report it by means of a fluorescent protein have been developed [15–17]. To be used in combination with biotech reactors, bacteria were encapsulated within giant unilammellar vesicles [16] or multilayer polymer shells [17]. These methods ensured confinement of the bacteria on short timescales (24 h or less), but the long-term behavior was not examined. Thus, we encapsulated the living L-lactate biosensors in DA 50 /DA 100 bilayers and tested their functionality.

To ensure that variability in medium oxygen concentrations do not affect the sensing performance, the bacteria were engineered to produce an oxygen-independent fluorescent protein, CreiLOV, as the reporter. Although this fluorescent protein shows lower fluorescence intensity and quicker bleaching than the GFP used in previous studies [15–17], the signal was high enough to be observed within the gels. In line with previous reports of encapsulated lactate sensing bacteria [17], fluorescence signals in response to 1 mM and 10 mM L-lactate were observed after 9 and 6 h, respectively (Fig. 4a). This slow response might be due to the dependence of fluorescent protein production on bacterial growth. In a second experiment, bacteria were allowed to grow inside the gels for 6 h after which L-lactate was added (Fig. 4b). An increase in the fluorescence signal with 10 mM lactate was observed already within the first 2 h, supporting the view that protein production is growth-dependent, which is in line with our previous study [5]. However, a higher degree of leaky expression was also observed in the absence of L-lactate, which overlapped with the signal generated by 1 mM lactate. This leaky expression of CreiLOV could be caused by incomplete repression of the promoter by the lldR repressor. The repressor expression is driven by a medium-strength constitutive promoter (BBa_J23118) [21] optimized for lactate-switchable repression in rapidly growing bacterial cultures. Once expressed, the main mechanism for removal of CreiLOV is by cell division. Therefore, small amounts of leaky expression can accumulate a high signal when the bacterial growth is restricted under encapsulation conditions. This effect is also observed when the bacterial biosensors are grown on agar plates as opposed to growth in culture (Fig. S7). This highlights the importance of understanding the unique characteristics of bacterial growth and functionality in confinement. Studies are underway to reduce the leaky expression of CreiLOV either through stronger expression of the repressor or through degradation of the reporter in the absence of L-lactate.

The possibility to store the bilayer thin-film sensor units at room temperature was tested. The bacteria in the hydrogels were allowed to grow for a day and the bilayer thin films were stored in phosphate buffered saline (PBS) for 2 days or 3 weeks (Fig. 4c and d), after which they were transferred to cell-culture medium containing L-lactate. The sensing capability and response rate of the sensor units remained unchanged: fluorescence increase was observed at between 2 and 4 h after

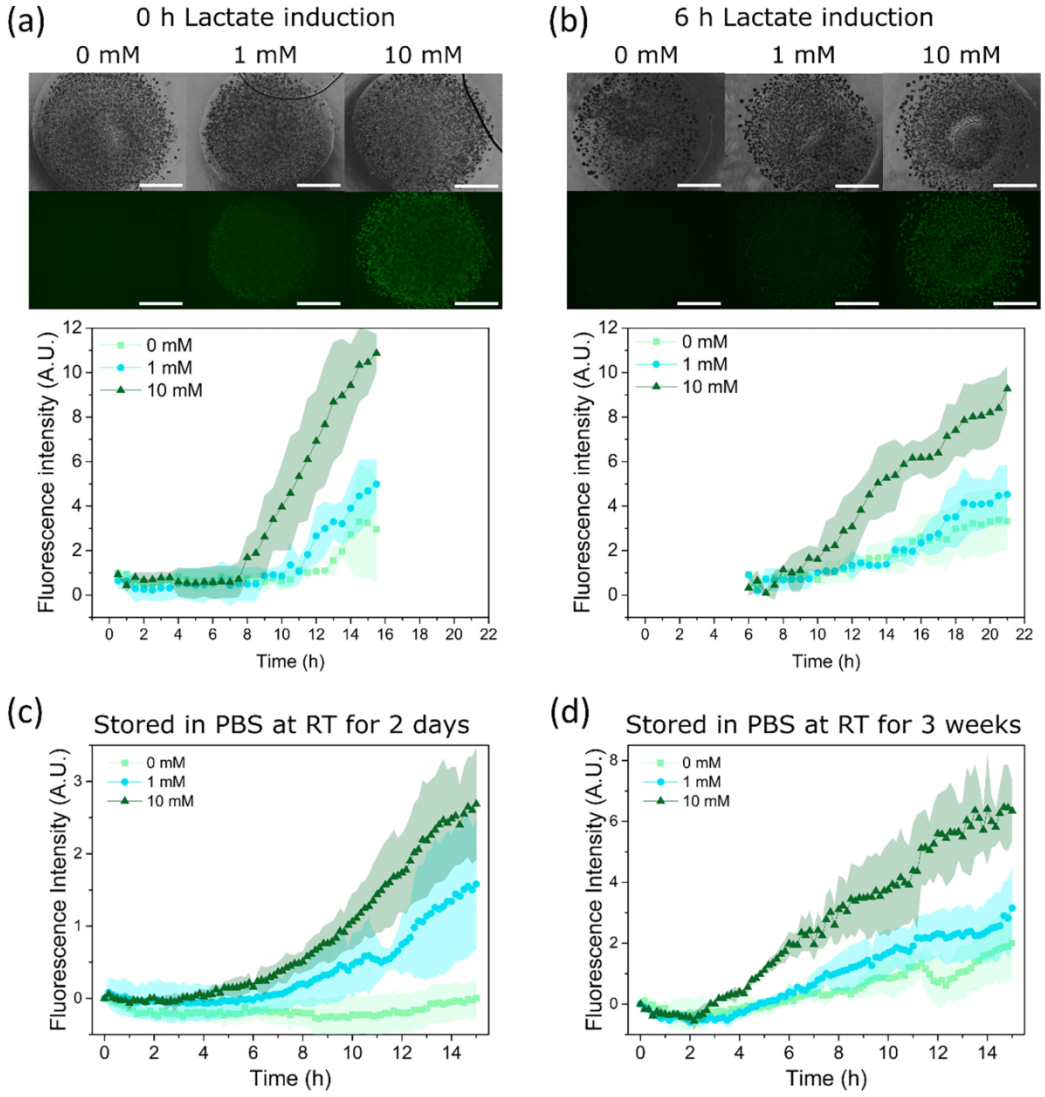

Fig. 4. Lactate inducible creiLOV production within the bilayer thin films: Brightfield and fluorescence microscopy images at 15:30 h (scale = 1000 μm) and quantification of fluorescence intensity within DA 50 bacterial gel thin films upon lactate induction at a) 0 h ($N = 2$) and b) 6 h ($N = 3$) indicating creiLOV production (mean ± standard deviation); quantification of fluorescence intensity within DA 50 bacterial gel thin films upon lactate induction post growth for 1 day and storage in PBS for c) 2 days (N = 2 for 0 and 1 mM, N = 3 for 10 mM) and d) 3 weeks (N = 3) indicating creiLOV production during 15:30 h (mean ± standard deviation).

addition of 10 mM L-lactate. Leaky expression in the absence of L-lactate was also observed to the same degree as with the 6 h incubation condition. Once again, this level of leaky expression overlapped with the response to 1 mM L-lactate, although the two conditions could be distinguished beyond 8 h. As a storage alternative, freeze drying was tested (Fig. S8). On reconstitution of the sensor units with medium containing L-lactate, fluorescence signals were observed to increase at around 4 h. However, freeze-drying damaged some of the samples and bacteria escaped into the surrounding medium. The fluorescence readouts from these samples were measured spectrophotometrically using a multiplate reader, indicating the possibility to develop these sensors for real-time sensing in a bioreactor using fluorimeters, similar to how sensing pads are currently used for monitoring O_2, CO_2 and pH in culture flasks [22–24].

3. Conclusions

This study describes a secure bacterial encapsulation format using Pluronic F127 based hydrogels for creating ELMs. Using hydrogel bilayers, the properties of the inner bacterial layer can be adjusted to maximize growth and metabolic function, while the outer, highly chemically cross-linked layer, is designed to prevent leakage of cells. These layers are polymerized onto a glass cover slip in one step and result in a transparent thin film that enables the use of this format for microscopy and spectroscopy analysis of bacterial behavior inside. We show that these hydrogels support bacterial growth and protein production. The highest rate of inducible protein production was observed in bilayers with DA 50 inner layer and could be maintained for at least 2 weeks. The produced RFP was released from within the gel from day 2 and increased in following days, indicating that the hydrogels are permeable and sustain diffusion of the produced molecules long term. By encapsulating L-lactate sensing bacteria, we illustrated the possible

application of bacterial bilayers as biosensors. Although the leaky expression of the protein needs to be addressed in the lactate sensing genetic circuit, our results show how the performance and safety of ELMs, which is crucial for application purposes, can be improved with dedicated but simple designs.

4. Materials and methods

4.1. Bacteria cultures

The endotoxin free strain of *E. coli* (ClearColi(R) BL21(DE3), BioCat) [6] was used for the bacterial studies. It was transformed with the plasmid pUC19 to enable Ampicillin resistance and minimize the risk of contamination in the culture. Transformation in ClearColi was performed by electroporation as described by the manufacturer of these competent cells. Bacterial cultures were grown for 16 h at 35 °C, 180 rpm in LB Miller medium supplemented with NaCl and 50 μg/mL of Ampicillin to an optical density at 600 nm wavelength (OD600) between 0.5 and 1. For the fluorescence based experiments, we used a previously optogenetically engineered strain of ClearColi that produces red fluorescence protein (RFP) when illuminated with blue light [6]. The RFP producing strain harbors the plasmid pDawn-RFP that encodes blue-light activatable gene expression and provides kanamycin resistance. The red fluorescence signal was used to quantify protein production in hydrogel-encapsulated bacterial populations. The bacteria were cultured for 16 h at 35 °C, 220 rpm in LB Miller medium supplemented with NaCl and 50 μg/mL of Kanamycin to an optical density at 600 nm wavelength (OD600) value between 0.5 and 1.5. All procedures with the light-inducible bacterial strain were performed either in the dark or under a laminar hood with an orange film that cuts off blue light to prevent their pre-mature induction.

4.2. Construction of the lactate biosensor

A plasmid of the lactate biosensor plasmid [17] derivative containing CreiLOV reporter was used to develop lactate biosensor for low oxygen conditions. *E. coli* DH5α cells were used for expression and characterization of all the plasmids constructs. Briefly, the reporter module carrying the lldR promoter and CreiLOV gene was digested with *Eco*RI and *Sac*I and cloned into the same sites of the biosensor plasmid [17]. The new construction was propagated in BW25113 (ΔArcA) strain, from the KEIO collection, to avoid repression of aerobic pathways [25]. Bacterial cultures were grown for 16 h at 35 °C, 180 rpm in LB Miller medium supplemented with 50 μg/mL of kanamycin to an optical density at 600 nm wavelength (OD600) between 0.5 and 1.

4.3. Functionalization of coverslips with (3-acryloxypropyl) trimethoxysilane to improve attachment of the bilayer hydrogel to the supporting glass

13/25 mm glass coverslips were sonicated in ethanol for 5 min and then rinsed with ethanol. The coverslips were treated with 1 % *v*/v solution of (3-acryloxypropyl)trimethoxysilane (APTS, Merck - Sigma Aldrich) in ethanol for 1 h. The coverslips were then rinsed in ethanol and dried for further use.

4.4. Preparation of bacteria-DA X thin films

Pluronic F127 (Plu, MW ~ 12,600 g/mol, Sigma-Aldrich) and Pluronic F127 diacrylate (PluDA) polymers with substitution degree of 70 % were used for the studies. The synthesis of PluDA has been reported elswhere [26]. DA 0 and DA 100 precursor solutions were prepared by diluting Plu or PluDA at 30 % (*w/v*) in milliQ water contining 0.2 % w/v Irgacure 2959 photoinitiator. DA 25, DA 50 and DA 75 precursor solutions were prepared from mixtures of DA 0 or DA 100 solutions in ratios as shown in Table S1. For the inner hydrogel with bacteria, precursor solutions at 4 °C were added to the bacterial suspension (OD600 of 0.5, ~4×10^7 cells/mL) at 9/1 (*v*/v) ratio to achieve a final OD600 of 0.05. The bacterial mixture was vortexed for 30 s to homogeneously disperse the bacteria.

To fabricate the thin films, 2 μL of the inner hydrogel precursor mixture containing the bacteria was placed on a coverslip previously functionalized with APTS and left at room temperature for 10 min for gelation. This step introduces acryl groups at the surface of the glass slide which react with DA X precursor solutions during the photopolymerization step [27,28]. This step covalently anchors DA X hydrogels to the glass slide and prevents detachment of the thin film from the glass slide during the experiment. To fabricate the DA 100 outer layer, 30 μL of DA 100 precursor solution was dropped on parafilm and allowed to physically crosslink at room temperature for 10 min. The coverslip with the bacterial gel was pressed against the DA 100 gel on the parafilm. The hydrogel sandwich was kept at room temperature for 10 min for physically crosslinked gelation to occur and exposed for 60 s to a UV Lamp inside Alpha Innotech FluorChem Q system (Biozym, Oldendorf, Germany) (6 mW/cm^2) which was the illumination step used to initiate the photopolymerization of the acrylate groups and covalent crosslinking of the hydrogels. After additional 10 min, the parafilm was peeled off. The thin-film construct was incubated in medium at 37 °C with 5 % CO_2.

4.5. Quantification of swelling ratio

DA X hydrogels discs (20 μL polymer precursor solution) were prepared on APTS coated glass coverslips using PDMS molds of diameter of 6 mm and height of 0.8 mm. The samples were irradiated with UV for 60 s, same as mentioned above. The hydrogels were immersed in 500 μL of MQ water and incubated at 37 °C and 5 % CO_2. The swelling ratios were gravimetrically determined in duplicate by dividing the wet hydrogel weight at timepoint t, W_t, by the initial hydrogel weight, W_i:

$$\text{Swelling ratio} = W_t/W_i$$

Samples were weighed at specific time points (1, 2, 3 and 24 h) and the supernatant was replaced with fresh MQ water at each timepoint.

4.6. GPC analysis of Pluronic in supernatant

DA X hydrogels films (10 μL polymer precursor solution, ca. 3 mg of polymer) were prepared on APTS coated glass coverslips by inverting them on different DA X hydrogels on parafilm and irradiated with UV. The hydrogels were immersed in 500 μL of MQ water and incubated at 37 °C and 5 % CO_2. At specific time points (10 s, 1 h, 4 h, 24 h and 72 h), the supernatant was taken out from the plate and immediately replaced with fresh MQ water. For the GPC measurement, PSS GPC-MALLS System was used. Injection volume was 100 μL with the mobile phase comprising of 100 % 0.5 g/L NaN_3 and 15 % ACN. Flow rate was 1 mL/min. A PSS SUPREMA LUX separation column was used (dimensions 8 × 50 mm^2, particle size 10 μm) and a PSS SUPREMA Linear M (dimensions 8 × 300 mm^2, particle size 10 μm). The measurements were performed at 25 °C and 37 bars pressure. An Agilent detector with positive signal polarity was used at temperature of 25 °C. Each sample at 10 s, 4 h, 24 h and 72 h was measured four times and samples at 1 h were measured three times. The concentration of the released pluronic in the supernatant was determined using a standard calibration curve of known pluronic concentrations (Fig. S3).

4.7. Bilayer thin film thickness

For visualising the bilayers, 0.2 μm FluoSpheres Carboxylate-Modified Microspheres (Invitrogen) were used at 0.02 % concentration within the DA 100 outer gel (yellow green) and DA 50 inner gel (crimson colored). The thin film was then imaged using Zeiss LSM 880 confocal laser scanning microscopy at 24 h using EC Plan-Neofluar 10×/

0.30 M27 objective. The green and red beads were excited using 488 nm and 633 nm laser and the emission spectra was detected at wavelength of 493–628 nm and 638–755 nm respectively. *Z*-stacks were taken in a z-step size of ca. 5.97 μm. Imaris software (Version 9.8.2, Bitplane, Zurich, Switzerland) was used to process the z-stacks to create 3D images.

4.8. Staining and imaging of bacterial colonies within thin films

The LIVE/DEAD BacLight Bacterial Viability kit (Thermo Fisher Scientific L7012) was used to visualize growth of bacterial colonies. Stock solutions of the stain were stored at −20 °C. To make the working solution, 3 μL of the stock solutions were added to 1 mL of phosphate buffered saline (PBS). The bacterial hydrogels were washed with PBS to remove traces of the medium and incubated with 100 μL of the stain solution for 30 min. The samples were washed with 0.5 mL PBS once and imaged under the microscope. For fluorescence imaging, BZ-X Filter TRITC OP-87764 (excitation 545/25, emission 605/70) was used for imaging the dead colonies while BZ-X Filter GFP OP-87763 (excitation 470/40, emission 525/50) was used for imaging the live colonies using the Keyence PlanFluor 4×/0.13 objective. Nikon Ti-Ecllipse (Nikon Instruments Europe B.V., Germany) microscope with S Plan Fluor ELWD 20×/0.45 objective used the Semrock filters (Semrock Inc., Rochester, USA) (LF488-C-000 filter, excitation 482/18, emission 525/45 for live colonies and LF561-B-000 filter, excitation 561/14, emission 609/54 for dead colonies). Image processing and analyses were performed using Fiji edition of ImageJ (ImageJ Java 1.8.0).

4.9. Analysis of RFP production by bacteria in bilayer thin film format

Bilayer thin films containing bacteria in the inner gels were freshly prepared and 400 μL of LB Miller medium supplemented with NaCl and 50 μg/mL of Kanamycin was added. RFP production was activated at 0–0.5 h by illuminating the thin films with blue light (BZ-X Filter GFP OP-87763, excitation 470/40, emission 525/50) pulses of 500 ms every 10 min for 24 h using the Keyence PlanFluor 4×/0.13 objective. The thin films were kept in static conditions at 37 °C and 5 % CO_2 using an incubation chamber (Stage Top Incubator, Tokai Hit) coupled to a BZ-X800 (Keyence, Osaka, Japan) microscope. For fluorescence imaging to detect the RFP production, BZ-X Filter TRITC OP-87764 (excitation 545/25, emission 605/70) was used. The light intensity and exposure settings were optimized for detecting early time-point generation of fluorescence and following increase in intensity for several hours without exceeding saturation limits. Image processing and analyses were performed using Fiji edition of ImageJ (ImageJ Java 1.8.0). Quantification of the overall fluorescence intensity of the film was done by determining the mean grey value post thresholding (Mean autothreshold) the colonies.

4.10. Long term stability and RFP production from bilayer films

For the long-term (2 weeks) studies of the stability and RFP production of the bacteria hydrogels, the bilayer thin film with DA 50 inner layer were stored in 400 μL of LB Miller medium supplemented with NaCl and 50 μg/mL of Kanamycin. The medium was changed every two days. The biofilms were illuminated with blue light pulses of 2 s every minute. The RFP protein production was measured using a black glass bottom 24 well plate in a plate reader (Tecan Infinite M200-Pro, excitation 545 nm, emission 605 nm) using the setting of multiple reads per well. A matrix of 3 × 3 reads were taken within the 24 well plate and the position in the middle of the plate, where the inner gel of the thin film was placed, was considered for the measurements. The growth of fluorescence was quantified with respect to the reading at 0 h. The absence of leakage of the thin films was observed under the microscope and confirmed by streaking 4 μL of the supernatants (day 10) on agar plates (made up of LB supplemented with NaCl and 50 μg/mL of Kanamycin) and incubated at 28 °C for 2 days. No colonies were seen on the agar plate (Fig. S4). To quantify RFP production, Strep-Tactin XT affinity beads (IBA Life Sciences) were spun down and washed twice with PBS at 300 rpm for 60 s. 20 μL of the beads were added to 50 μL of the supernatant solution and incubated for 1 h. The mixture solution was then pipetted in a 24-well plate and the beads were imaged using Nikon Ti-Ecllipse (Nikon Instruments Europe B.V., Germany) microscope with SPlanFluor 20× LWD/ 0.7 objective using the Semrock LF561-B-000 filter (excitation 561/14, emission 609/54).

For the brightfield microscopy analysis over 3 days, Nikon Ti-Ecllipse (Nikon Instruments Europe B.V., Germany) microscope with Plan Apo λ 10×/0.45. Thin films bacterial hydrogels were incubated at 37 °C and 5 % CO_2 using an Okolab incubation chamber (Okolab SRL, Pozzuoli, Italy) coupled to the microscope. Imaging locations were selected near the middle of the bacterial gel.

4.11. L-lactate biosensors

For the biosensing platform, BZ-X Filter GFP OP-87763 (excitation 470/40, emission 525/50) and Keyence PlanFluor 4×/0.13 objective were used to detect the production of creiLOV protein. The thin films were incubated in an incubation chamber (Stage Top Incubator, Tokai Hit) coupled to a BZ-X800 (Keyence, Osaka, Japan) microscope in 400 μL of RPMI 1640 (Thermo Fisher Scientific, Germany) medium supplemented with 50 μg/mL of Kanamycin to lower the background signal which was seen in case of LB medium. L-lactate solution in phosphate saline buffer was added in desired concentrations (0, 1 and 10 mM) to RPMI 1640 medium added to the samples. L-lactate was added to the samples at 0 h/6 h timepoints followed by incubation at 37 °C and 5 % CO_2 during which creiLOV fluorescence images were taken every 30 min and quantified by determining the mean grey value post thresholding (Mean autothreshold) the colonies and subtracting the mean grey value of the background. To test the storage efficacy of this living biosensors platform, the thin films were incubated at 37 °C and 5 % CO_2 to allow the bacteria to grow for 1 day and then stored in PBS for 2 days at room temperature. L-lactate was added and the development of the creiLOV fluorescence was then recorded in a TECAN plate reader every 15 min (excitation 447 nm, emission 497 nm) using the setting of multiple reads per well, as described earlier. For the freeze-drying experiments, the thin films were first soaked in 12 % *w/v* of sucrose solution for 1 day post growth of 1 day, dipped directly into liquid nitrogen for 2 min and freeze-dried using the freeze dryer (Christ Alpha 1–2 LDplus, Germany) at −20 °C at 1 mbar for 5 h. L-lactate was added to freshly added RPMI medium and the development of the creiLOV fluorescence was recorded as above.

4.12. Statistical analyses

One-way analysis of variance (ANOVA) with post hoc Tukey HSD test was performed with results involving more than three data points. Differences were considered statistically significant at $*p < 0.05$, $**p < 0.01$, $***p < 0.001$. Analyses were performed with Origin Pro 9.1 software.

CRediT authorship contribution statement

Shardul Bhusari: Methodology, Validation, Formal analysis, Investigation, Writing, Visualization.

Juhyun Kim: Methodology, Investigation.

Karen Polizzi: Conceptualization, Writing - Review & Editing.

Shrikrishnan Sankaran: Conceptualization, Formal analysis, Writing - Review & Editing, Supervision, Funding acquisition.

Aránzazu del Campo: Conceptualization, Methodology, Writing, Supervision, Funding acquisition.

Declaration of competing interest

The authors declare that they have no known competing financial interests or personal relationships that could have appeared to influence the work reported in this paper.

Data availability

Data will be made available on request.

Acknowledgements

SB, SS and AdC acknowledge funding support from the Collaborative Research Centre SFB 1027 (Deutsche Forschungsgemeinschaft) and from the Leibniz ScienceCampus Living Therapeutic Materials, LifeMat (W32/2019, Leibniz Gemeinschaft). Authors thank Dr. Mitchell Han and Dr. Cao Nguyen Duong for insights in image analysis, Ana Díaz Álvarez for functionalization of glass coverslips, Dr. Claudia Fink-Straube and Thi Vinh Ha Rimbach-Nguyen for gel permeation chromatography (GPC) measurements and Dr. Samuel Pearson for his support in the interpretation of GPC results.

Appendix A. Supplementary data

Supplementary data to this article can be found online at https://doi.org/10.1016/j.bioadv.2022.213240.

References

[1] L. Xu, X. Wang, F. Sun, Y. Cao, C. Zhong, W.-B. Zhang, Curr. Opin. Solid State Mater. Sci. (2021) 25.
[2] A. Rodrigo-Navarro, S. Sankaran, M.J. Dalby, A. del Campo, M. Salmeron-Sanchez, Nat. Rev. Mater. 6 (2021) 1175.
[3] H. Priks, T. Butelmann, A. Illarionov, T.G. Johnston, C. Fellin, T. Tamm, A. Nelson, R. Kumar, P.J. Lahtvee, ACS Appl. Bio Mater. 3 (2020) 4273.
[4] M. Schaffner, P.A. Rühs, F. Coulter, S. Kilcher, A.R. Studart, Sci. Adv. (2017) 3, https://doi.org/10.1126/sciadv.aao6804.
[5] S. Bhusari, S. Sankaran, A. del Campo, Adv. Sci. 2106026 (2022) 1.
[6] S. Sankaran, A. Campo, Adv. Biosyst. 3 (2019), 1800312.
[7] S. Sankaran, J. Becker, C. Wittmann, A. Campo, Small 15 (2019) 1804717.
[8] A. Saha, T.G. Johnston, R.T. Shafranek, C.J. Goodman, J.G. Zalatan, D.W. Storti, M. A. Ganter, A. Nelson, ACS Appl. Mater. Interfaces 10 (2018) 13373.
[9] T.G. Johnston, S.F. Yuan, J.M. Wagner, X. Yi, A. Saha, P. Smith, A. Nelson, H. S. Alper, Nat. Commun. 11 (2020) 563.
[10] T.C. Tang, E. Tham, X. Liu, K. Yehl, A.J. Rovner, H. Yuk, C. de la Fuente-Nunez, F. J. Isaacs, X. Zhao, T.K. Lu, Nat. Chem. Biol. 17 (2021) 724.
[11] X. Liu, T. Tang, E. Tham, H. Yuk, S. Lin, T.K. Lu, PNAS 114 (2017), https://doi.org/10.1073/pnas.1618307114.
[12] J.L. Connell, E.T. Ritschdorff, M. Whiteley, J.B. Shear, PNAS 110 (2013) 18380.
[13] X. Liu, H. Yuk, S. Lin, G.A. Parada, T.C. Tang, E. Tham, C. de la Fuente-Nunez, T. K. Lu, X. Zhao, Adv. Mater. 30 (2018) 1704821.
[14] C. Knierim, M. Enzeroth, P. Kaiser, C. Dams, D. Nette, A. Seubert, A. Klingl, C. L. Greenblatt, V. Jérôme, S. Agarwal, R. Freitag, A. Greiner, Macromol. Biosci. 15 (2015) 1052.
[15] L. Goers, C. Ainsworth, C.H. Goey, C. Kontoravdi, P.S. Freemont, K.M. Polizzi, Biotechnol. Bioeng. 114 (2017) 1290.
[16] T. Trantidou, L. Dekker, K. Polizzi, O. Ces, Y. Elani, Interface Focus (2018) 8, https://doi.org/10.1098/rsfs.2018.0024.
[17] I. Moya-Ramírez, P. Kotidis, M. Marbiah, J. Kim, C. Kontoravdi, K. Polizzi, ACS Synth. Biol. (2021), https://doi.org/10.1021/acssynbio.1c00577.
[18] M. Müller, J. Becher, M. Schnabelrauch, M. Zenobi-Wong, Biofabrication 7 (2015), 035006.
[19] B. Pabst, B. Pitts, E. Lauchnor, P.S. Stewart, Antimicrob. Agents Chemother. 60 (2016) 6294.
[20] M. Torres, C. Altamirano, A.J. Dickson, Curr. Opin. Chem. Eng. 22 (2018) 184.
[21] J. Anderson, Part : BBa _ J23118, can be found under, 2006, http://parts.igem.org/Part:BBa_J23118.
[22] M. Hill M. Kern S. Bose A. Apostolidis , "Evaluation of an Optical CO 2 Probe for Long-term Monitoring in Stirred-tank Bioreactors," can be found under https://www.presens.de/knowledge/publications/application-note/evaluation-of-an-optical-co2-probe-for-long-term-monitoring-in-stirred-tank-bioreactors-1715, n.d.
[23] M. Hill G. Laslo M. Kern S. Bose C. Krause , "Cell Culture Monitoring in Stirred-Tank Bioreactor With Optical pH Sensors," can be found under https://www.presens.de/knowledge/publications/application-note/cell-culture-monitoring-in-stirred-tank-bioreactor-with-optical-ph-sensors-1717, n.d.
[24] M. Hill G. Laslo M. Kern S. Bose C. Krause , "Evaluation of an Optical O2 Probe and Sensor Spots for Long-term Measurements in Stirred-tank Bioreactors," n.d.
[25] S. Iuchi, E.C.C. Lin, Proceedings of the National Academy of Sciences of the United States of America 85 (1888) (1988).
[26] M. Di Biase, P. De Leonardis, V. Castelletto, I.W. Hamley, B. Derby, N. Tirelli, Soft Matter 7 (2011) 4928.
[27] F. Yang, G.L. Nelson, J. Appl. Polym. Sci. 91 (2004) 3844.
[28] A. Farrukh, W. Fan, S. Zhao, M. Salierno, J.I. Paez, A. del Campo, ChemBioChem 19 (2018) 1271.

Supporting Information

Encapsulation of bacteria in bilayer Pluronic thin film hydrogels: a safe format for engineered living materials

Shardul Bhusari[1,2], Juhyun Kim[3,4,5], Karen Polizzi[3,4], Shrikrishnan Sankaran[1]*, Aránzazu del Campo[1,2]*

[1] INM - Leibniz Institute for New Materials, Saarbrücken, Germany

[2] Chemistry Department, Saarland University, 66123 Saarbrücken, Germany

[3] Department of Chemical Engineering, Imperial College London, London SW7 2AZ, United Kingdom

[4] Imperial College Centre for Synthetic Biology, Imperial College London, London SW7 2AZ, United Kingdom

[5] Current affiliation - School of Life Sciences, BK21 FOUR KNU Creative BioResearch Group, Kyungpook National University, Daegu 41566, Republic of Korea

*Corresponding authors

Email: shrikrishnan.sankaran@leibniz-inm.de, aranzazu.delcampo@leibniz-inm.de

Table S1: Hydrogel composition of the Plu-PluDA mixtures. Mechanical properties of DA 0-100 hydrogels with different compositions obtained from rheology; shear storage modulus (G') of the crosslinked hydrogels.[151]

Hydrogel Composition	Plu : PluDA	Shear storage modulus [kPa]
DA 0	100 : 0	17.8 ± 1.4
DA 25	75 : 25	20.4 ± 2.4
DA 50	50 : 50	25.9 ± 1.5
DA 75	25 : 75	32.7± 3.8
DA 100	0 : 100	42.9 ± 1.9

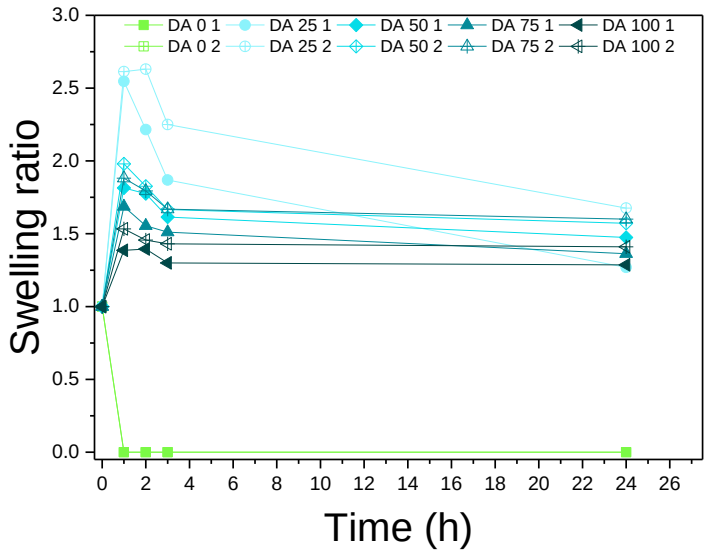

Figure S1: Swelling ratio (weight at time 't' compared to the initial weight) of the different DA X hydrogels in MQ water and stored at 37 °C and 5 % CO_2, where in DA X≥25, the ratio decreases with increasing X (i.e. covalent crosslinking) in the first hour. DA 0 dissolves in water. (n = 2)

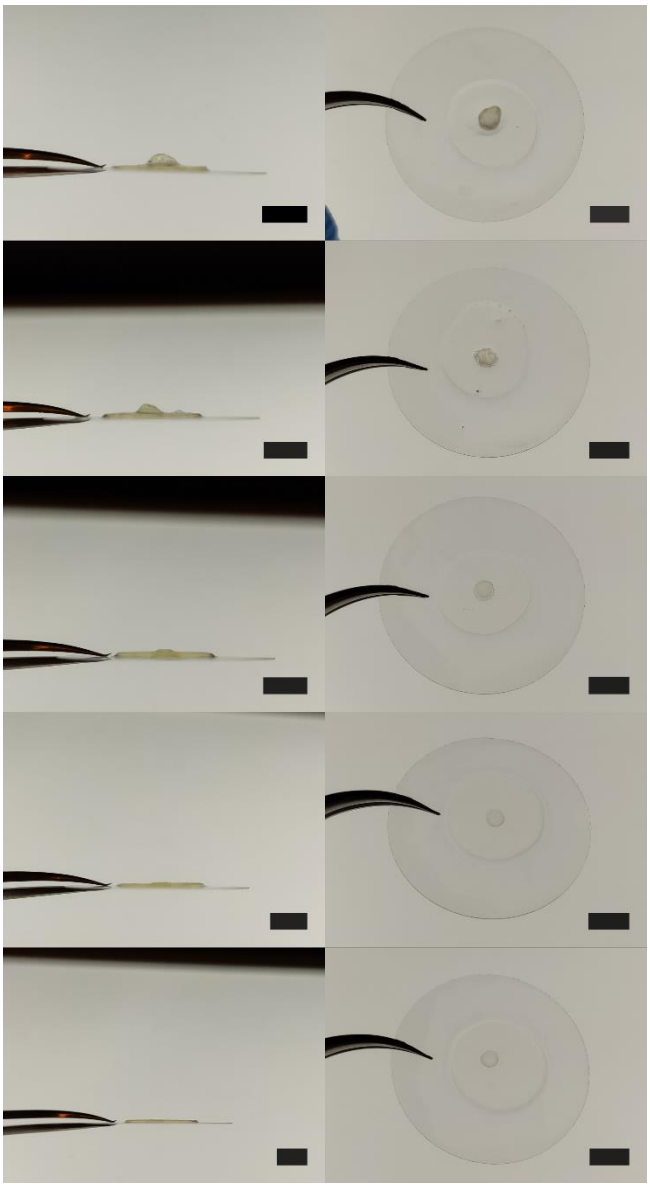

Figure S2: Images showing the swelling of the inner gels (DA X) of the bilayer thin films after 24 h incubation in medium at 37 °C and 5 % CO_2. (Scale = 5 mm)

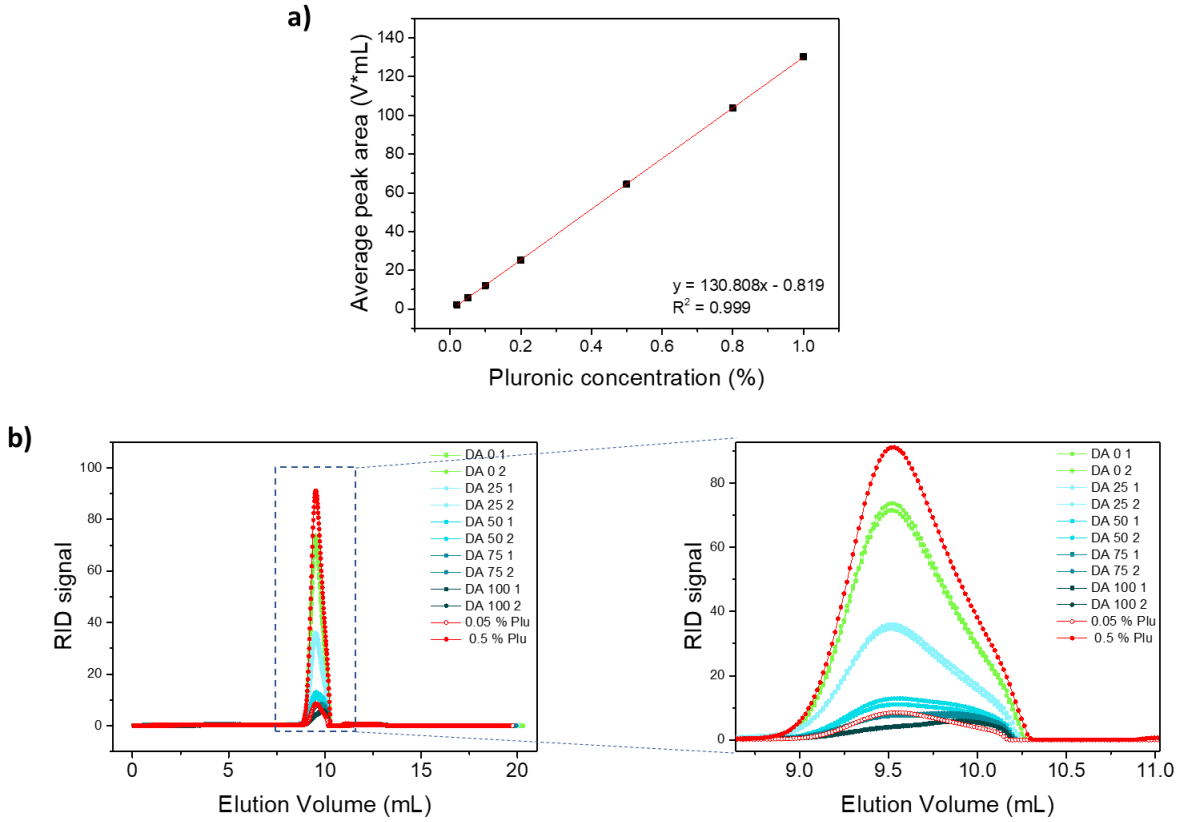

Figure S3: a) Standard curve with known pluronic concentrations and **b)** Representative GPC chromatograms of supernatants from DA X films after 1 h incubation. The chromatograms (in red) of solutions of known pluronic concentrations (0.05 and 0.5 % w/v) are also represented to compare the molecular weight distributions.

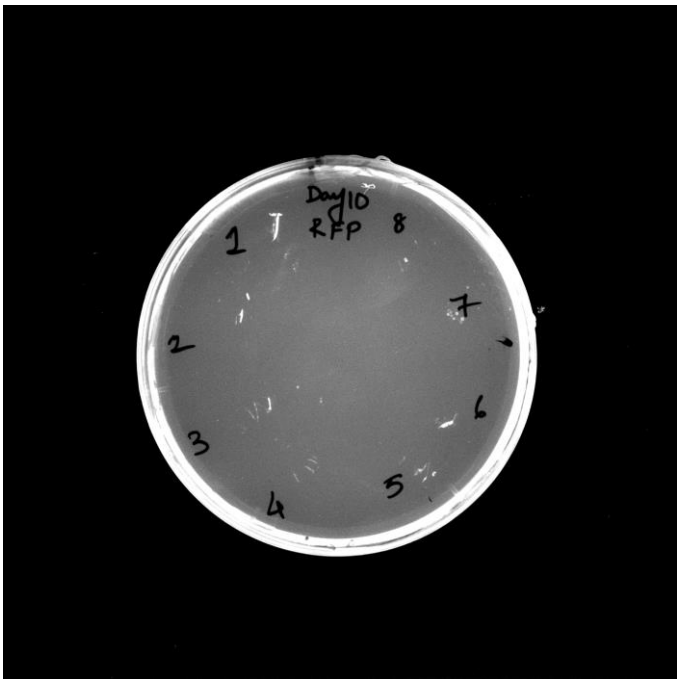

Figure S4: Supernatants of the thin films (N=8) embedding RFP producing bacteria for 10 days from (Figure 3d) streaked onto agar plates (made up of LB supplemented with NaCl and 50 µg/mL of Kanamycin) and incubated at 28 °C for 2 days showed no growth to confirm the absence of leakage of the thin films.

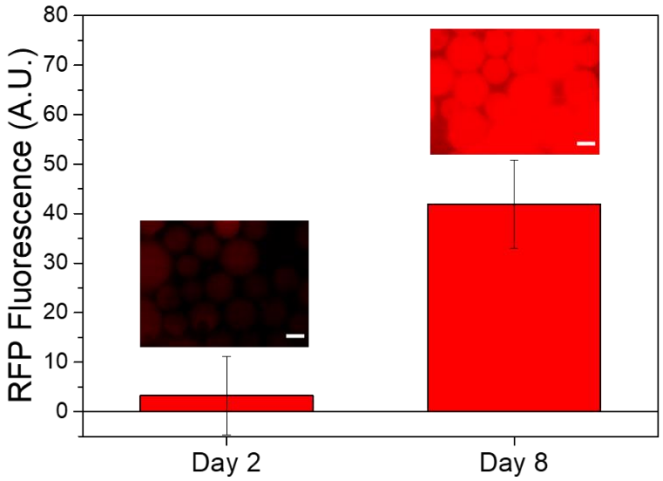

Figure S5: Fluorescence intensities of the Strep-Tactin affinity beads exposed to the supernatants of the thin films taken at day 2 and day 8. (scale = 50 µm)

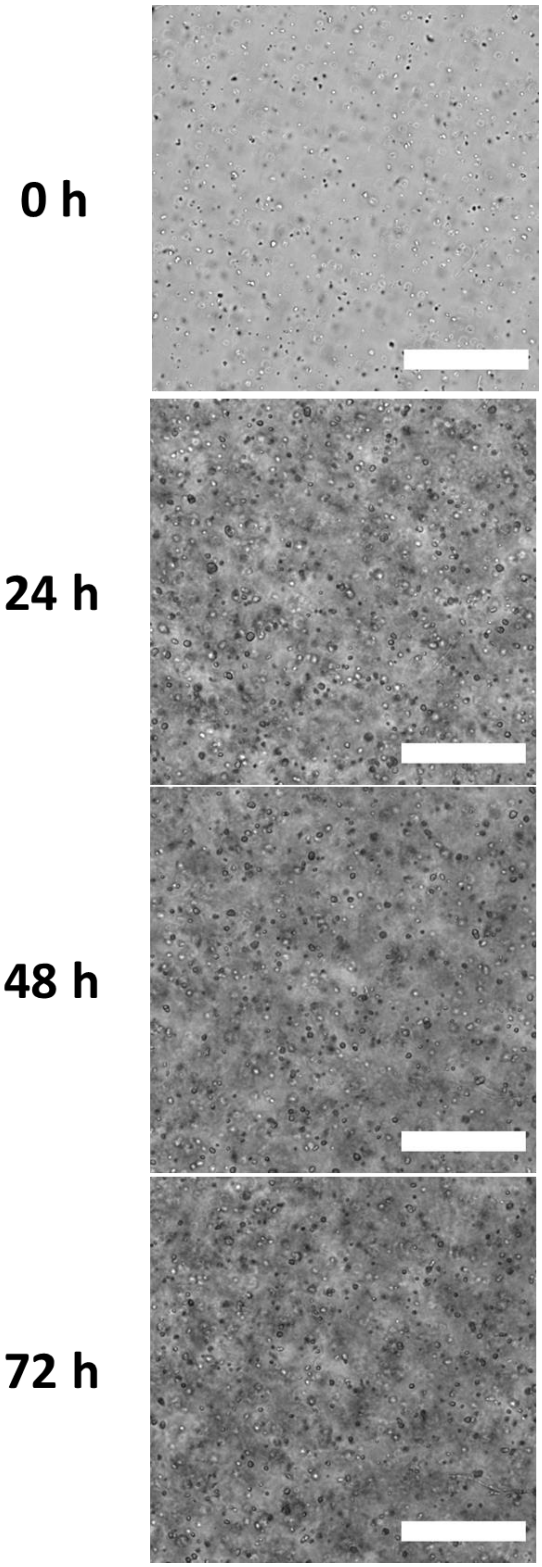

Figure S6: Representative images of E. coli (ClearColi) growing within the DA 50 thin film bilayers at 0, 24, 48 and 72 h. Images were taken near the middle of the bacterial gel height. (scale = 100 µm)

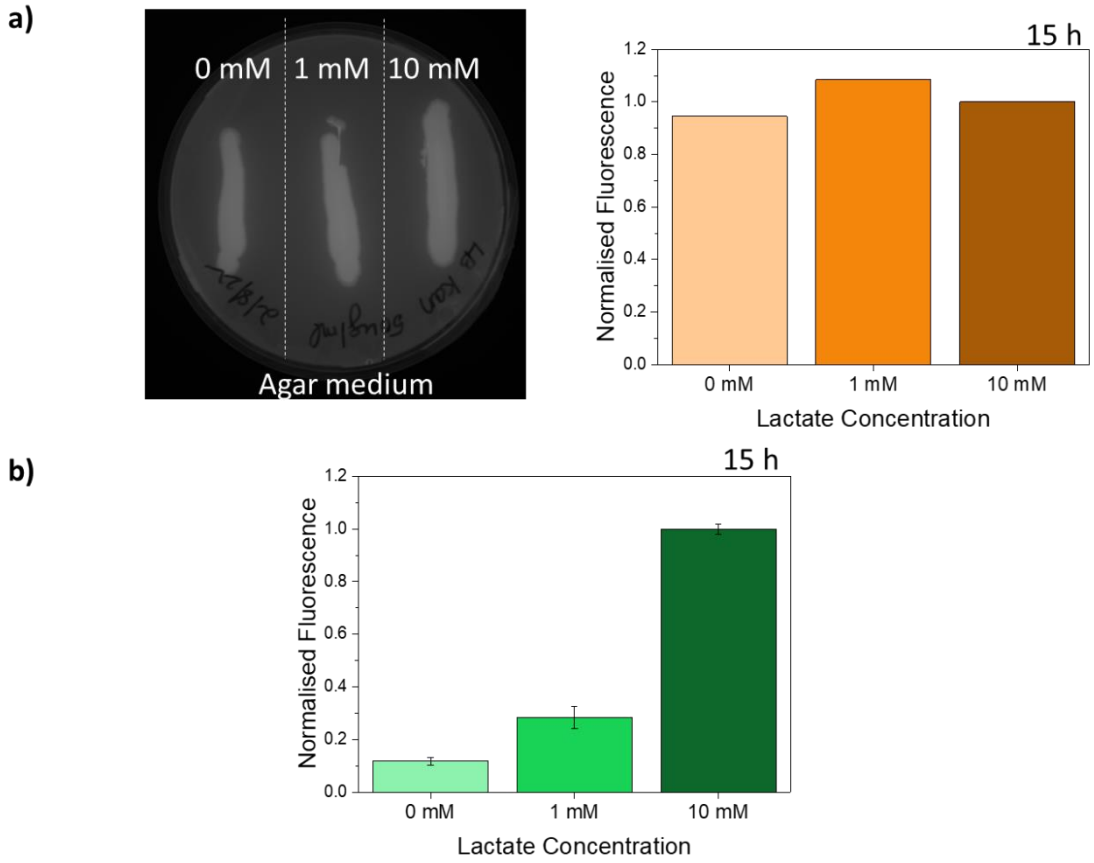

Figure S7: a) Fluorescence of the lactate sensing creiLOV production by the bacterial streaks on the agar plate at 15 h highlighting the strong leaky expression even in the absence of lactate (0 mM) (n = 1) and **b)** Fluorescence intensities upon lactate induction by the bacteria grown in liquid culture at 15 h. The fluorescence intensities were normalized to the corresponding 10 mM fluorescence values. (n = 2, mean ± SD)

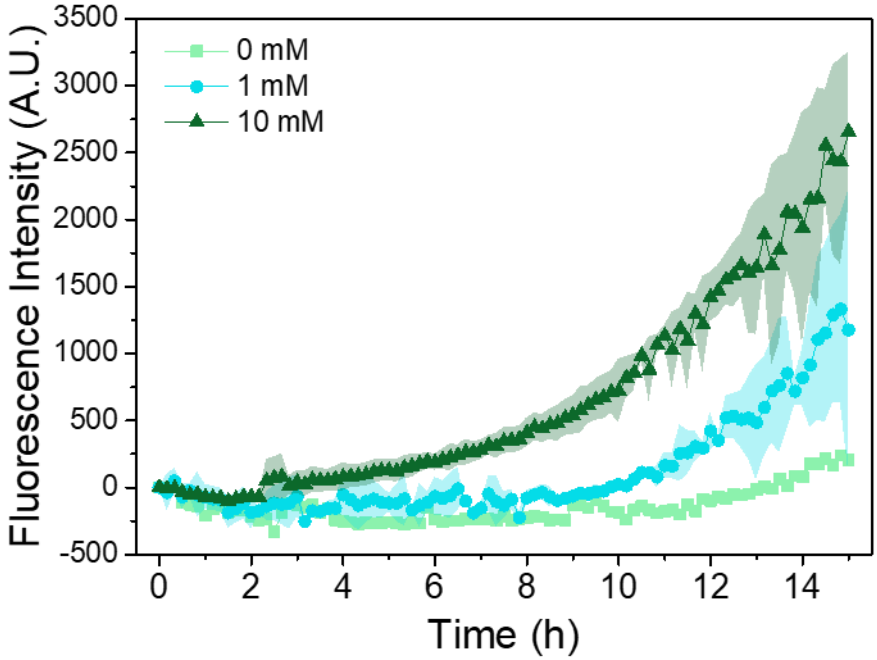

Figure S8: Quantification of fluorescence intensity upon lactate induction post growth for 1 day and storage in PBS for 2 days and freeze drying (N=2 for 1 and 10 mM, N=1 for 0 mM) indicating creiLOV production in the hydrogel DA 50 during 15:30 h (mean ± standard deviation)

6.4 *In vitro* evaluation of immune responses to bacterial hydrogels for the development of living therapeutic materials

Archana Yanamandra[1,2*], Shardul Bhusari[2,3*], Aránzazu del Campo[2,3], Shrikrishnan Sankaran[2#], Bin Qu[1,2#]

[1]Biophysics, Center for Integrative Physiology and Molecular Medicine (CIPMM), School of Medicine, Saarland University, Homburg, Germany

[2] INM - Leibniz Institute for New Materials, Saarbrücken, Germany

[3] Chemistry Department, Saarland University, 66123 Saarbrücken, Germany.

* Contributed equally

Corresponding authors

Email: bin.qu@uks.eu**,** shrikrishnan,sankaran@leibniz-inm.de

Unpublished original work (submitted)

Own Contribution: Methodology (sample fabrication, live dead assay, ATP assay, protein/DNA release study), Validation, Visualization, Formal analysis, Investigation, Writing (for parts with sample fabrication, live dead assay, ATP assay, protein/DNA release study)

Abstract

In living therapeutic materials (LTMs), organisms genetically programmed to produce and deliver drugs are encapsulated in porous matrices acting as physical barriers between the therapeutic organisms and the host cells. The therapeutic potential of such constructs has been studied in *in vitro* studies, however their translation to *in vivo* scenarios requires evaluation of the immune response to the LTMs. In this study, we investigate the response of human peripheral blood mononuclear cells (PBMCs) exposed to a LTM consisting of engineered *E. coli* encapsulated in Pluronic F127-based hydrogels. This bacteria/hydrogel combination has been frequently used in LTM designs but its immunogenicity has not been tested. The release of inflammation-related cytokines and cytotoxic proteins and the subsets of natural killer cells and T cells were examined. Encapsulation of the bacteria in hydrogels considerably lowers their immunogenicity. *ClearColi*, an endotoxin-free variant of *E. coli*, did not polarize NK cells into the more cytolytic $CD16^{dim}$ subset as *E. coli*. Our results demonstrate that *ClearColi*-encapsulated hydrogels generate low immunogenic response and are suitable candidates for the development of LTMs for *in vivo* testing to assess a potential clinical use. Nevertheless, we observed a stronger immune response in pro-inflammatory PBMCs, possibly from donors with underlying infections. This suggests that including anti-inflammatory measures in living therapeutic material designs could be beneficial for such recipients.

Introduction

Living therapeutic materials (LTMs) combine live cells with non-living materials to create devices with the potential to deliver therapeutic molecules when implanted in the body [1, 2]. Bacteria are frequently used as living component in LTMs due to their simple and adaptable nutritional requirements, and their robustness to survive harsh conditions (e.g. pH, hypoxia, osmosis) or processing steps for storage (e.g. freeze drying). These living cells are encapsulated in polymeric matrices, like agarose [3-5], alginate [6] or Pluronic F127 [7-9]. At adequate composition, the encapsulating matrices allow diffusion of nutrients, gas, and metabolites and can maintain the viability and function of the organisms while physically separating them from antagonistic external entities like competitive microbes or immune cells.

For the use of LTMs in biomedical applications, one major aspect is the immune responses they might elicit. LTMs in direct contact with tissues and biological fluids could potentially trigger innate and adaptive immune responses in the body. These can be originated by biochemical (release of proteins, oligonucleotides, chemical moieties, etc.) or physical (e.g. mechanical properties of the construct) factors [10-12]. Such responses have been observed during the development of encapsulated cell technologies, wherein mammalian cells engineered to secrete drugs are encapsulated in semipermeable matrices [13]. Most studies were conducted in cells encapsulated in degradable alginate microcapsules, and immune responses were observed in terms of the polymer, the cellular antigens, the therapeutic transgenes and the DNA vectors used to genetically engineer the cells [13]. Improved designs can solve many of these issues by using semi-permeable membrane interfaces to physically separate the engineered cells from the host [14].

Engineered bacteria are being developed as live biotherapeutic products to be freely administered in the body for curing a variety of diseases like inflammatory bowels disease, viral infections, cancer, etc [15, 16]. One of the prominent strains used in such studies is *E. coli* Nissle 1917, which is a probiotic in European markets. This strain has a defect in its LPS biosynthesis leading to truncated oligosaccharide chains that triggers low levels of immunogenicity when the LPS was exposed to PBMCs [17]. This strain is predominantly used to treat diseases in its natural habitat, the gut, but its use in other sites of the body to treat cancer has also been explored [18]. This has revealed that its intratumoral injection in mice leads to

considerable increase in IL-6 and TNFα levels, which is desirable for tumor immunotherapy [19]. Thus, outside the gut, this probiotic strain has been found to illicit immune responses. This strain is also susceptible to rapid immune attack and clearance from the body, which has been temporarily reduced by programming it to generate a surface capsular polysaccharide that encapsulates the bacterial cell [20]. Probiotic microencapsulation is a common strategy used to protect the bacteria from harsh factors within the body during administration [21]. However, the effect of encapsulation on immune responses has not been systematically evaluated.

Immunogenicity of LTMs can be associated to the material and to the living bacterial components. It is important to highlight that in LTMs, bacteria are not directly exposed to the host cells and, therefore, their possible immunogenicity should be associated with secreted substances or cell debris or with the properties of the encapsulating hydrogel, but not with a direct bacteria-host cell contact. The inflammatory host reactions are complex and involve neutrophils as the first dominant responder, followed by macrophages [10]. $CD4^+$ T helper cells and immune killer cells ($CD8^+$ cytotoxic T lymphocytes and natural killer cells) also participate in inflammation responses [22]. Upon detection of foreign bodies, inflammation-related cytokines (e.g. IL-6, IL-8, IL-10, tumor necrosis factor α (TNFα), interferon-gamma (IFNγ), and IL-17A) and cytotoxic proteins (e.g. perforin, granzyme A, granzyme B, granulysin, soluble Fas and soluble Fas ligand) are released by the effector immune cells [23-32]. Profiles of these cytokines and cytotoxic proteins can be therefore used as markers to evaluate LTM immunogenicity. Certain immune cells, including T cells and NK cells, can differentiate into functionally different subsets upon exposure to external stimuli [33, 34], offering another metric to evaluate LTM-induced immune response.

In this paper, we examine how the immune cells react to LTMs made from a commonly-reported material-bacteria combination: Pluronic F127-based hydrogels and *E. coli* strains. Pluronic F127 is a synthetic polymer approved for medical use and frequently used in drug delivery formulations. Pluronic solutions at concentrations >5 wt% and temperatures above 14°C self-assemble into micelles to form associative (physical) hydrogels [35, 36]. This thermoreversibility facilitates the use of Pluronic to encapsulate drugs or cells. *E. coli* has been frequently used in LTM design due to the availability of a broad genetic toolbox and medically relevant strains (e.g. Nissle 1917, *ClearColi*) [1]). *E. coli* hosts lipopolysaccharides (LPS) on the outer membrane, that engage with Toll-like receptor 4 (TLR4) and trigger strong endotoxic

responses, i.e. pro-inflammatory immune responses in mammals especially humans, which can result in a life-threatening cytokine storm. In the endotoxin-free strain *ClearColi* BL21DE3, the 7 genes that encode for LPS synthesis are deleted. Lysates of this strain have been proven to not elicit endotoxic responses [37]. In our recent work, we described light-responsive LTMs containing *ClearColi* engineered to produce and secrete a fluorescent protein as a model protein and deoxyviolacein as a potential antimicrobial drug [3, 4, 38]. We demonstrated that drug profiles could be tuned by light irradiation parameters and that release could be sustained for over a month in both cases, suggesting that such LTMs could be used to develop *in situ* controllable drug delivery devices. Inspired by these positive results, and with the aim to extend our future studies to *in vivo* scenarios, we examine here how donor-derived peripheral blood mononuclear cells (PBMCs) react to LTMs made of Pluronic F127 based hydrogels containing *ClearColi*. For comparison, similar studies with *E. coli* BL21DE3 (endotoxic), empty Pluronic F127 gels and free bacteria were also performed. The results of our study indicate that LTMs containing (and retaining) the endotoxin-free *ClearColi* within Pluronic hydrogels do not cause strong immune reactions by PBMCs, corroborating the suitability of this combination for LTM development. We also noticed that donors with pro-inflammatory status (high spontaneous IL-2 release) did show inflammatory response to the LTMs and, therefore, preventive strategies might need to be considered for the applicability of LTMs to such patients.

Materials and Methods

Antibodies and reagents

The following antibodies were purchased from BioLegend: BV421 anti-human CD3 antibody, PerCP anti-human CD8 antibody, PE anti-human CD45RO antibody, Alexa647 anti-human CCR7 antibody, APC anti-human CD56 antibody, PerCP anti-human CD16 antibody. Legendplex human CD8/NK panel was also purchased from BioLegend. Lymphocyte separation medium 1077 was purchased from PromoCell.

Bacteria cultures

E. coli BL21(DE3), from NEB (C2527H), and its endotoxin-free variant, *ClearColi* BL21(DE3), from Lucigen (60810-1), were used in this study. They were transformed with the plasmid pUC19 to provide them with ampicillin resistance and minimize the risk of contamination in the culture. Transformation in *E. coli* was performed by heat-shock and in *ClearColi* by

electroporation as described by the manufacturer of these competent cells. Bacterial cultures were grown for 16 h at 35°C, 180 rpm in LB Miller medium supplemented with 50 µg/mL of ampicillin to an optical density at 600 nm wavelength (OD600) between 0.5 – 1.

Functionalization of glass coverslips with (3-acryloxypropyl)trimethoxysilane

13 mm glass coverslips were sonicated in ethanol for 5 mins and then rinsed with ethanol. The coverslips were treated with 1% v/v solution of (3-acryloxypropyl)trimethoxysilane (APS, Merck - Sigma Aldrich) in ethanol for 1 h. The coverslips were then rinsed in ethanol and dried for further use.

Preparation of bacteria-encapsulated thin-film hydrogel constructs

Pluronic F127 (Plu, MW~12600 g/mol, Sigma-Aldrich) and Pluronic F127 diacrylate (PluDA) [39] with substitution degree of 70% was used for the studies. Stock solutions of 30% (w/v) Plu and PluDA in milliQ water with Irgacure 2959 photoinitiator at 0.2% w/v were prepared and stored at 4°C. 1:1 mixtures of the stock solutions of Plu and PluDA at 4°C were added to the bacterial suspension (OD600 of 0.5, ~ 4×10^7 cells/mL) at 9/1 (v/v) ratio to achieve a final OD600 of 0.05. The solutions were stored on ice to keep the Plu/PluDA solutions in liquid form. The Plu/PluDA/bacteria mixture was vortexed for 30 secs to obtain a homogeneous dispersion. 2 µL of the Plu/PluDA/bacteria mixture was placed on coverslips previously functionalized with (3-acryloxypropyl)trimethoxysilane and left at room temperature for 10 mins to form the physical hydrogel (Supporting information **Figure S1**). The silanization step ensures covalent bonding of the PluDA component with the glass substrate during the upcoming photopolymerization step.

The bacteria/Plu/PluDA physical hydrogel was covered by a PluDA envelope to avoid bacteria outgrowth. For this purpose, 30 µL of PluDA solution was dropped on parafilm and allowed to physically crosslink at room temperature for 10 mins. The coverslip with the bacterial gel was then placed on top of the gel on the parafilm. The hydrogel sandwich was exposed to UV light (365 nm, 6 mW/cm^2) for 60 secs using UV Lamp inside Alpha Innotech FluorChem Q system (Biozym, Oldendorf, Germany), which was the illumination step used to initiate the photopolymerization of the acrylate groups and covalent crosslinking of the hydrogels. After additional 10 mins, the parafilm was peeled off.

The thin-film construct was incubated at 37°C with 5% CO_2 for 3 days before incubation with the immune cells. In this time bacteria grew into colonies inside the Plu/PluDA hydrogel core

layer. Samples showing bacteria leakage (~1 out 10) were excluded for the study. From our and others' previous studies [7, 9, 38] we consider that the Pluronic F127 based gels allow free diffusion of nutrients. Plu/PluDA hydrogels might leak non-crosslinked chains to the medium during the first hours of incubation.

Live/Dead assay

The LIVE/DEAD BacLight Bacterial Viability kit (Thermo Fisher Scientific L7012) was used. Stock solutions of the stain were stored at −20°C. To make the working solution, 3 µL of the stock solutions were added to 1 mL of phosphate saline buffer (PBS). The bacterial hydrogels were washed with PBS to remove traces of the RPMI medium and incubated with 100 µL of the stain solution for 20 mins. The samples were washed with 0.5 mL PBS once and imaged under the microscope. For fluorescence imaging, BZ-X Filter TRITC OP-87764 (excitation 545/25, emission 605/70) was used for imaging the dead colonies while BZ-X Filter GFP OP-87763 (excitation 470/40, emission 525/50) was used for imaging the live colonies using the Keyence PlanFluor 4×/0.13 objective. Image processing and analyses were performed using Fiji edition of ImageJ (ImageJ Java 1.8.0). The thin-films were also imaged by Zeiss LSM 880 confocal laser scanning microscopy (CLSM) at days 3 and 7. The exposure conditions were optimized for minimizing cell photodamage using the objective LD C-Apochromat 40×/1.1 W Korr M27, detection wavelength 493-584 nm and 584-718 nm, laser wavelength of 488 and 583 nm and power of 0.2 and 1.5 % respectively for live and dead bacterial populations. Z-stacks of 100.204 µm were taken in a z-step size of 0.65 µm. Images of a size of (xy) 283.77 × 283.77 µm were acquired (512 × 512 pixels), two-fold line averaging, and pixel dwell time of 1.52 µs. The digital gain value was 760 and 720 for live and dead bacterial populations. Imaris software (Version 9.0, Bitplane) was used to process CLSM image z-stacks to create three-dimensional images.

ATP assay

Bacterial cell viability was assessed by the CellTiter-Glo luminescent cell viability assay (Promega) that quantifies ATP released in the culture medium as an indicator of metabolically active cells. A 1:1 mixture of the CellTiter-Glo reagent and the supernatant was shaken for 5 mins and the luminescence was measured using a Tecan Infinite M200- Pro plate reader. The experiments were performed for supernatants from different culture times.

Protein/DNA release studies

To quantify the amount of protein released in the supernatant medium of the thin films, a commercial BCA protein assay (Pierce BCA Protein Assay Kit, Thermo Fisher Scientific) was used. Quantification by absorbance measurements at 562 nm was performed using a Tecan Infinite 200 PRO microplate reader. To check the release of DNA into the supernatant, agarose gel electrophoresis was performed with the cell free supernatants mixed with the Tritrack Gel Loading Dye in a 3:1 ratio and loaded on the 1.5% (w/v) agarose gel premixed with SyBr Safe gel staining dye. The samples were run at constant voltage (100V) and visualized in the ChemiDoc TransIlluminator under UV light irradiation.

Isolation and cell culture of PBMCs

Human peripheral blood mononuclear cells (PBMCs) were isolated from Leucocyte reduction system chambers of healthy donors employing gradient centrifugation method where Lymphocyte Separation Medium 1077 was used. Virological test excluded infection by HIV and hepatitis B in the donors. Research carried out for this study is authorized by the local ethic committee of Saarland (declaration from 16.4.2015 (84/15; Prof. Dr. Rettig-Stürmer)).

To test the immune response to LTMs, PBMCs were cultured at 37°C with 5% CO_2 for 3 days in RPMI-1640 medium (Thermo Fisher Scientific) supplemented 10% FCS (Thermo Fisher Scientific) and 1 % ampicillin at a cell density of 3×10^6/mL per condition. Eight different conditions were used in the experiments: PBMCs alone (Ctrl), blank gel (without bacteria), *ClearColi* encapsulated gel, *E. coli* encapsulated gel, *ClearColi* in a transwell insert, *E. coli* in a transwell insert, *ClearColi* in direct contact with PBMCs, *E. coli* in direct contact with PBMCs. Bacteria suspensions with initial OD 0.05 were used for the studies.

Identification of subpopulations and subsets

PBMCs were collected on day 3 and washed twice with PBS/0.5% BSA, followed by staining with corresponding antibodies as specified in the figure notations for 30 mins at 4°C in dark. Control IgG was used to gate the positive cells. FACSVerse flow cytometer (BD Biosciences) was used for data acquisition and FlowJo v10 (FLOWOJO, LLC) for data analysis.

Multiplex cytokine assay

100 µL of cell culture media was collected carefully on days 1, 2 and 3 from each condition, centrifuged at 1000 g for 10 mins. Supernatant was collected and stored at -80°C until further analysis. Legendplex human CD8/NK panel (BioLegend) was used to determine cytokine

profiles of the samples according to the manufacturer's instructions. Culture media was used as the blank control.

Statistical analysis

GraphPad Prism 9 Software (San Diego, CA, USA) was used for statistical analysis. The differences between two columns were analyzed by the ratio paired t-test.

Results

In our previous studies we demonstrated that Plu/PluDA hydrogels at 30 wt% concentration supported the growth of *ClearColi* and kept their metabolic function [38, 40]. At this polymer concentration, Plu/PluDA mixtures are fluid below 14°C and form mechanically stable hydrogels at higher temperatures by self-association of the polymer micelles. The growth and activity of encapsulated bacteria in these Plu/PluDA hydrogels were dependent on the PluDA ratio in the hydrogel, which controls the covalent crosslinking degree of the network. In PluDA hydrogels, bacteria showed the lowest growth and remained confined within the hydrogel over days. In 1:1 Plu/PluDA hydrogels bacteria showed the highest protein production rate but they were able to grow out of the gels. For the current studies, we processed hydrogels in a bilayer thin film format, where 1:1 Plu/PluDA hydrogels containing bacteria were enveloped by PluDA hydrogels without bacteria (**Figure 1A**, Supplementary Information **Figure S1**). This composition of the inner layer provides optimum environment for bacterial proliferation while restricting their mobility within the layer as previously reported by us [40]. In this study, we showed that the hydrogel layers swell for the initial few hours, accompanied by the release of the uncrosslinked pluronic micelles to the surrounding medium. This release possibly led to increased porosity of the hydrogel after film formation and swelling, which can favor diffusion of nutrients and cell viability. The resulting hydrogel network is stable with the inner bacterial gel layer surrounded by an encapsulating layer of ca. 100-150 um thickness. This bilayer format supported bacterial growth and metabolic production while it prevented outgrowth and escape of the bacteria during at least 7 days. It also facilitated microscopy imaging of the encapsulated bacteria. At the used seeding density, bacteria grew inside the thin film hydrogel and formed individual colonies, as previously reported. The bacteria within these colonies remained viable for at least 7 days according to the live/dead staining (**Figure 1B**). The metabolic activity of the encapsulated bacteria was assessed by quantifying the extracellular ATP. This assay allows detection of the metabolic activity of bacterial cultures at

concentrations <50 nM [41]. In a classical bacteria culture, extracellular ATP peaks during the early log phase and decreases in the stationary phase [41]. A similar bell-shaped curve was observed in the supernatant of bilayer hydrogels. After a 6 h lag period, nearly 0.15 nM ATP was detected for the following 22 hours, followed by a progressive drop (**Figure S2**). We infer that the bacteria within the first 6 to 24 h of encapsulation and incubation within medium, are in the log phase, whereas bacteria at 48 and 72 h have reached the stationary phase. This time scale correlates with the observed colony growth rates discussed in previous reports [38, 40]. Analysis of the incubation medium after 4, 5, and 6 days of incubation with BCA protein assay and gel electrophoresis did not reveal significant release of proteins or DNA from the gels (Supporting information **Figure S3**) [42, 43]. This result suggests that no notable cell lysis occurs within this time.

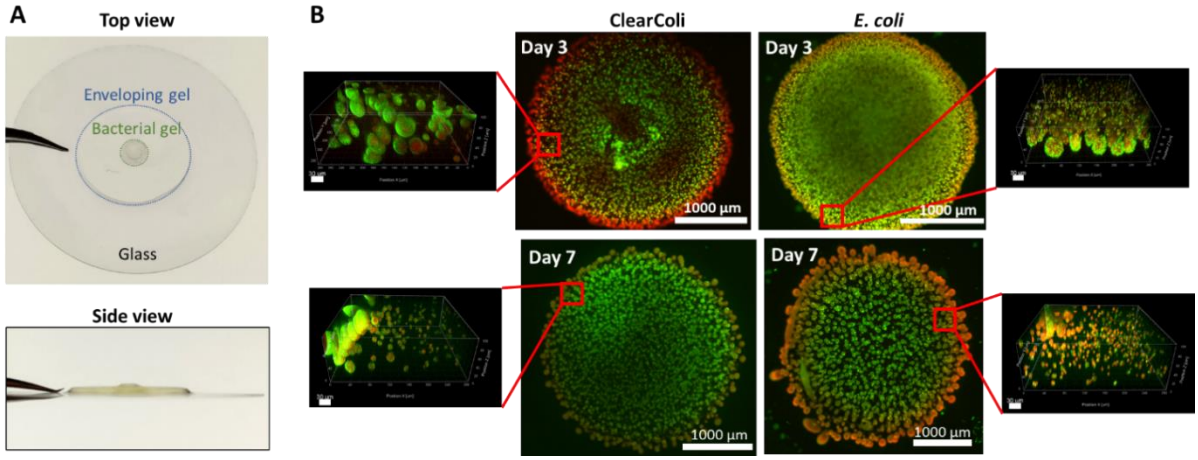

Figure 1: Bacteria/hydrogel thin-film constructs. A) Thin films (top and side view) showing the enveloping and bacterial Plu/PluDA gels. **B)** Confocal and fluorescence microscopy images of bacteria colonies of *ClearColi* and *E. coli* embedded in the hydrogels after staining with live-dead assay. The images show the presence of a viable population at day 3 and 7 post fabrication. (green/SYTO9 = live, red/propidium iodide = dead).

PBMC response to ClearColi, E. coli and PluDA hydrogels

We co-cultured PBMCs with the bacterial hydrogels on day 3 post fabrication and analyzed PBMC-released cytokines and cytotoxic proteins by multiplex cytokine assays for up to 3 days, since this is the relevant timespan for T cells to be fully activated [44]. Note that the bacterial hydrogels were kept in culture for 3 days before they were cocultured with the PBMCs. This step ensured that the bacteria had grown to their maximum colony sizes in all samples and allowed us to verify that they did not grow or leak out from the thin films. PBMCs from healthy

donors were used as they contain innate immune cells (e.g. monocytes and NK cells) as well as adaptive immune cells (e.g. T cells and B cells) [45] (Supplementary information **Figure S4**). As control experiments, we quantified the immunogenicity of the bacterial component (*E. coli* and *ClearColi* suspensions) and empty hydrogels in direct contact with PBMCs. The bacterial component was also physically separated by a nano-porous membrane in a transwell plate, i.e. ensuring exchange of bacteria-produced soluble factors (**Figure 2A**). Profiles of PBMC-released cytokines and cytotoxic proteins were analyzed on days 1, 2 and 3.

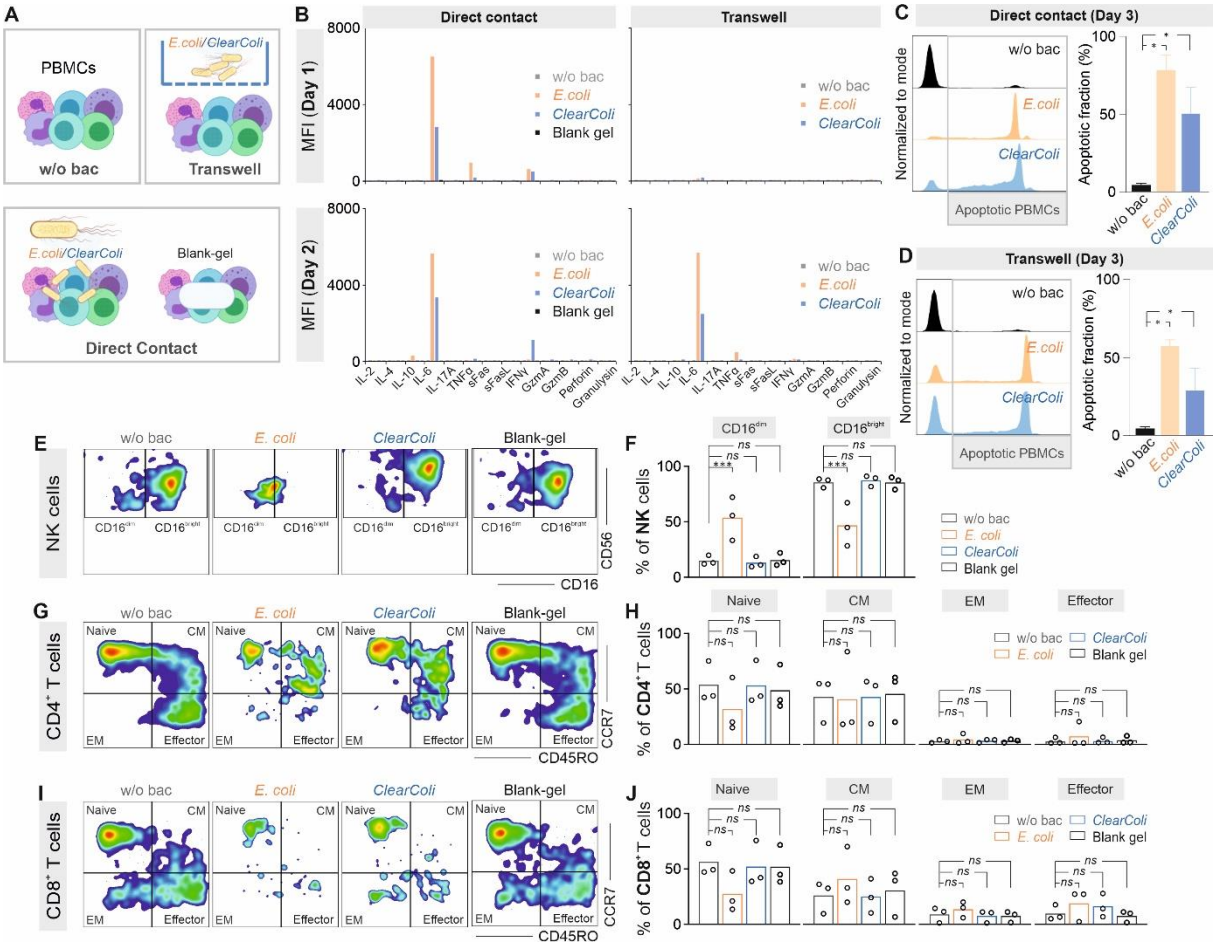

Figure 2: Immune response of PBMCs exposed to bacteria. A) Schematic for the different conditions tested: PBMCs cultured without bacteria (w/o bac), with bacteria or blank gels in the same well (Direct Contact), or with bacteria in a transwell, where PBMCs and bacteria are separated by a porous membrane that precludes direct contact (Transwell). **B)** Profiles of cytokines and cytotoxic proteins released by PBMCs determined by the multiplex cytokine assay. PBMCs were cultured as indicated in the figure. The supernatant was collected at the indicated time points. **C-D)** Viability of PBMCs on day 3 after direct contact with bacteria (**C**) or exposed to the soluble factors in a transwell (**D**). On day 3, PBMCs were stained with propidium iodide and the propidium iodide positive cells (gated in the frame) were considered

as apoptotic/dead cells. **E-J**) Differentiation of NK cells, $CD4^+$ T cells and $CD8^+$ T cells. PBMCs were stained with CD3/CD16/CD56 for NK cells (**E, F**), CD3/CD8/CD45RO/CCR7 for T cells (**G-J**). The CD3 negative (CD3-) population was gated for NK analysis. The CD3+CD8- population was gated for $CD4^+$ T cells, and the CD3+CD8+ population for $CD8^+$ T cells. Density plots are shown with pseudocolors to denote areas of high (red, orange), mid-range (yellow), and low (green, blue) population density. CM: central memory cells. EM: effector memory cells. All quantifications were from three donors and one representative donor is shown for plots.

The cytokines IL-2 [46, 47], IL-4 [48], IL10 [49], IL-6 [50-52], IL-17A [53], TNFα [54] and IFNγ [55] were selected for the panel as they play essential roles in both innate and adaptive immune response against infection. In addition, cytotoxic proteins (sFas, sFasL, GzmA, GzmB, perforin and granulysin) were included in the panel to access reaction of immune killer cells, mainly NK cells and CTLs, to bacteria-encapsulated hydrogels. When PBMCs were in direct contact with *E. coli*, IL-6 was predominantly released. TNFα and IFNγ were also detectable but at much lower levels (**Figure 2B**, left panel). *ClearColi* elicited release of the same cytokines, but at half the level of *E. coli* (**Figure 2B**, left panel). In comparison, concerning empty gel-induced release of cytokine or cytotoxic proteins, the levels were comparable to those of PBMCs controls and negligible compared to PBMCs in direct contact with *E. coli* or *ClearColi* (**Figure 2B**, left panel). When bacteria and PBMCs were separated by the transwell membrane with 400 nm pores, IL-6 release was triggered from day 2 onwards, which is one day later compared to the direct contact condition (**Figure 2B**). This result indicates that soluble factors from the bacteria, and not only direct contact, can trigger cytokine release. In the transwell condition, IL-6 release for *ClearColi* was 2-fold lowerthan for *E. coli* (**Figure 2B**, right panel). These results confirm that the lack of endotoxic LPS in *ClearColi* reduces immunogenicity, no matter if there is direct contact between bacteria and host or not.

Immune cells, especially NK cells, $CD4^+$ T cells and $CD8^+$ T cells, can differentiate into functionally different subsets upon activation. Thus, we also analyzed differentiation of these cells in response to the blank hydrogels on day 3. It should be noted that concerning the cytotoxicity of bacteria, more than half of PBMCs were apoptotic both in the direct bacterial contact (**Figure 2C**) and in transwell-separated (**Figure 2D**) cases, as identified by propidium iodide positive population. In comparison, for the controls, i.e. no bacteria present, the apoptotic fractions were lower than 3% in both cases (**Figure 2C, D**). In the remaining viable

PBMCs, NK cells were polarized to the more cytolytic $CD16^{dim}$ subset by *E. coli* but not by *ClearColi* or blank gels (**Figure 2E, F**). In terms of $CD4^+$ and $CD8^+$ T cells, four subsets were examined: naive ($CD45RO^-CCR7^+$), central memory ($CD45RO^+CCR7^+$), effector memory ($CD45RO^+CCR7^-$) and effector ($CD45RO^-CCR7^-$) cells. The effector memory and the effector sub-sets are ready to execute effector functions, whereas the naive and the central memory (CM) sub-sets are not fully activated. In the flow cytometry analysis, no change in differentiation of $CD4^+$ and $CD8^+$ T cells was detected (**Figures 2G-J**), although due to bacteria-induced apoptosis, the number of detected events was reduced as shown by the shrunk sizes of subsets compared to the condition without bacteria (**Figures 2G, I**). Taken together, these results indicate that the thin-film blank hydrogel construct is inert to immune cells *in vitro* and, therefore, Pluronic hydrogels are a reasonable material choice for the development of LTMs.

Characterization of immune responses to encapsulated E. coli and ClearColi hydrogels

We analyzed the response elicited by the bacterial thin-film hydrogels. PBMCs were co-cultured with the bacterial gels for 3 days and the cytotoxicity of the gels was examined with viability of PBMCs. In the case of *E. coli* hydrogels, 25 – 50% of the immune cells were found to be apoptotic on day 3, whereas for *ClearColi*-gels, the apoptotic fraction (i.e. the propidium iodide positive population) was only 5% (**Figure 3A**). In other words, immune cells in contact with *ClearColi*, encapsulated bacteria in Pluronic hydrogel retain viability at > 90% levels. This is a significantly higher viability than in the experiments where *ClearColi* were in direct contact or physically separated from the host cells through a porous membrane (<40 %).

Next, the release of cytokines or cytotoxic proteins on days 1, 2 and 3 post co-incubation of PBMCs and gels (corresponding to days 4, 5, 6 after bac-gel fabrication) was analyzed. Out of the 13 examined cytokines/cytotoxic proteins, mainly IL-6, IFNγ and GzmB were detected in the medium. In *E. coli* gels, the release of IL-6 peaked on day 2 (Donor #1 and Donor #2) or day 1 (Donor #3) and reduced afterwards, whereas in *ClearColi* gels, peak days for IL-6 release vary among donors (day 3 for Donor #1, day 2 for Donor #2, day 1 for Donor #3) (**Figure 3B**). The peak level of released IL-6 was comparable (Donor #1) or lower (Donor #2 and Donor #3) in *ClearColi*- than in *E. coli*-gels (**Figure 3B**). Release of IFNγ in *ClearColi*-gels was detectable from day 1, which was not always the case for GzmB (**Figure 3B**). The peak levels of IFNγ or GzmB were comparable between *E. coli*- and *ClearColi*-gels (**Figure 3B**). Considering that the number of viable immune cells in contact with *ClearColi*-gels was 1.5-2 fold higher than that

with *E. coli*-gels, these results indicate that the release of inflammatory cytokines induced by the *ClearColi*-gels is considerably lower compared to *E. coli*-gels.

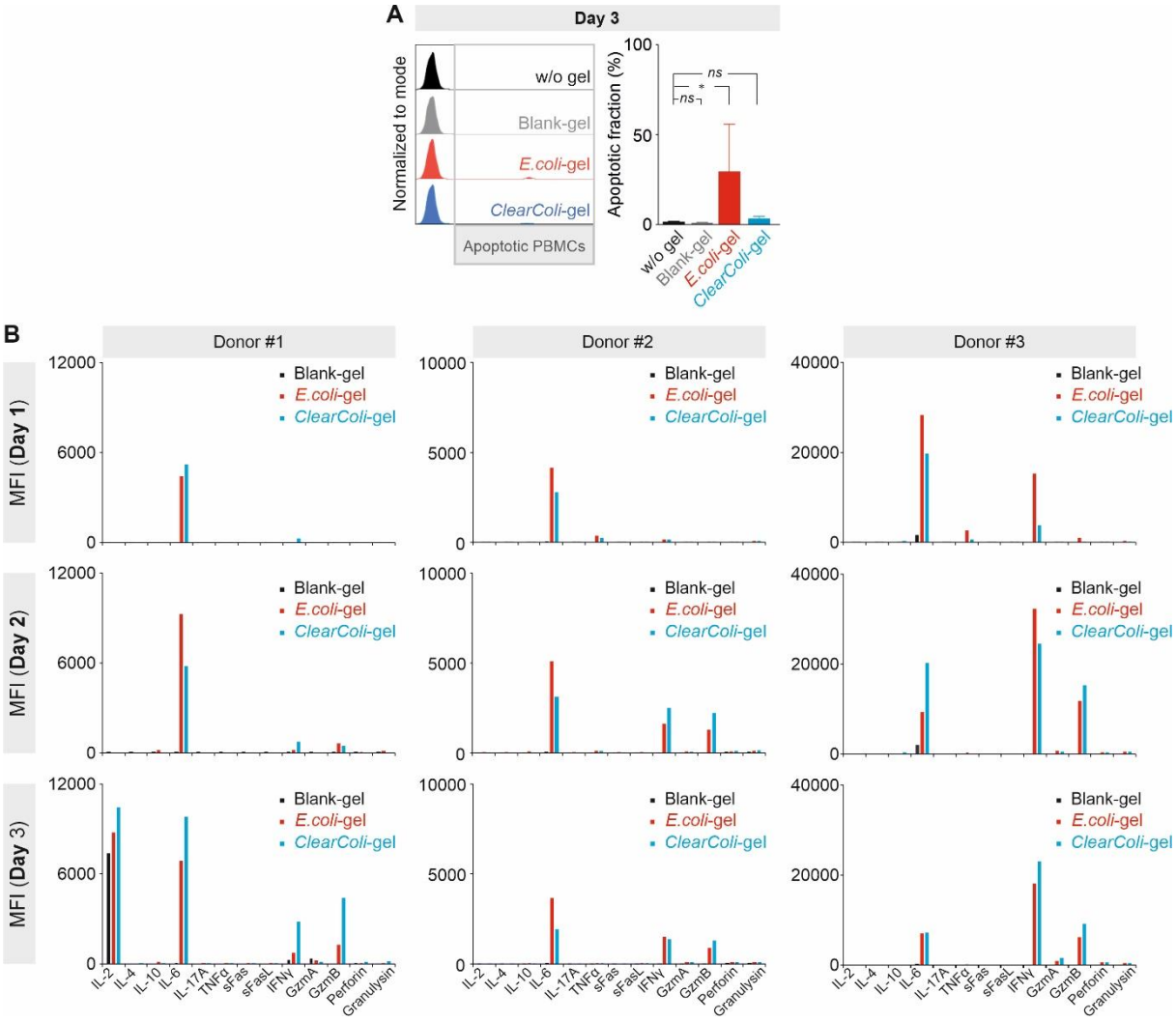

Figure 3: Profiles of cytokines and cytotoxic proteins in response to bacteria encapsulated hydrogels. PBMCs were cultured with empty hydrogels (Blank-gel), *E.coli*-encapsulated (*E.coli*-gel) or *ClearColi*-encapsulated gels (*ClearColi*-gel). **A)** Viability of PBMCs on day 3. PBMCs cultured alone (w/o gel) were used to access spontaneous apoptosis. On day 3, PBMCs were stained with propidium iodide and the propidium iodide positive cells (gated in the frame) were considered as apoptotic/dead cells. **B)** Profiles of cytokines and cytotoxic proteins released by PBMCs were determined by the multiplex cytokine assay. The supernatant was collected at the indicated time points. Results were from three donors. MFI: mean fluoresce intensity. Results were from three donors.

The NK or T cell subsets on day 3 were analyzed via flow cytometry. No significant difference in the differentiation of NK cells, CD4$^+$ T cells and CD8$^+$ T cells was observed in *E. coli*- or *ClearColi*-gels compared to blank hydrogels (**Figure 4**). Considering that NK cells are polarized to the more cytolytic CD16^{dim} subset by direct contact with *E. coli* (**Figures 2E, F**) and that high apoptosis of PBMCs (>50%) is induced by direct contact with bacteria (**Figures 2C**), these findings indicate that physical separation of *ClearColi* or *E. coli* from immune cells by encapsulation in Pluronic hydrogels significantly reduces activation and changes in the differentiation of NK cells or T cells and, therefore, in the overall immune response.

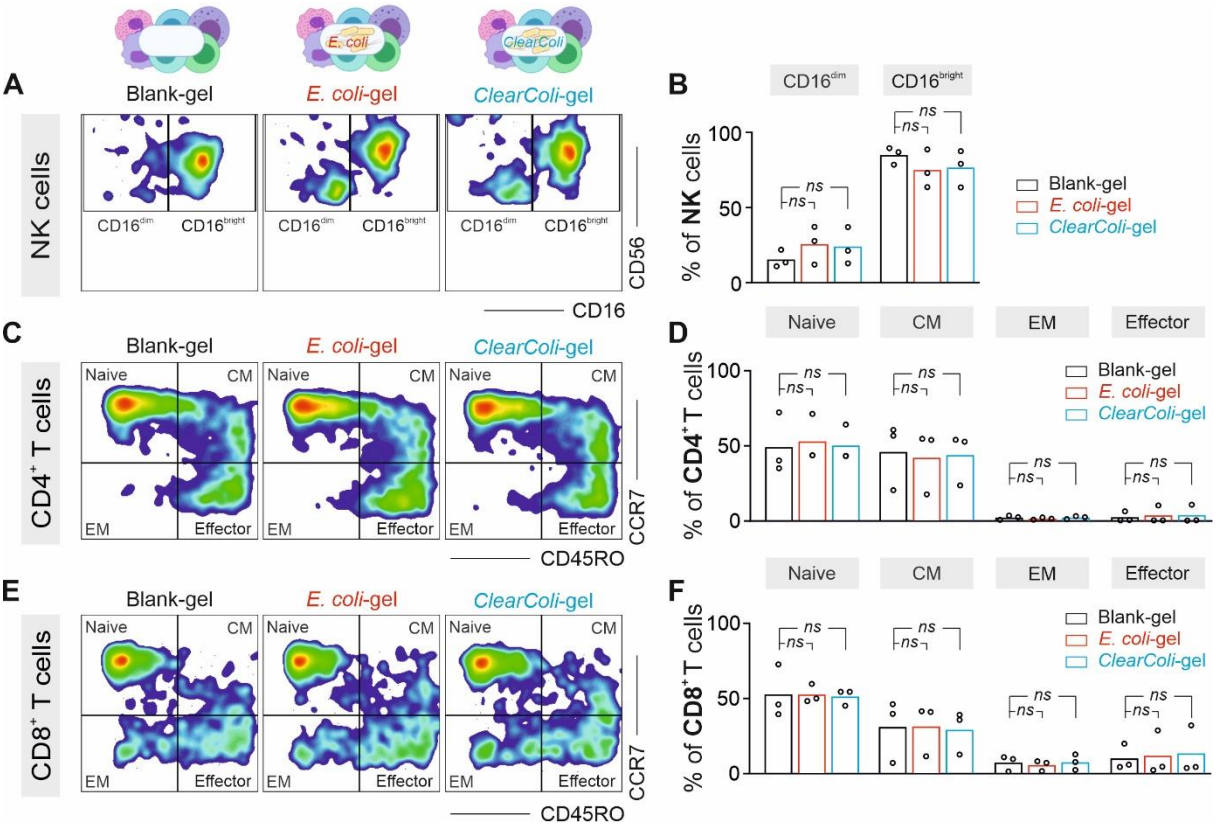

Figure 4: Differentiation of NK and T cells in response to bacteria encapsulated hydrogels. PBMCs were cultured with empty hydrogels (Blank-gel), *E.coli*-encapsulated (*E.coli*-gel) or *ClearColi*-encapsulated gels (*ClearColi*-gel). Differentiation of NK cells (**A, B**), CD4$^+$ T cells (**C, D**) and CD8$^+$ T cells (**E, F**) were examined using indicated surface markers. Results were from three donors. CM: central memory cells. EM: effector memory cells.

Strong IFNγ release is induced in PBMCs from pre-activated donors

During the analysis, we noticed that out of six donors, PBMCs from three donors showed high spontaneous IL-2 release in the negative control (no hydrogel or bacteria) right from day 1 (Supplementary information **Figure S5**). Since IL-2 is mainly produced by activated T cells,

especially $CD4^+$ T helper cells, immune cells in these donors were very likely in a pro-inflammatory status (termed pro-inflammatory donors henceforth). For these donors, direct contact of PBMCs with bacteria induced large IFNγ release, with variable peak time among donors, and with similar peak levels for *E. coli* and *ClearColi* hydrogels (Supplementary information **Figure S6A**). IFNγ release was 3-30 times higher than in normal PBMCs (Supplementary information **Figure 6B**), whereas IL-6 release stayed in a comparable range (**Figure 6C**). GzmA was released in large quantities (Supplementary information **Figure 6A**) and about 10-200 fold higher than normal donors (Supplementary information **Figure 6D**). In the control experiments with non-encapsulated bacteria strong cytokine release was also observed (Supplementary information **Figure S7**).

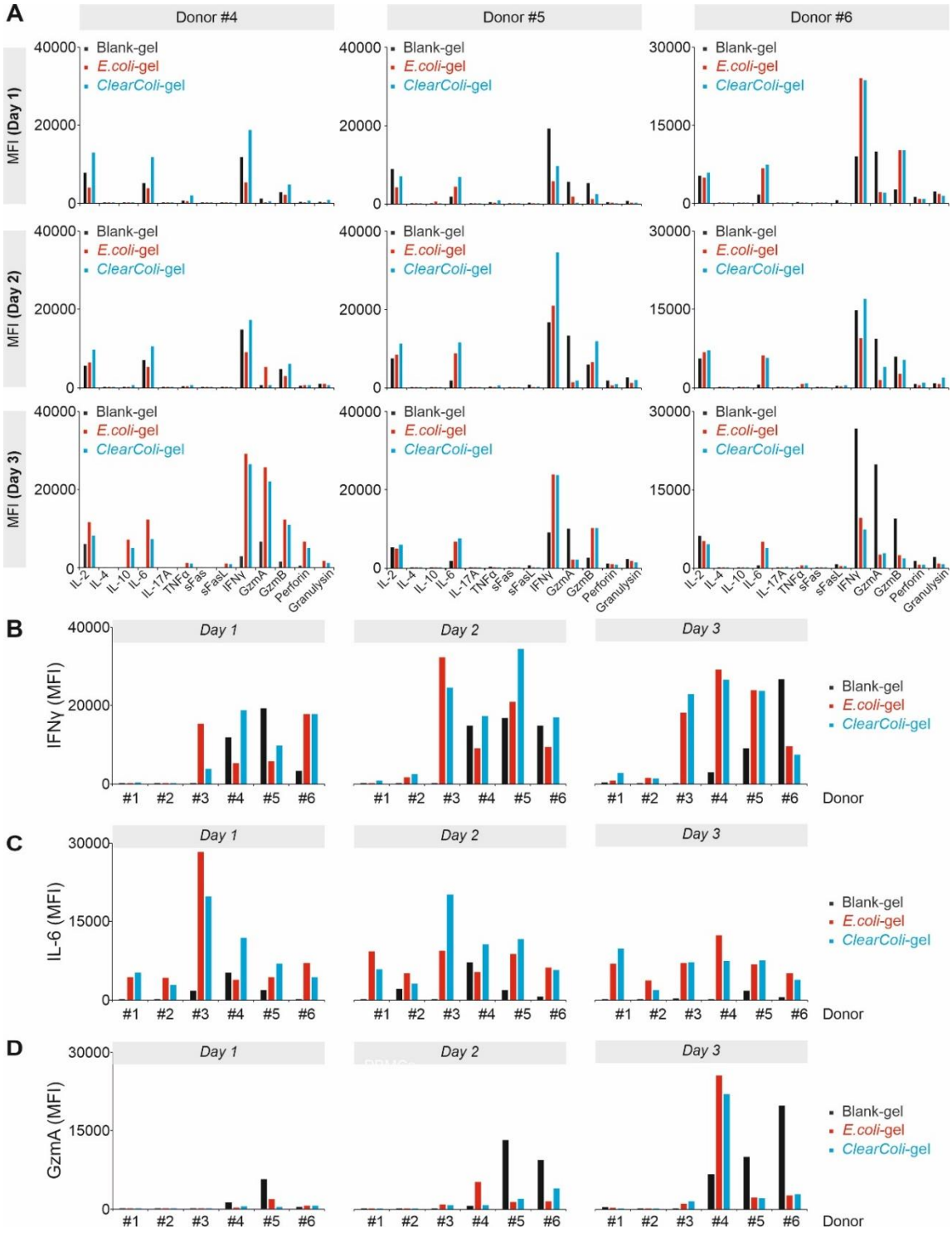

Figure 5: Profiles of cytokines and cytotoxic proteins from donors with high spontaneous IL-2 release in response to bacteria encapsulated hydrogels. A) Profiles of cytokines and cytotoxic proteins released by PBMCs were determined by the multiplex cytokine assay. PBMCs with high spontaneous IL-2 release were cultured with empty hydrogels (Blank-gel), *E.coli*-encapsulated (*E.coli*-gel) or *ClearColi*-encapsulated gels (*ClearColi*-gel). The supernatant was collected at the indicated time points. Results were from three donors, which are the same donors in Fig. 7. MFI: mean fluoresce intensity. **B-D)** Comparison of released cytokines

between donors with low (Donors #1-3) and high (Donors #4-6) spontaneous IL-2 release. IFNγ, IL-6 and granzyme A (GzmA) are shown in **B**, **C** and **D**.

In contact with bacterial gels, PBMCs from pro-inflammatory donors showed prominent release of IFNγ, IL-6, GzmA, GzmB, perforin, and granulysin (**Figure 5A**). Among those, IFNγ was 5-20 fold higher than in normal donors (Donors #1 and #2, **Figure 5B**). In comparison, levels of IL-6 were similar as the case of normal donors (**Figure 5C**). GzmA release was about 20-200 fold higher than normal donors (**Figure 5A, D**). Release of GzmB, perforin and granulysin were elicited in a considerably low level compared to IFNγ (**Figure 5A**). Remarkably, for pro-inflammatory donors, even blank Pluronic gels elicited significant release of cytokines (e.g. IL-6 and IFNγ) and cytotoxic proteins (e.g. GzmA, GzmB, perforin and granulysin) from PBMCs (**Figure 6**). These results indicate that in pro-inflammatory donors featured with high spontaneous release of IL-2, *E. coli* and *ClearColi* LTMs could trigger considerable immune reactions.

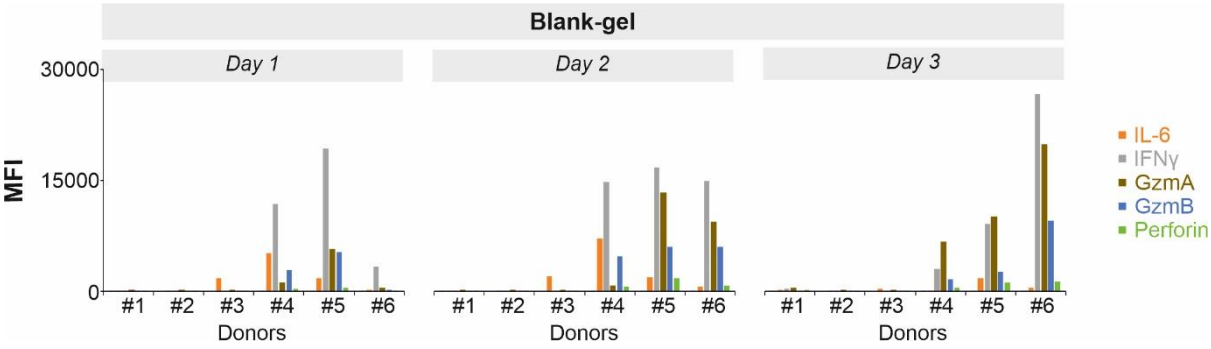

Figure 6: Comparison of cytokine profiles between donors with low or high spontaneous IL-2 release in response to empty hydrogels. PBMCs from Donors #1-3 were featured with low spontaneous IL-2 release, those from Donors #4-6) with high spontaneous IL-2 release. PBMCs were cultured with empty hydrogels (Blank-gel). The supernatant was collected at the indicated time points.IL-6, IFNγ, granzyme A (GzmA), granzyme B (GzmB), and perforin are shown. Data were extracted from Fig. 3B and Fig. 5A.

Discussion

In this work, we have studied the response of immune cells to LTMs made of the most common LTM bacteria, *E. coli,* and a synthetic, biocompatible, non-degradable polymer, Pluronic F127 diacrylate. The LTMs were designed with a Plu/PluDA core hydrogel containing the bacteria, enveloped in a thin PluDA hydrogel with higher crosslinking that prevents bacterial escape. The hydrogel envelope prevents physical contact between the bacteria and the immune cells in the culture. The novelty of our study lies in the development of a strategy to reliably assess possible immune responses to this new class of materials using patient-derived immune cells that can be adapted by others. Accordingly, the findings from this study provide a benchmark for the characterization of living therapeutic materials currently under development in the community.

Our results show that both empty hydrogels and *ClearColi*-encapsulated gels have no impact on differentiation of NK and T cells. Concerning cytokine release, for normal cases, empty hydrogels per se do not release of any cytokine or cytotoxic proteins, whereas *ClearColi*-encapsulated gels induce marginal/moderate release of limited number of cytokines/cytotoxic proteins (mainly IL-6, IFN-γ, and granzyme B). In comparison, for proinflammatory immune cells featuring with high spontaneous release of IL-2, high amounts of IL-6, IFN-γ, IL-10 and cytotoxic proteins (granzyme A, granzyme B and perforin) are secreted after being in contact with empty PluDA hydrogels and *ClearColi*-encapsulated gels.

Endotoxic LPS from Gram-negative bacteria, including *E. coli*, can elicit strong immune responses [56]. The *ClearColi,* with no LPS, has been shown not to trigger NFκB activity [37, 57]. In this work, we found that *ClearColi*- encapsulated hydrogels did not induced any changes in differentiation of NK cells and T cells, but elicited some release of the pro-inflammatory cytokines IL-6 and IFNγ from normal PBMCs. In this case, the levels of IL-6 and IFNγ are in a comparable range as the empty hydrogel-induced release in pro-inflammatory PBMCs. As empty Pluronic gels is shown/proven clinically safe, these levels of IL-6 and IFNγ can be considered as response from a normal 'foreign body reaction' [58, 59].

Of note, this *in vitro* study portrays an extreme case with high numbers (3 million) of immune cells in contact with the bacterial gels from the start. The bacterial density within the gels is estimated to be in the range of 10^9 – 10^{10} cfu/mL, which is equivalent to a bacterial culture at saturation levels of growth and the range in which probiotic formulations are made (e.g.

Mutaflor containing *E. coli* Nissle 1917 at 2.5–25 x 10^9 cfu/mL). Although the numbers of immune cells recruited to sites of inflammation or wounds have not been explicitly quantified, from the reported *in vivo* studies [60-62], we estimate the numbers are in the range of a few thousand to a few hundred of thousand. Thus, the measured response is very likely to be amplified/exaggerated compared to *in vivo* scenarios. Therefore, we conclude that *ClearColi*-encapsulating hydrogels do not elicit severe adverse events and are suitable for further *in vivo* studies.

It should be noted that in transwell inserts, i.e. within the culture medium, bacteria can freely grow during culture time and the resulting bacteria density to which cells are exposed might be orders of magnitude larger than bacteria number physically constrained within the hydrogels. Based on our previous study, the bacteria within the gels can grow to colony sizes with a conservative mean volume of 250 μm^3 [38] corresponding to ~400 cells (*E. coli* volume ~0.6 μm^3). Thus, in the 2 µL of the bacterial gel, the bacterial numbers starting from 8×10^3 cells are expected to reach between 10^6-10^7 cells. In the transwell inserts, at saturation levels of growth (OD 2 – 5) that are expected to be reached before day 3 in the 100 µL volume, the bacterial numbers are expected to reach between 10^8 – 10^9 cells. In direct contact with the PBMCs, a similar range can be expected although variations can occur due to killing of the bacteria by the immune cells. Additionally, since the colonies have already been allowed to form before initiation of the experiments with PBMCs, it is likely that growth, metabolic activity and death of the bacteria within these colonies will be occurring at a considerably diminished rate compared to those growing freely in medium. The differences in the immune responses observed in our data could be influenced by these additional factors to some extent.

Our results with PMBCs from pro-inflammatory donors indicate that LTMs might induce an elevated inflammatory reaction at the implantation site compared to donors with the immune system at a quiescent status. Considering the time of sample collection (between October and December 2020, a high season for seasonal flu and normal cold overlapped with the second wave of COVID-19 in Germany) the probability that some donors got infection a few weeks before the donation but were symptom-free at the time of donation was high. In this case, it is possible that the immune system could not have retracted to a quiescent status yet. The substantial difference between donors with low or high spontaneous IL-2 release highlights

the necessity to perform detailed studies of the immune response to LTMs, including individuals with different immune status. Depending on the clinical conditions of individual patients with a pro-inflammatory status, systemic or local anti-inflammation strategies should be applied to minimize adverse effects. A wide choice of non-steroidal anti-inflammatory drugs can be administered systemically to dampen inflammatory responses. Furthermore, for local inflammation, implementation of inflammation-controlling features [63] in LTMs, such as a temporal release of anti-inflammatory compounds from the material or the bacteria, could benefit recipients with a pro-inflammatory status.

Conflict of Interest

The authors declare that the research was conducted in the absence of any commercial or financial relationships that could be construed as a potential conflict of interest.

Author Contributions

AKY performed PBMC-related experiments and the corresponding analysis if not mentioned otherwise; SB prepared hydrogels, bacteria and bacteria-encapsulated hydrogels and carried out quality check; AdC helped with data interpretation and provided critical feedback on all aspects of the project; SS and BQ generated concepts; SS and SB designed hydrogel-related experiments and BQ designed PBMC-related experiments; All authors contributed to the writing, editing and cross-checking of the manuscript.

Acknowledgments

We thank the Institute for Clinical Hemostaseology and Transfusion Medicine for providing donor blood; Markus Bischoff and Philipp Jung for the bacteria culture facility, Carmen Hässig, Cora Hoxha, and Gertrud Schäfer for excellent technical help; Markus Hoth for inspiring discussion and continuous support. This project was funded by the Deutsche Forschungsgemeinschaft (SFB 1027 Project A2 to BQ, B6 to AdC, B8 to SS and GZ: INST 256/419-1 FUGG) and the Leibniz Science Campus on Living Therapeutic Materials, LifeMat.

Ethical considerations

Research carried out for this study with material from healthy donors (leukocyte reduction system chambers from human blood donors) is authorized by the local ethic committee Ethik-Kommission bei der Ärztekammer des Saarlandes (Identification Nr. 84/15, Prof. Dr. Rettig-Stürmer).

References

[1] A. Rodrigo-Navarro, S. Sankaran, M.J. Dalby, A. del Campo, M. Salmeron-Sanchez, Engineered living biomaterials, Nat Rev Mater 6(12) (2021) 1175-1190.

[2] L.R. Shang, C.M. Shao, J.J. Chi, Y.J. Zhao, Living Materials for Life Healthcare, Accounts Mater Res 2(1) (2021) 59-70.

[3] S. Sankaran, A. del Campo, Optoregulated Protein Release from an Engineered Living Material, Adv Biosyst 3(2) (2019).

[4] S. Sankaran, J. Becker, C. Wittmann, A. del Campo, Optoregulated Drug Release from an Engineered Living Material: Self-Replenishing Drug Depots for Long-Term, Light-Regulated Delivery, Small 15(5) (2019).

[5] L.M. Gonzalez, N. Mukhitov, C.A. Voigt, Resilient living materials built by printing bacterial spores, Nat Chem Biol 16(2) (2020) 126-+.

[6] K. Witte, A. Rodrigo-Navarro, M. Salmeron-Sanchez, Bacteria-laden microgels as autonomous three-dimensional environments for stem cell engineering, Mater Today Bio 2 (2019).

[7] X.Y. Liu, H. Yuk, S.T. Lin, G.A. Parada, T.C. Tang, E. Tham, C. de la Fuente-Nunez, T.K. Lu, X.H. Zhao, 3D Printing of Living Responsive Materials and Devices, Advanced Materials 30(4) (2018).

[8] M. Lufton, O. Bustan, B.H. Eylon, E. Shtifman-Segal, T. Croitoru-Sadger, A. Shagan, A. Shabtay-Orbach, E. Corem-Salkmon, J. Berman, A. Nyska, B. Mizrahi, Living Bacteria in Thermoresponsive Gel for Treating Fungal Infections, Adv Funct Mater 28(40) (2018).

[9] T.G. Johnston, S.F. Yuan, J.M. Wagner, X.N. Yi, A. Saha, P. Smith, A. Nelson, H.S. Alper, Compartmentalized microbes and co-cultures in hydrogels for on-demand bioproduction and preservation, Nat Commun 11(1) (2020).

[10] S. Franz, S. Rammelt, D. Scharnweber, J.C. Simon, Immune responses to implants - a review of the implications for the design of immunomodulatory biomaterials, Biomaterials 32(28) (2011) 6692-709.

[11] A. Carnicer-Lombarte, S.T. Chen, G.G. Malliaras, D.G. Barone, Foreign Body Reaction to Implanted Biomaterials and Its Impact in Nerve Neuroprosthetics, Front Bioeng Biotechnol 9 (2021) 622524.

[12] E. Mariani, G. Lisignoli, R.M. Borzi, L. Pulsatelli, Biomaterials: Foreign Bodies or Tuners for the Immune Response?, Int J Mol Sci 20(3) (2019).

[13] A. Ashimova, S. Yegorov, B. Negmetzhanov, G. Hortelano, Cell Encapsulation Within Alginate Microcapsules: Immunological Challenges and Outlook, Front Bioeng Biotechnol 7 (2019) 380.

[14] A. Lathuiliere, N. Mach, B.L. Schneider, Encapsulated cellular implants for recombinant protein delivery and therapeutic modulation of the immune system, Int J Mol Sci 16(5) (2015) 10578-600.

[15] A. Cubillos-Ruiz, T. Guo, A. Sokolovska, P.F. Miller, J.J. Collins, T.K. Lu, J.M. Lora, Engineering living therapeutics with synthetic biology, Nat Rev Drug Discov 20(12) (2021) 941-960.

[16] A. Maxmen, Living therapeutics: Scientists genetically modify bacteria to deliver drugs, Nat Med 23(1) (2017) 5-7.

[17] A.K. Guttsches, S. Loseke, U. Zahringer, U. Sonnenborn, C. Enders, S. Gatermann, A. Bufe, Anti-inflammatory modulation of immune response by probiotic Escherichia coli Nissle 1917 in human blood mononuclear cells, Innate Immun 18(2) (2012) 204-16.

[18] X. Yu, C. Lin, J. Yu, Q. Qi, Q. Wang, Bioengineered Escherichia coli Nissle 1917 for tumour-targeting therapy, Microb Biotechnol 13(3) (2020) 629-636.

[19] D.S. Leventhal, A. Sokolovska, N. Li, C. Plescia, S.A. Kolodziej, C.W. Gallant, R. Christmas, J.R. Gao, M.J. James, A. Abin-Fuentes, M. Momin, C. Bergeron, A. Fisher, P.F. Miller, K.A. West, J.M. Lora, Immunotherapy with engineered bacteria by targeting the STING pathway for anti-tumor immunity, Nat Commun 11(1) (2020) 2739.

[20] T. Harimoto, J. Hahn, Y.Y. Chen, J. Im, J. Zhang, N. Hou, F. Li, C. Coker, K. Gray, N. Harr, S. Chowdhury, K. Pu, C. Nimura, N. Arpaia, K.W. Leong, T. Danino, A programmable encapsulation system improves delivery of therapeutic bacteria in mice, Nat Biotechnol 40(8) (2022) 1259-1269.

[21] A.B. Shori, Microencapsulation Improved Probiotics Survival During Gastric Transit, HAYATI Journal of Biosciences 24(1) (2017) 1-5.

[22] F. Wei, S. Liu, M. Chen, G. Tian, K. Zha, Z. Yang, S. Jiang, M. Li, X. Sui, Z. Chen, Q. Guo, Host Response to Biomaterials for Cartilage Tissue Engineering: Key to Remodeling, Front Bioeng Biotechnol 9 (2021) 664592.

[23] Z. Sahbudak Bal, N. Karadas Ozdemir, S. Sen, D. Yilmaz Karapinar, E. Azarsiz, S. Aydemir, F. Vardar, Diagnostic Accuracy of Interleukin-6, Interleukin-8, and Interleukin-10 for Predicting Bacteremia in Children with Febrile Neutropenia, Turk J Haematol 34(3) (2017) 254-257.

[24] Q. Zhu, H. Li, S. Zheng, B. Wang, M. Li, W. Zeng, L. Zhou, Z. Guan, H. Wang, Y. Liu, Y. Gao, S. Qiu, C. Chen, S. Yang, Y. Yuan, H. Zhang, G. Ruan, X. Pan, IL-6 and IL-10 Are Associated With Gram-Negative and Gram-Positive Bacteria Infection in Lymphoma, Front Immunol 13 (2022) 856039.

[25] E.M. Rincon-Lopez, M.L. Navarro Gomez, T. Hernandez-Sampelayo Matos, D. Aguilera-Alonso, E. Duenas Moreno, J. Saavedra-Lozano, B. Santiago Garcia, M.D.M. Santos Sebastian, M. Garcia Morin, C. Belendez Bieler, J. Lorente Romero, E. Cela de Julian, F.D.S. Group, Interleukin 6 as a marker of severe bacterial infection in children with sickle cell disease and fever: a case-control study, BMC Infect Dis 21(1) (2021) 741.

[26] Y.V. Cavalcanti, M.C. Brelaz, J.K. Neves, J.C. Ferraz, V.R. Pereira, Role of TNF-Alpha, IFN-Gamma, and IL-10 in the Development of Pulmonary Tuberculosis, Pulm Med 2012 (2012) 745483.

[27] G.M. Boxx, G. Cheng, The Roles of Type I Interferon in Bacterial Infection, Cell Host Microbe 19(6) (2016) 760-9.

[28] A. Zganiacz, M. Santosuosso, J. Wang, T. Yang, L. Chen, M. Anzulovic, S. Alexander, B. Gicquel, Y. Wan, J. Bramson, M. Inman, Z. Xing, TNF-alpha is a critical negative regulator of type 1 immune activation during intracellular bacterial infection, J Clin Invest 113(3) (2004) 401-13.

[29] M.M. Curtis, S.S. Way, Interleukin-17 in host defence against bacterial, mycobacterial and fungal pathogens, Immunology 126(2) (2009) 177-85.

[30] M. Walch, F. Dotiwala, S. Mulik, J. Thiery, T. Kirchhausen, C. Clayberger, A.M. Krensky, D. Martinvalet, J. Lieberman, Cytotoxic cells kill intracellular bacteria through granulysin-mediated delivery of granzymes, Cell 157(6) (2014) 1309-1323.

[31] D.L. Leon, I. Fellay, P.Y. Mantel, M. Walch, Killing Bacteria with Cytotoxic Effector Proteins of Human Killer Immune Cells: Granzymes, Granulysin, and Perforin, Methods Mol Biol 1535 (2017) 275-284.

[32] D.H. Dockrell, The multiple roles of Fas ligand in the pathogenesis of infectious diseases, Clin Microbiol Infect 9(8) (2003) 766-79.

[33] A.M. Abel, C. Yang, M.S. Thakar, S. Malarkannan, Natural Killer Cells: Development, Maturation, and Clinical Utilization, Front Immunol 9 (2018) 1869.

[34] F.R. Shepherd, J.E. McLaren, T Cell Immunity to Bacterial Pathogens: Mechanisms of Immune Control and Bacterial Evasion, Int J Mol Sci 21(17) (2020).

[35] Y. Shachaf, M. Gonen-Wadmany, D. Seliktar, The biocompatibility of Pluronic (R) F127 fibrinogen-based hydrogels, Biomaterials 31(10) (2010) 2836-2847.

[36] R. Suntornnond, E.Y.S. Tan, J. An, C.K. Chua, A highly printable and biocompatible hydrogel composite for direct printing of soft and perfusable vasculature-like structures, Sci Rep-Uk 7 (2017).

[37] U. Mamat, K. Wilke, D. Bramhill, A.B. Schromm, B. Lindner, T.A. Kohl, J.L. Corchero, A. Villaverde, L. Schaffer, S.R. Head, C. Souvignier, T.C. Meredith, R.W. Woodard, Detoxifying Escherichia coli for endotoxin-free production of recombinant proteins, Microb Cell Fact 14 (2015) 57.

[38] S. Bhusari, S. Sankaran, A. Del Campo, Regulating Bacterial Behavior within Hydrogels of Tunable Viscoelasticity, Adv Sci (Weinh) (2022) e2106026.

[39] M. Di Biase, P. de Leonardis, V. Castelletto, I.W. Hamley, B. Derby, N. Tirelli, Photopolymerization of Pluronic F127 diacrylate: a colloid-templated polymerization, Soft Matter 7(10) (2011) 4928-4937.

[40] S. Bhusari, J. Kim, K. Polizzi, S. Sankaran, A. Del Campo, Encapsulation of bacteria in bilayer Pluronic thin film hydrogels: a safe format for engineered living materials, bioRxiv preprint doi: 10.1101/2022.09.29.510162 (2022).

[41] R. Mempin, H. Tran, C. Chen, H. Gong, K. Kim Ho, S. Lu, Release of extracellular ATP by bacteria during growth, BMC Microbiol 13 (2013) 301.

[42] J.B. Lee, J.J. Yoon, D.S. Lee, T.G. Park, Photo-crosslinkable, thermo-sensitive and biodegradable pluronic hydrogels for sustained release of protein, J Biomater Sci Polym Ed 15(12) (2004) 1571-83.

[43] S. You, D.H. Van Winkle, Single molecule observation of DNA electrophoresis in pluronic f127, J Phys Chem B 114(12) (2010) 4171-7.

[44] V. Pattu, B. Qu, E.C. Schwarz, B. Strauss, L. Weins, S.S. Bhat, M. Halimani, M. Marshall, J. Rettig, M. Hoth, SNARE protein expression and localization in human cytotoxic T lymphocytes, Eur J Immunol 42(2) (2012) 470-5.

[45] A. Knorck, S. Marx, K.S. Friedmann, S. Zophel, L. Lieblang, C. Hassig, I. Muller, J. Pilch, U. Sester, M. Hoth, H. Eichler, M. Sester, E.C. Schwarz, Quantity, quality, and functionality of peripheral blood cells derived from residual blood of different apheresis kits, Transfusion 58(6) (2018) 1516-1526.

[46] O. Boyman, J. Sprent, The role of interleukin-2 during homeostasis and activation of the immune system, Nat Rev Immunol 12(3) (2012) 180-90.

[47] Y. Wu, Z. Tian, H. Wei, Developmental and Functional Control of Natural Killer Cells by Cytokines, Front Immunol 8 (2017) 930.

[48] S.P. Gadani, J.C. Cronk, G.T. Norris, J. Kipnis, IL-4 in the brain: a cytokine to remember, J Immunol 189(9) (2012) 4213-9.

[49] K.N. Couper, D.G. Blount, E.M. Riley, IL-10: the master regulator of immunity to infection, J Immunol 180(9) (2008) 5771-7.

[50] T. Tanaka, M. Narazaki, T. Kishimoto, IL-6 in inflammation, immunity, and disease, Cold Spring Harb Perspect Biol 6(10) (2014) a016295.

[51] A. Santa Cruz, A. Mendes-Frias, A.I. Oliveira, L. Dias, A.R. Matos, A. Carvalho, C. Capela, J. Pedrosa, A.G. Castro, R. Silvestre, Interleukin-6 Is a Biomarker for the Development of Fatal Severe Acute Respiratory Syndrome Coronavirus 2 Pneumonia, Front Immunol 12 (2021) 613422.

[52] A. Shimabukuro-Vornhagen, P. Godel, M. Subklewe, H.J. Stemmler, H.A. Schlosser, M. Schlaak, M. Kochanek, B. Boll, M.S. von Bergwelt-Baildon, Cytokine release syndrome, J Immunother Cancer 6(1) (2018) 56.

[53] S. Xu, X. Cao, Interleukin-17 and its expanding biological functions, Cell Mol Immunol 7(3) (2010) 164-74.

[54] G.D. Kalliolias, L.B. Ivashkiv, TNF biology, pathogenic mechanisms and emerging therapeutic strategies, Nat Rev Rheumatol 12(1) (2016) 49-62.

[55] G. Kak, M. Raza, B.K. Tiwari, Interferon-gamma (IFN-gamma): Exploring its implications in infectious diseases, Biomol Concepts 9(1) (2018) 64-79.

[56] W. Schulte, J. Bernhagen, R. Bucala, Cytokines in sepsis: potent immunoregulators and potential therapeutic targets--an updated view, Mediators Inflamm 2013 (2013) 165974.

[57] U. Mamat, R.W. Woodard, K. Wilke, C. Souvignier, D. Mead, E. Steinmetz, K. Terry, C. Kovacich, A. Zegers, C. Knox, Endotoxin-free protein production—ClearColi™ technology, Nat Methods 10 (2013).

[58] T. Eigenbrod, A.H. Dalpke, Bacterial RNA: An Underestimated Stimulus for Innate Immune Responses, J Immunol 195(2) (2015) 411-8.

[59] N. Alphonse, R.E. Dickenson, C. Odendall, Interferons: Tug of War Between Bacteria and Their Host, Front Cell Infect Microbiol 11 (2021) 624094.

[60] H.C. Lee, J. Gaire, S.W. Currlin, M.D. McDermott, K. Park, K.J. Otto, Foreign Body Response to Intracortical Microelectrodes Is Not Altered with Dip-Coating of Polyethylene Glycol (PEG), Front Neurosci 11 (2017) 513.

[61] M. Burgess, K. Wicks, M. Gardasevic, K.A. Mace, Cx3CR1 Expression Identifies Distinct Macrophage Populations That Contribute Differentially to Inflammation and Repair, Immunohorizons 3(7) (2019) 262-273.

[62] C.E. Olingy, C.L. San Emeterio, M.E. Ogle, J.R. Krieger, A.C. Bruce, D.D. Pfau, B.T. Jordan, S.M. Peirce, E.A. Botchwey, Non-classical monocytes are biased progenitors of wound healing macrophages during soft tissue injury, Sci Rep 7(1) (2017) 447.

[63] Z. Tu, Y. Zhong, H. Hu, D. Shao, R. Haag, M. Schirner, J. Lee, B. Sullenger, K.W. Leong, Design of therapeutic biomaterials to control inflammation, Nat Rev Mater 7(7) (2022) 557-574.

Supplementary Information

In vitro evaluation of immune responses to bacterial hydrogels for the development of living therapeutic materials

Archana Yanamandra[1,2*], Shardul Bhusari[2,3*], Aránzazu del Campo[2,3], Shrikrishnan Sankaran[2#], Bin Qu[1,2#]

[1]Biophysics, Center for Integrative Physiology and Molecular Medicine (CIPMM), School of Medicine, Saarland University, Homburg, Germany

[2] INM - Leibniz Institute for New Materials, Saarbrücken, Germany

[3] Chemistry Department, Saarland University, 66123 Saarbrücken, Germany.

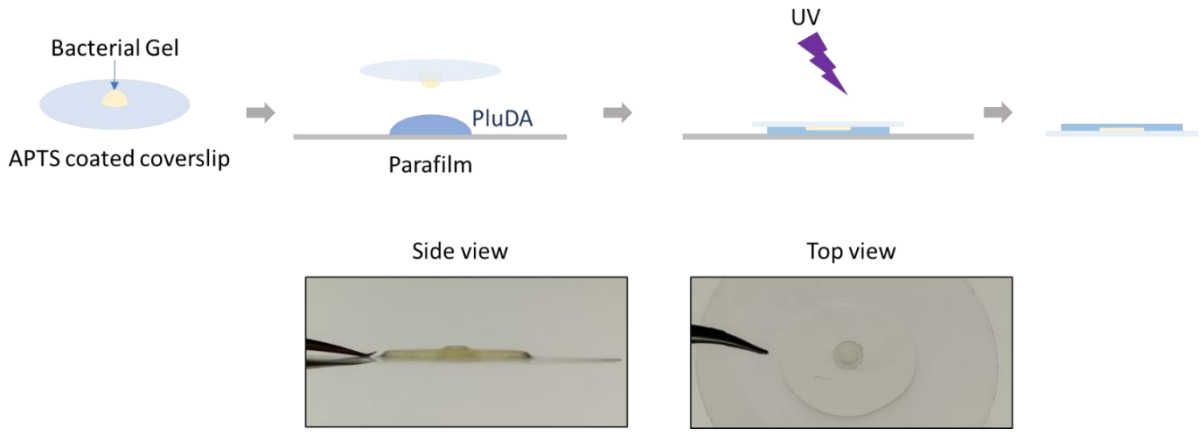

Figure S1: Schematic of the fabrication of a leak-proof thin-film bacterial hydrogel construct. The encapsulating gel, covalently crossliked to the APTS silanized glass coverslip upon UV irradiation, prevented the escape of bacteria from the bacterial gel upon contact with the surrounding medium.

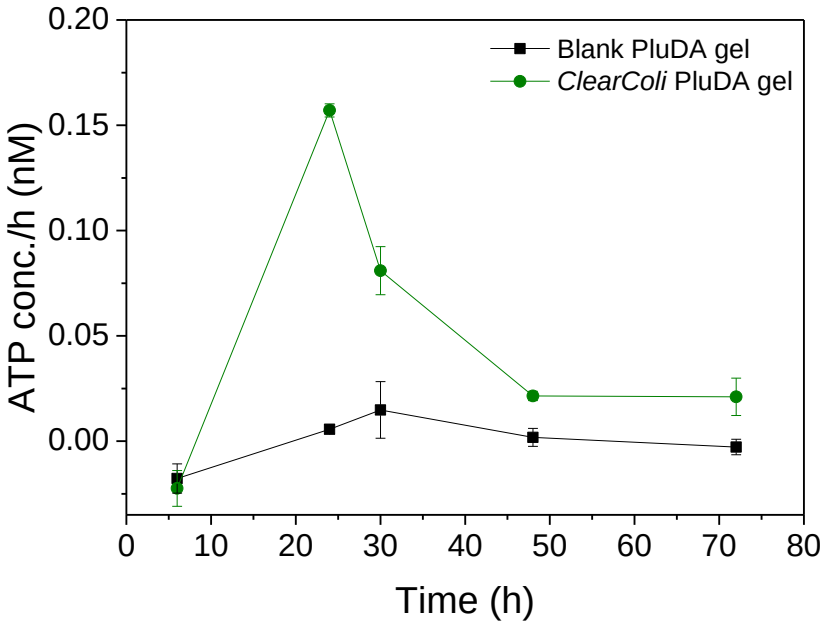

Figure S2: Extracellular ATP level changes in the surrounding medium. Samples were collected from the surrounding medium of Clearcoli bacteria encapsulated within the thinfilms at timepoints 6, 24, 30, 48 and 72 h, with blank (no bacteria) gels as a control. The concentration of the ATP was determined using a standard curve of ATP standard solution dilutions in culture medium. (n = 2, error bars represent standard deviation).

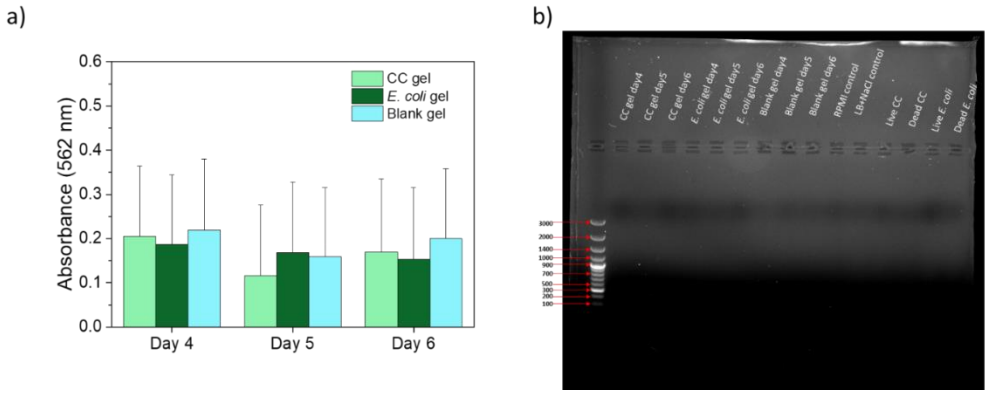

Figure S3: Protein and DNA release by the bacteria in encapsulated gels. A) The amount of protein released by the bacteria in the surrounding medium was measured using the BCA protein assay. The absorbance at 562 nm for the surrounding medium of the bacterial gels showed no significant difference compared to the blank gels; **B)** Agarose gels showing no indication DNA fragments released by the bacterial gels to the surrounding medium.

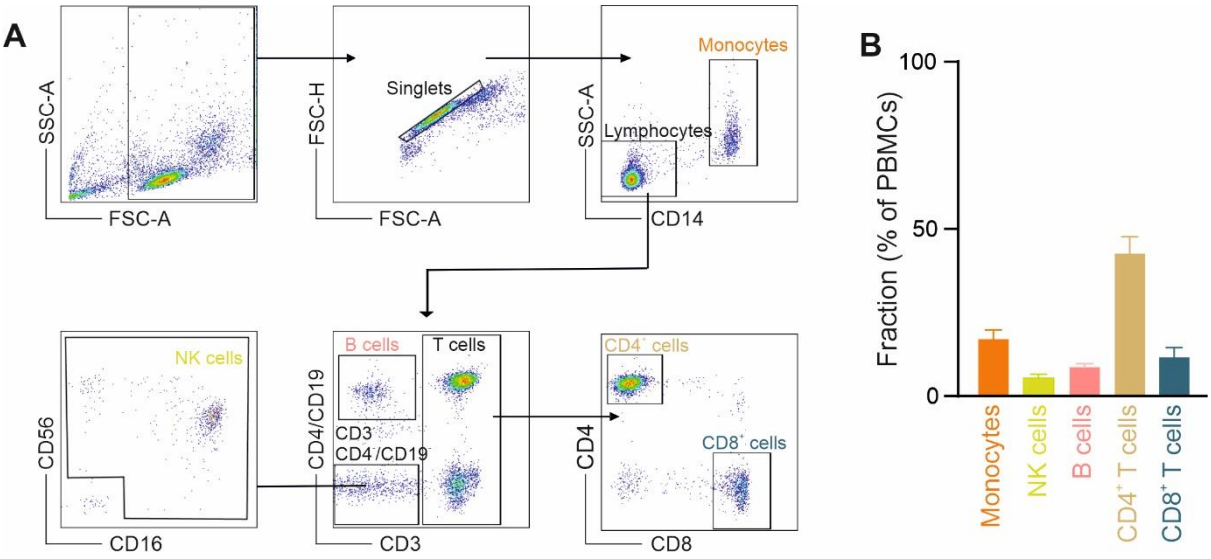

Figure S4: Sub-populations of PBMCs from healthy donors. A) Immunostaining was performed on PBMCs isolated from healthy donors and data was acquired using flow cytometer. Different immune cell population were gated from the lymphocytes as shown in the gating strategy by using the following antibodies with fluorophore conjugates: CD14-PE-Cy7, CD3-PerCP, CD4-BV421, CD19-BV421, CD56-APC, CD16-PE, and CD8-FITC as reported previously [1]. **B)** Fraction of each subpopulation in PBMCs. Data are presented as Results are from six donors.

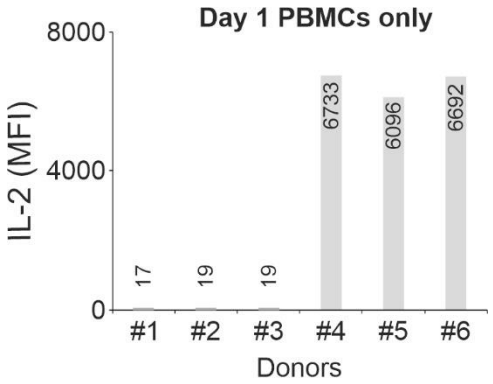

Figure S5: Spontaneous release of IL-2 in different donors. PBMCs from Donors #1-3 were featured with low spontaneous IL-2 release, those from Donors #4-6) with high spontaneous IL-2 release. PBMCs were cultured alone without bacteria or gels. The supernatant was collected on day 1. Data were extracted from Fig. 3 (Day 1) and Fig. 7A (Day 1).

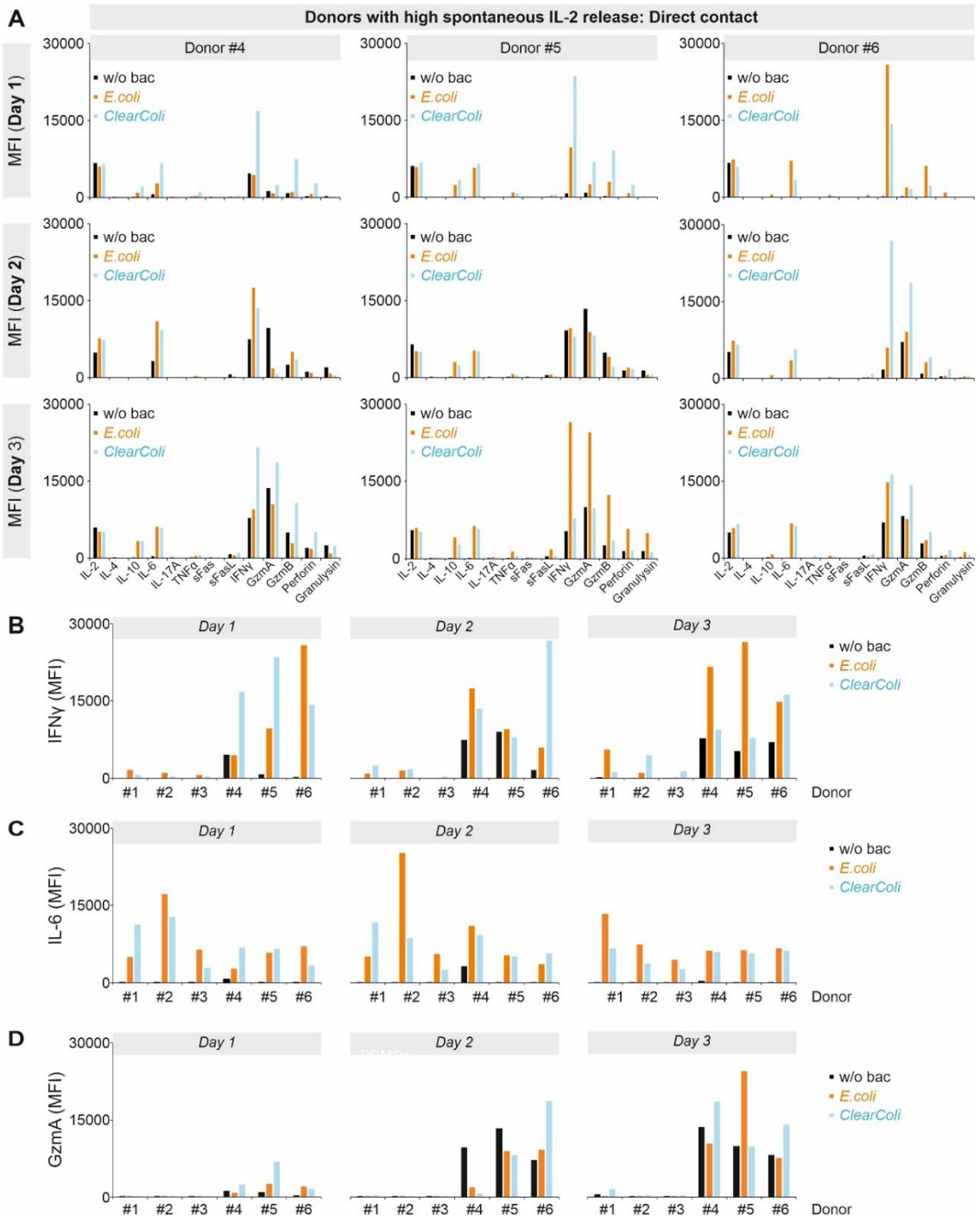

Figure S6: Profiles of cytokines and cytotoxic proteins from donors with high spontaneous IL-2 release upon bacterial contact. A) Profiles of cytokines and cytotoxic proteins released by PBMCs were determined by the multiplex cytokine assay. PBMCs with high spontaneous IL-2 release were cultured without bacteria (w/o bac) or in direct contact with *E.coli* or *ClearColi*. The supernatant was collected at the indicated time points. Results were from three donors. MFI: mean fluoresce intensity. **B-D)** Comparison of released cytokines between donors with low and high spontaneous IL-2 release. IFNγ, IL-6 and granzyme A (GzmA) are shown in **B**, **C** and **D**.

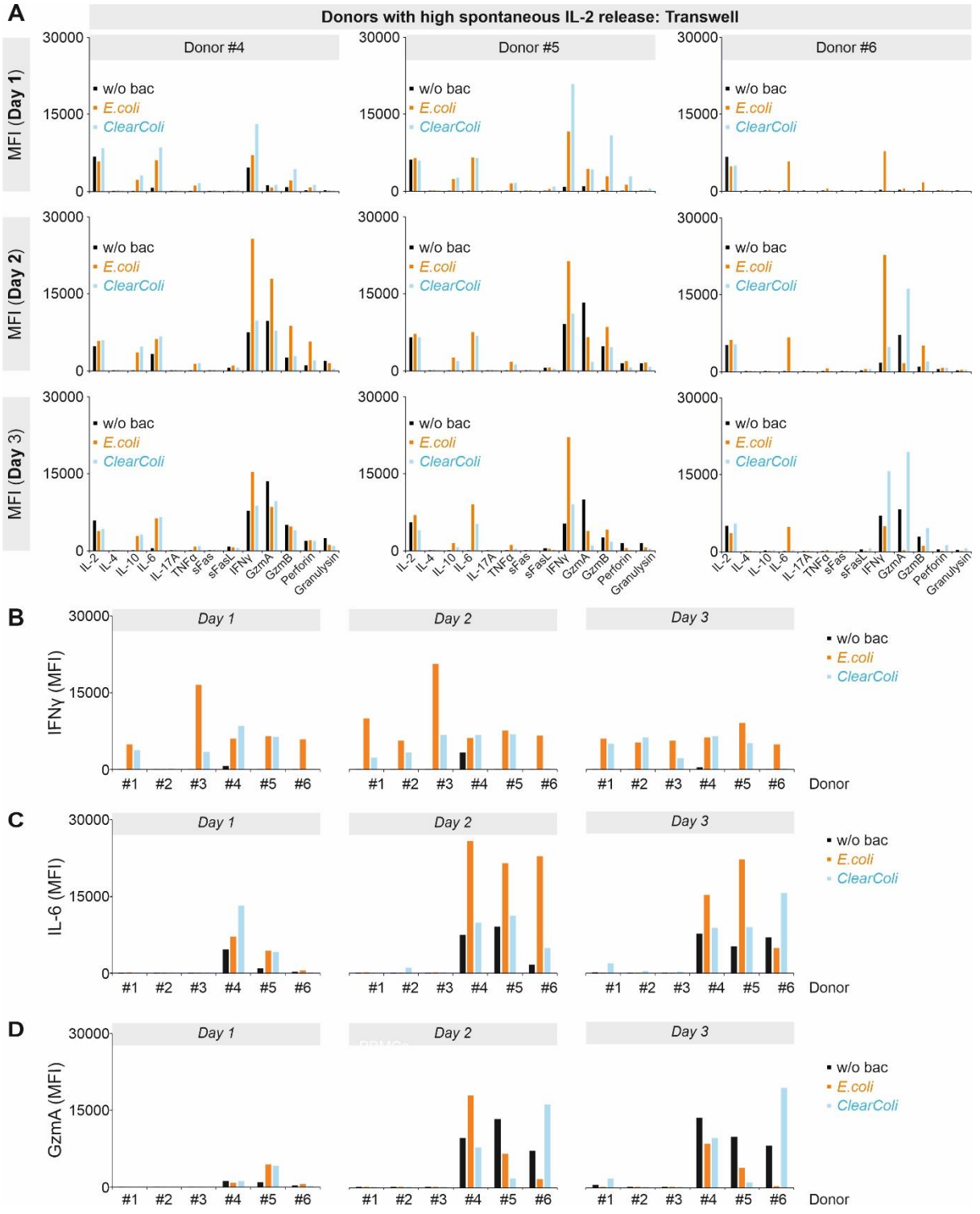

Figure S7: Cytokine profiles of PBMCs from donors with high spontaneous release of IL-2 with *E. coli* or *ClearColi* bacterial strains separated by a nano-porous transwell insert. A) PBMCs from donors with high spontaneous release of IL-2 were incubated with either *E. coli* or *ClearColi* strains separated by a nano-porous transwell insert for 3 days. Cell culture supernatant was collected on days 1, 2 and 3 to perform a multiplex cytokine assay. Cytokines and cytotoxic proteins released by PBMCs in response to soluble factors released by the

bacteria was determined which was compared to w/o bacteria condition (PBMCs alone). The data is represented with Mean fluorescence intensity (MFI) on Y-axis for donors 4, 5 and 6 for all the 3 days (n=3). **B-D**) A comparison between donors with modest release of IL-2 (donors 1,2,3) and high spontaneous release of IL-2 (donors 4,5,6) for IFNγ (**B**), IL-6 (**C**) and Granzyme A (**D**) released from PBMCs incubated with *E. coli* or *ClearColi* strains in a transwell insert and w/o bacteria condition (PBMCs alone).

Reference

1. Knorck, A. *et al.* Quantity, quality, and functionality of peripheral blood cells derived from residual blood of different apheresis kits. *Transfusion* **58**, 1516-1526 (2018).

7 PUBLICATIONS

Results obtained during the realization of this Thesis have led to the publications as listed below:

1. **Regulating bacterial behavior within hydrogels of tunable viscoelasticity**
   Authors: **Shardul Bhusari**, Shrikrishnan Sankaran and Aránzazu del Campo.
   Published: Advanced Science 9, no. 17 (2022): 2106026.
   DOI: 10.1002/advs.202106026

2. **Encapsulation of bacteria in bilayer Pluronic thin film hydrogels: a safe format for engineered living materials**
   Authors: **Shardul Bhusari**, Juhyun Kim, Karen M Polizzi, Shrikrishnan Sankaran and Aranzazu del Campo.
   Published: Biomaterials Advances 145 (2023): 213240.
   DOI: 10.1016/j.bioadv.2022.213240

3. ***In vitro* evaluation of immune responses to bacterial hydrogels for the development of living therapeutic materials**
   Authors: Archana Yanamandra*, **Shardul Bhusari***, Aranzazu del Campo, Shrikrishnan Sankaran and Bin Qu.
   Submitted

4. **Rheological behavior of Pluronic/Pluronic diacrylate hydrogel matrices used for bacteria encapsulation**
   Authors: **Shardul Bhusari**, Maxi Hoffmann, Petra Herbeck-Engel, Shrikrishnan Sankaran, Manfred Wilhelm and Aránzazu del Campo.
   Under preparation

5. **3D bioprinting mechanically robust core-shell living therapeutic fibers**
   Authors: **Shardul Bhusari**, Mokhamad Khamdan and Aránzazu del Campo.
   Under preparation

6. **Printed degradable optical waveguides for guiding light into tissue**

   Authors: Jun Feng, Yijun Zheng, **Shardul Bhusari**, Maria Villiou, Samuel Pearson**,** and Aranzazu del Campo.

   Published: Advanced functional materials 30, no. 45 (2020): 2004327

   DOI: 10.1002/adfm.202004327

7. **Plasmonic stimulation of gold nanorods for the photothermal control of engineered living materials**

   Authors: Selim Basaran, Sourik Dey, **Shardul Bhusari**, Shrikrishnan Sankaran and Tobias Kraus.

   Published: Biomaterials Advances (2023): 213332

   DOI: 10.1016/j.bioadv.2023.213332

8 CONFERENCE COMMUNICATIONS

Results obtained during the realization of this Thesis have been presented in numerous conferences listed below:

1. **ESB 2022 - The 32nd Annual Conference of the European Society for Biomaterials (Bordeaux, France)**

   Oral presentation: ‘‘Giving Life to Materials: Tuning bacterial behavior in Pluronic based bioinks for living therapeutic applications’’ Shardul Bhusari, Shrikrishnan Sankaran and Aránzazu del Campo.

2. **3rd International Conference Engineered Living Materials 2022 (Saarbrücken, Germany)**

   Oral presentation: ‘‘*In vitro* analysis of Immune Responses to Engineered Living Materials’’ Archana Yanamandra, Shardul Bhusari, Aránzazu del Campo, Shrikrishnan Sankaran, Bin Qu.

3. **6th International School and Conference on Biological Materials Science: Bioinspired Materials 2022 (virtual)**

   Oral presentation: ‘‘Therapeutic Materials with Life: Bacterial behavior in Pluronic based bioinks for smart drug delivery’’ Shardul Bhusari, Shrikrishnan Sankaran and Aránzazu del Campo.

4. **Biophilic Intelligence Seminar in the Future of Life Summer School 2022 (Karlsruhe, Germany)**

   Oral presentation: ‘‘Living materials for life’’ Shrikrishnan Sankaran, Shardul Bhusari, and Aránzazu del Campo.

5. **17th Zsigmondy Conference 2022 (Aachen, Germany)**

   Oral presentation: ‘‘Plasmonic stimulation of gold nanorods for the control of living materials’’ Selim Basaran, Sourik Dey, Shardul Bhusari, Aránzazu del Campo, Shrikrishnan Sankaran and Tobias Kraus.

6. **ESB 2021 – The 31st Annual Conference of the European Society for Biomaterials (virtual)**

   Oral presentation: ‘‘Bacteria Material Relationship - it's complicated! Bacterial behavior in Pluronic based bioinks for Living Therapeutic Devices.’’ Shardul Bhusari, Shrikrishnan Sankaran and Aránzazu del Campo.

7. **German Conference on Synthetic Biology 2021 - Engineering Living Systems (virtual)**

   Oral presentation: ‘‘Living therapeutic devices - Marrying synthetic biology with materials science’’ Shardul Bhusari, Shrikrishnan Sankaran and Aránzazu del Campo.

8. **German Conference on Synthetic Biology 2021 - Engineering Living Systems (virtual)**

   Oral presentation: ‘‘Living therapeutic materials - hydrogel-confined bacteria for smart drug delivery’’ Shrikrishnan Sankaran, Priyanka Dhakane, Shardul Bhusari, Sourik Dey, Marc Blanch Asensio, Florian Riedel, Aránzazu del Campo.

9. **Designer Biology Conference 2021 (virtual)**

   Oral presentation: ‘‘Living therapeutic materials for sustained drug release’’ Priyanka Dhakane, Varun Tadimarri, Shardul Bhusari, Aránzazu del Campo, Shrikrishnan Sankaran.

10. **Cell Physics 2021 (Saarbrücken, Germany)**

    Oral presentation: ‘‘Design of 3D printed hydrogel biofilm mimics’’ Shardul Bhusari, Shrikrishnan Sankaran and Aránzazu del Campo.

11. **2nd International Conference Engineered Living Materials 2021 (virtual)**

    Oral presentation: ‘‘Living therapeutic devices: bacterial behavior in viscoelastically tunable confinement’’ Shardul Bhusari, Shrikrishnan Sankaran, Aránzazu del Campo.

12. **1st International Conference Engineered Living Materials 2020 (Saarbrücken, Germany)**

    Poster presentation: ‘‘Living Therapeutic Materials: Light-mediated smart drug release from hydrogel-encapsulated bacteria’’ Shardul Bhusari, Shrikrishnan Sankaran, Judith Becker, Christoph Wittmann, Aránzazu del Campo.

13. **13th International Symposium on Frontiers in Biomedical Polymers 2019 (Tenerife, Spain)**

    Oral presentation: ‘‘Light-responsive drug release from living hydrogels’’ Shardul Bhusari, Shrikrishnan Sankaran, Aránzazu del Campo.

14. **International Summer School on Technology Transfer in Life Sciences 2019 (Dresden, Germany)**

    Oral presentation: ‘‘Living therapeutic materials - translation from bench to bedside’’ Shardul Bhusari, Shrikrishnan Sankaran and Aránzazu del Campo.

15. **Cell Physics 2019 (Saarbrücken, Germany)**

    Poster presentation: ‘‘Protein engineering strategy to design and develop a photo-respnosive ICAM-1 domain’’ Shardul Bhusari, Priyanka Dhakane, Shrikrishnan Sankaran and Aránzazu del Campo.